Université de Montréal
Faculté des arts et des sciences

Cette thèse intitulée:

Strategic Planning of Intracity Electric Vehicle Charging Station Locations with Integrated Advanced Demand Dynamics

présentée par:

Steven Lamontagne

a été évaluée par un jury composé des personnes suivantes:

Jean-Yves Potvin,	président-rapporteur
Margarida Carvalho,	directrice de recherche
Emma Frejinger,	codirectrice
Michel Gendreau,	membre du jury
Virginie Lurkin,	examinatrice externe
Dominic Rochefort,	représentant du doyen de la FESP

février, 2024

Thèse acceptée le: 3 mai 2024

Résumé

Dans des régions avec beaucoup d'électricité renouvelable, comme le Québec, une augmentation du nombre de Véhicules Électriques (VE) peut réduire les gaz à effet de serre. Par contre, l'autonomie réduite des VE et la présence limitée d'infrastructure publique pour recharger les véhicules peuvent contribuer à un phénomène nommé *anxiété de l'autonomie*, où les usagers n'achètent pas des VE par peur qu'ils tombent en panne. On peut alors planifier l'emplacement de l'infrastructure publique de recharge de manière stratégique pour combattre cet effet, menant alors à un taux d'adoption plus élevé pour les VE.

En utilisant des modèles de choix discret, nous incorporons des modèles économétriques de demande avancés capturant les préférences hétérogènes des usagers à l'intérieur de l'optimisation. En particulier, comme nous le démontrerons, ceci permet l'inclusion de nouveaux facteurs importants, tels qu'une disponibilité de la recharge à domicile et des effets de distance plus granulaire. Par contre, la méthodologie existante pour ce processus crée un modèle de programmation linéaire mixte en nombres entiers qui ne peut pas être résolue, même pour des instances de taille modeste. Nous développons alors une reformulation efficace en problème de couverture maximum qui, comme nous le démontrerons, permet une amélioration de plusieurs ordres de magnitude pour le temps de calcul.

Bien que cette reformulation dans un problème de couverture maximum améliore grandement la capacité à résoudre le modèle, celui-ci demeure difficile à résoudre pour des problèmes de grandes tailles, nécessitant des heuristiques pour obtenir des solutions de haute qualité. Nous développons alors deux méthodes de décomposition de Benders spécialisées pour cette application. La première est une méthode de décomposition de Benders accélérée, qui se spécialise à réduire l'écart d'optimalité et à la résolution de problèmes de petite taille ou de taille modeste. La deuxième approche rajoute un branchement local à la méthode de décomposition de Benders accélérée, qui sacrifie de l'efficacité lors de la résolution de problèmes

de plus petite taille pour une capacité augmentée afin d'obtenir des solutions réalisables de haute qualité.

Finalement, nous présentons une méthode pour dériver des valeurs de paramètres autrement difficiles à obtenir pour le modèle de choix discrets dans le modèle d'optimisation. Ces paramètres dictent les effets de l'infrastructure publique de recharge sur l'adoption des VE. Pour ce processus, nous regardons les facteurs qui encouragent les usagers courants des VE à utiliser l'infrastructure existante. De manière plus précise, nous utilisons des données de recharge réelles de la ville de Montréal (Québec) pour estimer les impacts des caractéristiques des stations, tels que la distance des usagers, le nombre de bornes de recharge, et les installations à proximité. Différents types d'infrastructure sont considérés, de manière parallèle avec des modèles de choix discrets qui peuvent tenir compte de plusieurs observations pour chaque individu.

Les contributions de cette thèse sont plus générales que simplement l'adoption de VE, étant applicable, par exemple, au problème de capture maximum, au problème de couverture maximum à multiples périodes, et à la prédiction de la station de recharge choisie par les conducteurs de VE.

Mots clés : Stations de recharge de véhicules électriques, modèles de choix discrets, modèle de couverture maximum, décomposition de Benders, préférences révélées

Abstract

In areas with large amounts of clean renewable electricity, such as Quebec, an increase to the number of electric vehicles (EVs) can reduce greenhouse gas emissions. However, the reduced range of EVs and the limited public charging infrastructure can contribute to a phenomenon known as *range anxiety*, where users do not purchase EVs out of concern they run out of charge while driving. We can strategically optimise the placement of public EV charging infrastructure to combat this effect, thus leading to increased EV adoption.

By utilising discrete choice models, we incorporate advanced econometric demand models capturing heterogeneous user preferences within the optimisation framework. In particular, as we demonstrate, this allows for the inclusion of new, important attributes, such as a more granular home charging availability and a continuous degradation of quality based on the distance. However, existing methodologies for this optimisation framework result in a mixed-integer linear program which cannot be solved for even moderately sized instances. We thus develop an efficient reformulation into a maximum covering location problem which, as we show experimentally, allows for multiple orders of magnitude of improved solving time.

While the reformulation into a maximum covering location problem greatly improves the solving capabilities for the model, it remains intractable for large-scale instances, relying on heuristics to obtain high-quality solutions. As such, we then develop two specialised Benders decomposition methods for this application. The first is an accelerated branch-and-Benders-cut method, which excels at solving small or medium-scale instances and at decreasing the optimality gap. The second approach incorporates a local branching scheme to the accelerated branch-and-Benders-cut method, which sacrifices some efficiency in solving smaller instances for an increased ability to obtain high-quality feasible solutions.

Finally, we discuss a method for deriving difficult-to-obtain parameter values of

the discrete choice model in the optimisation framework. These parameter values dictate the effects of the public charging infrastructure on EV adoption and, as such, play a crucial role in the optimisation model. For this process, we investigate the attributes that encourage current EV owners to utilise existing infrastructure. More specifically, we use real charging session data from the city of Montreal (Quebec) to determine the impacts of station characteristics such as the distance to the users, the number of outlets, and the nearby amenities. Different types of charging infrastructure are considered alongside discrete choice models which take into account multiple observations from individual users.

The contributions of this thesis lie more broadly than simply EV adoption, being applicable to, e.g., the maximum capture problem, the multi-period maximum covering location problem, and the prediction of the charging station selected by EV drivers.

Keywords: Electric vehicle charging stations, discrete choice models, maximum covering location problem, Benders decomposition, revealed preferences

Contents

List of Tables

List of Figures

List of Abbreviations

BDS	*Benders Dual Subproblem*
BEV	*Battery Electric Vehicle*
BPS	*Benders Primal Subproblem*
CIRRELT	*Centre Interuniversitaire de Recherche sur les Réseaux d'Entreprise, la Logistique, et le Transport*
EV	*Electric Vehicle*
GEV	*Generalised Extreme Value*
GF	*Growth Function*
GIS	*Geographical Information System*
GRASP	*Greedy Randomised Adaptive Search Procedure*
HEV	*Hybrid Electric Vehicle*
ICEV	*Internal Combustion Engine Vehicle*
km	*Kilometre*
kW	*Kilowatt*
kWh	*Kilowatt-hour*
LP	*Linear Programming*
MC	*Maximum Covering*
MCLP	*Maximum Covering Location Problem*
MCPRU	*Maximum Capture Problem with Random Utilities*
MILP	*Mixed-Integer Linear Program*
MNL	*Multinomial Logit*
MP	*Main Problem*

MXL	*Mixed Logit*
NSERC	*National Sciences and Engineering Research Council of Canada*
PHEV	*Plug-in Hybrid Electric Vehicle*
RFID	*Radio Frequency Identification*
RP	*Revealed Preference*
RUM	*Random Utility Maximisation*
SL	*Single Level*
SP	*Stated Preference*
VE	*Véhicule électrique*

Acknowledgements

J'aimerais premièrement offrir un remerciement solennel pour Bernard Gendron. C'est grâce à lui que j'ai entendu parler de la recherche opérationnelle, et sa joie de vivre et d'enseigner m'ont convaincu de faire un doctorat avec lui. Malheureusement, il nous a quittés trop tôt, et n'a jamais eu la chance de voir la complétude du projet. J'espère qu'il serait fier du progrès qu'on a fait.

I am also extremely grateful to my supervisors, Margarida Carvalho and Emma Frejinger. They have both been an incredible support and superb mentors throughout the process. The help and expertise they have given is immeasurable, from giving feedback on my first literature review (which was way too long, as usual), to staying late in one of our meetings to help me get CPLEX do what I want, to sitting down with me to translate statistics terms in Biogeme results, just to name a very few. This journey would have been impossible without them, and I am grateful beyond words to both of them.

I would also extend thanks to the amazing team for our project with Hydro-Québec. This includes, of course, our wonderful partners at Hydro-Québec and IREQ (Jean-Luc Dupre, Ribal Atallah, and Amira Dems) who have lent their incredible knowledge and vast experience about electric vehicle charging, the charging network, and network design. The insight and feedback from other members of the team have also helped shaped this work today, including Miguel Anjos, Nurit Oliker, Mahsa Moghaddass, Pierre-Luc Parent, Ismail Sevim, and Nagisa Sugishita.

I would also like to thank the following institutions for their financial support throughout the doctorate: Hydro-Québec, the Département d'Informatique et de Recherche Opérationelle (DIRO, Université de Montréal), the Centre Interuniversitaire de Recherche sur les Réseaux d'Entreprise, la Logistique, et le Transport (CIRRELT), the National Sciences and Engineering Research Council of Canada (NSERC), and the FRQ-IVADO Research Chair in Data Science for Combinatorial Game Theory.

Finally, I would also like to thank my friends and family who supported me throughout the doctorate process (while only occasionally asking when I would be done).

1 Introduction

Drastic reductions of CO_2 emissions are necessary to meet global goals. Among the different sectors of human activity, transportation accounted for 23% of CO_2 emissions worldwide in 2021 (International Energy Agency 2023), and 28% of the emissions in Canada in 2023 (Environment and Climate Change Canada 2023). In regions where most of the electricity is generated by nuclear power plants or renewable sources, which includes Quebec, increasing the number of electric vehicles (EVs) compared to Internal Combustion Engine Vehicles (ICEVs) can reduce these emissions (Woo et al. 2017, Axsen et al. 2015b).

To convince drivers that EVs are viable primary vehicles, sufficient charging opportunities must exist to combat the so-called *range anxiety* of users. For current EV owners, their charging needs are largely satisfied by home charging (see, e.g. Figenbaum and Nordbakke 2019, Tal et al. 2020). But this solution is not viable for all users, as those who make long-distance trips or who cannot install home chargers (e.g. those living in apartment buildings) may require additional public charging infrastructure. As this infrastructure is expensive, only a limited number of facilities may be constructed. It is then reasonable to ask which locations should be selected to maximise the adoption of EVs. In particular, this is an open question and ongoing process for our industrial partners, looking to construct public charging infrastructure within the province of Quebec.

There are multiple possible ways to view the charging station location problem. From a geographical standpoint, we can consider either intracity or intercity travel. While both are critical components of the public charging network, their use is quite different. For most users, the public charging infrastructure within the city is more a matter of convenience and a safety net, with users charging when already parked for an activity (Hardman et al. 2018, Figenbaum and Nordbakke 2019, Tal et al. 2020). However, this does not apply to users who cannot recharge at home, and are thus reliant on the public network. In the intercity context, the public

charging network is a necessity, enabling long-distance trips that would otherwise be impossible.

From a temporal standpoint, we can consider a tactical or strategic point of view. The tactical planning is geared towards improving the service quality for existing users, such as by increasing the capacity of heavily used stations or ensuring that charging stations can cover the demand for electricity (e.g. Parent et al. 2023). In the long-term context, the approach is geared towards improving the overall structure of the charging network, such as improving the regional availability of charging stations or increasing the portion of users who pass by charging infrastructure (e.g. Zhang et al. 2017a). From the perspective of a charging network operator, it also allows for the inclusion of factors such as seasonal effects, planned infrastructure from other network operators, and population shifts.

In our work, we consider the strategic and intracity context. More specifically, we assume we are given a list of both existing charging stations and potential locations for new charging stations within a city over a multi-year timespan. Each charging station may feature multiple connectors for recharging vehicles, which we call charging outlets (or chargers). Our goal is then to determine the optimal placement of these charging outlets to maximise the adoption of EVs.

Throughout this work, we use 'EV' as an umbrella term, which includes any vehicle that features a battery rechargeable via external connection to the power grid. Two subcategories exist within this context:

Plug-in Hybrid Electric Vehicle (PHEV): These vehicles feature both an internal combustion engine and a battery which can be recharged via a charging connector. Typically, they have a smaller battery capacity, and may not be able to take advantage of faster charging options.

Battery Electric Vehicle (BEV): These vehicles do not contain an internal combustion engine at all, relying solely on a battery. To compensate, they usually have much larger battery capacities and can take advantage of the fastest charging options.

In addition to these, some works on EVs also include Hybrid Electric Vehicles (HEVs, see Rezvani et al. 2015). However, while these can be propelled via the internal battery, this battery can only be recharged while driving the vehicle (such as by

braking). As such, they are effectively more fuel-efficient ICEVs, and are not affected by the placement of public charging infrastructure.

In the following we briefly outline the structure of the thesis and its contributions: In Chapter 2, we present background information, providing foundational insights to the readers. The following three chapters correspond to articles, each of which address a different aspect of the EV network design model. In Chapter 3, we formulate the EV network design model, based on a framework proposed in Pacheco Paneque et al. (2021). As the standard version of this framework demonstrates poor performance, we describe an efficient reformulation into a maximum covering location problem. This allows for tailored heuristic methods that can obtain high-quality feasible solutions. However, two particularities of this model warrant more detail: i) our exact method is not well suited for solving large-scale instances, and ii) the model requires specific parameters which reflect the impact of each candidate charging station to EV adoption. Chapter 4 assists with the first problem, and provides a more efficient solution method. More specifically, we develop specialised Benders decomposition approaches, tailored for the multi-year context. From there, Chapter 5 addresses the second problem, and aids in finding the required parameters for the optimisation framework. For this, we assume that a charging station which is better for users at the time of charging would result in a higher adoption of EVs. As a consequence, we use discrete choice models to predict the EV charging station selected by users, based only on readily available characteristics of charging stations and users. Finally, in Chapter 6, we conclude the thesis by discussing possible avenues of future research.

2 Background

In this chapter, we complement the literature reviews of Chapters 3, 4, and 5 with a discussion of selected topics. To avoid repetition, topics are abridged if they are discussed in the aforementioned chapters.

2.1 Application

In this section, we provide a background related to the optimal location of EV charging stations. This begins in Section 2.1.1 with some information about the charging requirements of vehicles and the different types of charging infrastructure. Then, in Section 2.1.2, we discuss existing methods for locating EV charging stations.

2.1.1 EV Charging

Analogous to the gas tank and fuel economy of ICEVs, each type of EV has a battery size (measured in kWh) and electricity consumption rate (measured in kWh/km). Combined, these factors determine the travel range of the EV and, consequently, the distance of trips for which public charging infrastructure would be required. In general, both PHEVs and BEVs have energy consumption rates around 20 kWh per 100 km, but PHEV feature smaller batteries around 10 kWh to 40 kWh, while (modern) BEVs feature batteries around 60 kWh to 100 kWh (Roulons Électrique 2023). This consumption rate translates to approximately 5 km of electric range per kWh of the vehicle, which is consistent with the conversion in the literature (van den Hoed et al. 2013, Hardman et al. 2018). As such, PHEVs can travel around 50 km to 200 km in electric mode, while BEVs have a range of around 300 km to 500 km. However, it is well known that the electric range of EVs is severely

reduced by cold weather, and can drop to 60% of its stated level (Roulons Électrique 2023). As such, trips as low as 30 km for PHEVs and 180 km for BEVs could constitute "long-distance trips" for which public charging would be necessary.

As for the equipment used for charging, the charging infrastructure is usually categorised into three levels depending on the power. In Table 2.1, we present characteristics about the different charging levels (Association des véhicules électriques du Québec 2024, Roulons Électrique 2023, Circuit Électrique 2023c, 2024, Hardman et al. 2018). We note that the power output can vary within the same charging level (with, notably, some level 3 charging stations reaching 350 kW, Circuit Électrique 2023c), and the values presented here are the most common for Quebec. In other words, these values are representative of the chargers that would be added to the public charging infrastructure, rather than what may be available more generally.

The charging behaviour of users is highly user-specific, but we note here some general trends which extend outside of Quebec, and that are useful for determining the importance and modelling the use of public charging infrastructure (van den Hoed et al. 2013, Axsen et al. 2015b, Tal et al. 2018, Figenbaum and Nordbakke 2019, Lee et al. 2020, Tal et al. 2020, Visaria et al. 2022, Anderson et al. 2023):

— The vast majority of EV owners (82% to 93%) have access to level 1 or level 2 chargers at home, and do most of their charging there.

— Some users (19% to 40%) additionally have access to workplace charging, which can be the main recharging source for those without home charging.

— The average number of daily charging sessions per user (at all locations) ranges from 0.71 to 1.47.

— Current usage of public charging infrastructure is overall low (for many users, less than once a month), though highly variable by individuals and by area.

— When using public charging, users prefer locations with activities or amenities, such as shopping facilities, supermarkets, or sports facilities.

We have discussed what kind of charging infrastructure can be installed, as well as where it might be used. We can now examine the current methods for placing this public charging infrastructure, thus creating a network of stations for EV owners to use.

	Level 1	Level 2	Level 3
Power output (kW)	1	7.2	50-100
Range added per hour (km)	6	40	240-400
Location	Home, Work	Home, Work, Public	Public
Typical charging session duration	8 hours or more	2 to 3 hours	25 to 30 minutes

Table 2.1 – Charging levels and characteristics

2.1.2 EV Charging Station Network Design

EV charging station network design problems –though they all aim to determine the optimal location for charging infrastructure – can be categorised by multiple interconnected facets, centered around the demand assumptions that are used (Kchaou-Boujelben 2021, Metais et al. 2022). In the node-based approach, the transportation network is composed of a series of nodes, a subset of which contain candidate charging station locations. Each node then generates demand for EV charging, which must be supplied by a nearby charging station node. This framework closely follows the general facility location problem, and thus lends itself well to many classic extensions. Examples include the set covering (minimising the cost for satisfying the demand of users, e.g. Wang and Lin 2009), p-median (minimise the median distance between users and charging stations, e.g. Gavranović et al. 2014), and maximum covering models (maximising the demand that can be satisfied given a limited budget for charging stations, e.g. Frade et al. 2011). Typically, these models do not consider individual drivers or paths and, as such, are best suited in the intracity environment, where daily travel typically falls well below the EV range.

In the path-based approach, users are travelling between a series of origin-destination pairs, the paths for which pass by candidate charging station locations. The charging stations are then selected to maximise the flow which passes by the stations, referred to either as Flow Capturing Location Model or Flow Interception Location Model (Hodgson 1990, Shukla et al. 2011). The Flow Refueling Location Model extension of Kuby and Lim (2005) can then require that multiple charging stations be necessary for long trips. Due to the high number of OD pairs (or arcs, in the case of the arc-cover reformulation of Capar et al. 2013), this approach is not well suited for the intracity case. As such, it is typically used for intercity travel.

While the node-based approach and the path-based approach are most common, other approaches are also used. Most notably, the works of Anjos et al. (2020) and Sun et al. (2020) combine the node-based and the path-based approaches for intracity and intercity travel respectively. Additionally, while more commonly used for electric taxis or buses rather than private vehicles, the activity-based approach considers the daily travel pattern of users and places charging stations near their series of destinations (see, e.g. Jung et al. 2014, Asamer et al. 2016). This highly user-focused approach allows for more detailed consideration of charging level and charging duration, at the cost of greatly increased complexity. Due to this complexity and the high data requirements, this approach is best suited for the intracity case.

In general, the demand is assumed to be constant, an exogenous parameter for the models. In other words, the number of EVs (in node-based models) or the traffic flow (in path-based models) are not dependent on the charging station infrastructure, with two exceptions. In Zhang et al. (2017a), the traffic flow in a path in a given year is a function of the flow in the previous year, the natural EV market share growth, the flow coverage in the path in the previous year, and the overall coverage of all paths in the previous year. In Anjos et al. (2020), the number of EVs in each area is assumed to increase following a piecewise linear growth function, but this growth is limited by the capacity of the charging network in that area.

To include more complex demand patterns, where the number of EVs can evolve based on the charging network, we must first determine the relationship between these two. For our purposes, we assume that there is a positive correlation between the beneficial characteristics of charging stations (distance to users, amenities, etc.) and the number of EVs. As such, we can examine the current methods for evaluating demand in the EV charging context, where users must decide which available charging stations they would use.

2.2 Modelling

To translate the problem of locating EV charging stations into a mathematical model, we rely on many different fields. In Section 2.2.1, we discuss the modeling of demand for charging stations, with a focus on discrete choice models (McFadden 1974). Incorporating the discrete choice models within our optimisation model leads to a bilevel programming framework, which we describe in Section 2.2.2. As we show in the first article (Chapter 3), the bilevel model can be reformulated into a variant of the maximum covering location problem. Both the original formulation and some variants are presented in Section 2.2.3.

2.2.1 Demand Modelling

To predict the probability of an EV owner selecting a given station, there are two fields of research we can explore. The first of these is econometrics, and in particular discrete choice modelling, which assumes a fixed utility structure between selected characteristics (such as the distance between users and the charging station). This results in a highly interpretable model, which can easily be extended to out-of-distribution cases. By contrast, in the second field of research – machine learning –, techniques such as deep learning can involve highly nonlinear models, which can reach higher predictive power at the cost of reduced interpretability. A discussion of these techniques and their strengths are presented in, e.g. Hillel (2020) and Hillel et al. (2021). However, in our application, interpretability and out-of-distribution generalisation are crucial, as results must be extended to locations which do not yet exist. Additionally, a framework proposed in Pacheco Paneque et al. (2021) provides a method for incorporating advanced discrete choice models directly within the optimisation model, allowing for complex demand patterns. This makes discrete choice models the natural option for our work. For more general discussions about using machine learning for combinatorial problems or EV demand modelling, we refer to the reviews of Bengio et al. (2021) and Deb (2021). There has also been recent work to integrate machine learning and discrete choice modelling together, which leverages the predictive power of the former while maintaining the interpretability of the latter (Sifringer et al. 2020).

Within the discrete choice modeling, our work considers additive Random Util-

ity Maximisation (RUM) models, which we describe below. However, specific applications of discrete choice modelling to EV charging demand is analysed in detail in Chapter 5. As such, to avoid repetition, we limit the current discussion to the general context and to the models which will be used in Chapter 5.

The models and procedures described here are based on Train (2002). In RUM models, a user i in a set N must select one alternative j from among a set M based on the attributes $k = 1, \ldots, K$. We note that the term *factor* is sometimes used for an attribute in econometrics, while *feature* is prevalent in the machine learning community (see, e.g. Train 2002, Hillel et al. 2021, Bengio et al. 2021). Each alternative is assumed to have a *utility function* u_{ij}, reflecting the value of alternative j for user i, which combines *observable* attributes known by the modeller and *unobservable* attributes which are known only to the user. More specifically, the utility function can be given by

$$u_{ij}(\beta_{ij}, x_{ij}) = V_{ij}\left(\beta_{ij}, x_{ij}\right) + \varepsilon_{ij},\ i \in N, j \in M$$

where β_{ij} (respectively, x_{ij}) is a K-dimensional vector of parameters (respectively, attribute values) for observable attributes, V_{ij} is a function of β_{ij} and x_{ij}, and ε_{ij} is an error term to account for the unobservable attributes. User i observes all attributes, and is assumed to choose the alternative which maximises their utility. To predict this choice, the modeller defines the functions $V_{ij}\left(x_{ij}\right)$ based on the application, and selects appropriate distributions for the error terms. The predicted probability that a user i chooses alternative j given the vector of attributes x_{ij} is then the probability that it is associated with the highest utility, that is,

$$P_{ij}(\beta_{ij}, x_{ij}) = \text{Prob}\left(V_{ij}\left(\beta_{ij}, x_{ij}\right) + \varepsilon_{ij} > V_{ij'}\left(\beta_{ij}, x_{ij'}\right) + \varepsilon_{ij'}, j' \neq j \in M\right).$$

We note that here, and in what follows, we have opted to explicitly write out $\beta_{ij}, u_{ij}(\beta_{ij}, x_{ij})$ and $P_{ij}(\beta_{ij}, x_{ij})$ rather than the more common shorthand of β, u_{ij}, P_{ij}. This is to emphasise the dependence on the user i, both in β_{ij} itself as well as in the calculation of $u_{ij}(\beta_{ij}, x_{ij})$ and $P_{ij}(\beta_{ij}, x_{ij})$ via the vectors β_{ij} and x_{ij}.

In the standard multinomial logit (MNL) specification, we have that: i) the function $V_{ij}\left(\beta, x_{ij}\right)$ is linear in the parameters β, ii) the parameters β are inde-

pendent of the user i, and iii) the error terms ε_{ij} are independent and identically extreme-value distributed across alternatives and users. In other words, the utility function is given by

$$u_{ij}(\beta, x_{ij}) = \sum_{k=1}^{K} \beta_k x_{ijk} + \varepsilon_{ij},\ i \in N, j \in M,$$

where $\beta_k \in \mathbb{R}$ is the parameter value for attribute k. Under these assumptions, for a given vector of parameter values β and vector of attribute values x_{ij}, the resulting probability for selecting alternative j is then given by

$$P_{ij}(\beta, x_{ij}) = \frac{\exp\left(\sum_{k=1}^{K} \beta_k x_{ijk}\right)}{\sum_{j' \in M} \exp\left(\sum_{k=1}^{K} \beta_k x_{ij'k}\right)}. \tag{2.1}$$

For a set of vectors $x_{ij}, i \in N$, the parameters β_k can then be estimated efficiently by maximising the log-likelihood function

$$LL(\beta) = \sum_{i \in N} \sum_{j \in M} y_{ij} \ln\left(P_{ij}(\beta, x_{ij})\right), \tag{2.2}$$

were $y_{ij} = 1$ if user i selected alternative j and 0 otherwise.

In the random-parameters mixed logit (MXL) model with panel effects, the utility for user $i \in N$ is given by

$$u_{ij}(\tilde{\beta}_i, x_{ij}) = \sum_{k=1}^{K} \tilde{\beta}_{ik} x_{ijk} + \varepsilon_{ij},$$

where the parameters $\tilde{\beta}_{ik} \in \mathbb{R}$ depend on the user i, while the error terms ε_{ij} are independent and identically extreme-value distributed across alternatives and users. Given the vector of attribute values x_{ij}, if the vector $\tilde{\beta}_i$ were known, the choice probabilities could then be given by the logit probabilities in Equation (2.1), resulting in the function

$$L_{ij}(\tilde{\beta}_i, x_{ij}) = \frac{\exp\left(\sum_{k=1}^{K} \tilde{\beta}_{ik} x_{ijk}\right)}{\sum_{j' \in M} \exp\left(\sum_{k=1}^{K} \tilde{\beta}_{ik} x_{ij'k}\right)},$$

which is called the logit kernel for alternative j. In general, the vectors $\tilde{\beta}_i$ are unknown for individual users. However, it is assumed that the set of parameters $\tilde{\beta}$ are distributed over the users i with density $f_\beta(\tilde{\beta})$, where β are the parameters of the distribution f. In this thesis, we assume that $\tilde{\beta}$ follow normal distributions, with mean β_k^μ and standard deviation β_k^σ for each parameter k. We remark that, for the sake of consistency, the parameters of the density f are denoted β, as they are the values to be estimated in this model. Therefore, the vector β may not be K-dimensional and, as such, this does constitute a slight abuse of notation.

The probability of selecting alternative j, for given parameter values β and vector of attribute values x_{ij}, is then given by

$$P_{ij}(\tilde{\beta}, x_{ij}) = \int L_j\left(\tilde{\beta}, x_{ij}\right) f_\beta(\tilde{\beta}) d\,\tilde{\beta}. \tag{2.3}$$

To take into account panel effects, the choice probabilities in Equation (2.3) are modified as to take the product of all observations from each user. However, for the sake of simplicity, the following development omits this product.

The choice probabilities in Equation (2.3) do not have a closed form but, for any given value of β (i.e. parameters of the density f), can be approximated via simulation. Let R be the total number of draws used in the approximation, and let $\tilde{\beta}^r, r = 1, \ldots, R$ denote the draws of $\tilde{\beta}$ from the density $f_\beta(\tilde{\beta})$. Then the simulated choice probability in Equation (2.3), for given parameters β and vector of attribute values x_{ij}, is given by

$$\hat{P}_{ij}(\tilde{\beta}, x_{ij}) = \frac{1}{R} \sum_{r=1}^{R} L_{ij}\left(\tilde{\beta}^r, x_{ij}\right). \tag{2.4}$$

The parameters β can then be estimated by maximising the simulated log-likelihood function

$$SLL(\beta) = \sum_{i \in N} \sum_{j \in M} y_{ij} \ln\left(\hat{P}_j(\tilde{\beta}, x_{ij})\right). \tag{2.5}$$

To emphasise the difference between the MNL and MXL models, the former assumes that the parameter values β_k are constant across the population, while the latter allows for variance. As a result, the MXL model aims to find the distribution of preferences which best matches the population, which it does by estimating the

parameter values β of the distribution. Crucially, the probability functions for both models in Equations (2.1) and (2.4) only depend on the attribute values of user i, rather than their (unknown) individual preferences. As such, they can be applied to users unobserved in the estimation process.

If we use discrete choice models for demand modelling and embed the utility functions directly within the optimisation framework for EV charging network design (following the framework of Pacheco Paneque et al. 2021), we obtain a hierarchical structure to our problem. More specifically, the choices of the users depend intrinsically upon the network design decisions, as the selection by the user can only be determined once all the set of alternatives and their characteristics are decided. This application thus falls within the framework of *bilevel optimisation*, which we can discuss more in detail next.

2.2.2 Bilevel Optimisation

In many applications, there is a natural hierarchical structure embedded within the decision processes, where decisions are made in a sequential order. In the bilevel optimisation context, this takes the form of two groups called the upper level (or *leader*) and the lower level (or *followers*):

1. The upper level takes a decision first, with a specific objective in mind (which typically depends on both the upper and lower level decisions). They know the objective of the lower level, but cannot directly control their decisions.
2. After the decisions of the upper level have been revealed, the lower level make their decisions. The lower level have a separate objective from the upper level, which depends upon the decisions of the upper level.

We present the simplest case, where both the upper and lower level problems are linear and the lower level variables are continuous, as that is the context of our work. More specifically, consider the following model:

$$\text{Minimise}_{x,w} \sum_{j=1}^{J} F_j^x x_j + \sum_{i=1}^{I} F_i^w w_i, \tag{2.6a}$$

$$\text{subject to } \sum_{j=1}^{J} G_{jk}^x x_j + \sum_{i=1}^{I} G_{ik}^w w_i \geq B_k, \quad 1 \leq k \leq K, \tag{2.6b}$$

$$w \in \text{argmax} \left\{ \sum_{i=1}^{I} f_i^w w_i' : \begin{array}{c} \sum_{j=1}^{J} g_{jl}^x x_j + \sum_{i=1}^{I} g_{il}^w w_i' \geq b_l,\ 1 \leq l \leq L, \\ w' \geq 0 \end{array} \right\}, \tag{2.6c}$$

$$x \in X, \tag{2.6d}$$

where $x_j, j \in J$ (respectively, $w_i, i \in I$) denote the decision variables for the upper level (lower level), and X denotes the upper-level domain, which includes integrality requirements.

The presence of the lower-level subproblem (2.6c) makes the problem much more difficult to solve, and not directly solvable by a Mixed-Integer Linear Program (MILP) solver. However, we can reduce the Problem (2.6) to a single-level program. Indeed, since the lower-level subproblem is a continuous linear program, we can use standard duality theory to derive necessary and sufficient conditions to guarantee optimality. More specifically, the dual of lower level problem is given by

$$\text{Minimise } \sum_{l=1}^{L} (b_l - \sum_{j=1}^{J} f_{jl}^x x_j) \pi_l, \tag{2.7a}$$

$$\text{subject to } \sum_{l=1}^{L} g_{il}^w \pi_l \leq f_i^w, \quad 1 \leq i \leq I, \tag{2.7b}$$

$$\pi \geq 0. \tag{2.7c}$$

From there, optimality is given by the complementary slackness constraints

$$\left(f_i^w - \sum_{l=1}^{L} g_{il}^w \pi_l\right) w_i = 0, \quad 1 \le i \le I, \tag{2.8a}$$

$$\left(\sum_{j=1}^{J} g_{jl}^x x_j + \sum_{i=1}^{I} g_{il}^w w_i - b_l\right) \pi_l = 0, \quad 1 \le l \le L. \tag{2.8b}$$

In the more general case, where the lower level is concave, these complementary slackness conditions are replaced by the Karush-Kuhn-Tucker conditions in the single-level reduction (Sinha et al. 2017).

The Constraints (2.8) involve the product of variables, rendering them non-linear. However, they can be linearised through the use of the following so-called Big-M constraints

$$f_i^w - \sum_{l=1}^{L} g_{il}^w \pi_l - M_i \alpha_i \le 0, \quad 1 \le i \le I, \tag{2.9a}$$

$$w_i - M_i(1 - \alpha_i) \le 0, \quad 1 \le i \le I, \tag{2.9b}$$

$$\sum_{j=1}^{J} g_{jl}^x x_j + \sum_{i=1}^{I} g_{il}^w w_i - b_l - M_l \beta_l \le 0, \quad 1 \le l \le L, \tag{2.9c}$$

$$\pi_l - M_l(1 - \beta_l) \le 0, \quad 1 \le l \le L, \tag{2.9d}$$

$$\alpha_i, \beta_l \in \{0, 1\}, \quad 1 \le l \le L, 1 \le i \le I, \tag{2.9e}$$

where M_i, M_l are sufficiently large constants, and α and β are auxiliary variables.

These linearised complementary slackness constraints (2.9) along with the primal feasibility constraints in (2.6c) and the dual feasibility constraints in (2.7) can then replace the lower-level subproblem itself (2.6c). The resulting model is a single-level, mixed-integer linear program, which can be given directly to generic MILP solvers. However, we note that the complementary slackness constraints (2.9) involve auxiliary binary variables α_i and β_i, and the values of M_i, M_l may result in poor bounds (Pineda and Morales 2019, Kleinert et al. 2020). As a consequence, the solver may exhibit slow convergence. In an ideal situation, this slow convergence may be significantly improved by reformulating the problem to avoid this bilevel structure entirely and, consequently, avoiding the need for the big-M con-

straints. As we will see in Chapter 3, the reformulation we employ results in a maximum covering location problem.

2.2.3 Maximum Covering Location Problem

The Maximum Covering Location Problem (MCLP), first proposed in Church and ReVelle (1974), is a subclass of the general facility location problem. In it, there is a set of facilities I which can be opened, and a set of users J which can be assigned to facilities. A user is then considered to be "covered" if it is assigned to a suitable facility (with the definition of "suitable" depending on the application). As there is no benefit to covering the same user multiple times, this formulation encourages the spreading of locations so as to cover new users. In general, due to resource limitations, it is not possible for all users to be covered. As such, the goal is to cover as much demand from users as possible, while remaining below the resource thresholds. This distinguishes the MCLP from the set covering formulation, where the goal is to minimise the cost for maintaining a fixed level of service.

More specifically, the classical MCLP model takes the form

$$\text{Maximise} \sum_{j \in J} d_j z_j, \tag{2.10a}$$

$$\text{subject to} \sum_{i \in I} x_i = p, \tag{2.10b}$$

$$\sum_{i \in I} a_{ij} x_i \geq z_j, j \in J, \tag{2.10c}$$

$$x_i \in \{0,1\}, \quad i \in I, \tag{2.10d}$$

$$z_j \in \{0,1\} \qquad j \in J. \tag{2.10e}$$

The variables x_i indicate whether or not a facility $i \in I$ is open, while the variables z_j indicate whether a user $j \in J$ is covered. From there, the objective function (2.10a) maximises the value of covering users, with d_j the weight of user j. In general, the weights d_j are assumed to be non-negative. Since opening a facility can only be beneficial in this situation, the cardinality constraint (2.10b) limits the total number of facilities which may be opened. This constraint can also be replaced with a knapsack-style budget constraint. The covering constraints (2.10c) ensure that at

least one appropriate facility must be opened for the user j to be considered covered, where the predefined parameter $a_{ij} \in \{0, 1\}$ indicates whether the facility i covers the user j. For many applications, this coverage is determined via Euclidean distance, with each facility i covering users within a predefined radius (see, e.g. Church and ReVelle 1974, Cordeau et al. 2019). The Constraints (2.10d) and (2.10e) restrict the variables to be binary. However, it is well-known that integrality can be relaxed on the variables $z_j, j \in J$ (Murray 2016).

Since the formulation of the MCLP is quite simple while the applicability is quite vast, many variations of the MCLP have been developed. Some notable examples include:

Budgeted MCLP: While not always identified as a variant, this formulation replaces the cardinality constraint (2.10b) by a budget constraint (Khuller et al. 1999, Li et al. 2021).

Capacitated MCLP: This variant adds an additional constraint, which imposes a capacity limit to each facility (de Assis Corrêa et al. 2009, Alizadeh et al. 2021). As such, it requires a more precise tracking of the assignment of users to facilities.

Dynamic (or Multi-period) MCLP: In some applications, facility construction or allocation can take place over an extended period of time, with sequences of facilities built over time. Correspondingly, the formulation is modified by allowing the decision variables x_i, z_j, the cardinality p, and the demands d_j to vary by time period (Gunawardane 1982, Porras et al. 2019).

Partial (or Cooperative) MCLP: Rather than the all-or-nothing approach to coverage in the classical MCLP with $a_{ij} \in \{0, 1\}$, this variant allows for a facility to only partially cover a user, with $a_{ij} \in [0, 1]$ (Berman et al. 2013, Han et al. 2019). In this approach, multiple facilities may need to cooperate to cover a single user.

Stochastic MCLP (or Under Uncertainty): In the classical MCLP, all of the parameters $p, d_j, a_{ij}, i \in I, j \in J$ are assumed to be known in advance and fixed. This variant allows for some of these parameters to be uncertain, and rely on the distribution of the parameters instead (Berman et al. 2013, Vatsa and Jayaswal 2016, Nelas and Dias 2020).

Regardless of the formulation used, the model must then be solved. As the MCLP is known to be NP-hard (Murray 2016), techniques have evolved over the years to solve more and more complex instances. Naturally, when possible, it is desirable to use an exact method for obtaining an optimal solution to our problem.

2.3 Solution Methods for the MCLP

With the model reformulated into an MCLP, we have access to a variety of existing methods for solving the model, which can be adapted for our application. We begin by discussing exact methods in Section 2.3.1, with a focus on the application of decomposition techniques. By contrast, we present specialised heuristic approaches for the MCLP in Section 2.3.2.

2.3.1 Exact Methods

As the MCLP is a mixed-integer linear program, the simplest solution method is to give the model to a generic MILP solver. However, while effective for small instances, it has repeatedly been shown that these solvers are unable to solve large instances (see, e.g. Church and ReVelle 1974, ReVelle et al. 2008, Cordeau et al. 2019). As such, recent exact approaches have been focused on decomposition approaches, with specialised column generation and Benders decomposition approaches.

The column generation procedure of Senne and Lorena (2002) and Pereira et al. (2007) is based on reformulating the MCLP to a p-median problem, and is particularly well suited when the set of possible configurations of facilities is extremely large. Expressed in maximum covering terms, this approach defines a *cluster* as an assignment of users i to a facility $j \in J$, with the resulting value as the sum of the covered demand within the cluster. The objective is then to select the p clusters which result in the largest possible coverage. As explicitly enumerating all possible clusters would be computationally infeasible, this method iteratively generates new ones by computing the currently unsatisfied demand. Clusters which result

in a strictly positive unsatisfied demand are added to the set of clusters, while the procedure ends when no such cluster can be found.

The Benders decomposition approach of Cordeau et al. (2019) is particularly well suited when the set of users J is much larger than the set of facilities I. Rather than explicitly stating the covering constraints (2.10c), these constraints are replaced by a cutting plane procedure. This procedure is described in detail in Section 4. In essence, for a given configuration of facilities $x_i, i \in I$, this approach generates a cut reflecting that the optimal objective value is bounded by the demand which is covered in the configuration x_i, plus the unsatisfied demand which can be covered by new facilities.

As alluded to previously, the column generation and Benders decomposition methods are best suited for different types of problems. The former is particularly effective when the set of users J is much larger than the set of facilities I, while the latter will perform better when the set of users and facilities are closer in size. This can be seen in the size of the instances solved, with the column generation method in Pereira et al. (2007) successfully solving instances with $|I| = |J| = 818$, while the Benders decomposition method in Cordeau et al. (2019) solved instances with $|I| = 100$, $|J| = 15,000,000$. By point of comparison, the generic MILP solver CPLEX was able to solve instances with $|I| = 100$ and $|J| = 100,000$ in Cordeau et al. (2019).

For problems beyond these sizes, or for which additional constraints are present, these methods may be insufficient to obtain a solution. For such cases, we can turn to the vast array of heuristic techniques, specialised for the MCLP.

2.3.2 Heuristic Methods

We describe the principle mechanisms behind commonly used heuristics below, which are all a general class of heuristic methods. We list adaptations of the methods for the MCLP though, for the sake of simplicity, some particularities may be omitted. For more specific details, we refer to the accompanying references.

Greedy: The greedy algorithm (Church and ReVelle 1974) is an iterative and deterministic method. It begins with a null solution (that is, $x_i = 0, i \in I$), then selects the facility i which covers the largest amount of the unsatisfied

demand. This procedure is then repeated, with the unsatisfied demand updated with each new facility, until the full set of facilities have been selected. A variation of this method is proposed in Church and ReVelle (1974) as well, called the greedy-substitution algorithm. After a facility is selected using the above procedure, the method iterates over each selected facility, and attempts to replace it with an unselected facility. If this substitution results in an increased coverage, the solution is replaced.

Lagrangian relaxation: Discussed in Downs and Camm (1996) and Galvão and ReVelle (1996), this approach applies Lagrangian relaxation on the covering constraints (2.10c). Dual multipliers are then found using subgradient optimisation, providing an upper bound for the Linear Programming (LP) value. Meanwhile, lower bounds are provided via the greedy algorithm, both of which are embedded within a branch-and-bound framework. Slow convergence requires the use of explicit stopping criteria, rendering this a heuristic method. However, when solved to optimality, this method is equivalent to the column generation procedure described above.

Simulated annealing: First applied to the MCLP in Murray and Church (1996), the simulated annealing heuristic emulates the cooling of metals. Starting from a randomly generated solution (that is, the p facilities such that $x_i = 1$ are determined randomly), the method arbitrarily selects one open facility and one closed facility. If exchanging these facilities results in an increase to the coverage, the solution is updated. Otherwise, there is a chance that this exchange is still accepted, with the likelihood depending on the current *temperature* parameter and how recently the solution was updated.

Tabu search: Similar to the simulated annealing method, the tabu search heuristic (Adenso-Díaz and Rodríguez 1997, Gendreau et al. 1997) begins with a starting solution (such as via the greedy algorithm). The method then iteratively exchanges one open facility and one closed facility, selecting the exchange with the best coverage (even if that coverage is less than the current solution). To avoid cycling back to previously visited solutions, a list of previous exchanges is maintained, and may not be reversed.

GRASP: As with the greedy algorithm, the Greedy Randomised Adaptive Search

Procedure (GRASP, Resende 1998) is an iterative method which adds facilities to the null solution, but the best facility is not always selected. Instead, in each iteration, the additional coverage from each facility is determined, and the selected facility is randomly determined among those with additional coverage within a given threshold of the best option. After this, a local search phase is conducted, which performs the substitution procedure, as with the greedy-substitution algorithm.

Genetic algorithm: Adapted for the MCLP in Arakaki and Lorena (2001) and Xia et al. (2009), the genetic algorithm mimics the processes of natural selection, with *generations* of solutions that provide beneficial solution characteristics to future generations. This begins with an initial pool of feasible solutions, which are then combined together in pairs of *parents* to form an *offspring* by selecting a subset of the open facilities in each of the parents. The offspring from a pair of parents which produces the best coverage then progresses to the next generation.

Heuristic concentration: The heuristic concentration method (ReVelle et al. 2008) uses a pool of high-quality solutions to fix facilities to be either open or closed, thus reducing the feasible space for a generic MILP solver. This begins with a pool of random solutions, which are improved by using the substitution procedure, as per the greedy-substitution algorithm. From there, facilities which are selected in all of the solutions in the pool are fixed to be open, while facilities whose selection rate in the pool falls below a given threshold are fixed to be closed. All remaining facilities are then determined by using a generic MILP solver.

2.4 Relation to Our Work

The background provided in this chapter allow us to next summarise and position the demand modeling and optimisation procedures developed in this thesis. In Chapter 3, we formulate a mathematical model for determining the optimal

location of public charging infrastructure in an intracity context, which can include both level 2 and level 3 charging outlets. This model follows a node-based approach, where the potential EV owners and the candidate charging station locations form nodes on the grid. Daily travel patterns are not available, and EV charging preferences (and thus the benefits of each candidate charging location) arise solely from the characteristics of the charging station and the user. The impact of these characteristics is codified via discrete choice models, including MNL and MXL specifications. Using the method of Pacheco Paneque et al. (2021), these discrete choice models can be embedded directly within the optimisation framework. The resulting formulation can be viewed as a bilevel model, for which we use a single-level reduction (via complementary slackness conditions) to enable it to be solved by a generic MILP solver. We then reformulate the model into a dynamic MCLP, enabling it to be solved significantly faster. However, even with this reformulation, the model is intractable for large-scale instances. We thus propose greedy and GRASP heuristic methods for obtaining high-quality solutions, with adaptations for the multi-period context. We then progress in Chapter 4 to design exact algorithms for our model, which modify and accelerate the Benders decomposition approach proposed in Cordeau et al. (2019). Finally, in Chapter 5, we delve more deeply into the discrete choice models, and use maximum likelihood to estimate appropriate parameter values. More specifically, we estimate multinomial logit and random parameters mixed logit models for predicting the selection of EV charging station by current EV users.

3 Optimising Electric Vehicle Charging Station Placement using Advanced Discrete Choice Models

Preface

In Chapter 3, we develop the mathematical program, which uses the framework of Pacheco Paneque et al. (2021) to model the interaction between the public charging network and the adoption of EVs. To this end, we specify a discrete choice model, representing the user's choice of the primary recharging method for an EV. These recharging choices include public charging infrastructure or a home charging alternative (if available to that user), which all correspond to the purchase of an EV. In addition, there is a single 'opt-out' alternative, for which the user does not purchase an EV.

The primary contribution of this work for the EV charging station location problem lies in the integration of discrete choice models via the framework of Pacheco Paneque et al. (2021). As we show experimentally, this creates more realistic demand dynamics compared with the existing literature, and affects the optimal decision of the problem. A more general contribution lies in the efficient reformulation of the model of Pacheco Paneque et al. (2021) to a maximum covering formulation. This reformulation is applicable not only in our context, but to any model using the embedded simulated utility framework of Pacheco Paneque et al. (2021), subject to some assumptions. A comparison of this reformulation against similar methods was examined in the work of Legault and Frejinger (2023), while an in-depth discussion about the limiting assumptions of this reformulation and possible extensions are discussed in Chapter 6. Additionally, we have adapted heuristics for the classic MCLP, such as the greedy and GRASP methods discussed in Chapter 2, to our application. As we demonstrate experimentally, these methods are effective tools for obtaining high-quality solutions, which can then be applied to similar multi-period MCLP applications.

This work contains a few important limitations, which we address in future chapters:

— We are not able to solve large-scale instances. Further, our experiments showed that not even the LP relaxation could be solved within a two-hour timespan. As such, in Chapter 4, we develop specialised Benders decomposition algorithms for obtaining better quality results.

— The utility functions for each charging station alternative require very specific coefficients, which are not trivial to obtain. These coefficients relate the impact of that public charging alternative to the EV adoption rate. In Chapter 5, we propose discrete choice models for predicting the choice of public charging stations by users. Under some assumptions, these could then be transformed into the required coefficients for the model in this chapter.

The contents of this chapter were published in *INFORMS Journal of Computing*. This publication can be cited as follows:

Lamontagne, S., Carvalho, M., Frejinger, E., Gendron, B., Anjos, M.F., Atallah, R., 2023. Optimising electric vehicle charging station placement using advanced discrete choice models. INFORMS Journal on Computing 35, 1195–1213.

Contributions of Steven Lamontagne and the coauthors

— The original topic of electric vehicle charging station placement was proposed by Bernard Gendron, while the research ideas were developed by the student, Bernard Gendron, Emma Frejinger, and Margarida Carvalho. In particular, the bilevel optimisation model, the subsequent maximum covering reformulation, and the adaptations to existing heuristic methods were conceptualised and created by the student.

— All code was written by the student, including the implementations of the branch-and-cut method and rolling horizon heuristic via CPLEX software, as well as the greedy and GRASP heuristics. In addition, the test instances were developed and produced by the student.

— The original draft (including all tables and images) were produced by the student, while it was revised by Margarida Carvalho, Emma Frejinger, Miguel Anjos, and Ribal Atallah.

Abstract

We present a new model for finding the optimal placement of electric vehicle charging stations across a multi-period time frame so as to maximise electric vehicle adoption. Via the use of stochastic discrete choice models and user classes, this work allows for a granular modelling of user attributes and their preferences in regard to charging station characteristics. We adopt a simulation approach and pre-compute error terms for each option available to users for a given number of scenarios. This results in a bilevel optimisation model that is, however, intractable for all but the simplest instances. Our major contribution is a reformulation into a maximum covering model, which uses the pre-computed error terms to calculate the users covered by each charging station. This allows solutions to be found more efficiently than for the bilevel formulation. The maximum covering formulation remains intractable in some instances, so we propose rolling horizon, greedy, and GRASP heuristics to obtain good quality solutions more efficiently. Extensive computational results are provided, which compare the maximum covering formulation with the current state-of-the-art, both for exact solutions and the heuristic methods.

Keywords: Electric vehicle charging stations, facility location, integer programming, discrete choice models, maximum covering

3.1 Introduction

In order to meet CO_2 emissions goals, major changes at the global level are necessary. This includes the transportation sector, which in 2019 was responsible for 27% of global CO_2 emissions (International Energy Agency 2021) and 30% of emissions in Canada (Environment and Climate Change Canada 2021). One initiative that has been proposed to reduce these emissions is the adoption of electric vehicles (EVs), rather than internal combustion engine vehicles (ICEVs). Depending on the electricity generation mix, this may be effective in reducing emissions (Axsen et al. 2015c, Woo et al. 2017).

Due to the limits of the internal battery, EVs require more frequent refuelling than CVs. While early adopters of EVs may have access to home charging (Bailey et al. 2015), this can be supplemented with public charging infrastructure to increase accessibility. The availability of the latter has been found to increase EV adoption (e.g. Coffman et al. 2017). However, this scenario has been noted to suffer from a "chicken-and-egg" dilemma (Anjos et al. 2020), where users require charging infrastructure in order to purchase an EV, while businesses and infrastructure operators have little incentive to install charging stations when there are few users. To this end, governmental organisations can alleviate this problem by investing in public charging infrastructure, thus allowing users to recharge EVs and encourage EV adoption.

The problem we examine is that of the decision makers responsible for public charging infrastructure, and the optimal placement of that infrastructure within a city. They have a set of candidate locations for charging stations, and must decide which charging stations to open as well as how many charging outlets to place at each open station. These decisions take place over a long-term planning horizon, and investment in each period is limited by a budget. The decision makers take into account the users who are purchasing a vehicle in each period. Depending on the placement of charging infrastructure, these users may purchase an EV. We assume that the users anticipate the need to recharge an EV, and will only purchase one if they have access to charging infrastructure (either public or at home). Additionally, we assume that more convenient charging (e.g. by a charging station being closer to home, or having more charging outlets) increases the probability that a user will purchase an EV. The goal of the decision makers is to plan the placement of charging infrastructure so that it maximises EV adoption.

The existing literature for this problem is quite narrow, and has limitations that we address in this work. In the intercity context, the optimisation model of Zhang et al. (2017a) accounts for EV adoption growth depending on the coverage of paths, but their method is not applicable to the intracity case. To the best of our knowledge, in the intracity context, only Anjos et al. (2020) formulate an optimisation model for locating charging stations accounting for EV adoption growth based on the location of charging stations. There, the total number of EVs increases according to a piecewise-linear growth function, which accounts for

natural growth. This growth function is applied indiscriminately to all locations. Additionally, the fraction of users who have access to home charging is assumed to be constant across locations in the network. In reality, the EV growth rate varies by location (Association des Véhicules Électrique du Québec 2021), and access to home charging depends on the type of residences (Nicholas et al. 2019).

This work presents modelling, algorithmic, and computational contributions. For the modelling side, we consider user classes, allowing for parameter values to be considered more specifically for groups of users rather than the entire population. Additionally, within each user class, the optimisation model supports the use of advanced discrete choice models. Acknowledging the uncertainty associated with demand distribution, these models assign a probability distribution over available alternatives. This allows to model heterogeneous user preferences and complex substitution patterns. The combination of the user classes and the ability to use advanced discrete choice models results in a highly flexible model, which the decision makers can design to suit their specific problem and available data sources. The user behaviour is incorporated in the decision-maker's problem as in Pacheco Paneque et al. (2021), leading to a bilevel program. While the bilevel optimisation model presented here can only solve small instances, the maximum covering reformulation allows for instances to be solved significantly faster. To the best of our knowledge, such a reformulation has not been presented in the context of the simulation-based approach of Pacheco Paneque et al. (2021). We note that this reformulation is effective for our optimisation model, but is also applicable to more general, uncapacitated bilevel models using the same framework. On the algorithmic side, we propose three heuristics to solve the optimisation models. First, a rolling horizon method, which was also used in Anjos et al. (2020). Second, a greedy method (Church and ReVelle 1974), and third, a GRASP method (Resende 1998). We extend the latter two to a multi-period setting with sizing decisions. On the computational side, we present extensive experimental comparisons examining: the capabilities of our optimisation model versus the model presented in Anjos et al. (2020), the bilevel formulation versus maximum covering formulation, and the heuristic methods. Where possible, parameter values and user class characteristics are based on real data.

We structure the remainder of the paper as follows: Section 3.2 reviews the

relevant literature for the problem. Section 3.3 describes the framework of the problem, as well as briefly presenting the bilevel model and its single-level reformulation. Section 3.4 gives the maximum covering reformulation for the bilevel model. Section 3.5 discusses various heuristic methods for solving large instance sizes of practical interest. Section 3.6 provides computational results.

3.2 Literature Review

We review three topics of research that relate closely to our work. First, EV charging station location models, which determines the optimal location for charging stations. Second, vehicle acquisition, more specifically relating to EVs, which discusses factors that affect whether users purchase EVs. Third, Maximum Capture Problem with Random Utilities (MCPRU), which examines the optimal placement of facilities in a competitive environment.

On the topic of EV charging station location models, the model proposed by Anjos et al. (2020), which we refer to as the *Growth Function* (GF) model, is the closest to our work. Whereas most charging station location models are examined with the objective to maximise profits or minimise costs, the GF model is designed solely to encourage electric vehicle adoption. Its use of a combination of node-based and path-based approaches allows for the inclusion of a general highway charging station network while allowing for increased precision within the city. EV adoption and charging stations are linked via capacity constraints, with users willing to recharge at any charging station within a fixed distance of their home.

There is an existing literature for EV charging station placement (an excellent review is presented in Kadri et al. 2020), however two notable differences separate it from our work. First, in all cases, the users under consideration are those who already own EVs, and are deciding on a charging station to recharge. Second, the objective of the decision maker are different, such as profit maximisation (Luo et al. 2015), maximising the EV flow that can travel each path given a limited EV range (Lim and Kuby 2010), minimising the users' costs for recharging the EV and travel time (González et al. 2022), or maximising the EV charging demand that can

be covered (Frade et al. 2011). We provide a summary of the key characteristics of related works in Table 3.1.

Unlike our work, EV recharging demand at each station or along each path is generally taken to be deterministic. However, in Luo et al. (2015) and Cui et al. (2019) the demand for each station is estimated using the analytic choice probabilities from a nested logit model. The demand model they use considers station characteristics such as the distance to the EV owner and the proximity of the charging station to amenities (such as restaurants and shopping centres). In Kadri et al. (2020), the evolution each year of the demand for each path is modelled with a discrete scenario tree. In the tree, the demand for the current year is assumed to be known, as are the transition probabilities for each of the possible states in each subsequent year. This allows for the estimation of the expected demand of each path considering all subsequent years.

The inclusion of capacity constraints in EV charging station location models is not consistent. Several models (including our work, as well as others in Table 3.1) do not consider capacity. For those that do include capacity constraints, the modelling assumptions differ. In Frade et al. (2011) and Zhang et al. (2017a), the demand that may be satisfied by each charging station is limited by the number of outlets installed at that location. In Luo et al. (2015), the decision maker must ensure that charging stations meet minimum quality of service requirements, including waiting time and service coverage. In Cui et al. (2019), the decision maker must ensure that the amount of electricity supplied at each charging station is sufficient for the expected amount of demand. In González et al. (2022), the number of recharging sessions that will be required at each station is estimated, and used as a bound for the capacity of the station.

The vehicle acquisition problem examines the attributes that increase the likelihood of purchasing EVs, and are useful for determining exogenous attributes for the demand model and defining user classes. Importantly, the availability of electric vehicle charging stations increases the likelihood of users purchasing an EV; This availability (also referred to as 'fuel availability'), was a significant factor in the decision to purchase an EV in most articles examining the subject (Achtnicht et al. 2012, Javid and Nejat 2017, Hackbarth and Madlener 2013, Ziegler 2012, Rezvani et al. 2015, Coffman et al. 2017). This finding is not unanimous, however,

	Objective	Model Type	Demand	Time Periods	Capacity	Intracity or Intercity
Lim and Kuby (2010)	Maximise flow refueled	FRLM	D	Single	No	Inter
Frade et al. (2011)	Maximise coverage of EV charging demand	Maximum Covering	D	Single	Yes	Intra
Shukla et al. (2011)	Maximise flow intercepted	FILM	D	Single	No	Intra
Capar et al. (2013)	Maximise flow refueled	FRLM	D	Single	No	Inter
Luo et al. (2015)	Maximise profit of decision maker	MINLP	S	Multi	Yes	Intra
Zhang et al. (2017a)	Maximise flow refueled	FRLM	D	Multi	Yes	Inter
Cui et al. (2019)	Minimise cost of decision maker	MINLP	S	Multi	Yes	Intra
Badri-Koohi et al. (2019)	Minimise costs, p-median, flow interception (weighted sum)	MILP	D	Single	No	Intra
Kadri et al. (2020)	Maximise flow refueled	FRLM	S	Multi	No	Inter
González et al. (2022)	Minimise users' travel cost	Bilevel	D	Single	Yes	Intra

Legend: FRLM = Flow Refueling Location Model, FILM = Flow Interception Location Model, MINLP = Mixed Integer Non-Linear Problem, MILP = Mixed Integer Linear Problem, D = Deterministic, S = Stochastic.

Table 3.1 – Summary of key characteristics of EV charging station location models.

as Bailey et al. (2015) propose that a predisposition to EVs makes the users more likely to notice existing charging infrastructure, not the converse. The conclusions of Bailey et al. (2015) are also present in Axsen et al. (2015a), an article based on the same dataset and project. Several studies focus on assessing preferences in regard to various types of attributes (Hidrue et al. 2011, Achtnicht et al. 2012, Ziegler 2012, Hackbarth and Madlener 2013, Axsen et al. 2015a, Bailey et al. 2015, Javid and Nejat 2017). For reviews of EV acquisition models, we refer to Rezvani et al. (2015), Javid and Nejat (2017), and Coffman et al. (2017).

In this work, we formulate the problem as a MCPRU, generally attributed to Benati (1999) and Benati and Hansen (2002). In the MCPRU, a company is looking to place facilities in an environment where competitors have existing facilities. A *Random Utility Maximisation* (RUM) discrete choice model is used to assign choice probabilities of users, based on the set of facilities available to them. The company aims to place the new facilities to maximise the market share that the new facilities capture. In general, the MCPRU focuses on two key attributes of facilities in order to determine which one users choose to patronise: distance to the users, and *facility attractiveness* (Berman et al. 2014). It is possible to consider market expansion in the MCPRU, where the placement of facilities attracts customers that were not originally in the market (see, e.g., Aboolian et al. 2007). Since a vehicle (EV or otherwise) is an expensive purchase, it is assumed that the additions to the charging infrastructure are not sufficient to attract users who were not planning on purchasing a vehicle at all in the given period. We thus do not include market expansion in our optimisation model.

Almost all work on the MCPRU has been done in the context of using the multinomial logit (MNL) model for characterising user behaviours, due to the existence of an analytic formula for calculating choice probabilities. For recent examples, the linear formulation in Freire et al. (2016) (which improves on the linear formulation in Haase 2009) and the outer approximation and submodular cut methods in Ljubić and Moreno (2018) both rely on the logit choice probabilities. Exceptions to the use of MNL model include the work of Mai and Lodi (2020), who express a mixed logit choice probability as a sum of probabilities of MNL models (though they do not conduct any computational experiments using this method), and the work of Dam et al. (2021), who use a method that makes use of the submodularity

of the objective function for all discrete choice models in the Generalised Extreme Value (GEV) family (of which MNL and mixed logit are included). Since we do not assume the use of MNL or the GEV family (in addition to the added complexity of multi-period and sizing considerations), the methods proposed in these works cannot be applied directly to our model.

While it can be used more generally, the simulation-based approach in Pacheco Paneque et al. (2021) can be applied to the MCPRU. Rather than embedding an analytic probability that users will select an alternative into the objective function, this approach instead generates error terms for each alternative for a given number of *scenarios*. These error terms, pre-computed and given to the optimisation model as an input, allow for the utility to be calculated for each alternative and each scenario. Using the RUM principle, users then select, in each scenario, the alternative which has the highest utility. Alternatives which are not available to users (such as, in the case of the MCPRU, facilities which are closed) are set to a lower bound, ensuring they are not selected. This approach supports the use of any discrete choice model rather than being limited to the MNL model (or even the GEV family). However, it is computationally difficult to solve in larger instances.

We emphasise that the simulation-based approach of Pacheco Paneque et al. (2021) differs from the linearisation typically presented for the MCPRU (e.g. Benati and Hansen 2002, Haase 2009, Haase and Müller 2014, Freire et al. 2016). In the latter case, the analytic choice probabilities for each alternative are linearised by setting the variable coefficients appropriately. However, this linearisation can only be done when analytic choice probabilities are known for the discrete choice model (e.g. MNL). On the contrary, the simulation-based approach assumes that the utility functions are linear in the decision variables and works directly in the space of utilities. Under the RUM principle, this allows for linearisation of the sample average approximation of the choice probabilities (which can be derived for any discrete choice model for which error terms can be drawn). As a consequence, the choice probabilities are approximations of their exact form, but also renders the approach suitable for any discrete choice model. This includes, notably, discrete choice models for which the choice probabilities are typically estimated via sample average approximation (e.g. mixed logit Train 2002).

Our work aims to bridge the gap between the EV charging station placement

models, EV acquisition models, and the MCPRU. Most EV charging station placement models are designed to benefit existing EV owners, instead of maximising EV adoption. The existing works which include EV growth based on the placement of EV charging stations, namely the models of Zhang et al. (2017a) and Anjos et al. (2020), use an aggregate approach for EV growth. However, the literature on EV acquisition shows that significant factors for determining EV acquisition are individual characteristics of the users (e.g. income, education level, access to home charging). This highlights the benefit of user classes in our optimisation model, as they allow for these individual characteristics to be considered. Moreover, we note the heterogeneity within each preference class (which function equivalently as a user class in our work) in the latent class models of Hidrue et al. (2011) and Axsen et al. (2015a). This suggests the use of a discrete choice model for demand modelling, and naturally leads to a MCPRU formulation for the optimisation model. As is the case for the MCPRU, in addition to user characteristics, characteristics from the charging station also impact the choice of users. While the specification of the discrete choice model for the users is outside the scope of this work, we note in Appendix A.1.1 characteristics of the demand modelling which makes the MNL model less suitable. Because of this, we use the simulation-based approach of Pacheco Paneque et al. (2021).

3.3 Problem Formulation and Modelling

In our problem, we consider the placement of charging infrastructure in a city, wherein there are two parties with different motives: a decision maker placing the infrastructure, and the users choosing whether to purchase an EV (depending on the charging infrastructure). An illustration of this process is given in Figure 3.1.

3.3.1 Decision Maker

The decision maker is planning charging infrastructure over a planning horizon with T periods (e.g., seasons or years) indexed by $1 \leq t \leq T$.

The decision maker has a candidate set of locations M where charging stations $j \in M$ may be installed or expanded with additional outlets to a maximum number m_j. In each period t, there is a budget B^t, which limits the total investment (both opening stations and installing outlets). Let c^t_{jk} denote the cost to go from $k-1$ to k outlets at charging station $j \in M$ in period t. Note that this cost concept is flexible, and accounts for additional costs to be incorporated at certain thresholds if significant infrastructure upgrades are required. Notably, this includes initial infrastructure installation for $k = 1$ but can also include, e.g., increasing electric power capacity at the station.

Let x^t_{jk} be a binary variable indicating if station $j \in M$ has *at least* k outlets in period t (with $1 \leq k \leq m_j$). We denote $\mathbf{x} = \left\{x^t_{jk}\right\}, j \in M, 1 \leq k \leq m_j, 1 \leq t \leq T$. Let x^0_{jk} denote the initial state of each charging station j.

3.3.2 Users

We consider users who are are planning on purchasing a vehicle and, depending on public charging infrastructure, may choose to purchase an EV. These users are composed of a set of user classes N. The population size for each user class is given by $N^t_i, i \in N, 1 \leq t \leq T$. These parameters provide a flexible modelling. For instance, they can correspond to the number of potential new EVs in a class or be configured to prioritise early adopters by decreasing the population size in later time periods. This would have an effect similar to the classical approach of discounting future time periods.

Each user considers whether they have a primary option for recharging an EV. If such an option is available and sufficient for their needs, they decide to purchase an EV. This decision is modelled via a discrete choice model, with users in user class $i \in N$ selecting an alternative j in choice set $\mathcal{C}^t_i(\mathbf{x})$. The inclusion of $\mathbf{x}$ in the notation for the choice set emphasises the dependence on the set of open stations, since stations without at least one outlet cannot be used to recharge an EV. The choice set $\mathcal{C}^t_i(\mathbf{x})$ contains a subset of the public charging infrastructure, home charging (if available to user class i), and an opt-out. The latter corresponds to the alternative to not purchase an EV, while all other alternatives indicate the user purchases one. In what follows, we denote the opt-out alternative as $j = 0$.

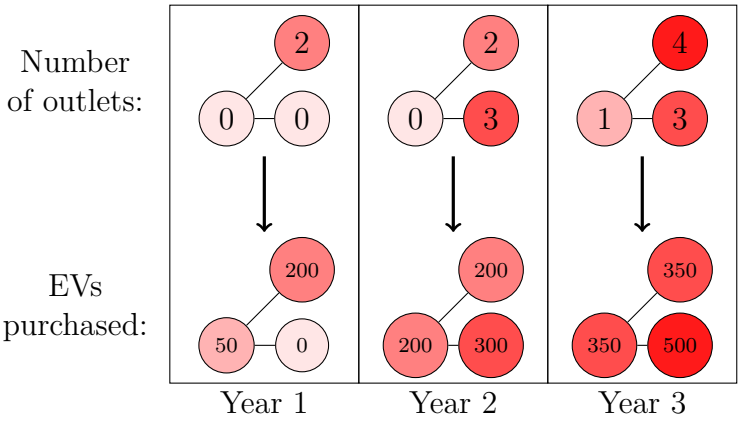

Figure 3.1 – The decision maker decides where to place charging infrastructure (stations and number of outlets) on the simple example network. In response, a subset of users decide to purchase EVs.

We note that the use of the index j for both alternatives and stations is deliberate because, as we discuss in Section 3.3.3, the charging stations are the alternatives for the most part.

At the strategic-level planning, we assume that each charging station $j \in M$ that is opened is *uncapacitated*, in the sense that there is no limit to the number of users that may select it. However, we assume that the likelihood of users selecting a given station increases with the number of outlets. The rationale being that the higher the number of outlets, the more likely one may be available when required. This allows us to implicitly take into account that users perceive the capacity as finite.

3.3.3 Simulation-based Model

We adopt the simulation-based method of Pacheco Paneque et al. (2021) to the users' decision to purchase an EV. More specifically, for each user class $i \in N$, let R_i be the number of scenarios used to approximate the choice probabilities. We assume that the decision to purchase an EV is separable for each user class, each period, and each scenario, meaning that there is no interaction among them. Therefore, in what follows, we concentrate on detailing a given triplet $(t, i, r) \in P = \{(t', i', r') : 1 \leq t' \leq T, i' \in N, 1 \leq r' \leq R_{i'}\}$. For each alternative $j \in \mathcal{C}_i^t(x)$, let u_{ji}^{rt} be the *simulated utility*.

We previously remarked that the choice set $\mathcal{C}_i^t(\mathbf{x})$ depends on which stations are open. For notational simplicity, we define the two choice sets: C_i^{0t} and C_i^{1t}. The set C_i^{0t} includes all alternatives exogenous to the optimisation model (i.e. unaffected by decision variables), for which the availability is not under the control of the decision maker. This always includes the opt-out alternative, but may also, for example, include the alternative for home charging. The simulated utility u_{ji}^{rt}, for $j \in C_i^{0t}$, is thus given by

$$u_{ji}^{rt} = \kappa_{ji}^t + \varepsilon_{ji}^{rt}, \tag{3.1}$$

where the parameter κ_{ji}^t is the alternative-specific constant. In general, the alternative-specific constants can be any function which does not depend on the decision variables. Note that we assume only one opt-out alternative as multiple options can be replaced by a single alternative given by the maximum utility across all opt-out alternatives.

The set C_i^{1t} includes the alternatives for charging stations which have a non-zero probability of being chosen (e.g. sufficiently close to be considered). If station $j \in C_i^{1t}$ is open, we consider the utility u_{ji}^{rt} to be a function of the number of charging outlets available at that station as well as the alternative-specific constant. This leads to the formulation: $u_{ji}^{rt} = \sum_{k=1}^{m_j} \beta_{jik}^t x_{jk}^t + \kappa_{ji}^t + \varepsilon_{ji}^{rt}$. We recall that m_j is the maximum number of outlets at station j. The parameter β_{jik}^t is the incremental benefit of going from $k-1$ to k outlets. The model does not impose any restrictions on the form of the utility coefficients, however, we assume that the coefficients are non-negative. As before, the alternative-specific constant can be any function which does not depend on the decision variables. If the station is closed, the utility is set to a lower bound $\underline{a}_i^t$ to ensure that it will not be selected.

3.3.4 Single-Level Model

Given $\mathbf{x}$ and a triplet (t, i, r), a user selects the alternative maximising the simulated utility, i.e., $k \in \arg\max_{j \in \mathcal{C}_i^t(\mathbf{x})} u_{ji}^{rt}$. If we now integrate the goal of the decision maker, which is to maximise the purchase of EVs, we naturally obtain a bilevel formulation. Following the simulation-based method of Pacheco Paneque et al. (2021), we can reduce the bilevel formulation to a single-level form. Indeed,

the Single-Level (SL) model of the problem is given by

$$\text{Minimise} \sum_{(t,i,r)\in P} \frac{N_i^t}{R_i} w_{0i}^{rt}, \tag{3.2a}$$

$$\text{subject to} \sum_{j\in M}\sum_{k=1}^{m_j} c_{jk}^t \left(x_{jk}^t - x_{jk}^{t-1}\right) \le B^t, \qquad 1 \le t \le T. \tag{3.2b}$$

$$x_{jk}^t \le x_{jk-1}^t, \qquad 1 \le t \le T, j \in M, 1 \le k \le m_j, \tag{3.2c}$$

$$x_{jk}^t \ge x_{jk}^{t-1}, \qquad 1 \le t \le T, j \in M, 1 \le k \le m_j, \tag{3.2d}$$

$$u_{ji}^{rt} = \kappa_{ji}^t + \varepsilon_{ji}^{rt}, \qquad (t,i,r) \in P, j \in C_i^{0t}, \tag{3.2e}$$

$$u_{ji}^{rt} \ge \underline{a}_i^t, \qquad (t,i,r) \in P, j \in C_i^{1t}, \tag{3.2f}$$

$$u_{ji}^{rt} \le \underline{a}_i^t + \nu_{ji}^{rt} x_{j1}^t, \qquad (t,i,r) \in P, j \in C_i^{1t}, \tag{3.2g}$$

$$u_{ji}^{rt} \ge \sum_{k=1}^{m_j} \beta_{jik}^t x_{jk}^t + \kappa_{ji}^t + \varepsilon_{ji}^{rt} - \nu_{ji}^{rt}\left(1 - x_{j1}^t\right), (t,i,r) \in P, j \in C_i^{1t}, \tag{3.2h}$$

$$u_{ji}^{rt} \le \sum_{k=1}^{m_j} \beta_{jik}^t x_{jk}^t + \kappa_{ji}^t + \varepsilon_{ji}^{rt}, \qquad (t,i,r) \in P, j \in C_i^{1t}, \tag{3.2i}$$

$$u_{ji}^{rt} - \alpha_i^{rt} + \left(1 - w_{ji}^{rt}\right)\mu_{ji}^{rt} \ge 0, \qquad (t,i,r) \in P, j \in C_i^{0t} \cup C_i^{1t}, \tag{3.2j}$$

$$\sum_{j\in C_i^{0t}} w_{ji}^{rt} + \sum_{j\in C_i^{1t}} w_{ji}^{rt} = 1, \qquad (t,i,r) \in P, \tag{3.2k}$$

$$\alpha_i^{rt} \ge u_{ji}^{rt}, \qquad (t,i,r) \in P, j \in C_i^{0t} \cup C_i^{1t}, \tag{3.2l}$$

$$w_{ji}^{rt} \in \{0,1\}, \qquad (t,i,r) \in P, j \in C_i^{0t} \cup C_i^{1t},$$

$$\alpha_i^{rt} \in \mathbb{R}, \qquad (t,i,r) \in P,$$

$$u_{ji}^{rt} \in \mathbb{R}, \qquad (t,i,r) \in P, j \in C_i^{0t} \cup C_i^{1t},$$

$$x_{jk}^t \in \{0,1\}, \qquad 1 \le t \le T, j \in M, 1 \le k \le m_j.$$

The objective function (3.2a) minimises the number of users who do not purchase an EV (or, equivalently, maximises those who do) with the auxiliary variables w_{ji}^{rt} representing the selection of alternative j by the triplet (t, i, r). Recall that w_{0i}^{rt} corresponds to the opt-out alternative, and indicates that the triplet (t, i, r) does not purchase an EV. Budget constraints (3.2b) are given for each time period t. It would be possible to supplement the per-period budget with an overall budget, as was done in Anjos et al. (2020). Constraints (3.2c) impose that to have at least k outlets, we must have at least $k-1$ outlets. Constraints (3.2d) forbid us from removing outlets once installed. Constraints (3.2e) set the utility for exogenous alternatives (opt-out, home charging, etc.). Constraints (3.2f)-(3.2i) set the utility for endogenous alternatives (charging stations). Constraints (3.2j)-(3.2l) ensure that the alternative with the highest utility is selected for each triplet (t, i, r). We present the details around the model in Appendix A.1.1.

We note that Constraints (3.2e) set the utility for all exogenous alternatives in C_i^{0t}, which includes opt-out and may include home charging. However, in practice, it is better to preprocess any triplets which have access to home charging: if the utility associated with home charging is lower than that of the opt-out, then home charging can be ignored (as it will never be selected). If it is higher than for the opt-out, then the associated opt-out choice variable w_{0i}^{rt} can be fixed to 0, as we can guarantee that it will not be selected. As such, the set C_i^{0t} can be reduced to only contain the opt-out alternative.

3.4 Maximum Covering Model

While the SL model (3.2) is a Mixed-Integer Linear Programming (MILP) optimisation problem that can be given directly to a general purpose solver, large-scale instances can be hard to solve. This is due to the Big-M constraints for the utility (3.2f)-(3.2i) and the linearised lower-level problem (3.2j)-(3.2l), as well as both sets of binary variables $\mathbf{x}$ and $\mathbf{w}$. While the Big-M values are tight given the bounds, as we will see in Section 3.6, the model is intractable for all but the simplest of instances. For this reason, we propose to reformulate the problem into a maximum covering problem using the pre-computed error terms ε_{ji}^{rt}.

For $j \in C_i^{1t}$, define $u_{jik}^{rt} = \sum_{k'=1}^{k} \beta_{jik'}^t + \kappa_{ji}^t + \varepsilon_{ji}^t$. In other words, u_{jik}^{rt} is the utility for the triplet (t, i, r) for charging station j having k outlets in period t. This is equivalent to the utility u_{ji}^{rt} with $x_{jk'}^t = 1$ if $k' \leq k$ and $x_{jk'}^t = 0$ if $k' > k$.

Definition 1. *A charging station j with k charging outlets* covers *the triplet (t, i, r) if the following conditions hold:* (i) $k \geq 1$, (ii) $j \in C_i^{1t}$, *and* (iii) $u_{jik}^{rt} \geq u_{0i}^{rt}$, *where u_{0i}^{rt} represents the opt-out utility for triplet (t, i, r). We say that (t, i, r) is covered by $\mathbf{x}$ if $\exists j \in M, \exists k \in \{1, \ldots, m_j\}$ such that $x_{jk}^t = 1$ and charging station j with k charging outlets covers (t, i, r).*

Intuitively, a charging station covers a triplet if the station has at least one outlet (and is thus open), it is available to and considered by the user class in question, and the charging station is a better option than the opt-out for that triplet.

Example 2. *We consider a given scenario r, user class i, and period t. In Figure 3.2, we see the utilities u_{ji}^{rt} for each option $j \in C_i^{0t} \cup C_i^{1t}$. For each option, the error terms and alternative-specific constants are all pre-computed, which defines the values for utility with no charging outlets. The opt-out utility does not depend on the number of outlets, and so it is constant. Stations 1 and 3 only cover the triplet (t, i, r) if they have at least one and four outlets, respectively. Station 2 is not able to cover (t, i, r) even with six outlets.*

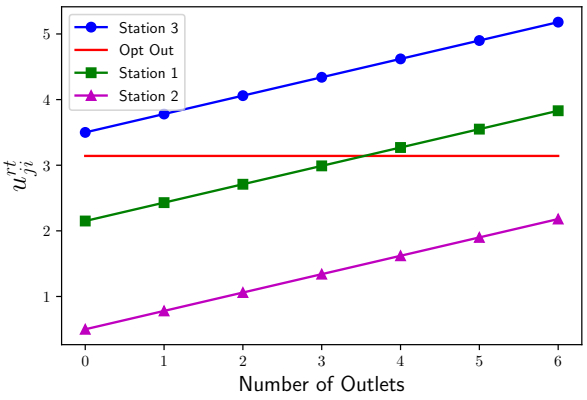

Figure 3.2 – Utilities for user class i, under scenario r, at period t.

Next, we define $a^{rt}_{jik} = 1$ if station j with k outlets covers (t, i, r), and 0 otherwise. This vector a of parameters can be pre-computed after the error terms have been calculated. In the maximum covering formulation, we keep the variables $\mathbf{x}$. We then define the covering decision variables $w^{rt}_i = 1$ if (t, i, r) is covered by $\mathbf{x}$, and 0 otherwise.

The Maximum Covering (MC) model is then

$$\text{Maximise} \sum_{(t,i,r)\in P} \frac{N^t_i}{R_i} w^{rt}_i, \tag{3.3a}$$

$$\text{subject to (3.2b)} - \text{(3.2d)}$$

$$\sum_{j\in M} \sum_{k=1}^{m_j} a^{rt}_{jik} x^t_{jk} \geq w^{rt}_i, (t, i, r) \in P, \tag{3.3b}$$

$$x^t_{jk} \in \{0, 1\}, \qquad 1 \leq t \leq T, j \in M, 1 \leq k \leq m_j,$$

$$w^{rt}_i \in [0, 1], \qquad (t, i, r) \in P.$$

The objective function (3.3a) is the maximisation equivalent to the objective in the SL model (3.2a). Constraints (3.3b) model whether the triplet (t, i, r) is covered by a given $\mathbf{x}$. We note that due to the direction of the optimisation, these inequalities are satisfied with equality at an optimum. Since these constraints are the only ones on the variables w^{rt}_i, it is well-known that their integrality can be relaxed (Murray 2016). These constraints replace the utility constraints for choice set C^{0t}_i (3.2e), the utility constraints for choice set C^{1t}_i (3.2f)-(3.2i) and the maximisation of the users' utilities given by (lower-level problem) constraints (3.2j)-(3.2l). They thus eliminate all Big-M constraints from the model. It is important to note that the maximum covering reformulation is possible because we consider the case where stations are uncapacitated. However, if we wished to include capacity constraints, this would be straightforward for the SL model (3.2) (as was done in Pacheco Paneque et al. 2021).

3.5 Heuristic Methods

While the reformulation from the SL model (3.2) to the MC model (3.3) significantly improves tractability, the latter is still unable to solve larger instances, as shown in Section 3.6. We propose three heuristic methods for solving the MC model (3.3), including rolling horizon, greedy, and Greedy Randomised Adaptive Search Procedure (GRASP).

We note that, for the greedy and GRASP methods, it is required to calculate the quality of a candidate solution $\mathbf{x}$. We denote it by

$$f(\mathbf{x}) = \sum_{(t,i,r)\in P} \frac{N_i^t}{R_i} \min\left(1, \sum_{j\in M} \sum_{k=1}^{m_j} a_{jik}^{rt} x_{jk}^t\right). \tag{3.4}$$

3.5.1 Rolling Horizon Heuristic

Several variants of the rolling horizon heuristic exist, which form a standard approach in a multi-period setting. The basic version treats each period independently. We use this approach as a baseline. More precisely, we solve the MC model (3.3) for one period at a time, $1 \leq t \leq T$. Given the potential difficulty of solving the MC model (3.3) even when restricted to one period, a time limit is added. The best incumbent solution found within this time limit is returned by the heuristic.

An alternate version of the rolling horizon heuristic was tested, where for each time period $1 \leq t \leq T$ the variables x_{jk}^t are discrete, but taken as continuous for $x_{jk}^{t'}, t' > t$. The variables x_{jk}^t are then fixed, and we repeat the procedure for $t = t + 1$. However, this method did not perform well in our application, due to the increased time required to solve each time period. Thus, we do not discuss this heuristic further in the rest of the paper.

3.5.2 Greedy Heuristics

The maximum covering problem is generally attributed to Church and ReVelle (1974), where they also present a simple greedy heuristic. The algorithm presented here is a natural extension, where we iteratively place outlets one at a time, selecting the one which increases the number of new EVs the most.

More specifically, when considering the number of new EVs covered by a new outlet, there are two possible search modes. In the *myopic* search mode, only new EVs from the current period are counted. In the *hyperoptic* search mode, since any outlets placed in the current time period cannot be removed, the EVs in future time periods that result from these outlets are also counted. Namely, we consider the following *score* functions when examining a candidate solution $\tilde{x}$ in time period t':

$$f_m\left(\tilde{\mathbf{x}}, t'\right) = \sum_{i \in N} \sum_{r=1}^{R_i} \frac{N_i^{t'}}{R_i} \min\left(1, \sum_{j \in M} \sum_{k=1}^{m_j} a_{jik}^{rt'} \tilde{x}_{jk}^{t'}\right),$$
$$f_h\left(\tilde{\mathbf{x}}, t'\right) = \sum_{t=t'}^{T} \sum_{i \in N} \sum_{r=1}^{R_i} \frac{N_i^{t}}{R_i} \min\left(1, \sum_{j \in M} \sum_{k=1}^{m_j} a_{jik}^{rt} \tilde{x}_{jk}^{t}\right),$$

with f_m and f_h being (respectively) for the myopic and hyperoptic search modes.

Independently of the search mode, each greedy heuristic starts with the trivial, zero solution (which is always feasible). It then iterates over each time period. Given a time period, for each station, the heuristic determines whether adding an outlet is feasible. If so, it computes the number of new EVs covered accordingly with the score function for the search mode (f_m or f_h). The outlet which maximises the value of the score function is then selected, and the candidate solution updated. The iteration over stations for the given period continues until no outlets can feasibly be added (either due to the budget or the maximum number of outlets at each station), or the total number of EVs does not increase after adding a station. The latter is possible if all triplets covered by a possible outlet are already covered in the incumbent solution. The heuristic then proceeds to the next time period and repeats the process.

3.5.3 GRASP

GRASP is characterised by two phases. The first utilises a greedy approach to generate solutions, where each greedy move is randomly selected from all possible moves that result in a solution with an objective value that is within a factor α of the optimal greedy move. The second phase performs a local search procedure on each solution from the first phase. This method was first applied to the maximum

covering problem by Resende (1998). However, the algorithm described in this work makes several adaptations in order to support the multi-period and sizing considerations.

First phase The solution construction phase is similar to the Greedy algorithm, with the addition of the parameter $\alpha \in [0, 1]$. We randomly select one outlet to place from amongst the set of outlets that result in an increase within $100 \times \alpha$ % of the best possible outlet. The myopic and hyperoptic search modes also apply in the GRASP method.

Solution Filtering In our method, the second phase of GRASP takes considerably longer than the first phase. As such, it is beneficial to filter out unpromising solutions early on. In a method proposed in Resende and Ribeiro (2018), we examine whether the local search method, when applied to a candidate solution, is likely to result in a better objective value than our incumbent solution. For a given number of candidate solutions, we examine the relative increase to the objective function before and after applying the local search. For all subsequent candidate solutions, we then estimate the maximum objective value from the second phase by multiplying the objective value of the candidate solution by the maximum relative increase that was observed. If this results in an objective value that is less than our current best, we filter the candidate solution and do not start the second phase.

Second Phase When examining a candidate solution $\hat{\mathbf{x}}$, we consider the three following moves:

Add: If the budget permits, we add an outlet to the given station j in period t. To ensure feasibility of the solution, we also increase the number of outlets for all subsequent periods $t + 1, \ldots, T$ for station j.

Transfer: If the station j has at least one outlet, we consider each station $j', j' \neq j$, and transfer all resources spent on station j in each period $t, t + 1, \ldots, T$ to be spent on station j' instead. To ensure feasibility of the solution, we set the number of outlets at station j for periods $t' \geq t$ to the value in period $t - 1$ (or x^0_{jk} if $t = 1$). If station j' reaches the maximum number of outlets and there are resources remaining, they are spent on station j.

Split: If the station j has at least one outlet, we consider each station $j', j' > j$, and we evenly split the resources spent on stations j and j' in each period $t, t+1, \ldots, T$. We note that this move is symmetric, and so it is only necessary to attempt this move if $j' > j$. In order to ensure feasibility of the solution, we can only use this move if the resources spent on these stations and the prior values of the solution for these stations in period $t-1$ allow us to open both stations and place at least one outlet in each.

The moves can be applied to the candidate solution using either the "first improvement" or "best improvement" methods as described in Resende and Ribeiro (2018). In the first improvement method, the candidate solution $\hat{\mathbf{x}}$ is updated whenever a move is found which improves the objective function $f(\hat{\mathbf{x}})$. In the best improvement method, the candidate solution $\hat{\mathbf{x}}$ is updated with the move from amongst all stations j which resulted in the highest objective function $f(\hat{\mathbf{x}})$.

Stopping Criteria We wish to prevent the local search from spending considerable time making very minor improvements to the candidate solution. At the end of each loop through the stations, we check the increase in the objective function via the local search. If the relative increase to the objective function falls below a given threshold, the local search immediately ends the search in the given period and proceeds to the following one.

The GRASP algorithm terminates when one of the following conditions have been satisfied: i) a threshold number of candidate solutions have been examined, ii) a threshold number of candidate solutions have been filtered out or, iii) a time limit has been reached.

3.6 Computational Results

In this section, we analyse the results from computational experiments using the models and heuristic methods discussed in the previous sections. In Section 3.6.1, we describe the network and datasets used in our experiments. In Section 3.6.2, we assess the advantage of the MC model (3.3) over the SL model (3.2) when solving

both with a MILP solver. In Section 3.6.3, we compare the capabilities of the GF model and the MC model. We show that the MC model (3.3) can more accurately reflect effects which are known from the literature to affect EV purchase. Finally, in Section 3.6.4, we discuss the limitations of the MC model (3.3) motivating, in Section 3.6.5, a computational study comparing it with our heuristic methods.

All tests were run on a server running Linux version 3.10, with an Intel Core i7-4790 CPU with eight virtual cores and 32 GB of RAM. The code is written in Python 3.7, and is publicly available [1]. We use CPLEX version 12.10, accessed via the DoCPLEX module (version 2.21). Parameter values can be found in Appendix A.1.2, and instances used in the simulations are publicly accessible [2].

3.6.1 Test Environment

The network used for the simulations is based on the smallest aggregation level in the 2016 census (Statistics Canada 2017) for the city of Trois-Rivières, Québec. This defines 317 zones within the city, with populations and aggregate characteristics given for each zone. Nodes in the graph are given by the centroids of each zone. The edges in the graph are created between adjacent zones, with the edge length being the Euclidean distance between the centroids. We note that the Saint Lawrence river divides the city into two parts. Edges have been added to the graph to account for the Laviolette bridge, which connects both parts. The network is shown in Figure 3.3, with the nodes shown as points.

We generated five datasets , each containing 20 instances with a list of candidate stations, a set of user classes, and pre-computed error terms. The parameters and the generation method for the error terms for each dataset are discussed in Appendix A.1.2, with key parameter values given in Table 3.2. We give a summary of the important distinctions in each dataset:

Simple A small-scale dataset where key parameter values are fixed such that the resulting instances are easy to solve. This is the only dataset which the SL model (3.2) can solve.

Distance This dataset increases the penalisation term in the alternative-specific

1. https://github.com/StevenLamontagne/EVChargingStationModel
2. https://doi.org/10.7488/ds/3850

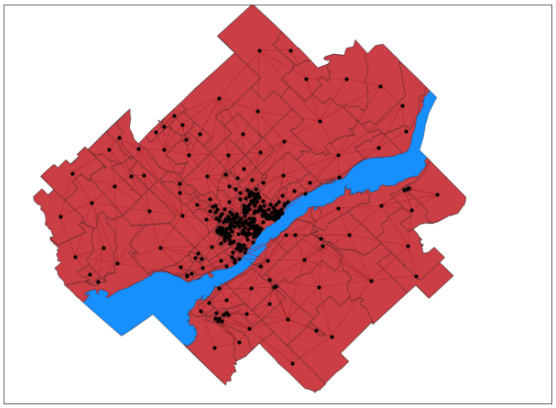

Figure 3.3 – Trois-Rivières network

constant for each station to account for distance.

HomeCharging For this dataset, we create two user classes in each node: one with and one without access to home charging.

LongSpan This dataset increases the number of years from four to ten, but the user classes remain consistent across the planning horizon.

Price In this dataset, we simulate a decrease in the price of the EV year-by-year, which affects user classes differently based on their income. The alternative-specific constant for each station is modified based on the income level of the user class and the current year.

The Simple, Distance, and HomeCharging datasets have a candidate location set with ten options, and users will not consider any station which is more than ten kilometres away. In contrast, the LongSpan and Price datasets have a candidate location with 30 options, and users may consider any charging station regardless of the distance. This results in significantly more difficult problems to solve. In general, CPLEX is not able to solve the exact models for these instances.

Parameter	Simple	Distance	HomeCharging	LongSpan	Price
T	4	4	4	10	4
$\|M\|$	10	10	10	30	30
$\|N\|$	317	317	734	317	1397
R_i	$15-105$	$15-105$	$15-105$	465	465
m_j (all stations)	2	6	6	6	6

Table 3.2 – Parameter values for the generated instances.

3.6.2 Comparison of the Single-Level and Maximum Covering Models

In order to illustrate the advantages of the maximum covering formulation over the single-level version, we solve all instances in the Simple dataset using both formulations. Table 3.3 reports the following statistics averaged over the 20 instances: The CPU time for the root and branch-and-cut, as well as the optimality gaps for each phase and the number of nodes, are as reported in the CPLEX log file. For the number of instances solved, we consider an instance to be solved if the solver terminates with a provably-optimal solution. For the CPU time in the linear relaxation, neither the Python API nor the CPLEX log directly give the time to solve the linear relaxation of the model. Since CPLEX may run additional methods at the root node to more rapidly solve a discrete optimisation problem (e.g. cuts or heuristics) rather than simply solving its linear relaxation, we ran the solver a second time with the continuous versions of all the variables. As such, the CPU time for the linear relaxation may be higher than for the root node, due to run-time differences.

We note a large difference in the solving time of the models. In addition to the average improvement between the MC model (3.3) and the SL model (3.2), we also note that the former displays small variance: for the SL model (3.2), the solving times ranged from 1,978.21 to 4,724.34 seconds, whereas for the MC model (3.3), the solving times ranged from 0.22 to 0.32 seconds. We also observe improvements in the optimality gap at the root node as well as in the number of nodes explored, likely due to the presence of the Big-M constraints in the SL model (3.2).

3.6.3 Comparison of the Maximum Covering and GF Models

We compare the capabilities of the GF model (Anjos et al. 2020) with those of the MC model (3.3). To accurately compare the models, we only use the node-based, intracity part of the GF model. Parameter values are chosen to match as closely as possible between both models. The modified GF model, as well as the parameters, are presented in Appendix A.1.3.

	MC	SL
CPU time (LP, sec)	0.83	4466.75
CPU time (root, sec)	0.23	2294.71
CPU time (B&C, sec)	0.03	729.24
Optimality gap (root, %)	0.69	2.15
Optimality gap (B&C, %)	0.00	0.00
Nodes explored	8.50	769.85
Instances solved	20	20

Table 3.3 – Average performance of CPLEX applied to the MC model and the SL model in the Simple dataset; LP denotes the linear relaxation and B&C denotes the branch-and-cut.

We assume that the capacity of each charging outlet is infinite in the GF model. This is consistent with the assumption in the MC model that the stations are uncapacitated.

In Sections 3.6.3 and 3.6.3, we consider two cases. In the first case, we force the solver to use the same solution for both the GF and the MC models. This allows for comparing the spread of EVs around charging stations. In the second case, we find the solution returned by the solver for the GF model. We then calculate the objective value of the MC model (3.3) using that solution (by using (3.4)). This allows us to analyse if the differences in the spread of EVs has an impact on solution quality.

Distance to Charging Station

Distance is a key factor in determining which facility users choose to patronise in the maximum capture problem (Benati and Hansen 2002, Eiselt et al. 2019) as well as in models that examine existing EV owners' choice of charging location (Luo et al. 2015, Vermeulen et al. 2019, Wolbertus et al. 2021). These works all find that users are less likely to select a facility as the distance increases. To our knowledge, there are no studies which examine the impact of the distance of charging stations to users in the decision to purchase an EV, but we assume that similar results hold in this case. That is, the utility of a charging option (and thus the likelihood that the charging option acts as a primary recharging method) decreases with distance.

In the GF model, all users have a maximum distance within which they consider

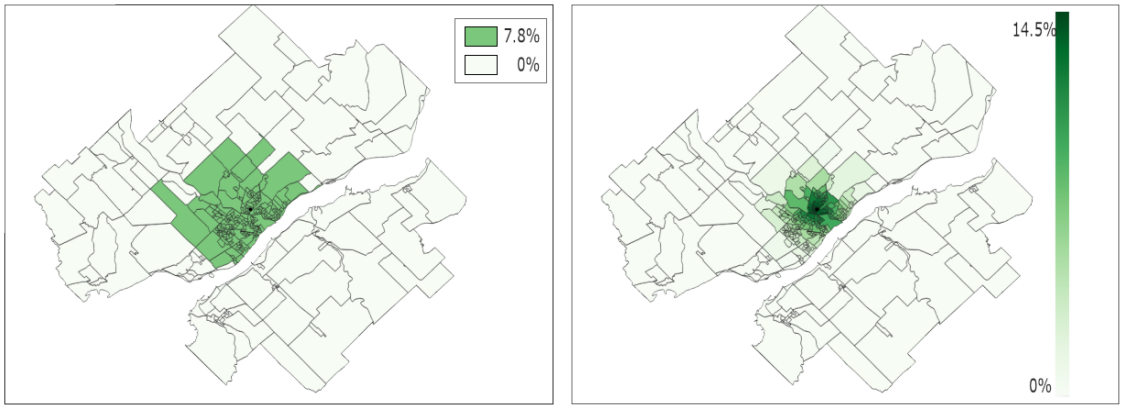

Figure 3.4 – Percentage of population in each zone which purchases an EV by the end of the simulation when examining the distance to the charging station. GF model on left side, MC model on right side.

charging stations. At a given node, users consider charging at any charging station within that maximum distance.

In the MC model (3.3), we also assume that the users have a maximum distance for considering charging stations. However, additionally, the utility decreases with distance. For this comparison, we use the Distance dataset described in Section 3.6.1.

In Figure 3.4, we see the percentage of the population that purchases an EV (at the end of the planning horizon) when one station is opened. On the left, in the GF model, we see that the EV adoption rate is the same across the entire region that considers that station. By comparison, on the right in the MC model, we see that the EV adoption rate decreases as the distance increases.

In Table 3.4, we report the value of (3.4) for the solutions from both models. We see that the optimal objective values for the GF model are around 42% lower than those for the MC model. However, the incentive for the GF model to place more outlets is linked to the capacity of each station. Thus, in the uncapacitated case, it will only place one outlet at any station it opens. To counteract this effect and compare the models more fairly, we examine the objective values of adjusted solutions. These set the capacity of each station selected to be open by the GF model to its maximum capacity of 6 outlets. Despite this being an infeasible solution (due to the budget), the optimal objective values for the adjusted GF model are still around 20.6% lower than those for the MC model.

	GF	GF (Adjusted)	MC
5th percentile	9117.18	12954.33	16496.45
Median	9266.85	13113.74	16592.65
95th percentile	9407.89	13244.96	16764.57

Table 3.4 – Number of EVs from the solutions of the GF and MC models.

We note the difference in the spread of EVs observed in Figure 3.4, with the spread in the MC case being more consistent with the literature (Benati and Hansen 2002, Eiselt et al. 2019). Additionally, as we report in Table 3.4, the quality of the solutions are considerably different between the two models. This indicates that these differences have an important impact in the solutions, and highlights the benefits of the maximum covering formulation.

Access to Home Charging

Given it is a significant factor in the decision to purchase an EV, accurately modelling access to home charging is critical (Hidrue et al. 2011, Bailey et al. 2015).

In the GF model, it is assumed that a given fraction of new EV owners will have access to home charging (which depends on the year, but not the location). The total number of EVs at each location, including both those who have access to home charging and those who do not, is then bound by the capacity of nearby stations. Consequently, if there are no charging outlets sufficiently close to the users, not even those with home charging access may purchase EVs. We note this effect in Figure 3.6.

In the maximum covering model (3.3), the population and home charging access for each user class can be set independently. By creating two user classes for each area, with appropriately set populations, we can more accurately model the percentage of the population that has access to home charging. Additionally, since the two user classes are separate in the model, the users who have access to home charging are allowed to purchase EVs, even if no public charging infrastructure is sufficiently close. For this comparison, we use the HomeCharging dataset described in Section 3.6.1.

In Figure 3.5, we depict the percentage of the population in each area that purchase EVs by the end of the simulation period simply because of home charging

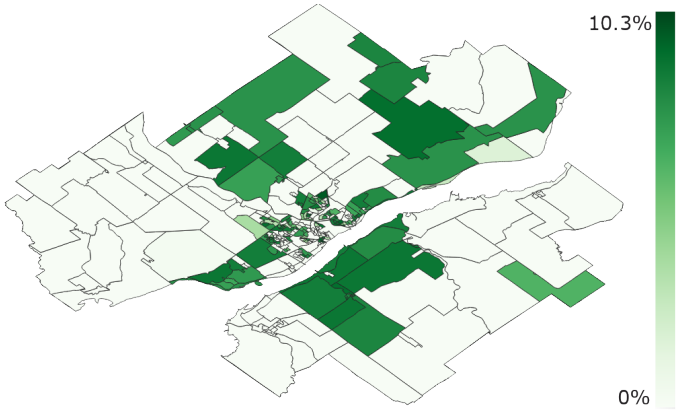

Figure 3.5 – Percentage of Population Covered by Home Charging Access.

	GF	GF (Adjusted)	MC
5th percentile	13648.43	15990.52	17975.55
Median	13737.12	16091.57	18036.37
95th percentile	13780.56	16133.63	18085.95

Table 3.5 – Number of EVs from the solutions of the GF and MC models.

access (according to the MC model (3.3)). In other words, even if no public charging infrastructure is installed, these users can charge at home and decide to purchase an EV. By contrast, in Figure 3.6, we depict the percentage of the population at the end of the simulation period that purchase EVs when one station is opened. On the left, in the GF model, we note that only users near the charging station have purchased EVs. By comparison on the right, in the MC model (3.3), we note that the users that were covered by home charging in Figure 3.5 have purchased EVs. Additionally, we see that near the charging station there is an increase to the percentage of the population that purchases EVs, as users who were not covered by home charging access are now covered by the charging station.

In Table 3.5, we report the value of (3.4) for the solutions from both models. We see that not accounting for home charging access results in a decrease in the number of EVs of around 23.8%. As before, we examine an adjusted solution to take the infinite capacity into account. Despite this being an infeasible solution, it results in a decrease in the numbers of EVs of around 10.8% compared to the MC model. Clearly, the same findings emerge as in Section 3.6.3.

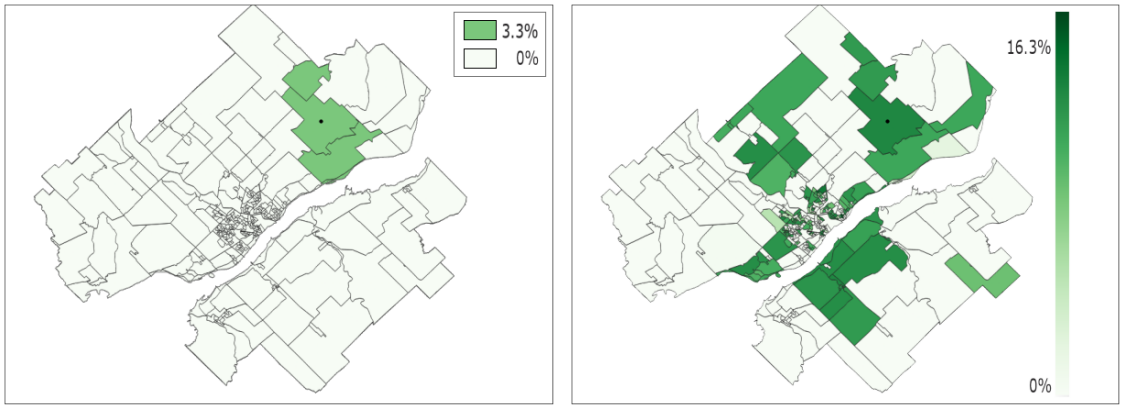

Figure 3.6 – Percentage of population in each zone which purchases an EV by the end of the simulation when examining the home charging access. GF model on left side, MC model on right side.

3.6.4 Limitations of the Maximum Covering Model

While the maximum covering formulation significantly improves tractability by MILP solvers compared to the single-level formulation, our problem remains difficult to solve for large instances. To demonstrate this, we solve the MC model (3.3) over all instances in all five datasets, restricting CPLEX to a time limit of 7,200 seconds. In Table 3.6, we report the average performance, using the same statistics reported in Section 3.6.2.

We first note that CPLEX is not able to solve any of the instances in the LongSpan and Price datasets within the time limit. Moreover, not only can it not complete the root node, it is not even able to solve the LP relaxation This highlights the complexity of the problem, even for a moderate-sized city and only 30 candidate locations. Concerning the three smallest datasets (Simple, Distance, and HomeCharging) which are all solved to optimality, we remark that the optimality gap at the root node is quite good, suggesting that the majority of the difficulty lies in solving the root node. Finally, we note that, while most of the statistics of each instance are close to the average, the number of nodes explored and the CPU time for the branch-and-cut phase vary, depending on how quickly the optimal solution is found.

	Simple	Distance	HomeCharging	LongSpan	Price
CPU time (LP, sec)	0.83	1.01	4.33	-	-
CPU time (root, sec)	0.23	2.12	6.29	7202.90	7203.88
CPU time (B&C, sec)	0.03	0.53	4.51	-	-
Optimality gap (root, %)	0.69	2.47	2.41	37.34	75.14
Optimality gap (B&C, %)	0	0	0	37.34	75.14
Nodes explored	8.50	99.95	447.75	0	0
Instances solved	20	20	20	0	0

Table 3.6 – Average performance of CPLEX applied to the MC model. The entries for the Simple dataset are copied from Table 3.3, for ease of comparison.

3.6.5 Comparing Heuristics

We compare solving the MC model (3.3) via the standard branch-and-cut approach used by CPLEX (labelled as "Exact" in the results) and the heuristics presented in Section 3.5. We impose a time limit of two hours (7,200 seconds) for the Exact and all heuristic methods. In the cases of the Exact method and the Rolling Horizon method, this time limit is given directly to CPLEX, and thus only limits the CPLEX solving time. The Greedy procedure is tested using both the myopic and hyperoptic search methods. For the Rolling Horizon method, we examine two ways of distributing the time across the years. In the first, we divide the time evenly amongst all years ("Even"). In the second, the time limit is divided geometrically, with the first year having a time limit of 3,600 seconds and each successive year having half of the previous time ("Geometric"). For the GRASP procedure, we test both the myopic and hyperoptic search methods. We set the value of α to 0.85, as recommended for the maximum covering problem in Resende and Ribeiro (2018). The GRASP procedures run until 300 solutions have been examined, or until 500 solutions have been filtered out. The second phase of the GRASP procedure uses the first improvement method.

Solving Time

In Table 3.7, we report the 5th percentile, the 95th percentile, and the average solving time across all instances of a given dataset and method. For the small datasets (Simple, Distance, HomeCharging), the solving time of the Exact method is only surpassed by the Greedy and Rolling Horizon methods. Both

Greedy methods are undoubtedly the fastest. This is the case in the Simple and Distance datasets (with the Rolling Horizon methods being nearly as fast in the Simple dataset), however, it is more noticeable in the HomeCharging, Price, and LongSpan datasets.

The Rolling Horizon methods both solve quickly for the small datasets. In the LongSpan test set, the Rolling Horizon methods solve more quickly than the Exact method. Since the user classes are the same for each year, solutions from previous years act as good quality warmstart solutions. This allows the later years in the Rolling Horizon method to terminate before the time limit. However, this does not occur in the Price test set. Since the user classes change each year, the quality of the solution for previous years is poorer, which causes the solver to reach the time limit.

While the GRASP methods took longer to solve than the RollingHorizon methods in the small datasets, they scaled better for the Price dataset. This resulted in a solving time around a sixth that of the RollingHorizon and Exact methods. In the LongSpan dataset, the solving times for the GRASP method are relatively high. This is due to the fact that both the first and second phases iterate over every year, which causes the solving time to increase substantially as the number of time years increases. The hyperoptic method is solved noticeably slower than the myopic method.

Solution Quality

In Table 3.8, we report the 5th percentile, the 95th percentile, and the average gaps to the best known solution for all instances of a given test set and method. More specifically, for each instance, we examine which method found the solution with the highest objective, whose value is denoted as $bestSol$. The gap for each method is then given by $gap(x^\star) = \frac{bestSol - f(x^\star)}{bestSol}$, where $x^\star$ is the solution found by the given method.

Additionally, we give the number of instances in which a method has found a solution with objective value equal to that of the best known solution. In the case of the Simple, Distance, and HomeCharging datasets, the exact solution is known, thus the corresponding entries for the heuristic methods are the optimality gaps.

While the Exact method produces the best solution value for the smaller tests

		Simple	Distance	HomeCharging	Price	LongSpan
Exact	5th percentile	0.22	2.26	9.17	7203.50	7202.70
	Average	0.27	2.66	10.80	7203.98	7202.99
	95th percentile	0.30	3.04	11.89	7204.51	7203.27
GreedyOne (Myopic)	5th percentile	0.10	0.15	0.15	1.03	1.17
	Average	0.10	0.16	0.39	1.06	1.23
	95th percentile	0.10	0.17	1.07	1.09	1.65
GreedyOne (Hyperoptic)	5th percentile	0.21	0.29	0.29	2.20	4.98
	Average	0.21	0.31	0.57	2.27	5.09
	95th percentile	0.21	0.33	1.19	2.36	5.12
RollingHorizon (Even)	5th percentile	0.17	0.37	1.92	7201.49	3557.43
	Average	0.18	0.40	2.09	7226.27	3919.75
	95th percentile	0.19	0.41	2.22	7298.76	4238.00
RollingHorizon (Geometric)	5th percentile	0.17	0.37	1.92	7201.47	7096.51
	Average	0.18	0.40	2.08	7219.97	7163.96
	95th percentile	0.19	0.41	2.21	7314.78	7186.91
GRASP (Myopic)	5th percentile	66.48	78.20	88.06	851.76	1593.75
	Average	71.22	83.74	91.55	873.47	1635.97
	95th percentile	81.70	87.18	101.45	896.95	1666.46
GRASP (Hyperoptic)	5th percentile	99.27	119.29	128.16	1405.71	3058.92
	Average	105.07	122.85	132.76	1433.38	3121.60
	95th percentile	113.94	127.47	138.17	1478.21	3197.92

Table 3.7 – Comparison of solving times for heuristic methods across all datasets. Times are given in seconds.

(Simple, Distance, HomeCharging), it is unable to find solutions which are as good as the heuristic methods in the Price and LongSpan datasets.

The Greedy methods performed slightly worse than the other heuristic methods in the Simple, Distance, and Home Charging datasets, but they performed surprisingly well in the LongSpan and Price datasets. They frequently found the best solution, and with gaps under 0.1% even in cases where the method did not find the best solution.

The Rolling Horizon methods perform well in the smaller test sets but, similar to the Exact method, they do not perform as well in the LongSpan and Price datasets as the other heuristic methods. Both GRASP methods performed comparable to each other, and comparable with the Greedy methods. However, the GRASP methods were more consistently able to produce good-quality solutions across all datasets as compared to the Greedy methods, as can be seen in the Distance dataset.

		Simple	Distance	HomeCharging	Price	LongSpan
Exact	5th percentile	0.00	0.00	0.00	12.67	8.86
	Average	0.00	0.00	0.00	12.74	8.94
	95th percentile	0.00	0.00	0.01	12.83	9.01
	# of best	20	20	20	0	0
GreedyOne (Myopic)	5th percentile	0.00	1.66	0.46	0.00	0.00
	Average	0.02	2.08	0.53	0.01	0.01
	95th percentile	0.07	2.76	0.68	0.05	0.03
	# of best	14	0	0	11	15
GreedyOne (Hyperoptic)	5th percentile	0.00	1.47	0.44	0.00	0.00
	Average	0.07	2.03	0.61	0.02	0.02
	95th percentile	0.19	2.53	0.84	0.06	0.05
	# of best	9	0	0	8	10
RollingHorizon (Even)	5th percentile	0.00	0.00	0.00	12.33	4.11
	Average	0.00	0.07	0.02	12.66	4.19
	95th percentile	0.00	0.38	0.06	12.83	4.27
	# of best	20	14	12	0	0
RollingHorizon (Geometric)	5th percentile	0.00	0.00	0.00	12.51	2.52
	Average	0.00	0.07	0.02	12.72	3.95
	95th percentile	0.00	0.38	0.06	12.83	4.26
	# of best	20	14	12	0	0
GRASP (Myopic)	5th percentile	0.00	0.14	0.16	0.00	0.10
	Average	0.02	0.43	0.26	0.02	0.18
	95th percentile	0.12	0.68	0.36	0.04	0.24
	# of best	16	0	0	5	0
GRASP (Hyperoptic)	5th percentile	0.00	0.19	0.12	0.00	0.10
	Average	0.03	0.44	0.23	0.04	0.19
	95th percentile	0.16	0.67	0.36	0.07	0.26
	# of best	14	0	0	3	0

Table 3.8 – Comparison of gaps to the best known solution for heuristic methods in all five datasets (in percentage).

3.7 Conclusion

In this work, we proposed a model for determining the optimal location of EV charging stations in a long-term planning environment so as to maximise the total number of EVs. To consider user-specific characteristics, we used discrete choice models to represent the decision of the users to purchase EVs. When compared to the existing model for this problem (the GF model in Anjos et al. 2020) this allowed for more intuitive user behaviour with regards to charging station location and home charging access. Additionally, solutions for the GF model were significantly different than those for the MC model, highlighting the benefits of using the latter.

Using the simulation-based approach of Pacheco Paneque et al. (2021) resulted in a bilevel model. By reformulating the model as a maximum covering problem, the sets of Big-M constraints were removed, thus improving the tractability. We note that this reformulation can be applied to other applications of the simulation-based method (including the MCPRU) if no capacity constraints are present.

For more difficult instances, several heuristic methods were proposed for obtaining feasible solutions. While the Rolling Horizon heuristic was not as effective for more difficult instances, the Greedy and GRASP algorithms both performed very well. In particular, we note that the Greedy methods were able to find solutions within a few seconds, even on the most difficult instances. Additionally, the GRASP methods can obtain solutions of near-optimal quality within a few minutes for the small instances, and they can easily surpass the quality of the best solution obtained from the exact method, within less than half the time limit. The similar performances of the Greedy and GRASP methods suggests that more complex local search moves may be necessary to find better solutions.

While the heuristic methods were able to quickly find feasible solutions, we are not able to verify the quality of these solutions on the larger instances. Further research will examine an exact method specifically tailored for larger scale instances. A few approaches are possible. Firstly, the structure of the problem resembles the resource-constrained production scheduling problem (RCPSP), for which a specialised algorithm exists (Bienstock and Zuckerberg 2010, Muñoz et al. 2018). The method (which is similar to column generation) has a mechanism for bounding the number of basis elements. However, when this bound is applied to

our problem, it is greater than the maximum number of basis elements. As such, a complete enumeration is possible, and the method may require solving the full MC model (3.3). A successful modification and implementation of this algorithm for our problem would be the subject of future research. A second possible approach is the Bender's decomposition method proposed in Cordeau et al. (2019), which is designed for large-scale maximum covering problems. Since the restricted master problem does not include the full set of covering constraints, and solutions to the subproblem can be calculated analytically, the method seems quite well-suited. However, in our preliminary testing, we have found poor convergence. In part, this is likely due to the higher ratio of stations to users as compared with the original paper, which the authors note to be an important factor. As such, research is ongoing to improve the performance of this method in our problem.

Since the MC model (3.3) was designed for the intracity network, it is not applicable to larger geographical areas. For example, in the MC model (3.3), there are no constraints related to the range of EVs, which would be necessary for intercity travel. This is a notable difference with the GF model of Anjos et al. (2020), which was designed for intracity and intercity networks, and was applied to the province of Québec. As such, further research will examine an extension of the MC model (3.3) which includes the intercity network.

Acknowledgements

The authors thank the anonymous reviewers whose comments helped to improve the manuscript. In particular, one reviewer proposed a reformulation of the model which greatly improved the convergence rate, and led to the version presented here.

The authors gratefully acknowledge the assistance of Jean-Luc Dupré from *Direction Mobilité* of *Hydro-Québec*, for both providing and helping to understand EV charging data, as well as for sharing his expertise on EV charging stations and the network. We gratefully acknowledge the work of Mahsa Moghaddass in estimating the parameter values used in the models.

This research was supported by Hydro-Québec, NSERC Collaborative Research and Development Grant CRDPJ 536757 - 19, and NSERC Discovery grant 2017-06054.

4 Accelerated Benders Decomposition and Local Branching for Dynamic Maximum Covering Location Problems

Preface

In Chapter 3, we reformulated the single-level model of Pacheco Paneque et al. (2021) with simulated utilities to an efficient maximum covering formulation. More specifically, due to the time periods, the resulting model can be described as a dynamic (or multi-period) MCLP. However, even with this reformulation, there remain challenges with solving hard instances. Notably, the general-purpose linear programming solver CPLEX cannot solve the LP relaxation of the problem within a two-hour time limit. As such, in this chapter, we develop specialised Benders decomposition algorithms for the multi-period model, expanding the single-period MCLP method proposed in Cordeau et al. (2019). This includes an accelerated branch-and-Benders-cut algorithm and a local branching scheme, both of which exploit separability of our problem by time period to improve convergence and find better quality solutions.

These specialised algorithms can be applied to any dynamic MCLP with the only constraint on the users being the covering constraints (2.10c). In other words, any constraints on the facilities (or stations, in our application) can be used, such as budgetary, cardinality, or precedence constraints. However, constraints such as a capacity for the facilities (which link the facility and user variables) or requiring repeated coverage of users (which act on the user variables between time periods) are not valid within this framework. Further discussion around these limitations is presented in Chapter 6.

The contents of this chapter are in the second round of revision for *Computers & Operations Research*. A pre-print publication can be cited as follows:

Lamontagne, S., Carvalho, M., Atallah, R., 2023. Accelerated Benders Decomposition and Local Branching for Dynamic Maximum Covering Location Problems.

https://arxiv.org/abs/2309.00702.

Contributions of Steven Lamontagne and the coauthors

— The research ideas were developed by the student and Margarida Carvalho. In particular, the adaptations of the Benders decomposition and the acceleration techniques were conceptualised and incorporated by the student. Additionally, the inclusion of the local branching method and the development of its specialised methods was conducted by the student.

— All code was written by the student, including the (re)implementations of the branch-and-cut, (accelerated and unaccelerated) branch-and-Benders-cut, and local branching methods via the CPLEX software, and the greedy algorithm.

— The original draft (including all tables and images) were produced by the student, while it was revised by Margarida Carvalho and Ribal Atallah.

Abstract

The maximum covering location problem (MCLP) is a key problem in facility location, with many applications and variants. One such variant is the dynamic (or multi-period) MCLP, which considers the installation of facilities across multiple time periods. To the best of our knowledge, no exact solution method has been proposed to tackle large-scale instances of this problem. To that end, in this work, we expand upon the current state-of-the-art branch-and-Benders-cut solution method in the static case, by exploring several acceleration techniques. Additionally, we propose a specialised local branching scheme which exploits the separability of the problem by time period. This scheme uses a novel distance metric in its definition of subproblems and features a new method for efficient and exact solving of the subproblems. These methods are then compared through extensive computational experiments, highlighting the strengths of the proposed methodologies.

Keywords: Maximum covering, dynamic, Benders decomposition

4.1 Introduction

A classic problem in operations research is the optimal location of facilities according to different aspects such as users' preferences and installation cost. Within this category of problems is the maximum covering location problem (MCLP), attributed to Church and ReVelle (1974). In the MCLP, each facility covers the users within a certain radius and, due to limited resources, it is not possible to open every facility. Thus, a decision maker must select a subset of facilities to open, with the goal of maximising the total coverage. Due to its simplicity and versatility, the MCLP has been used in a wide range of applications, including emergency services location (Gendreau et al. 2001, Degel et al. 2015, Nelas and Dias 2020), healthcare services (Bagherinejad and Shoeib 2018, Alizadeh et al. 2021), safety camera positioning (Dell'Olmo et al. 2014, Han et al. 2019), ecological monitoring or conservation (Church et al. 1996, Martín-Forés et al. 2021), bike sharing (Muren et al. 2020), and disaster relief (Zhang et al. 2017b, Iloglu and Albert 2020, Yang

et al. 2020). For a review of the MCLP and its applications, we refer to Murray (2016).

To include more complex interactions and restrictions, several variants of the MCLP have been developed. The one we consider is the dynamic (or multi-period) MCLP, where the decision maker conducts facility planning over a long time horizon, divided into discrete time periods (Schilling 1980, Gunawardane 1982). The intrinsic consideration of the time horizon is vital in many situations, such as when the demand to be covered varies across time (Porras et al. 2019), when planning infrastructure that persists throughout future planning periods (Gunawardane 1982, Lamontagne et al. 2023), or in real-time operations of emergency services where exact positioning is important (Gendreau et al. 2001). Throughout the time horizon, open facilities may be forced to remain open for the duration of the time horizon (Lamontagne et al. 2023), may be allowed to change location with or without cost (Marín et al. 2018), or a subset may be required to be relocated each time period (Dell'Olmo et al. 2014).

To the best of our knowledge, no exact method exists for solving large-scale dynamic MCLPs. More specifically, the only exact method employed in the literature for the dynamic MCLP is branch-and-bound, which has successfully solved instances with 300 users, 300 facilities, 9 time periods (Dell'Olmo et al. 2014), and $49,905$ users, 60 facilities, 4 time periods (Lamontagne et al. 2023). Meanwhile, in terms of heuristic methods, Porras et al. (2019) used simulated annealing to solve instances with 547 users, 547 facilities, 4 time periods, while Lamontagne et al. (2023) used a greedy method to solve instances with $649,605$ users, 180 facilities, 4 time periods. This compares with specialised methods for the static MCLP, which have successfully solved instances with 818 users, 818 facilities (Pereira et al. 2007), and $15,000,000$ users, 100 facilities (Cordeau et al. 2019). Most notably, the method proposed in Cordeau et al. (2019) is specifically designed for problems in which there are significantly more users than facilities. This situation can occur when using a very fine discretisation of a continuous demand (e.g. Lamontagne et al. 2023) or when creating many different scenarios to model uncertainty in the problem (Daskin 1983, Berman et al. 2013, Vatsa and Jayaswal 2016, Nelas and Dias 2020). These categories of use cases support the need for a specialised method for the dynamic MCLP which can handle large-scale instances.

In this work, we present several contributions to the literature on the dynamic MCLP. First, we extend the branch-and-Benders-cut approach for the static MCLP of Cordeau et al. (2019) to the dynamic case. Second, we detail a suite of acceleration techniques tailored for the dynamic MCLP, which can be selected based on the structure of the application. This includes an intuitive and effective multi-cut generation technique based on separability by time period, an efficient Pareto-optimal cut generation technique with a closed-form solution, a partial Benders decomposition strategy which leverages the problem structure, and a Benders dual decomposition approach which can further strengthen cuts for fractional solutions. Third, we present a specialized local branching method embedded within the branch-and-Benders cut framework. This method makes use of a new distance metric for defining subproblems, which relies on the separability of the problem by time period. We then present a novel subproblem solution method, which can efficiently solve the local branching subproblems in an exact and proven-valid manner. Fourth, we present extensive computational results comparing our proposed methods. Part of these experiments are carried out with instances based on real data from an electric vehicle charging station placement case study, underlying the practical interest of the dynamic MCLP. Our results validate the suitability of our methodological contributions to provide high-quality solutions to instances involving a large number of users, candidate locations and a planning horizon. In particular, our methods can produce solutions with a higher demand covered compared to the greedy heuristic in Lamontagne et al. (2023), in addition to providing performance guarantees via optimality gaps.

The rest of this paper is organized as follows: Section 4.2 discusses the literature about solution methods for the static and dynamic MCLP. Section 4.3 presents the general model for the dynamic MCLP. Section 4.4 is dedicated to the branch-and-Benders-cut methods, extending the work in Cordeau et al. (2019) and implementing improvement methods to the general framework. Section 4.5 then presents the local branching method, based on the work in Rei et al. (2009), with special consideration for the distance metric and the branching scheme. Finally, Section 4.6 provides our computational results, while Section 4.7 concludes our work.

4.2 Literature Review

Despite its long history, few exact solution methods have been developped for the MCLP, while heuristic methods are most commonly used (Murray 2016). We provide a summary of solution methods for both the static and dynamic MCLP in Table 4.1.

The most common exact method uses standard branch-and-bound techniques, in conjunction with off-the-shelf mixed-integer linear programming solvers. This method is commonly used for small-scale instances, or as a benchmark approach for heuristics. However, it has been repeatedly noted that this is insufficient for solving large-scale instances (see, e.g., ReVelle et al. 2008, Zarandi et al. 2013, Cordeau et al. 2019, Lamontagne et al. 2023). In addition, three other exact methods have been presented for the static MCLP. In Downs and Camm (1996), a lower bound is generated via a greedy procedure, similar to the one presented in Church and ReVelle (1974), while an upper bound is generated via Lagrangian relaxation of the covering constraints. Both are combined within a branch-and-bound framework to ensure optimality. In Pereira et al. (2007), the MCLP is reformulated as a p-median problem, with a column generation procedure used to solve the resulting model. In the procedure, stabilisation techniques are proposed to help improve the convergence rate, and limits are placed on both the number of columns generated and the total number of iterations. In Cordeau et al. (2019), the variables associated with the coverage of users are projected out in the Benders subproblem. An analytic solution is then given for the solution of the Benders dual subproblem, allowing for rapid generation of Benders cuts. This process is embedded within a branch-and-Benders-cut framework, allowing for large-scale problems to be solved efficiently.

In terms of heuristics, we note a wide variety of methods. However, two approaches which are used repeatedly include greedy methods and simulated annealing. In the greedy method (e.g. Church and ReVelle 1974), a solution is constructed by repeatedly opening a facility, each time selecting the one which causes the largest increase in coverage. In simulated annealing (e.g. Murray and Church 1996), the process simulates the cooling of metals, with a temperature parameter that varies across the solving process and which controls the mutability of our current solution (e.g. swapping an open facility for a closed one). In Xia et al. (2009), these two

Article	Variant	Methods proposed	Exact versus heuristic
Church and ReVelle (1974)	Static	Greedy, branch-and-bound	Both
Schilling (1980)	Dynamic	Weighing method	Heuristic
Gunawardane (1982)	Dynamic	Branch-and-bound	Exact
Downs and Camm (1996)	Static	Greedy + Lagrangian relaxation + Branch-and-bound	Exact
Galvão and ReVelle (1996)	Static	Greedy + Lagrangian relaxation	Heuristic
Murray and Church (1996)	Static	Greedy, simulated annealing	Heuristic
Adenso-Díaz and Rodríguez (1997)	Static	Tabu search	Heuristic
Resende (1998)	Static	GRASP	Heuristic
Galvão et al. (2000)	Static	Lagrangian relaxation, surrogate relaxation	Heuristic
Arakaki and Lorena (2001)	Static	Genetic algorithm	Heuristic
Gendreau et al. (2001)	Dynamic	Parallel tabu search	Heuristic
Pereira et al. (2007)	Static	Column generation	Exact
ReVelle et al. (2008)	Static	Heuristic concentration	Heuristic
Xia et al. (2009)	Static	Greedy, simulated annealing, genetic algorithm, tabu search	Heuristic
Rodriguez et al. (2012)	Static	Iterative greedy	Heuristic
Zarandi et al. (2013)	Dynamic	Simulated annealing	Heuristic
Dell'Olmo et al. (2014)	Dynamic	Branch-and-bound	Exact
Colombo et al. (2016)	Static	Variable neighbourhood search, heuristic concentration	Heuristic
Calderín et al. (2017)	Dynamic	Simulated annealing, evolutionary algorithm	Heuristic
Máximo et al. (2017)	Static	Intelligent-guided adaptive search	Heuristic
Marín et al. (2018)	Dynamic	Lagrangian relaxation	Heuristic
Cordeau et al. (2019)	Static	Branch-and-Benders-cut	Exact
Porras et al. (2019)	Dynamic	Simulated annealing	Heuristic
Lamontagne et al. (2023)	Dynamic	Greedy, GRASP, rolling horizon	Heuristic

Table 4.1 – Articles proposing solution methods for the static or dynamic MCLP.

heuristics (along with greedy plus substitution, genetic algorithm and tabu search) were compared, with the simulated annealing method finding solutions of the best quality. By comparison, the greedy method solved instances faster, with solutions of value within a 1% relative gap of those of simulated annealing.

Our work contributes to the literature on exact methods for dynamic MCLPs, which, to our knowledge, is limited to branch-and-bound techniques. These have proved inadequate for tackling large-scale instances.

4.3 Problem Formulation

We present a general formulation for the dynamic MCLP. Let T be the number of time periods, J be the set of users and I be the set of facilities. We use the index $1 \leq t \leq T$ to denote a time period, the index $j \in J$ for a user, and the index $i \in I$ for a facility. We define the parameters a_{ij}^t such that $a_{ij}^t = 1$ if facility i covers user j in period t, and 0 otherwise. Let $d_j^t > 0$ denote the demand of user j in time period t. We introduce a binary decision vector x with entries x_i^t such that

$x_i^t = 1$ if and only if facility i exists in period t. We also include in the model an auxiliary decision vector z with entries z_j^t such that $z_j^t = 1$ if user j is covered by some facility at period t, and 0 otherwise. Then, the dynamic maximum covering location is formulated as

$$\text{Maximise} \sum_{t=1}^{T} \sum_{j \in J} d_j^t z_j^t, \tag{4.1a}$$

$$\text{subject to } x \in \Omega, \tag{4.1b}$$

$$\sum_{i \in I} a_{ij}^t x_i^t \geq z_j^t, 1 \leq t \leq T, j \in J, \tag{4.1c}$$

$$x_i^t \in \{0,1\}, \quad 1 \leq t \leq T, i \in I, \tag{4.1d}$$

$$z_j^t \in \{0,1\} \qquad 1 \leq t \leq T, j \in J. \tag{4.1e}$$

The objective function (4.1a) maximises the demand covered over all time periods. Constraint (4.1b) defines the feasible domain Ω for the variables x, which can be any polytope not involving the variables z_j^t. Typically, this includes either a cardinality constraint (e.g. Calderín et al. 2017) or a knapsack constraint (e.g. Cordeau et al. 2019) to restrict the number of facilities. The set Ω can also include, for instance, diversification constraints imposing that the set of facilities must change in each time period (Dell'Olmo et al. 2014), or precedence constraints imposing that some facilities must be constructed before others (Lamontagne et al. 2023). Constraints (4.1c) impose that a suitable facility must exist for our users to be considered covered. Constraints (4.1d) and (4.1e) indicate that both sets of variables x and z must be binary. However, as noted in Murray (2016), integrality on the variables z_j^t can be relaxed in Constraints (4.1e).

We emphasise that the constraints in Ω may only depend on the variables x. Most notably, some acceleration techniques in Section 4.4.2 and the local branching method in Section 4.5 may no longer be valid with additional linking constraints between the variables x and z, or even uniquely on the variables z. Some examples include capacity constraints on the facilities in the dynamic MCLP problem of Alizadeh et al. (2021), or continual coverage constraints such as in the multi-period incremental facility location of Albareda-Sambola et al. (2009).

For a given solution $x \in \Omega$, it is easy to calculate the resulting coverage or, in

other words, the total demand covered by the set of facilities defined via x. Let $f(x)$ denote the coverage of solution $x \in \Omega$. Then, as described in ReVelle et al. (2008), Cordeau et al. (2019), this value can be calculated as

$$f(x) = \sum_{t=1}^{T} \sum_{j \in J} \min \left\{ 1, \sum_{i \in I} a_{ij}^t x_i^t \right\} d_j^t. \tag{4.2}$$

4.4 Benders Decomposition

In this section, we present an accelerated branch-and-Benders-cut approach tailored for the dynamic MCLP. This begins by generalising the current state-of-the-art approach in the static MCLP, the branch-and-Benders-cut method proposed by Cordeau et al. (2019), to the dynamic case. We then discuss acceleration techniques which aim to strengthen the formulation and accelerate convergence, applied within our dynamic context.

4.4.1 Single Cut Benders Decomposition

We detail the development of the branch-and-Benders-cut method proposed in Cordeau et al. (2019). While the process is nearly identical in the dynamic case as the static case, the development process is a prerequisite for the acceleration techniques we discuss below. As in Cordeau et al. (2019), we define $J_s = \left\{ j \in J : \sum_{t=1}^{T} \sum_{i \in I} a_{ij}^t = 1 \right\}$ as the set of users which are covered by only one facility.

Like in the classical Benders decomposition (Benders 1962), we project out the (continuous) z variables of model (4.1). The value of the z variables in the objective function is replaced with an auxiliary variable, θ. Then, in iteration v, the main

problem (MP) can be written as

$$\text{Maximise } \theta, \tag{4.3a}$$

$$\text{subject to (4.1b), (4.1d)}$$

$$\text{Opt}_{\pi^r,\sigma^r}(x) \geq \theta, \quad 1 \leq r \leq v, \tag{4.3b}$$

$$\theta \geq 0, \tag{4.3c}$$

where π^r and σ^r are the optimal dual vectors associated with the Benders subproblem in iteration r. To simplify the presentation, the index r is omitted when there is no risk of confusion. Since the Benders subproblem is feasible $\forall x \in \Omega$, it is not necessary to include feasibility cuts. We note that an initial upper bound on θ must be provided to ensure that the problem is bounded, such as $\theta \leq \sum_{t=1}^{T} \sum_{j \in J} d_j^t$.

We denote —now and throughout this paper— $\tilde{x}$ as the candidate solution in iteration v. Unless otherwise specified, it is assumed that this solution is integer feasible, i.e. that $\tilde{x} \in \Omega$ and $\tilde{x}_i^t \in \{0,1\}, 1 \leq t \leq T, i \in I$. For each $1 \leq t \leq T$ and $j \in J$, let $I_j^t(x) = \sum_{i \in I} a_{ij}^t x_i^t$ denote the coverage of user j in period t by solution x. When there is no risk of confusion, we use $\tilde{I}_j^t = I_j^t(\tilde{x})$.

The Benders Primal Subproblem (BPS) is then given by

$$\text{Maximise } \sum_{t=1}^{T} \sum_{j \in J} d_j^t z_j^t, \tag{4.4a}$$

$$\text{subject to } z_j^t \leq \tilde{I}_j^t, \qquad 1 \leq t \leq T, j \in J, \tag{4.4b}$$

$$z_j^t \leq 1, \qquad 1 \leq t \leq T, j \in J, \tag{4.4c}$$

$$z_j^t \geq 0, \qquad 1 \leq t \leq T, j \in J. \tag{4.4d}$$

Let π_j^t and σ_j^t denote the dual variables associated with Constraints (4.4b)

and (4.4c). The Benders Dual Subproblem (BDS) is then

$$\text{Minimise} \sum_{t=1}^{T} \sum_{j \in J} \left(\tilde{I}_j^t \pi_j^t + \sigma_j^t \right), \tag{4.5a}$$

$$\text{subject to } \pi_j^t + \sigma_j^t \geq d_j^t, \qquad 1 \leq t \leq T, j \in J, \tag{4.5b}$$

$$\pi_j^t, \sigma_j^t \geq 0, \qquad 1 \leq t \leq T, j \in J. \tag{4.5c}$$

Similar to Cordeau et al. (2019), this subproblem can be easily solved by inspection: If $\tilde{I}_j^t < 1$, then the optimal solutions are $\tilde{\pi}_j^t = d_j^t, \tilde{\sigma}_j^t = 0$. If $\tilde{I}_j^t > 1$, then $\tilde{\pi}_j^t = 0, \tilde{\sigma}_j^t = d_j^t$. If $\tilde{I}_j^t = 1$, then any solution $\tilde{\pi}, \tilde{\sigma} \geq 0$ such that $\tilde{\pi}_j^t + \tilde{\sigma}_j^t = d_j^t$ will be optimal. The optimality cut associated with these values is then

$$\sum_{t=1}^{T} \sum_{j \in J} \left(\left(\sum_{i \in I} a_{ij}^t x_i^t \right) \tilde{\pi}_j^t + \tilde{\sigma}_j^t \right) \geq \theta.$$

The resulting cut, reformulated as a function of the variables x, is presented in Proposition 4.4.1. We set $\pi^{v+1}, \sigma^{v+1} = \tilde{\pi}, \tilde{\sigma}$, and the left-hand side of the cut forms the term $\text{Opt}_{\pi^{v+1}, \sigma^{v+1}}$ in (4.3b).

Proposition 4.4.1. *The optimality cuts associated with the Benders subproblem take the form,*

$$\sum_{t=1}^{T} \sum_{i \in I} \left(\sum_{j \in \Gamma^t(\tilde{x}^t)} d_j^t a_{ij}^t \right) x_i^t + \sum_{t=1}^{T} \sum_{j \in J \setminus \Gamma^t(\tilde{x}^t)} d_j^t \geq \theta \tag{4.6}$$

where the set $\Gamma^t(\tilde{x}^t)$ can be defined as any of the following expressions:

$$\Gamma^t(\tilde{x}^t) = \left\{ j \in J : \tilde{I}_j^t < 1 \right\}, \tag{B0}$$

$$\Gamma^t(\tilde{x}^t) = \left\{ j \in J \setminus J_s : \tilde{I}_j^t < 1 \right\} \cup \left\{ j \in J_s : \tilde{I}_j^t \leq 1 \right\}, \tag{B1}$$

$$\Gamma^t(\tilde{x}^t) = \left\{ j \in J : \tilde{I}_j^t \leq 1 \right\}. \tag{B2}$$

We remark that the names of the cuts (B0), (B1), and (B2) correspond to those of the equivalent cuts in Cordeau et al. (2019).

We note the following observations about these optimality cuts:

— As in Cordeau et al. (2019), the cuts (B0) are dominated by the cuts (B1).

— By definition of the set J_s, the condition $\tilde{I}_j^t \leq 1$ will always be satisfied for $j \in J_s$.

— The optimality cuts (4.6) are valid for both integer and fractional candidate solutions $\tilde{x}$. As described in Cordeau et al. (2019), optimality cuts can be generated for fractional solutions to improve the convergence rate.

So far, we have presented a simple generalisation of the Benders procedure of Cordeau et al. (2019) to the dynamic MCLP. However, as we will see in Section 4.6.2, this method can exhibit slow convergence. We next explore improvements with respects to its convergence rate.

Remark: While this work focuses on developing a framework for branch-and-Benders-cut, it is also possible to use a branch-and-cut framework with submodular cuts. In particular, there are submodular cuts which are analogous to the Benders cuts described in both Cordeau et al. (2019) and in this work. These are presented in a more general context in Coniglio et al. (2022). In A.2.2, we provide more detail as to the links between these approaches, as that may provide additional insight for the reader.

4.4.2 Improvements to the Single-Cut Method

In this section, we demonstrate and discuss the application of known techniques to our particular dynamic MCLP. These approaches aim to strengthen the Benders optimality cuts and improve the dual bound for the decomposition. For the sake of simplicity, the acceleration techniques are presented separately in relation to the decomposition presented in Section 4.4.1. However, it is possible to incorporate multiple techniques simultaneously. For a discussion of acceleration techniques in the general context of Benders decomposition, we refer to Rahmaniani et al. (2017).

There exist classes of improvement methods which heavily depend on the structure of Ω, but which do not affect the structure of the Benders subproblems. Since they involve Ω, their use is application-specific. However, since they do not impact the Benders subproblems, they can be applied to the methods in this work without affecting their validity. An example of such a technique would be a primal heuristic providing warmstart solutions. This can be used to obtain a good lower

bound on the optimal objective value, which otherwise can be difficult during the early iterations of the Benders decomposition method (Rahmaniani et al. 2017). Another example would be valid cuts, which can be added to the main problem to tighten its linear programming (LP) relaxation. Examples for both techniques can be found in Santoso et al. (2005), Codato and Fischetti (2006), Costa et al. (2012).

The remainder of the techniques discussed in this section modify the Benders subproblems in some way, whether by changing the set of users J (which, in turn, changes the amount of computational work required for the generation of cuts), modifying the frequency or type of cuts, or by directly providing reformulations for the BPS (4.4) or the BDS (4.5).

Preprocessing Preprocessing techniques which aggregate users reduce the size of J and, consequently, the number of $\tilde{I}_j^t$ to be calculated in each iteration of the Benders decomposition. A method for doing this such that the resulting problem is equivalent is given in Legault and Frejinger (2023). Their method aggregates users based on their coverage from facilities, i.e., if users j and j' are covered by exactly the same set of facilities then they can be aggregated. An equivalent exact preprocessing technique is presented, among other techniques, in Chen et al. (2023). Heuristic methods also exist such as the ones by Dupačová et al. (2003) and Crainic et al. (2014). However, we note that, due to the analytic solution for the Benders dual subproblem, the marginal effects of each user is negligible in terms of the cut generation time.

Multi-cut method Since the variables z_{ij}^t are only involved in the covering Constraints (4.1c), the Benders primal subproblem (4.4) can be separated per time period. This allows for more optimality cuts to be generated each iteration of the Benders decomposition, which accelerates convergence, as noted by Birge and Louveaux (1988) and Contreras et al. (2011). More specifically, we replace the auxiliary variable θ by the sum of new variables θ^t for $1 \leq t \leq T$. Then, for each iteration v, we have the following MP:

$$\text{Maximise} \sum_{t=1}^{t} \theta^t, \tag{4.7a}$$

$$\text{subject to (4.1b), (4.1d)} \tag{4.7b}$$

$$\text{Opt}_{\pi^{rt},\sigma^{rt}}(x^t) \geq \theta^t, \quad 1 \leq t \leq T, 1 \leq r \leq v, \tag{4.7c}$$

$$\theta^t \geq 0, \tag{4.7d}$$

where, as before, π^{rt} and σ^{rt} are the optimal dual vectors associated with the Benders subproblem in time period t and iteration r. As in the single-cut case, an initial upper bound must be added on $\sum_{t=1}^{T} \theta^t$.

The BPS (4.4) and the BDS (4.5) as well as the process for deriving the Benders cuts is identical to the single-cut case, with the summations (and, as a consequence, indices) shifted from the subproblem to the main problem. The optimality cuts themselves are presented in Proposition 4.4.2.

Proposition 4.4.2. *For each $1 \leq t \leq T$, the optimality cuts associated with the Benders subproblem take the form,*

$$\sum_{i \in I} \left(\sum_{j \in \Gamma^t(\tilde{x}^t)} d_j^t a_{ij}^t \right) x_j^t + \sum_{j \in J \setminus \Gamma^t(\tilde{x}^t)} d_j^t \geq \theta^t. \tag{4.8}$$

The sets $\Gamma^t(\tilde{x}^t)$ are as defined in Proposition 4.4.1.

Pareto-optimal cuts The optimal solution to the Benders dual subproblem may not be unique, and the strength of the resulting Benders cut may vary depending on the solution selected. This phenomenon is the principle behind the B0, B1, and B2-type cuts introduced in Proposition 4.4.1, with the strength of the resulting cuts discussed in depth in Cordeau et al. (2019). In the context of general Benders decomposition, the selection of an optimal solution leading to a Benders cut is introduced in Magnanti and Wong (1981).

More specifically, in our context, a Benders optimality cut of the form $\theta \leq$

$\sum_{t=1}^{T}\sum_{i\in I}\beta_i^t x_i^t + \gamma$ is said to dominate another cut $\theta \leq \sum_{t=1}^{T}\sum_{i\in I}\beta_i'^t x_i^t + \gamma'$ if

$$\sum_{t=1}^{T}\sum_{i\in I}\beta_i^t x_i^t + \gamma \leq \sum_{t=1}^{T}\sum_{i\in I}\beta_i'^t x_i^t + \gamma'$$

for all $x \in \Omega$ and if there exists at least one $x \in \Omega$ for which the inequality is strict. A Benders cut is said to be *Pareto-optimal* if it is not dominated by any other cut of the same form.

In Magnanti and Wong (1981), the authors propose a model for finding a Pareto-optimal cut based on a *core point*, a point in the relative interior of the convex hull of Ω. This technique was employed in Santoso et al. (2005), Contreras et al. (2011), and discussed further in Papadakos (2008).

Let $\tilde{x}$ be the candidate solution from the main problem (4.3) and $\tilde{\pi}, \tilde{\sigma}$ be an associated optimal solution of the dual subproblem (4.5). Let $\overset{c}{x}$ denote a core point of Ω. Magnanti and Wong (1981) define a Pareto-optimal cut with respect to a core point $\overset{c}{x}$ and a candidate solution $\tilde{x}$ as the one obtained by solving the following subproblem:

$$(\overset{c}{\pi}, \overset{c}{\sigma}) \in \operatorname{argmin} \sum_{t=1}^{T}\sum_{j\in J}\left(I(\overset{c}{x})_j^t \pi_j^t + \sigma_j^t\right), \tag{4.9a}$$

$$\text{subject to } \pi_j^t + \sigma_j^t \geq d_j^t, \qquad 1 \leq t \leq T, j \in J, \tag{4.9b}$$

$$\sum_{t=1}^{T}\sum_{j\in J} I(\tilde{x})_j^t \pi_j^t + \sigma_j^t = \sum_{t=1}^{T}\sum_{j\in J} I(\tilde{x})_j^t \tilde{\pi}_j^t + \tilde{\sigma}_j^t, \tag{4.9c}$$

$$\pi_j^t, \sigma_j^t \geq 0, \qquad 1 \leq t \leq T, j \in J, \tag{4.9d}$$

where $(\overset{c}{\pi}, \overset{c}{\sigma})$ is called a Pareto-optimal point.

Due to the presence of Constraint (4.9c), the Magnanti-Wong subproblem (4.9) is not quite identical to the Benders dual subproblem (4.5). Nevertheless, we are still able to describe the determination of an optimal solution to subproblem (4.9):

Proposition 4.4.3. *For a given candidate solution $\tilde{x}$ and core point $\overset{c}{x}$, the Pareto-optimal solutions $\overset{c}{\pi}, \overset{c}{\sigma}$ for problem* (4.9) *can be calculated pointwise as follows: For $1 \leq t \leq T, j \in J$,*

— *If $I(\tilde{x})_j^t < 1$, then $\overset{c}{\pi}{}_j^t = d_j^t, \overset{c}{\sigma}{}_j^t = 0$.*

— *If* $I(\tilde{x})_j^t > 1$, *then* $\overset{c}{\pi}{}_j^t = 0, \overset{c}{\sigma}{}_j^t = d_j^t$.

— *If* $I(\tilde{x})_j^t = 1$ *and* $I(\overset{c}{x})_j^t < 1$, *then* $\overset{c}{\pi}{}_j^t = d_j^t, \overset{c}{\sigma}{}_j^t = 0$.

— *If* $I(\tilde{x})_j^t = 1$ *and* $I(\overset{c}{x})_j^t > 1$, *then* $\overset{c}{\pi}{}_j^t = 0, \overset{c}{\sigma}{}_j^t = d_j^t$.

— *If* $I(\tilde{x})_j^t = 1$ *and* $I(\overset{c}{x})_j^t = 1$, *then any value such that* $\overset{c}{\pi}{}_j^t + \overset{c}{\sigma}{}_j^t = d_j^t$ *is Pareto-optimal.*

Proof. We first emphasise that the solution to the Magnanti-Wong subproblem (4.9) must also be an optimal solution to the BDS (4.5) for $\tilde{x}$, as specified in Magnanti and Wong (1981). This is enforced through Constraints (4.9b) and (4.9d) (which enforce feasibility), combined with Constraint (4.9c) (which enforces optimality). As described in Section 4.4.1, there is a set of optimal solutions to BDS (4.5) which can be analytically determined for each period t and customer j based on $I(\tilde{x})_j^t$. Hence, let us denote by Φ_j^t the set of optimal solution pairs $(\tilde{\pi}_j^t, \tilde{\sigma}_j^t)$. Concretely, recall that if $I(\tilde{x})_j^t < 1$, then $\Phi_j^t = \big\{(d_j^t, 0)\big\}$. Likewise, $I(\tilde{x})_j^t > 1$ implies that $\Phi_j^t = \big\{(0, d_j^t)\big\}$. Finally, if $I(\tilde{x})_j^t = 1$ then $\Phi_j^t = \big\{(\pi_j^t, \sigma_j^t) : \pi_j^t + \sigma_j^t = d_j^t, \pi_j^t \geq 0, \sigma_j^t \geq 0\big\}$.

In this way, we can equivalently formulate subproblem (4.9) with Constraint (4.9c) replaced by the following constraint:

$$(\pi_j^t, \sigma_j^t) \in \Phi_j^t.$$

This eliminates the linking constraint which involves all variables, reformulating the Magnanti-Wong subproblem (4.9) into the following:

$$\text{Minimise } I(\overset{c}{x})_j^t \pi_j^t + \sigma_j^t, \tag{4.10a}$$

$$\text{subject to } (4.9\text{b}), (4.9\text{d})$$

$$\pi_j^t, \sigma_j^t \in \Phi_j^t. \tag{4.10b}$$

Now, it is easy to verify the feasibility and optimality of the solution described in the proposition statement. □

Corollary 4.4.1. *If the set* $\big\{(t, j) : 1 \leq t \leq T, j \in J, I(\tilde{x})_j^t = 1\big\}$ *is empty, then the Benders optimality cut is unique.*

In practice, Proposition 4.4.3 states that, when determining if $j \in \Gamma^t(\tilde{x}^t)$, we only need to consider the core point when $I_j^t(\tilde{x}) = 1$. In those cases, rather than solely using information from j and $\tilde{x}$ (as is the case for the cuts in Proposition 4.4.1), we can instead look to the coverage in the core point to determine if $j \in \Gamma^t(\tilde{x}^t)$. If both $I_j^t(\tilde{x}) = 1$ and $I(\overset{c}{x})_j^t = 1$, then a different method is required. For example, it is possible to create analogous cuts to (B0), (B1), or (B2).

The calculation of Pareto-optimal points relies on finding a core point $\overset{c}{x}$. For simple domains Ω, a core point can be easily found, such as the point $\overset{c}{x} = (0.5, 0.5, 0.5)$ in the example of A.2.1. However, depending on the domain Ω, it may not be possible to find a core point analytically. An iterative method is proposed in Papadakos (2008), which starts with a feasible solution and takes the average with the candidate solution at every iteration to take the role of core point. Alternatively, one can use the analytic center of the MP (4.3) as a core point, which can be estimated by solving the linear relaxation with the barrier method and without objective (Atkinson and Vaidya 1995, Bonami et al. 2020). By using this analytic center, the Pareto-optimal cut generation procedure is similar to the *in-and-out* stabilisation technique presented in, e.g., Ben-Ameur and Neto (2007).

Benders Dual Decomposition In Benders Dual Decomposition, information from the main problem is added to the Benders subproblems to generate better quality cuts. This is done via allowing some (or potentially all) of the upper level variables to change based on the dual information. Following the work in Rahmaniani et al. (2020), auxiliary variables y_i^t are created by duplicating the decision variables x_i^t. These auxiliary variables are then forced to match a fractional or integer candidate solution $\tilde{x}_i^t$ in the Benders subproblem, resulting in the following subproblem:

$$\text{PSP}\left(\tilde{x}\right) = \text{Maximise} \sum_{t=1}^{T} \sum_{j \in J} d_j^t z_j^t, \tag{4.11a}$$

$$\text{subject to } y_i^t = \tilde{x}_i^t, \qquad 1 \leq t \leq T, i \in I, \tag{4.11b}$$

$$z_j^t \leq \sum_{i \in I} a_{ij}^t y_i^t, 1 \leq t \leq T, j \in J, \tag{4.11c}$$

$$y \in \Omega, \tag{4.11d}$$

$$z_j^t \in [0,1], \qquad 1 \leq t \leq T, j \in J. \tag{4.11e}$$

In its current form, the subproblem (4.11) is entirely equivalent to the original subproblem (4.4). However, by applying Lagrangian relaxation on the Constraints (4.11b), for a given Lagrangian multiplier λ_i^t for each $1 \leq t \leq T$ and $i \in I$, we obtain the following Lagrangian subproblem:

$$\text{LSP1}\left(\tilde{x}, \lambda\right) = \text{Maximise} \sum_{t=1}^{T} \sum_{i \in I} \left(d_j^t z_j^t - \lambda_i^t \left(y_i^t - \tilde{x}_i^t\right)\right), \tag{4.12a}$$

$$\text{subject to } (4.11\text{c}) - (4.11\text{e}). \tag{4.12b}$$

If we take $\lambda_i^t = \tilde{\lambda}_i^t$ as the optimal dual variables associated with Constraints (4.11b) after solving the subproblem (4.11) and $\bar{y}, \bar{z}$ as the optimal solutions of subproblem $\text{LSP1}\left(\tilde{x}, \tilde{\lambda}\right)$, this results in the optimality cuts

$$\theta \leq \sum_{t=1}^{t} \sum_{j \in J} d_j^t \bar{z}_j^t - \sum_{t=1}^{T} \sum_{i \in I} \tilde{\lambda}_i^t \left(\bar{y}_i^t - x_i^t\right). \tag{4.13}$$

In Rahmaniani et al. (2020), it was shown that the cuts (4.13) are equivalent to the standard optimality cuts (4.6) when generated from an integer candidate solution $\tilde{x}$. On the other hand, the authors also show that the cuts (4.13) are stronger than cuts (4.6) when generated from a fractional candidate solution.

If we further solve the full Lagrangian subproblem

$$\text{LSP2}\left(\tilde{x}\right) = \text{Minimise}_{\lambda}\left(\text{LSP1}\left(\tilde{x}, \lambda\right)\right), \tag{4.14}$$

with optimal solutions $\bar{\lambda}, \bar{y}, \bar{z}$, we obtain the following optimality cuts:

$$\theta \leq \sum_{t=1}^{t} \sum_{j \in J} d_j^t \bar{z}_j^t - \sum_{t=1}^{T} \sum_{i \in I} \bar{\lambda}_i^t \left(\bar{y}_i^t - x_i^t \right). \tag{4.15}$$

As before, Rahmaniani et al. (2020) show that the cuts (4.15) are only useful for a fractional candidate solution, where the cuts (4.15) are stronger than both the standard optimality cuts (4.6) and the cuts (4.13).

However, in order to apply the Benders dual decomposition approach, we must repeatedly solve Lagrangian subproblems. Notably, depending on the structure of Ω and the sizes of I, solving the Lagrangian subproblems (4.12) or (4.14) may be computationally infeasible. As such, contrary to the other acceleration techniques discussed in this work, the viability of this method is dependent on the application.

Partial Benders Decomposition In Partial Benders Decomposition, information from the Benders subproblem is added to the main problem to improve the dual bound. This is done via including some variables of the Benders subproblem in the main problem. Following the work in Crainic et al. (2021), we partition J into two sets, $\bar{J}$ and $J \setminus \bar{J}$, and define the following reformulation of the maximum covering problem:

$$\text{Maximise} \sum_{t=1}^{T} \left(\sum_{j \in \bar{J}} d_j^t z_j^t + \sum_{j \in J \setminus \bar{J}} d_j^t z_j^t \right), \tag{4.16a}$$

$$\text{subject to (4.1b), (4.1d)} \tag{4.16b}$$

$$\sum_{i \in I} a_{ij}^t x_j^t \geq z_j^t, \qquad 1 \leq t \leq T, j \in \bar{J}, \tag{4.16c}$$

$$\sum_{i \in I} a_{ij}^t x_j^t \geq z_j^t, \qquad 1 \leq t \leq T, j \in J \setminus \bar{J}, \tag{4.16d}$$

$$z_j^t \in \{0,1\} \qquad 1 \leq t \leq T, j \in \bar{J}, \tag{4.16e}$$

$$z_j^t \in \{0,1\} \qquad 1 \leq t \leq T, j \in J \setminus \bar{J}. \tag{4.16f}$$

This formulation is, clearly, equivalent to the original formulation (4.1). However, when we project the z variables for the Benders decomposition, we keep the variables $z_j^t, j \in \bar{J}$ in the main problem. More specifically, in iteration v of the Benders

decomposition method, our main problem is given by

$$\text{Maximise } \theta + \sum_{t=1}^{T} \sum_{j \in \bar{J}} d_j^t z_j^t, \tag{4.17a}$$

$$\text{subject to } (4.1\text{b}), (4.1\text{d}), (4.3\text{b}), (4.3\text{c}) \tag{4.17b}$$

$$\sum_{t=1}^{T} \sum_{i \in I} a_{ij}^t x_j^t \geq z_j^t, \qquad 1 \leq t \leq T, j \in \bar{J}, \tag{4.17c}$$

$$z_j^t \in \{0, 1\} \qquad 1 \leq t \leq T, j \in \bar{J}, \tag{4.17d}$$

and the Benders primal subproblem is then given by

$$\text{Maximise } \sum_{t=1}^{T} \sum_{j \in J \setminus \bar{J}} d_j^t z_j^t, \tag{4.18a}$$

$$\text{subject to } z_j^t \leq \tilde{I}_j^t, \qquad 1 \leq t \leq T, j \in J \setminus \bar{J}, \tag{4.18b}$$

$$z_j^t \in [0, 1], \qquad 1 \leq t \leq T, j \in J \setminus \bar{J}, \tag{4.18c}$$

for which optimality cuts can be derived as before.

The users j' in J_s are particularly well-suited for scenario retention, i.e. to make $\bar{J} = J_s$. If we take $j' \in J_s$, by definition,, we have that $\sum_{t=1}^{T} \sum_{i \in I} a_{ij'}^t = 1$. Next, we take the period t' and the facility i' such that $a_{i'j'}^{t'} = 1$. Then, since $d_j^t > 0$ by definition, we have that Constraint (4.17c) will be satisfied with equality. As such, the variable $z_{j'}^{t'}$ can be removed from the main program (4.17), and the objective function can be replaced by

$$\theta + \sum_{t=1}^{T} \sum_{i \in I} \left(\sum_{j \in J_s} a_{ij}^t d_j^t \right) x_i^t.$$

This scenario retention process is equivalent to the *singleton aggregation* pre-processing technique used in Güney et al. (2021), Chen et al. (2023), which replaces z_j^t by x_i^t if $j \in J_s$ and $a_{ij}^t = 1$. We note that, after this process, the Benders cuts of type (B0) and (B1) coincide (as do their multi-cut equivalents).

In addition to the scenario-retention method proposed in Crainic et al. (2021), the authors also propose a scenario-creation method. This involves the creation of artificial scenarios given by a convex combination of real scenarios. These artificial scenarios are then kept in the main problem as a proxy for their subproblem counterparts. A more recent approach proposed in Ramírez-Pico et al. (2023), called *adaptive Benders cuts*, follows a similar procedure. Rather than creating artificial scenarios *a priori*, it dynamically bundles scenarios which share the same dual solution. However, these methods rely on the variables z_j^t, which are no longer present in the branch-and-Benders-cut framework presented in Section 4.4.1. As such, these approaches are not well-suited for this framework, and further research would be necessary for their successful integration.

4.5 Local Branching for Branch-And-Benders-Cut

In the local branching method by Fischetti and Lodi (2003) for tackling mixed-integer programs, small subdomains of the feasible space are defined via distance-based neighbourhoods around solutions. These small subdomains are then solved in a separate subproblem via a black-box solver, and excluded from the feasible space, thus gradually reducing the size of the search space. In Rei et al. (2009), this process was applied to a branch-and-Benders-cut framework, with the goal of simultaneously improving the upper and lower bounds for the search tree.

We start in Section 4.5.1 by presenting the framework (following the work in Rei et al. 2009) for embedding a local branching approach within our branch-and-Benders-cut method. This defines a modified main problem and the necessary subproblems, which are all reliant on a distance metric. In Section 4.5.2, we propose a new distance metric for the dynamic MCLP. Via this distance metric, we then provide a novel solution method for quickly solving subproblems. Finally, in Section 4.5.3, we discuss methods for separating the feasible subdomains explored in our subproblems.

4.5.1 Overview

We implement the local branching scheme within the framework of our branch-and-Benders-cut methods, as proposed in Rei et al. (2009). Since it is based on our branch-and-Benders-cut methods, any of the acceleration techniques presented in Section 4.4.2 can be applied to the local branching method as well. To that end, contrary to Section 4.4.2, we present this section using the multi-cut version of the Benders optimality cuts. Due to the central role of the time period in the proceeding developments, the multi-cut formulation allows for a more natural and interpretable explanation. Thus, at iteration v of the Benders decomposition, we consider the following local branching main problem:

$$\text{Maximise} \quad \sum_{t=1}^{T} \theta^t, \tag{4.19a}$$

$$\text{subject to} \quad (4.1b), (4.1d), (4.3c)$$

$$\sum_{i \in I} \left(\sum_{j \in \Gamma^t(x^{rt})} d_j^t a_{ij}^t \right) x_j^t \geq \theta^t - \sum_{j \in J \setminus \Gamma^t(x^{rt})} d_j^t, \quad 1 \leq t \leq T, 1 \leq r \leq v, \tag{4.19b}$$

$$\text{Dist}_{x^s}(x) \geq \kappa^s, \qquad 1 \leq s \leq u, \tag{4.19c}$$

where x^s for $1 \leq s \leq u$ are feasible facility location decisions previously determined. We omit the index s when there is no risk of confusion. The function Dist_{x^s} represents a distance metric, indicating that only solutions found at a distance κ^s from solution x^s may be considered. We note that Constraints (4.19b) are the Benders optimality cuts (4.7c) provided by Proposition 4.4.2.

Our goal, given an integer candidate solution $\tilde{x}$ and a threshold distance $\tilde{\kappa}$, is to find the optimal solution to our original problem (4.1) restricted to distance $\tilde{\kappa}$ around $\tilde{x}$. As described in Rei et al. (2009), we can then generate Benders optimality cuts (4.8) for this high-quality solution, thus improving the upper bound in the local branching main problem (4.19). Simultaneously, the solution may also improve upon the incumbent, thus also increasing the lower bound. We can then exclude the subdomain of distance $\tilde{\kappa}$ around $\tilde{x}$ from the local branching main problem (4.19) by adding a constraint of type (4.19c).

Formally, let $\hat{x}$ denote the optimal solution to the *restricted subproblem* centered around $\tilde{x}$, given by the solution to the following subproblem:

$$\text{Maximise} \sum_{t=1}^{T} \sum_{j \in J} d_j^t z_j^t, \tag{4.20a}$$

$$\text{subject to } (4.1\text{b}), (4.1\text{d}), (4.4\text{d}), (4.4\text{c}), (4.19\text{c}),$$

$$\text{Dist}_{\tilde{x}}(x) \leq \tilde{\kappa}. \tag{4.20b}$$

If $\hat{x}$ has a strictly higher objective than $\tilde{x}$, we generate Benders optimality cuts (4.8) for $\tilde{x}$, and we set $x^{s+1} = \tilde{x}, \kappa^{s+1} = \tilde{\kappa} + 1, s = s + 1$ and repeat the restricted problem (4.20) centered around $\hat{x}$. If $\hat{x} = \tilde{x}$, we create a *diversified subproblem* which replaces the threshold distance $\tilde{\kappa}$ in Constraint (4.20b) with $\tilde{\kappa}' > \tilde{\kappa}$, and adds the constraint $\text{Dist}_{\tilde{x}}(x) \geq 1$. This guarantees that the resulting optimal solution $\hat{x}$ is different than $\tilde{x}$, and we create Benders optimality cuts (4.8) from $\hat{x}$.

By setting $x^{s+1} = \tilde{x}, \kappa^{s+1} = \tilde{\kappa} + 1$, we ensure that the feasible domain in the restricted subproblem (4.20) in iteration v and the main problem in iteration $v+1$ are complementary. More specifically, the restricted subproblem only considers solutions with distance $\text{Dist}_{\tilde{x}}(x) \leq \tilde{\kappa}$, whereas the main problem considers solutions with distance $\text{Dist}_{\tilde{x}}(x) \geq \tilde{\kappa}+1$. Since the candidate solution $\tilde{x}$ is integer feasible, it is not necessary to consider solutions with distance $\text{Dist}_{\tilde{x}}(x) \in (\tilde{\kappa}, \tilde{\kappa}+1)$, as these correspond to fractional solutions.

We remark that the local branching main problem (4.19) and the restricted subproblem (4.20) can be defined via any distance metric and with any threshold distance $\tilde{\kappa}$. By increasing the size of the subdomain, we can remove a larger area from the feasible space of the local branching main problem (4.19), but at the cost of a restricted subproblem (4.20) that is harder to solve than that of a smaller size. We also note that any method can be used to find the optimal solution $\hat{x}$ to the restricted subproblem (4.20). In Fischetti and Lodi (2003), a general-purpose mixed-integer linear solver is used, while the branch-and-Benders-cut approach with the acceleration techniques proposed in Section 4.4.2 is a natural choice in our case. However, by carefully selecting our distance metric and threshold distance

$\tilde{\kappa}$, we can derive an exact solution method for the restriced subproblem (4.20) which is more effective than the accelerated branch-and-Benders-cut method.

4.5.2 An Effective Formulation for a Tailored Distance Metric

The distance metric typically used is the Hamming distance (see, e.g., Fischetti and Lodi 2003, Rei et al. 2009). This results in Constraint (4.20b) taking the form

$$\sum_{t=1}^{T} \sum_{i \in I: \tilde{x}_i^t = 1} \left(1 - x_i^t\right) + \sum_{t=1}^{T} \sum_{i \in I: \tilde{x}_i^t = 0} x_i^t \leq \tilde{\kappa}. \tag{4.21}$$

However, we propose to use a modified distance metric in the dynamic case, which enforces that the Hamming distance in each time period must be within our threshold. This results in Constraint (4.20b) taking the form

$$\sum_{i \in I: \tilde{x}_i^t = 1} \left(1 - x_i^t\right) + \sum_{i \in I: \tilde{x}_i^t = 0} x_i^t \leq \tilde{\kappa}, \ 1 \leq t \leq T. \tag{4.22}$$

The motivation behind this new distance metric derives from infrastructure contexts, where the facilities under consideration correspond to significant investments (e.g. warehouses, stores, etc.). In those contexts, facilities which are added in early time periods are likely to persist throughout the time horizon. In the case of the general Hamming distance, this incurs a repeated penalty in each time period, increasing the total distance. As an illustration, consider the example in A.2.1 and the two solutions $x^t = (1, 0, 0)$ and $\hat{x}^t = (1, 1, 0), 1 \leq t \leq T$, and a time horizon $T = 4$. These solutions are at distance 4 when considering the general Hamming distance, whereas they are only at distance 1 using the new metric.

An important benefit of this new distance metric allows for an efficient solving method if we consider $\tilde{\kappa} = 2$. To describe this method we first note that, for a candidate solution $\tilde{x}$ and time period t, there are only two sets of modifications which result in an integer solution at distance exactly 1:

1a) Add one facility which is currently not selected.

1b) Remove one facility which is currently selected.

Likewise, at distance exactly 2, there are only three sets of modifications:

2a) Add two facilities which are currently not selected.

2b) Remove one facility which is currently selected, and add one facility which is currently not selected.

2c) Remove two facilities which are currently selected.

Since, by assumption $a_{ij}^t \in \{0,1\}$ and $d_j^t > 0$, options 1b) and 2c) cannot lead to an increase in the objective function, and hence, can be disregarded.

As a consequence, there is a limited number of feasible solutions contained within the restricted subproblem (4.20) when considering $\tilde{\kappa} = 2$. We can then use Proposition 4.5.1 to evaluate the quality of feasible solutions (as given in Equation (4.2)) based on Benders optimality cuts.

Proposition 4.5.1. *Let x be an (integer) feasible solution to the maximum covering model* (4.1)*, and let t be any time period, $1 \leq t \leq T$. Let $\hat{i} \in I$ be such that $x_{\hat{i}}^t = 0$. Then the modified solution $\hat{x}$ with $\hat{x}_{\hat{i}}^t = 1$ and $\hat{x}_i^t = x_i^t, i \neq \hat{i}$ satisfies*

$$\sum_{i \in I} \left(\sum_{j \in \Gamma^t(x^t)} d_j^t a_{ij}^t \right) \hat{x}_i^t + \sum_{j \in J \setminus \Gamma^t(x^t)} d_j^t = \sum_{j \in J} \min \left\{ 1, \sum_{i \in I} a_{ij}^t \hat{x}_i^t \right\},$$

when $\Gamma^t(x^t)$ is given by (B0) *or* (B1)*.*

Proof. We first note that, by rearranging the terms in the left-hand side, we have that

$$\sum_{i \in I} \left(\sum_{j \in \Gamma^t(x^t)} d_j^t a_{ij}^t \right) \hat{x}_i^t + \sum_{j \in J \setminus \Gamma^t(x^t)} d_j^t = \sum_{j \in \Gamma^t(x^t)} \left(\sum_{i \in I} a_{ij}^t \hat{x}_i^t \right) d_j^t + \sum_{j \in J \setminus \Gamma^t(x^t)} d_j^t.$$

Now, we concentrate on both cases for $\Gamma^t(x^t)$.

If $\Gamma^t(x^t)$ is given by (B0), then we have that

$$\begin{aligned} \sum_{j \in \Gamma^t(x^t)} \left(\sum_{i \in I} a_{ij}^t \hat{x}_i^t \right) d_j^t + \sum_{j \in J \setminus \Gamma^t(x^t)} d_j^t &= \sum_{j \in J : I(x)_j^t < 1} \left(\sum_{i \in I} a_{ij}^t \hat{x}_i^t \right) d_j^t + \sum_{j \in J : I(x)_j^t \geq 1} d_j^t, \\ &= \sum_{j \in J : I(x)_j^t = 0} \left(\sum_{i \in I \setminus \{i\}} a_{ij}^t x_i^t + a_{\hat{i}j}^t \right) d_j^t + \sum_{j \in J : I(x)_j^t \geq 1} d_j^t, \end{aligned}$$

where $I(x)_j^t = \sum_{i \in I} a_{ij}^t x_i^t < 1$ implies that $I(x)_j^t = 0$, since all elements in the summation are binary.

From there, for the first term, $a_{\hat{i}j}^t$ being binary also implies that $\sum_{i \in I} a_{ij}^t \hat{x}_i^t = \sum_{i \in I \setminus \{\hat{i}\}} a_{ij}^t x_i^t + a_{\hat{i}j}^t = I_j^t(x) + a_{\hat{i}j}^t \leq 1$. As such, we have that

$$\sum_{j \in J: I(x)_j^t = 0} \left(\sum_{i \in I \setminus \{\hat{i}\}} a_{ij}^t x_i^t + a_{\hat{i}j}^t \right) d_j^t = \sum_{j \in J: I(x)_j^t = 0} \min\{1, \sum_{i \in I} a_{ij}^t \hat{x}_i^t\} d_j^t.$$

For the second term, we note that since $\hat{x}$ has an extra facility compared to x, we also have that the coverage for each user must be equal or greater. Concretely, $I(x)_j^t = \sum_{i \in I} a_{ij}^t x_i^t \leq \sum_{i \in I} a_{ij}^t \hat{x}_i^t$, and thus

$\sum_{j \in J: I(x)_j^t \geq 1} d_j^t = \sum_{j \in J: I(x)_j^t \geq 1} \min\{1, \sum_{i \in I} a_{ij}^t \hat{x}_i^t\} d_j^t$.

As a consequence, we have that

$$\sum_{j \in J: I(x)_j^t = 0} \left(\sum_{i \in I \setminus \{\hat{i}\}} a_{ij}^t x_i^t + a_{\hat{i}j}^t \right) d_j^t + \sum_{j \in J: I(x)_j^t \geq 1} d_j^t = \sum_{j \in J} \min\{1, \sum_{i \in I} a_{ij}^t \hat{x}_i^t\} d_j^t.$$

If $\Gamma^t(x^t)$ is given by (B1), then we have that

$$\begin{aligned} &\sum_{j \in \Gamma^t(x^t)} \left(\sum_{i \in I} a_{ij}^t \hat{x}_i^t \right) d_j^t + \sum_{j \in J \setminus \Gamma^t(x^t)} d_j^t \\ =& \sum_{j \in J_s} \left(\sum_{i \in I} a_{ij}^t \hat{x}_i^t \right) d_j^t + \sum_{j \in J \setminus J_s: I(x)_j^t < 1} \left(\sum_{i \in I} a_{ij}^t \hat{x}_i^t \right) d_j^t + \sum_{j \in J \setminus J_s: I(x)_j^t \geq 1} d_j^t. \end{aligned}$$

We note that, by definition of the set J_s, we always have that $\sum_{i \in I} a_{ij}^t \hat{x}_i^t \leq 1$. As a consequence, we have that $\sum_{j \in J_s} \left(\sum_{i \in I} a_{ij}^t \hat{x}_i^t \right) d_j^t = \sum_{j \in J_s} \min\{1, \sum_{i \in I} a_{ij}^t \hat{x}_i^t\} d_j^t$. The last two terms can be transformed using reasoning similar to that of the prior case, which gives our result.

□

We remark that Proposition 4.5.1 does not hold in general if $\Gamma^t(x^t)$ is given by (B2). As a counterexample if $\Gamma^t(x^t)$ is given by (B2), consider the example in

A.2.1, the candidate solution $x = (1, 0, 0)$, and $\hat{i} = i_2$. We then have that

$$\sum_{i \in I} \left(\sum_{j \in \Gamma^t(x^t)} d_j^t a_{ij}^t \right) \hat{x}_j^t + \sum_{j \in J \setminus \Gamma^t(x^t)} d_j^t = 36, \tag{4.23}$$

$$\sum_{t=1}^{T} \sum_{j \in J} \min \left\{ 1, \sum_{i \in I} a_{ij}^t \hat{x}_i^t \right\} = 28. \tag{4.24}$$

Put more simply, Proposition 4.5.1 states that if we take a given solution x and only add one facility to it, then the Benders optimality cuts for x accurately give the coverage for the modified solution.

We can then derive an efficient method for finding the optimal solution of distance two around $\tilde{x}$ by combining the limited number of valid modifications to $\tilde{x}$ along with Proposition 4.5.1. For this, let e^i denote the elemental vector with 1 in position i and 0 elsewhere. We then denote $x^t + e^i$ (respectively, $x^t - e^i$) as the modified solution which adds the currently unused facility i in period t (respectively, removes the currently used facility i). We present this method in Proposition (4.5.2).

Proposition 4.5.2. *Let $\hat{x}_j^t$ denote the optimal values for the variables x_j^t in the restricted subproblem* (4.20) *around an integer candidate solution $\tilde{x}$ at distance $\tilde{\kappa} = 2$. Then $\hat{x}_j^t$ are also the optimal values for the variables x_j^t in the following*

problem:

$$\text{Maximise} \sum_{t=1}^{T} \theta^t, \tag{4.25a}$$

$$\text{subjectto} (4.1b), (4.1d), (4.3b), (4.3c), (4.19c),$$

$$\sum_{i \in I : \tilde{x}_i^t = 1} \left(1 - x_i^t\right) + \sum_{i \in I : \tilde{x}_i^t = 0} x_i^t \leq 2, \qquad 1 \leq t \leq T, \tag{4.25b}$$

$$\sum_{i \in I} \left(\sum_{j \in J \setminus \Gamma^t(\tilde{x}^t)} a_{ij}^t d_j^t \right) x_i^t + \sum_{j \in \Gamma^t(\tilde{x}^t)} d_j^t \geq \theta^t, \qquad 1 \leq t \leq T, \tag{4.25c}$$

$$\sum_{i \in I} \left(\sum_{j \in J \setminus \Gamma^t(\tilde{x}^t + e^{\hat{i}})} a_{ij}^t d_j^t \right) x_i^t + \sum_{j \in \Gamma^t(\tilde{x}^t + e^{\hat{i}})} d_j^t \geq \theta^t, 1 \leq t \leq T, \hat{i} : \tilde{x}_{\hat{i}}^t = 0, \tag{4.25d}$$

$$\sum_{i \in I} \left(\sum_{j \in J \setminus \Gamma^t(\tilde{x}^t - e^{\hat{i}})} a_{ij}^t d_j^t \right) x_i^t + \sum_{j \in \Gamma^t(\tilde{x}^t - e^{\hat{i}})} d_j^t \geq \theta^t, 1 \leq t \leq T, \hat{i} : \tilde{x}_{\hat{i}}^t = 1. \tag{4.25e}$$

Proof. The feasible space for the variables x_j^t are defined via

Constraints (4.1b), (4.1d), (4.19c),

and (4.25b). Since these constraints are present in both models, it follows that the set of feasible values for x_j^t are the same. We now show that the objective value for every feasible solution x is the same in both models.

From our previous discussion, there is a limited number of feasible solutions which we must consider: the solution $\tilde{x}$ itself, as well as the resulting solutions from modifications 1a), 2a) and 2b). The value of the solution $\tilde{x}$ is given by Constraint (4.25c). For all other solutions, we make use of Proposition 4.5.1. More specifically, for each type of modification, we have generated an optimality cut for a solution with exactly one fewer facilities:

— Constraints (4.25c) generate optimality cuts for the solution $\tilde{x}^t$ for all time periods t. As a consequence, all solutions which add one facility to $\tilde{x}$ (i.e. modifications of type 1a) are evaluated correctly.

— Constraints (4.25d) generate optimality cuts for the solutions $\tilde{x}^t + e^{\hat{i}}$ for all time periods t and for all facilities $\hat{i}$ which are currently not installed. As a consequence, all solutions which add one additional facility beyond $\tilde{x}^t + e^{\hat{i}}$ (thus modifications of type 2a) are evaluated correctly.

— Constraints (4.25e) generate optimality cuts for the solutions $\tilde{x}^t - e^{\hat{i}}$ for all time periods t and for all facilities $\hat{i}$ which are currently not installed. As a consequence, all solutions removing $\hat{i}$ and then adding another facility (thus modifications of type 2b) are evaluated correctly.

□

We note the following observations about Proposition 4.5.2:

— Due to the presence of Constraints (4.1d), model (4.25) is a mixed-integer linear program, which can be solved directly via a generic MILP solver. When solving model (4.25) directly with a generic solver is the strategy for finding the optimal solution to the restricted subproblem (4.20), we denote this as SubD. When, instead, the restricted subproblem (4.20) is solved via the branch-and-Benders-cut method, we denote this SubB.

— Some of Constraints (4.25c)-(4.25e) may be redundant, in the sense that they allow for the evaluation of solutions which can either be evaluated using other constraints within the model or which correspond to infeasible solutions. In general, verifying the feasibility of the solutions before generating the associated Constraints (4.25d) or (4.25e) is unlikely to be beneficial, due to the speed at which these constraints can be built. Instead, infeasible solutions can be detected by the MILP solver via Constraints (4.1b) and (4.19c). However, some structures of Ω may make the detection of some infeasible solutions a trivial task, such as the use of precedence constraints, and thus justify the computational effort of the verification process.

— From the proof of Proposition 4.5.2, it is clear that the optimal objective value of the restricted subproblem (4.20) and of model (4.25) are the same. This is important, as it allows us to verify if the newly found solution has a better objective value than the incumbent, and update the incumbent accordingly.

Remark: As with the Benders cuts themselves, Propositions 4.5.1 and 4.5.2

can be interpreted quite naturally through the lens of submodular optimisation. The submodular versions of these propositions are presented in A.2.2.

4.5.3 Branching

Using Proposition 4.5.2, we can thus easily solve the restricted subproblem (4.20). However, this ease of solving comes at a cost when moving to solve the full problem (4.19).

After each candidate solution $\tilde{x}$ and the set of restricted and diversified subproblems, the Constraints (4.19c) ensure that the solver removes the subdomain examined during the subproblems, thus avoiding unnecessary work. In Rei et al. (2009), the Hamming distance is used in Constraints (4.19c), and hence, the complement of the set $\tilde{\Omega} = \{x \in \Omega : (4.1\text{d}), \text{Dist}_{\tilde{x}}(x) \leq \tilde{\kappa}\}$ is simply

$$\tilde{\Omega}^{\mathbf{c}} = \left\{ x \in \Omega : (4.1\text{d}), \sum_{t=1}^{T} \sum_{i \in I : \tilde{x}_i^t = 1} \left(1 - x_i^t\right) + \sum_{i \in I : \tilde{x}_i^t = 0} x_i^t \geq \tilde{\kappa} + 1 \right\}.$$

However, using the distance metric in Section 4.5.2, the set $\tilde{\Omega}^{\mathbf{c}}$ requires the Hamming distance to be at least $\tilde{\kappa}+1$ in at least one time period, which cannot be modeled as a single linear constraint. Therefore, we must create a branch for each time period in order to mimic $\tilde{\Omega}^{\mathbf{c}}$ through T disjoint problems. More specifically, for every $1 \leq t' \leq T$, we generate the following problem:

$$\begin{aligned}
\text{Maximise} \quad & \sum_{t=1}^{T} \theta^t, && (4.26\text{a}) \\
\text{subject to} \quad & (4.1\text{b}), (4.1\text{d}), (4.3\text{c}), (4.19\text{b}), (4.19\text{c}), \\
& \sum_{i \in I : \tilde{x}_i^{t'} = 1} \left(1 - x_i^{t'}\right) + \sum_{i \in I : \tilde{x}_i^{t'} = 0} x_i^{t'} \geq \tilde{\kappa} + 1, && (4.26\text{b}) \\
& \sum_{i \in I : \tilde{x}_i^{t} = 1} \left(1 - x_i^{t}\right) + \sum_{i \in I : \tilde{x}_i^{t} = 0} x_i^{t'} \leq \tilde{\kappa}, t < t'. && (4.26\text{c})
\end{aligned}$$

Each of these problems can be viewed as a branch at node $\tilde{x}$ in the search tree. In this way, the Constraints (4.19c) are formed of the branching constraints (4.26b) and (4.26c) from the prior nodes in the search tree. In essence, these branches

progressively select each time period as the one that exceeds the threshold distance, and impose all prior years to be below the threshold in order to ensure distinct sets. When using these branches to separate the subdomains of the restricted and diversified subproblems, we refer to the method as SepB.

Alternatively, we can model this disjunction through a set of cuts, requiring the introduction of auxiliary binary variables and Big-M constraints. More specifically, the set $\tilde{\Omega}^{\mathbf{c}}$ can be obtained by adding to Constraints (4.19c) the constraints

$$\sum_{i:\tilde{x}_i^t=1}(1-x_i^t)+\sum_{i:\tilde{x}_i^t=0}x_i^t+\tilde{\delta}^t(\tilde{\kappa}+1)\geq\tilde{\kappa}+1,\quad 1\leq t\leq T, \tag{4.27a}$$

$$\sum_{t=1}^{T}\tilde{\delta}^t\leq T-1, \tag{4.27b}$$

$$\tilde{\delta}^t\in\{0,1\},\quad 1\leq t\leq T. \tag{4.27c}$$

However, since we are adding the binary variables $\tilde{\delta}^t$ and the Big-M constraints (4.27a) to the main program (4.19), the problem gets progressively more difficult to solve as more subdomains are removed. When using this disjunction to separate the subdomains of the restricted and diversified subproblems, we refer to the method as SepD.

We note that in the case that the distance $\tilde{\kappa}=0$, the Constraints (4.27) are equivalent to (and thus can be replaced by) the typical no-good cut:

$$\sum_{t=1}^{T}\left(\sum_{i:\tilde{x}_i^t=1}(1-x_i^t)+\sum_{i:\tilde{x}_i^t=0}x_i^t\right)\geq 1, \tag{4.28}$$

which does not require the use of binary auxiliary variables.

4.6 Computational Experiments

In this section, we compare the performance of the variations of the Benders decomposition techniques presented in this work. We start in Section 4.6.1 by giving the background information for the problem instances, which are obtained from an

electric vehicle (EV) charging station location model, and based on real-life data. In Section 4.6.2, we then examine the performance metrics when using our Benders decomposition methods to solve these problem instances, which clearly demonstrates the capabilities and limitations of each method on a practical example. To better demonstrate the effects of each acceleration technique, in Section 4.6.3 we present new synthetic instances. These instances allow us to compare performance metrics of the proposed methods, along with applying each technique in isolation. In Section 4.6.4, we evaluate the options for the local branching method presented in Section 4.5.2 for the restricted subproblem solution method. These experiments demonstrate the efficiency of solving our reformulated restricted subproblem (4.25), validating its use in Section 4.6.2. Similarly, in Section 4.6.5, we compare the options for eliminating feasible space already explored within the local branching method, as presented in Section 4.5.3. Additionally, we discuss the technical limitations that face the implementation of the SepB method, and the consequences of using either the SepD or SepBmethods.

To more easily distinguish between the methodologies discussed in this paper, we present the following nomenclature:

1. The unaccelerated branch-and-Benders-cut procedure in Cordeau et al. (2019) as described in Section 4.4.1 is referred to as the U-B&BC method.
2. The accelerated branch-and-Benders-cut procedure presented in Section 4.4.2 is referred to as the A-B&BC method. We describe the set of acceleration techniques in more detail in Section 4.6.1.
3. The accelerated branch-and-Benders-cut procedure with local branching presented in Section 4.5 is referred to as the A-B&BC+LB-Sub-Sep method, where Sub indicates the restricted subproblem solution method as described in Section 4.5.2 and Sep indicates the subdomain separation scheme as described in Section 4.5.3. In all cases, we impose a time limit of 60 seconds for the solving of each restricted and diversified subproblem, after which the the best incumbent solution is used for the subsequent procedures.

The tests were run on a server running Linux version 3.10, with an Intel Core i7-4790 CPU with eight virtual cores and 32 GB of RAM. The code is written in

C++, and is publicly available [1]. We use CPLEX version 22.1.1 limited to a single thread, and with the Benders cuts implemented via the generic callback feature. Other than the removal of incompatible preprocessing and reformulation options in the cases which use the callback feature, the only notable parameters which are not set at default value are the memory management and numerical precision. The Eigen library (Guennebaud et al. 2010) is used for efficient dense and sparse matrix calculations, notably for the calculation of $\tilde{I}_j^t$ and the subsequent generation of cuts. In all tests, we impose a two-hour (7,200 second) time limit for solving each instance.

4.6.1 Application: Electric Vehicle Charging Station Placement

We apply the proposed methods to the instances of the electric vehicle (EV) charging station placement problem by Lamontagne et al. (2023). We chose these problem instances because of their practical interest and the large number of users, which leads to large-scale dynamic MCLPs and therefore allows us to demonstrate the capabilities of our methodological contributions.

In this problem, there are two groups making sequential decisions over a multi-period time span. First, a decision maker which decides where to place public charging infrastructure. And second, users purchasing a vehicle in the given time period, who must elect between an EV or a conventional vehicle (a choice which depends on the charging network). If a user is covered by a charging station (in the maximum covering sense), then they elect to purchase an EV. The objective of the decision maker is to place the charging infrastructure in such a way as to maximise EV adoption.

In addition to determining which charging stations to open, this problem also aims to find the optimal sizing (i.e. number of charging outlets) of each open station. For this purpose, the decision variables are binary, indicating if a charging station i has *at least* k outlets (with k ranging from 1 to an upper bound m_i). The set Ω is then composed of three sets of constraints: precedence constraints imposing for each station that in order to have at least $k+1$ outlets, one must first

1. https://github.com/StevenLamontagne/DynamicMCLP-AcceleratedBranchAndBendersCut

have at least k outlets, constraints that forbid the removal of outlets between time periods, and budget constraints which force the cost of installing new outlets to be below a budget B^t in each time period t. For these budget constraints, the first outlet at a charging station costs 150 while subsequent outlets each cost 50, with the budget $B^t = 400, 1 \leq t \leq T$.

The test instances are divided into five datasets, each with different characteristics and each containing 20 instances. The main characteristics of each dataset are shown in Table 4.2, though we refer to Lamontagne et al. (2023) for a detailed description. However we note that the Simple, Distance, and HomeCharging datasets are easier to solve than the LongSpan and Price datasets. Notably, no instance in the latter two datasets was solved exactly in Lamontagne et al. (2023), with the best incumbent objective value in the branch-and-cut method (via CPLEX 12.10) being below that of the greedy method described in that paper. As a consequence, we refer to the set of instances in the Simple, Distance, and HomeCharging datasets as the "easy instances", while those from the LongSpan and Price datasets are called the "hard instances".

Parameter	Simple	Distance	HomeCharging	LongSpan	Price
T	4	4	4	10	4
$\|I\|$	20	60	60	180	180
$\|J^t\|$ (per time period)	22575	22575	49905	147405	649605

Table 4.2 – Notable parameter values for the generated instances. The set of users J^t is generated separately in each time period, i.e. user j in period t has no relation to user j in period $t + 1$.

Next, we discuss the customisation of the acceleration techniques described in Section 4.4.2 used for this problem.

— There are two preprocessing techniques we can use to eliminate users from consideration, without affecting the objective value. The first technique, as proposed in Legault and Frejinger (2023), is to eliminate any users for which $a^t_{ij} = 0, \forall j \in J$. Note that such users they can never be covered regardless of our efforts, implying that their elimination does not affect the objective. The second technique is to eliminate any user which is "precovered" (in the sense that there is an existing facility or option which guarantees coverage, regardless of decisions in the model). In particular, in the HomeCharging

dataset, there are users who have access to a home charging system for their EV. As a consequence, a subset of those users will purchase an EV, regardless of the state of the public charging network, and can be eliminated from consideration.

— For a heuristic warmstart, we use the greedy method proposed in Lamontagne et al. (2023). This is achieved via the warmstart feature present in CPLEX.

— We keep the users $j \in J_s$ within the main problem, as described in Section 4.4.2.

— For the Benders optimality cuts, we use the multicut equivalent of the Pareto-optimal cuts in Proposition 4.4.3, using B1-type cuts. In other words, for $1 \leq t \leq T$, the sets $\Gamma^t(\tilde{x}^t)$ in Proposition 4.4.2 are given by

$$\Gamma^t(\tilde{x}^t) = \left\{ j \in J \setminus J_s : \tilde{I}_j^t < 1 \right\} \cup \left\{ j \in J \setminus J_s : \tilde{I}_j^t = 1, \overset{c^t}{I}_j < 1 \right\}. \tag{4.29}$$

The users $j \in J_s$ do not need to be considered, due to the partial Benders decomposition strategy mentioned above. We use the iterative method proposed in Papadakos (2008) for estimating a core point.

— In the cases of the LongSpan and Price datasets, CPLEX is unable to solve even the linear programming relaxation of model (4.1) as shown in Lamontagne et al. (2023). As such, we do not use Benders dual decomposition, as repeatedly solving the Lagrangian subproblems (4.12) or (4.14) would be computationally infeasible.

4.6.2 Comparison of Methodologies

In this section, we compare the performance of the U-B&BC, A-B&BC, and A-B&BC+LB-SubD-SepD methods for solving the instances. As will be discussed later, these options for the local branching method are the best suited for our application. Additionally, we compare these with a standard branch-and-cut tree via CPLEX, and the greedy method from Lamontagne et al. (2023). These last two methods are referred to as the B&C and Greedy methods, respectively.

We run the experiments both with and without using the greedy solution as a warmstart. This allows us to compare the ability of the methods to find high-

quality solutions, and to reduce the optimality gap. In Tables 4.3 and 4.4, we summarise our computational results for each methodology and instance set , respectively, without and with the greedy warmstart. The solving time, objective value, optimality gap, and number of nodes are reported as given by CPLEX. Notably, the"objective value" field presents the value of the incumbent solution if the optimality threshold has not been reached within the two-hour time limit. However, we note that the number of nodes in the local branching case only includes the ones for the main problem. In addition to these metrics, we also include the gap to the best solution, calculated as the relative gap in each instance between the objective value of a method and the best objective value among all methods.

Performance profiles for each method in the easy instances (combining all instances both with and without warmstart) are presented in Figure 4.1, indicating the percentage of instances solved by each method as a function of time. Additional performance details are presented in A.2.3 , including disaggregate performance profiles for the Simple, Distance, and HomeCharging datasets both with and without considering the warmstart solution.

By examining the results, we note that:

— The U-B&BC method without a warmstart is able to find a non-trivial solution (i.e. a solution which places at least one facility) for almost all instances, only failing to find a solution in one instance in the LongSpan dataset. However, it found worse quality solutions on average than the Greedy method, A-B&BC, and A-B&BC+LB-SubD-SepD methods in the hard instances. When given a warmstart solution, both the U-B&BC and the A-B&BC methods perform comparably to each other in regards to reducing the optimality gap.

— Without a warmstart, the A-B&BC method is able to find solutions of better quality than the U-B&BC method and reduce the optimality gap significantly more, on average. However, the A-B&BC method also failed to find non-trivial solutions in eight instances of the LongSpan dataset, significantly more than the U-B&BC method. In terms of solving time, the A-B&BC method was able to outperform the U-B&BC method in all instances. In addition, in the easy instances, the A-B&BC method is able to run faster than the B&C method. However, while it is able to reduce the

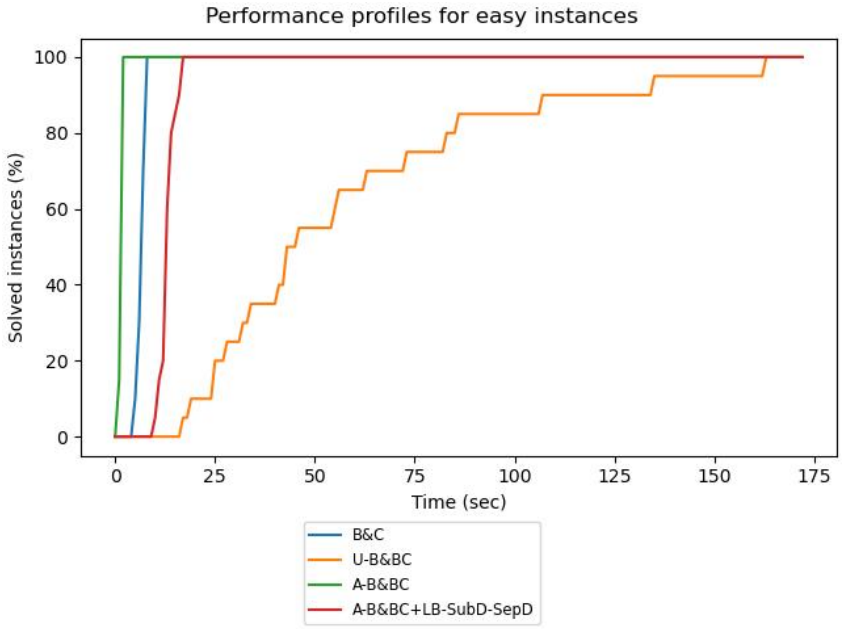

Figure 4.1 – Performance profiles showing the percentage of Simple, Distance, and Home-Charging instances solved by each method as a function of time, combining both with and without the warmstart solution.

optimality gap in the hard instances compared to the U-B&BC method, the objective value is only slightly better than the GREEDY method. In fact, when given the warmstart solution, the A-B&BC method only improved the objective value compared to the GREEDY method in two instances in the LongSpan dataset, and two instances in the Price dataset.

— The performance of the A-B&BC+LB-SUBD-SEPD method was nearly identical both with and without the warmstart solution. It required more time than either the A-B&BC or the B&C methods in the easy instances, and the optimality gap is considerably higher than the A-B&BC method in the hard instances. However, combining both with and without the warm-start, the A-B&BC+LB-SUBD-SEPD method improves the objective value compared to the GREEDY method in 39 instances in the LongSpan dataset and 37 instances in the Price dataset, which is notably more than the A-B&BC method.

Table 4.3 – Average performance details without greedy warmstart. Starred entries only include instances for which non-zero incumbent solutions were found. Entries in **bold** indicate the best performance across the exact methods in that dataset and metric.

		Simple	Distance	HomeCharging	LongSpan	Price
Solve time (sec)	Greedy	< 0.01	< 0.01	< 0.01	0.05	0.10
	B&C	0.20	0.70	6.56	7186.12	7194.97
	U-B&BC	0.15	1.57	68.24	7184.25	7184.76
	A-B&BC	**0.11**	**0.51**	**1.37**	7184.35	7184.57
	A-B&BC+LB-SubD-SepD	4.65	4.74	12.70	7313.04	7344.53
Objective value	Greedy	31814.20	16591.75	18016.47	133724.37	33641.74
	B&C	**31820.15**	**16627.14**	**18030.50**	0.00	0.00
	U-B&BC	**31820.15**	**16627.14**	**18030.50**	122803.68*	32563.31
	A-B&BC	**31820.15**	**16627.14**	**18030.50**	133613.34*	33623.02
	A-B&BC+LB-SubD-SepD	**31820.15**	**16627.14**	**18030.50**	**133772.68**	**33655.97**
Gap to best known solution (%)	Greedy	0.02	0.21	0.08	0.04	0.04
	B&C	**0.00**	**0.00**	**0.00**	-	-
	U-B&BC	**0.00**	**0.00**	**0.00**	8.20*	3.25
	A-B&BC	**0.00**	**0.00**	**0.00**	0.11*	0.10
	A-B&BC+LB-SubD-SepD	**0.00**	**0.00**	**0.00**	**0.00**	**0.00**
Optimality gap (%)	B&C	< **0.01**	< **0.01**	< **0.01**	-	-
	U-B&BC	< **0.01**	< **0.01**	< **0.01**	15.79*	15.00
	A-B&BC	< **0.01**	< **0.01**	< **0.01**	**6.20***	**11.49**
	A-B&BC+LB-SubD-SepD	< **0.01**	< **0.01**	< **0.01**	12.04	18.91
Number of nodes	B&C	59.25	43.35	**131.95**	0.00	0.00
	U-B&BC	**52.40**	**27.85**	228.50	0.00	0.00
	A-B&BC	152.10	84.50	1012.55	455.30	0.00
	A-B&BC+LB-SubD-SepD	65.05	187.30	795.25	**6435.35**	**1099.60**

Table 4.4 – Average performance details with greedy warmstart. Entries in **bold** indicate the best performance across the exact methods in that dataset and metric.

		Simple	Distance	HomeCharging	LongSpan	Price
Solve time, (sec)	Greedy	< 0.01	< 0.01	< 0.01	0.05	0.10
	B&C	0.23	0.70	6.46	7187.77	7196.19
	U-B&BC	0.14	1.13	58.23	7184.00	7185.39
	A-B&BC	**0.09**	**0.52**	**1.34**	7184.54	7185.04
	A-B&BC+LB-SubD-SepD	4.67	4.81	13.00	7291.34	7305.71
Objective value	Greedy	31814.20	16591.75	18016.47	133724.37	33641.74
	B&C	**31820.15**	**16627.14**	**18030.51**	133724.36	33641.73
	U-B&BC	**31820.15**	**16627.14**	**18030.51**	133724.36	33641.74
	A-B&BC	**31820.15**	**16627.14**	**18030.51**	133728.65	33642.19
	A-B&BC+LB-SubD-SepD	**31820.15**	**16627.14**	**18030.51**	**133781.88**	**33650.81**
Gap to best known solution (%)	Greedy	0.02	0.21	0.08	0.04	0.03
	B&C	**0.00**	**0.00**	**0.00**	0.04	0.03
	U-B&BC	**0.00**	**0.00**	**0.00**	0.04	0.03
	A-B&BC	**0.00**	**0.00**	**0.00**	0.04	0.03
	A-B&BC+LB-SubD-SepD	**0.00**	**0.00**	**0.00**	**0.00**	**0.00**
Optimality gap (%)	B&C	< **0.01**	< **0.01**	< **0.01**	25.07	52.84
	U-B&BC	< **0.01**	< **0.01**	< **0.01**	6.25	11.34
	A-B&BC	< **0.01**	< **0.01**	< **0.01**	**6.12**	**11.32**
	A-B&BC+LB-SubD-SepD	< **0.01**	< **0.01**	< **0.01**	11.86	18.66
Number of nodes	B&C	47.40	35.00	**109.30**	0.00	0.00
	U-B&BC	**41.90**	**17.65**	200.75	0.00	0.00
	A-B&BC	65.35	75.05	860.45	0.00	**1499.60**
	A-B&BC+LB-SubD-SepD	65.05	205.60	797.35	**7282.65**	1202.50

4.6.3 Comparison of Acceleration Techniques

To the best of our knowledge, the instances in Section 4.6.2 (from Lamontagne et al. 2023) are the only publicly available instances for the uncapacitated, dynamic MCLP. However, they are not sufficient to illustrate the performance differences among each of the acceleration techniques. As such, we use a modified version of the generation procedure in Zarandi et al. (2013) to create new instances, each with $T = 5$:

1. We randomly generate 20 facility locations on a 2D plane, with both coordinates drawn from a uniform $[0, 30)$ distribution. Each facility can be of size $k = 1, 2, 3$, or 4, with corresponding costs $150, 50, 50$ and 50. The total budget in each time period is 200.
2. For each time period t, we randomly generate 50,000 demand nodes, with both coordinates drawn from a uniform $[0, 30)$ distribution and with demand from a uniform $[0, 100)$ distribution.
3. A facility is considered to cover a demand node if the Euclidean distance between the facility i and the demand node j is below a threshold, which varies based on the size of the facility. For each value of S in $\{3.25, 3.75, 4.25\}$ we generate coverage parameters a as $a^t_{ijk} = 1$ if $\Delta(i, j) \leq S + 0.25k$, where $\Delta(i, j)$ denotes the Euclidean distance between facility i and user j. As such, the coverage depends not only on the initial coverage S but also on the size of the facility k.

The above procedure is repeated five times, creating a new dataset of 15 instances which we call *Medium*. This modified procedure maintains a similar Ω structure as the instances in Lamontagne et al. (2023), as well as a similarly high ratio of users to facilities. We recall that, as in Cordeau et al. (2019), this method is designed for applications with much larger numbers of users than facilities.

We note that these instances are designed for comparing the performances of the acceleration techniques. As such, they are principally designed to be more difficult for the branch-and-Benders-cuts methodologies, rather than the standard B&C method. To better compare these techniques, we create new methods which add a single acceleration technique to the unaccelerated branch-and-Benders-cut method of Cordeau et al. (2019). These new methodologies are denoted U-

B&BC+XX, where XX is MC for multi-cut generation, PO for Pareto-optimal cut generation, or PB for partial Benders decomposition.

In Table 4.5, we summarise our computational results for each methodology, with no warmstart applied in any method. The performance fields are identical to the prior section, with the addition of the number of instances solved. Further computational results are presented in A.2.3. We make the following observations about the performances:

— The comparative performances of the U-B&BC and A-B&BC methods are consistent with those presented in Section 4.6.2, with the solve time and optimality gap of the U-B&BC method higher than with the A-B&BC method. Additionally, the A-B&BC method was able to solve all instances for all values of S, contrary to the U-B&BC method.

— The average solve time and the number of nodes of the A-B&BC method were worse than the B&C method for $S = 3.25$, but better for $S = 3.75$ and $S = 4.25$. As both methods were able to solve all instances, the objective value and number of solved instances were identical.

— Similar to the U-B&BC method, the A-B&BC+LB-SubD-SepD method was outperformed in all metrics by the A-B&BC method. The A-B&BC+LB-SubD-SepD method was able to find the optimal solution in all instances (as indicated by the "Objective value" entries), but was not able to reduce the optimality gap as effectively.

— Comparing the effects of each acceleration technique in isolation, we see that each technique shows improvements compared to the unaccelerated method in terms of the average solve time. However, it is clear that the multi-cut generation has the largest impact on the effectiveness of the techniques, as the U-B&BC+MC method outperformed all but the A-B&BC method (and the B&C method in the instances with $S = 3.25$). Notably, the U-B&BC+MC, B&C, and A-B&BC methods were the only ones able to solve all 15 instances in the dataset.

— By comparison, the effects from the Pareto-optimal cut generation are more minor, with the U-B&BC+PO performing worse than the U-B&BC method in some instances for the objective value, but performing better or compara-

bly in terms of the solve time and the optimality gap.

— Finally, the U-B&BC+PB method also showed improvements compared to the U-B&BC method, with better solve time and optimality gap (even in the instances with $S = 3.75$, for which the objective value was worse).

As in Section 4.6.2, we complement these results with performance profiles in Figure 4.2. In it, we present the percentage of instances solved by each method, aggregating across all values of S, as a function of time. Separate performance profiles for each value of S are presented in A.2.3.

These results clearly demonstrate the benefits of the acceleration techniques discussed in Section 4.4.2, even when used in isolation. However, none of the individual acceleration techniques performed as well as the combination, via the A-B&BC method.

Additionally, the results from this section combined with Section 4.6.2 highlight the different use cases for the A-B&BC and the A-B&BC+LB-SubD-SepD methods. The A-B&BC method excels at reducing optimality gaps and proving optimality. However, it can struggle to produce or improve solutions for hard instances, which makes it ideally suited for small to medium difficulty instances that can be solved to proven optimality. By contrast, the performance of the A-B&BC+LB-SubD-SepD method is the opposite. Even when given the same warmstart solution, it cannot reduce the optimality gap as effectively as the A-B&BC method. However, its performance is nearly identical both with and without a warmstart solution, finding high-quality solutions even in hard instances. This makes it best suited for hard to solve instances, for which a heuristic solution is sought.

4.6.4 Further Results: Local Branching Restricted Subproblem Solution Method

In this section, we compare the methods for solving the restricted subproblems (4.20) of the local branching procedure. Since these subproblems are solved many times in each instance, it is imperative that they are solved efficiently. For this, we use the SubD and SubB procedures presented in Section 4.5.2. We recall that the SubD method solves the restricted subproblem (4.20) by directly pro-

Table 4.5 – Average performance details in Medium instances. Entries in **bold** indicate the best performance across the exact methods in that dataset and metric.

		$S = 3.25$	$S = 3.75$	$S = 4.25$
Solve time, MIP (sec)	B&C	**23.40**	187.48	73.31
	U-B&BC	7110.49	6515.51	5001.91
	U-B&BC+MC	79.44	86.67	40.71
	U-B&BC+PO	5009.42	4928.70	4711.18
	U-B&BC+PB	4516.99	4300.18	3403.50
	A-B&BC	56.11	**51.88**	**36.80**
	A-B&BC+LB-SubD-SepD	2077.59	2943.88	3725.03
Objective value	B&C	**1877854.46**	**2398990.73**	**2970338.08**
	U-B&BC	1877081.97	2398147.48	2968357.31
	U-B&BC+MC	**1877854.46**	**2398990.73**	**2970338.08**
	U-B&BC+PO	1877040.15	2396647.52	2967975.96
	U-B&BC+PB	1877179.18	2397067.08	2969571.91
	A-B&BC	**1877854.46**	**2398990.73**	**2970338.08**
	A-B&BC+LB-SubD-SepD	**1877854.46**	**2398990.73**	**2970338.08**
Gap to best known solution (%)	B&C	**0.00**	**0.00**	**0.00**
	U-B&BC	0.04	0.04	0.07
	U-B&BC+MC	**0.00**	**0.00**	**0.00**
	U-B&BC+PO	0.04	0.10	0.08
	U-B&BC+PB	0.04	0.08	0.03
	A-B&BC	**0.00**	**0.00**	**0.00**
	A-B&BC+LB-SubD-SepD	**0.00**	**0.00**	**0.00**
Optimality gap (%)	B&C	$<$ **0.01**	$<$ **0.01**	$<$ **0.01**
	U-B&BC	2.60	1.77	3.00
	U-B&BC+MC	$<$ **0.01**	$<$ **0.01**	$<$ **0.01**
	U-B&BC+PO	1.98	1.89	2.96
	U-B&BC+PB	0.85	1.47	0.93
	A-B&BC	$<$ **0.01**	$<$ **0.01**	$<$ **0.01**
	A-B&BC+LB-SubD-SepD	0.07	0.19	1.13
Number of nodes	B&C	8351.60	62989.40	24196.40
	U-B&BC	22776.80	24473.60	9865.80
	U-B&BC+MC	103045.80	86509.80	52664.80
	U-B&BC+PO	30834.00	25441.00	10147.80
	U-B&BC+PB	19181.20	13130.00	8498.00
	A-B&BC	68917.80	58596.60	49838.20
	A-B&BC+LB-SubD-SepD	**2631.60**	**8132.00**	**4233.40**
Number of solved instances	B&C	**5**	**5**	**5**
	U-B&BC	0	1	2
	U-B&BC+MC	**5**	**5**	**5**
	U-B&BC+PO	2	2	2
	U-B&BC+PB	3	3	3
	A-B&BC	**5**	**5**	**5**
	A-B&BC+LB-SubD-SepD	4	4	4

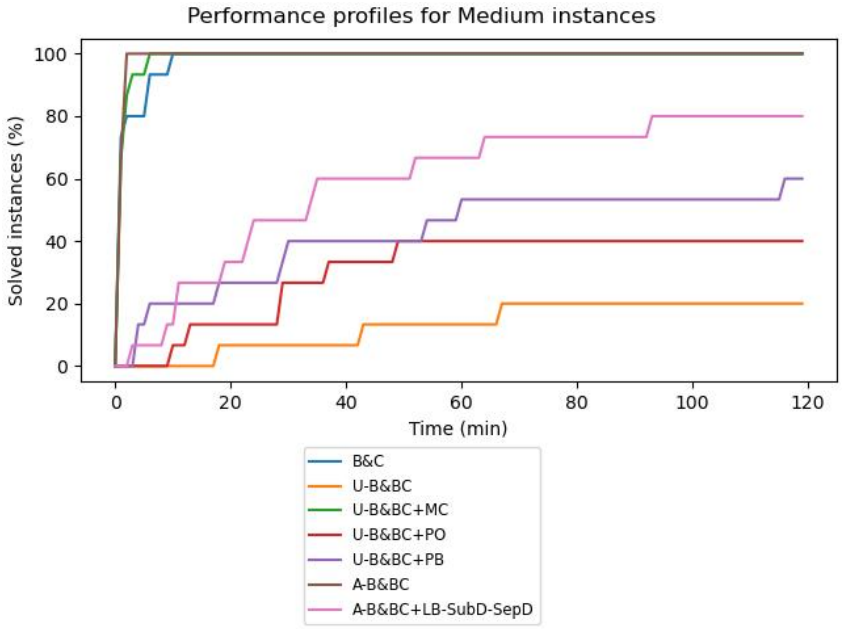

Figure 4.2 – Performance profiles showing the number of Medium instances solved (across all values of S) by each method as a function of time.

viding the reformulation (4.25) to a generic MILP solver (in this case, CPLEX), while the SubB procedure solves the restricted subproblem (4.20) with the A-B&BC method.

For a more accurate comparison between the SubD and SubB methods, we simulate the entire solving process. This starts with the MP (4.19), with no optimality cuts (4.7c) nor feasible space reductions (4.19c). We then generate randomly a sequence of 255 feasible candidate solutions $\tilde{x}$, which are used for both SubD and SubB methods. For each solution, we solve the resulting restricted problem (4.20) using each method. Then, we add the Constraints (4.27) and the Benders optimality cuts derived from the set (4.29) for $\tilde{x}$, and continue to the next solution.

In Table 4.6, we report the average results across all instances in each dataset. The objective value and solve times are as reported as CPLEX, however only instances which terminate before the time limit are included in the solve time. For the subproblems solved it is indicated the percentage of the subproblems which were successfully solved before the time limit was reached.

Examining the results, we note that both methods performed nearly identically in the easy instances. Additionally, in terms of solving time, both methods were

		Simple	Distance	HomeCharging	LongSpan	Price
Objective value	SubD	**25382.61**	**12539.70**	**15817.63**	**130526.42**	**32559.12**
	SubB	**25382.61**	**12539.70**	**15817.63**	130462.23	32544.02
Solve time (fully solved, sec)	SubD	**0.07**	0.16	0.21	**30.78**	14.67
	SubB	0.08	**0.14**	**0.20**	38.84	**14.39**
Subproblems solved (%)	SubD	**100.00**	**100.00**	**100.00**	**89.04**	**100.00**
	SubB	**100.00**	**100.00**	**100.00**	1.75	5.69

Table 4.6 – Comparison of cutting planes solution method and accelerated Benders decomposition for restricted subproblems. Entries in **bold** indicate the best performance across the exact methods in that dataset and metric.

very similar in the hard instances. By contrast, the percentage of subproblems solved within the time limit is drastically different between the two methods, with the SubD method successfully solving nearly all instances whilst the SubB method is able to solve very few. This can also be seen in the objective values, with the average objective value for the SubD method being better than the SubB method in the hard instances. These results demonstrate quite clearly that the proposed method is much better for solving the subproblem in hard problems compared to the SubB method.

A detailed view of the evolution of the solve times in terms of the number of evaluated solutions is presented in A.2.3. In brief, we observe a similar increase in the solve time for both methods, with more variability in the SubB method.

4.6.5 Further Results: Local Branching Subdomain Separation Scheme

In this section, we compare the two distinct approaches presented in Section 4.5.3 for exploring the disjoint search spaces in the local branching subproblems. We recall that the SepB approach consists in creating a series of branches indicating the time period for which the distance from our candidate exceeds the distance threshold. These branches can be created after any feasible solution, and so we compare branching after every iteration of the Benders decomposition with branching only in iterations of the Benders decomposition for which the solution found is better than the current incumbent. The SepD approach consists in using the Constraints (4.27) to model the disjunctive set. These constraints are added for

every candidate solution encountered during the series of restricted and diversified subproblems.

From technical standpoint, it is only possible to create two branches at every branch-and-bound node of CPLEX (IBM 2022). As the SepB approach demands a branch per time period, this comparison is only possible for $T = 2$. Since all of the problem instances contain at least four time periods, we modify the instances in this section by not considering any time periods beyond the first two.

In Table 4.7, we see the average results across all instances in each dataset. The solve time, objective value, and optimality gap are reported directly by CPLEX. The number of diversified subproblems and restricted subproblems are collected as part of the callback, and include all subproblems regardless of their solution status. The number of local branching separations is also collected as part of the callback, and reports the number of branches created as part of the separation procedure.

By examining the results, we observe that the SepB method which branches after every iteration had the worst performance overall. In particular, the objective value is lower and the optimality gap is higher than both other methods. Comparing the SepD and the SepB method which branches only after improving solutions, we see a trade-off in terms of objective value and optimality gap. There is also a notable difference in terms of the number of restricted subproblems, with the SepD method performing roughly 50% more subproblems.

To better explain this difference, it is important to keep in mind how both the SepB and SepD methods work at a high level. On the one hand, the SepB method creates two branches at the candidate solution, corresponding to the threshold distance being exceeded in either the first time period or the second. As such, each of these branches solves the main problem (4.19) at a local level, within relatively large subdomains. By selecting to explore a subdomain which contains better quality solutions, the solver can then improve the incumbent. However, as the subdomains get more restrictive, the bounds provided by the Benders optimality cuts become more accurate, making it more difficult to find new, improving nodes to explore. Additionally, as a consequence of this branching procedure, any upper bounds that are found are locally valid, leading to a decreased optimality gap in unexplored branches. On the other hand, the SepD method effectively creates a hole within the feasible domain, imposing that all solutions must exceed the

Table 4.7 – Average performance details for different feasible space reduction methods. Entries in **bold** indicate the best performance across the exact methods in that dataset and metric. Metrics or datasets with no clear "best" value do not have any entries in bold.

		Simple	Distance	HomeCharging	LongSpan	Price
Solve time (sec)	SepB, all solutions	46.52	2.32	1460.34	7176.68	9045.39
	SepB, improving solutions	**0.72**	**1.17**	8.95	7192.53	7269.47
	SepD	1.12	1.68	**4.99**	7175.38	7292.31
Objective value	SepB, all solutions	**13718.14**	**6635.17**	**8151.72**	18473.34	13439.35
	SepB, improving solutions	**13718.14**	**6635.17**	**8151.72**	**18882.63**	**13601.62**
	SepD	**13718.14**	**6635.17**	**8151.72**	18851.94	13552.85
Optimality gap (%)	SepB, all solutions	$<$ **0.01**	$<$ **0.01**	0.21	21.92	22.41
	SepB, improving solutions	$<$ **0.01**	$<$ **0.01**	$<$ **0.01**	13.38	18.05
	SepD	$<$ **0.01**	$<$ **0.01**	$<$ **0.01**	**12.47**	**17.47**
Number of nodes	SepB, all solutions	509.10	100.60	3061.90	1003.45	589.73
	SepB, improving solutions	12.75	73.95	216.35	2654.30	1117.95
	SepD	**10.00**	**64.10**	**170.80**	**4273.90**	**1592.75**
Number of diversified subproblems	SepB, all solutions	662.45	26.70	2892.20	760.50	278.27
	SepB, improving solutions	13.60	13.05	61.80	889.15	276.30
	SepD	18.00	15.85	30.55	876.80	268.90
Number of restricted subproblems	SepB, all solutions	1424.90	98.25	13127.65	4838.15	1708.62
	SepB, improving solutions	31.25	41.60	195.60	4783.15	1338.45
	SepD	87.75	101.95	170.40	6773.35	1973.20
Number of user-created branches	SepB, all solutions	654.70	27.00	2887.90	741.20	260.38
	SepB, improving solutions	2.20	4.70	6.70	12.40	9.30

threshold distance. As such, the main problem (4.19) is working at a global level, not divided into subdomains. This may make it easier to find new, improving nodes, as the solver may easily move to areas of the feasible domain which have not been explored and, thus, areas in which the bounds from the Benders optimality cuts are less accurate. Additionally, since the main problem works at a global level, any upper bounds that are found are globally valid, leading to an improved optimality gap overall. Due to the black-box nature of the solver, it is not possible to verify this hypothesis. However, it is supported by the progressively increasing number of nodes and the progressively decreasing optimality gap from the SepB method at all solutions, to the SepB method at improving solutions, and then to the SepD method.

These results suggest that it may be beneficial to consider the SepB method for subproblem separation at improving solutions when higher-quality feasible solutions are sought. However, the limitations in terms of the number of time periods would need to be addressed in order to apply the SepB method more generally.

Additional performance details are presented in A.2.3.

4.7 Conclusion

In this work, we present two new methods for solving the dynamic MCLP in an exact manner. The accelerated branch-and-Benders-cut method expands upon the current state-of-the-art in the static case, the Benders decomposition in Cordeau et al. (2019), adding several acceleration techniques from the literature to improve convergence. Computational experiments showed that the proposed method resulted in better performance across solving time, objective value, and optimality gap compared to the state-of-the-art. Most notably, while each acceleration technique was able to improve convergence in some instances compared with the unaccelerated method, the best performance was obtained via the combination of the techniques.

Additionally, the general nature of the model and the acceleration techniques may allow for the improved method to be applied to different structures of Ω. For example, the dynamic equivalent to the budgeted MCLP (Khuller et al. 1999, Li et al. 2021, Wei and Hao 2023) or the MCLP under uncertainty (Daskin 1983, Berman et al. 2013, Vatsa and Jayaswal 2016, Nelas and Dias 2020). The accelerated branch-and-Benders-cut method could also be extended to the MCLP with partial coverage (Karasakal and Karasakal 2004), also known as the cooperative MCLP (Berman et al. 2010). This variant allows for the coverage a_{ij}^t to be fractional, and thus may require multiple facilities to cover a user. While the Benders primal subproblem solution and Benders cuts themselves are equivalent in the partial coverage case, we note that the integrality property does not hold for the Benders primal subproblem. As such, a generalised Benders decomposition approach would be required (see, e.g. Rahmaniani et al. 2017).

In addition to the dynamic versions of these variants of the MCLP, the ideas behind our methods can also be applied to related facility location problems. An example would be the partial set covering model, which minimises the cost for maintaining a predetermined level of coverage for users. As discussed in Cordeau et al. (2019), this problem features an analogous Benders decomposition approach as for the MCLP. As such, when considering the dynamic variant of this problem, the separability would allow analogous acceleration techniques and a similar local branching approach. This dynamic variant of the partial set covering model is

similar to the incremental facility location problems studied in Albareda-Sambola et al. (2009) and Arulselvan et al. (2019). Though we note that the models in these works include constraints which break separability of the subproblems by time period, for which the multi-cut acceleration technique and the local branching method are no longer valid.

The accelerated branch-and-Benders-cut method with local branching develops a specialised local branching scheme for the dynamic MCLP. This combines an intuitive distance metric with an innovative subproblem solution method to find improved feasible solutions. Indeed, in computational experiments, this method was the only one able to consistently find better quality feasible solutions compared to the warmstart solution. However, in instances which can be solved to optimality by the accelerated branch-and-Benders-cut method, this method outperformed the local branching approach. As such, the local branching method is best used in difficult instances, where attaining higher-quality feasible solutions is paramount.

Both the accelerated branch-and-Benders-cut and the local branching methods were applied to an existing problem in the literature, an EV charging station placement model (Lamontagne et al. 2023). This provided faster solution methods with better performance guarantees, as well as improved lower bounds. These results validate the methodological contributions provided in this work for the dynamic MCLP.

From our experiments, we conclude that potential speedups should exploit the structure of Ω. In other words, it is crucial to obtain primal formulations in which the linear relaxation is tight in the main problem variables. Hence, future work on specific dynamic MCLPs could follow this research direction in order to improve the performance of our Benders framework. In another potential research direction, recent work has explored the integration of mixed integer rounding cuts within the branch-and-Benders-cut framework (Bodur and Luedtke 2017). This framework does not depend on the structure of Ω, and thus may be applicable for the dynamic MCLP.

Acknowledgements

The authors gratefully acknowledge the assistance of Jean-Luc Dupre from *Direction Mobilité* of *Hydro-Québec* for sharing his expertise on EV charging stations and the network, as well as Ismail Sevim for his insights into the project. We also gratefully acknowledge the assistance of Walter Rei of Université de Québec à Montréal and Mathieu Tanneau of Georgia Institute of Technology in discussion about Benders decomposition techniques.

This research was supported by Hydro-Québec, NSERC Collaborative Research and Development Grant CRDPJ 536757 - 19, and the FRQ-IVADO Research Chair in Data Science for Combinatorial Game Theory.

5 What makes for a good public electric vehicle charging station? A revealed preference study

Preface

In Chapter 3, we described how to embed advanced demand patterns (via, e.g., discrete choice models) directly into the optimisation framework. However, these discrete choice models must describe the interaction between the placement of public charging infrastructure and the adoption of EVs. Notably, this is controlled by the parameters of the utility functions β^t_{jik} and κ^t_{ji}, $1 \leq t \leq T, i \in N, j \in C^{0t}_i \cup C^{1t}_i, 1 \leq k \leq m_j$. As these parameters are quite specific to our case-study, in this chapter, we make progress towards obtaining appropriate values. More specifically, we investigate the high-level factors which affect the selection of public charging stations by existing EV users, under the assumption that stations which would exhibit a higher preference should result in higher EV adoption when opened. For our case study, we consider the real-world charging preferences obtained from EV users and charging sessions within the city of Montreal (Quebec).

The model in this chapter is designed explicitly for inclusion within optimisation models for EV charging network design, as it does not require user-specific information such as daily travel or battery state of charge. It can thus be applied for any such optimisation context, even beyond the EV adoption model we propose. Furthermore, the discrete choice model itself is designed to predict charging station selection. As such, this makes it suitable for estimating the usage of candidate charging station locations before such facilities exist, or determining favourable locations for charging stations.

The contents of this chapter are being prepared for submission to a peer-reviewed international journal in the domain of operations research.

Contributions of Steven Lamontagne and the coauthors

— The research ideas were developed by the student, Emma Frejinger and Margarida

Carvalho. In particular, the specification of the discrete choice models was done by the student, following the thorough research of existing work and an extensive testing process.

— All code was written by the student, including the estimation and analysis of the discrete choice models via Biogeme software. The analysis and filtering process for the real data were also developed and implemented by the student.

— The original draft (including all tables and images) were produced by the student, while it was revised by Emma Frejinger, Margarida Carvalho, and Ribal Atallah.

Abstract

To determine the optimal locations for electric vehicle charging stations within a charging network, optimisation models must predict which charging stations users will select. However, existing demand models are typically estimated using stated preference data, and include user-specific characteristics which may not be available for charging network operators, such as daily trips and vehicle state of charge. To that end, we estimate discrete choice models to predict the usage of charging stations, based only on readily available information for charging network operators. Notably, the parameter values are estimated using a unique dataset of real charging sessions within the city of Montreal, Quebec. We find that the distance between the charging stations and the users, the close proximity of the charging station to the area of the users home, and the number of outlets at each station are significant factors for predicting station usage. Additionally, the value of amenities near the charging station tend to have an overall neutral effect, with some users demonstrating strong preference or aversion for these locations. High variability among the preferences of users highlight the importance of models which incorporate panel effects.

Keywords: Electric vehicles, discrete choice models, mixed logit, revealed preferences

5.1 Introduction

Scope Whether operated by a private company or a governmental entity, electric vehicle (EV) public charging station network operators want their charging stations to be used frequently. Each charging station is expensive to install, and as such, private companies require many customers to recuperate this cost, while high usage of charging stations demonstrates a wise deployment of resources for governmental entities. To aid in this, a tool for predicting aggregate usage of public charging stations can inform on the potential impacts of candidate locations for new stations. Moreover, such a tool can then be embedded within optimisation models for

charging network planning, with the goal of selecting future public charging station locations in a long-term context.

A crucial component of this optimisation is the prediction of demand for each station. In charging station placement models, the demand for a charging station is based on either the location of the users and charging stations on the network (so called *node-based models*), or the path of a user between origin and destination on a trip (*flow-based models*, or *activity-based models* if considering a sequence of trips) (Kchaou-Boujelben 2021, Metais et al. 2022). Since it only requires the locations of users and charging stations, the node-based approach is particularly well-suited to intracity charging network optimisation, which may have limited data on the daily activities of their users. However, the level of demand in these models is typically determined via distance-based coverage or p-median models, which do not allow for more complex behaviours such as cannibalisation of demand between stations or limited charging capacity (Metais et al. 2022).

By contrast, the state-of-the-art in charging station demand modeling is dominated by discrete choice models, where the alternatives are the charging stations available to the driver (Potoglou et al. 2023). The flexibility and interpretability of discrete choice models make it an ideal choice for predicting existing behaviour and extending these predictions for candidate charging stations. In addition, the underlying behavioral assumptions in these models can allow for the more complex behaviours described above. However the integration of existing discrete choice demand models to charging network operation is non-trivial. Additionally, while discrete choice models can be estimated using stated preference (SP) or revealed preference (RP) data, the vast majority are from SP data. More specifically, the surveys for these SP-driven works present hypothetical trip and charging stations to respondent in order to simulate real-time decision making. As a consequence, these experiments typically include real-time operation attributes such as remaining vehicle range, parking time at destination, or sociodemographic characteristics (e.g. Wang et al. 2021, Visaria et al. 2022, Anderson et al. 2023). Since these attributes cannot be known in advance by the charging network operator, their inclusion in the demand models renders them ill-suited for strategic optimisation.

In this work, we estimate discrete choice models specifically tailored for integration within intracity, node-based charging network optimisation. More con-

cretely, the models predict charging station choices based on vehicle-agnostic and trip-agnostic characteristics, for example, the home area of the user and station characteristics. Such information is readily available by charging network operators, thus allowing for *a priori* estimation of demand of both existing and candidate stations. Recent advances in competitive facility location problems then describe the integration of these discrete choice models directly within optimisation frameworks (e.g., Mai and Lodi 2020, Pacheco Paneque et al. 2021, Lamontagne et al. 2023, Legault and Frejinger 2023). These frameworks embed the evaluation of charging station demand directly into the optimisation model, preserving the underlying behavioural assumptions of the demand models, and thus enabling the selection of optimal charging station locations. Public charging infrastructure is available with different power outputs, referred to as level 2 and level 3 charging, and which exhibit drastically different usage and behaviour (Hardman et al. 2018, Figenbaum and Nordbakke 2019, Tal et al. 2020). As such, we estimate separate parameter values for each of these charging levels.

Contributions Our work presents several contributions to EV demand modeling. Firstly, we specify models tailored for charging station operators, ensuring their high interpretability and rendering seamless their integration into network optimisation models. More specifically, we estimate multinomial logit (MNL) and mixed logit (MXL), with the latter including the panel effect of repeated observations from individual users. Secondly, we estimate our models from revealed preference (RP) data rather than stated preference data, thus avoiding the well-studied hypothetical bias (Haghani et al. 2021a,b). To the best of our knowledge, only Sun et al. (2016) uses RP data for charging station demand estimation, and only in the context of intercity EV charging. In addition, the dataset we use for estimation is unique in that the charging network represents 90% of charging stations within the province (Association des véhicules électriques du Québec 2023), thus accounting for nearly all available alternatives. By point of comparison, the charging network operator in Pevec et al. (2018) is reported to only account for 15% of the total network. Thirdly, we complement this unique usage data with Geographical Information System (GIS) data from OpenStreetMap (OpenStreetMap contributors 2017), allowing us to examine the travel network and amenities in

proximity to the stations when each session took place. Notably, the presence of amenities has been observed to affect EV charging decisions in Philipsen et al. (2016), Anderson et al. (2018), Sheldon et al. (2019) but, to the best of our knowledge, has not yet been included in RP studies with discrete choice models. We note that RP data and GIS information have been used in machine learning models for charging station prediction (Pevec et al. 2018, Straka et al. 2020). However the resulting machine learning models are not well-suited for selecting multiple new charging stations simultaneously, thus making for a difficult integration into charging network optimisation. Our key findings indicate, unsurprisingly, that the distance between the charging stations is the most significant factor for predicting charging station usage. Additionally, the number of outlets at each station and the charging station being within a short walk of the home area of the user are also found to increase usage of a station. In the MNL models, the average effects of some amenities are significant. However, the MXL models indicate an overall neutral average effect and significant variance among users. This suggests that the significant average effect observed in the MNL models may be caused by a high number of sessions from users with strong preferences or aversions, rather than an overall trend within the population. As a consequence, optimisation models which employ MNL formulations for demand modeling may incorrectly relate the usage of stations with amenities.

Paper Organisation In Section 5.2, we present a review of the relevant literature on charging preferences and charging station selection. Section 5.3 presents general characteristics about EV charging in Quebec, along with the process for generating the value of the attributes in our models. In Section 5.4, we discuss the specifications of our MNL and MXL models. The results of the estimation process are presented in Section 5.5, while they are discussed in Section 5.6. Finally, we conclude our work in Section 5.7.

5.2 Literature Review

There is a vast literature on EV charging habits. Thus, for the sake of brevity, we present here works relating to the use or selection of charging stations by private EV owners. We start with a focus toward the data used, followed by an exploration of literature addressing charging preferences. This specifically includes preferences related to the public charging network. Lastly, we delve into the methodologies employed for predicting charging station selection. For recent reviews of these and other aspects of charging activity, we refer to Hardman et al. (2018) and Potoglou et al. (2023).

5.2.1 Charging Behaviour and Requirements

We start by noting the works detailing the charging behaviour for private vehicle users. These allow us to identify and validate charging behaviour of real users, as well as isolate irregular behaviour. Collectively, these works report on millions of charging sessions and thousands of EV owners across the Netherlands, British Columbia (Canada), Norway, Ireland, California (United States), and New Zealand (van den Hoed et al. 2013, Axsen et al. 2015d, Figenbaum and Kolbenstvedt 2016, Morrissey et al. 2016, Figenbaum and Nordbakke 2019, Nicholas et al. 2017, Tal et al. 2018, 2020, Burroughs et al. 2021). Additionally, while other works focus on a specific research question, they may also present survey results or revealed data on charging behaviour. Examples include the surveys of Franke and Krems (2013), Chakraborty et al. (2019), Lee et al. (2020), Visaria et al. (2022), and Anderson et al. (2023). By combining this vast literature, we obtain a diverse portfolio of preferences of EV drivers across multiple years and geographical regions, thus rendering it possible to compare against existing behaviour and identify irregularities.

The dependency on the public charging network varies greatly depending on the user. When charging their vehicle, users may have access to private charging outlets located at their home or workplace. Indeed, currently, the majority of users charge primarily at home, with between 82% and 93% of EV owners recharging frequently at home (Figenbaum and Nordbakke 2019, Lee et al. 2020, Tal et al. 2020, Visaria et al. 2022, Anderson et al. 2023). For workplace charging, there is

more variability in terms of availability and frequency of use, with the percentage of frequent users ranging from 19% to 40% (*ibid.*). Notably, in Helmus et al. (2020) they find that a minority of sessions in the Netherlands are associated with workplace charging, at around 14%. This compares with 35% associated with non-workplace daytime charging and 50% associated with overnight public charging. The attributes contributing to the frequency of each type of charging location were examined in more detail in Chakraborty et al. (2019) and Lee et al. (2020), which included income, dwelling type, access to level 2 charging at home versus level 1 charging, and the electric range of the vehicle. The access to home or workplace charging can decrease the reliance on the public charging network, and can thus lead to a disproportionate representation of public charging sessions by those without access to these other types of charging.

5.2.2 Predicting Charging Station Selection

Once a user has opted to use the public charging network, they must then select a charging station to use. Depending on its characteristics, each station may successfully draw the demand of that user. In this sense, this viewpoint is similar to the approach of node-based optimisation models, with the demand of each charging station depending on multiple attributes rather than simply the distance. In the demand modeling literature, researchers have then tried to characterise or predict this selection. In many cases, they use a discrete choice model to predict a charging station choice, with significant attributes including cost, charger availability or waiting time, distance to home or detour time, location type, proximity to amenities, number of chargers at the station, electricity obtained from a renewable source, and the rating of the charging station on a mobile phone application (Luo et al. 2015, Cui et al. 2019, Moon et al. 2018, Sheldon et al. 2019, Wang et al. 2021, Lamontagne et al. 2023, Ma et al. 2022, Visaria et al. 2022, Anderson et al. 2023). In the case of Luo et al. (2015), Cui et al. (2019), Lamontagne et al. (2023), charging demand was predicted using discrete choice models, and embedded within optimisation models. No parameter values or estimation results are presented in Luo et al. (2015), Cui et al. (2019), while parameter values for a MNL model are presented in Lamontagne et al. (2023) based on real charging session data. In all

other cases, the models are estimated based on a curated survey, where respondents are presented a set of charging options with different characteristics and must select an option.

Of particular note for our study is the work in Sheldon et al. (2019), involving a choice experiment with 1,261 drivers (not necessarily EV) in California, as it includes the proximity to amenities as an attribute. More specifically, the proximity of a station to amenities is treated as a categorical characteristic which classifies charging stations into one of the following location types: workplace, grocery stores, shopping malls, public transit, sports facilities, schools, entertainment venues, level 3 near home, and level 3 near the highway. They find that respondents exhibited a preference for locations identified as near grocery stores, shopping malls, and having level 3 charging stations near their homes and close to the highway network, as opposed to the baseline location near entertainment locations. Moreover, respondents demonstrated indifference or a tendency to disfavor locations identified as being near transit, sports facilities, and schools (even students). In all cases, these public charging locations were favoured less than workplace charging. However, the authors find that these preferences vary significantly among the respondents.

Under a similar node-based viewpoint but not using discrete choice models, in Philipsen et al. (2015), they ask a discussion group of 15 non-EV drivers from Germany about their preferences for charging. As part of this, a series of evaluation criteria for charging stations were brought up: combining the charging session with everyday activities (dual use), compatibility with existing habits, avoiding detours or added delays (accessibility), easy to find and see (visibility), availability of chargers when needed (reliability), safe to leave vehicle or to stay for extended periods of time, allowing for longer trips that could otherwise not be done, and connection to the public transportation network. The participants also proposed several locations which fit the above criteria, such as supermarkets, public authorities, gas stations, motorway service stations, medical centres, recreational facilities, and sports venues. These findings were validated in Philipsen et al. (2016) through a survey of 252 respondents in Germany, asking each to rank to importance of the evaluation criteria and locations proposed in Philipsen et al. (2015). For the ranking of criteria, reliability and dual use were most important, followed by accessibility and visibility. For location type, motorway service stations were deemed

most important, followed by workplace, gas stations, and shopping facilities (at roughly equal importance), then leisure facilities and educational facilities. These preferences for evaluation criteria and location were found to vary based on sociodemographic (notably, based on gender) and if the respondent was presently an EV driver. In a similar approach, in Anderson et al. (2018), they conduct a survey of 761 EV owners in Germany in which respondents were asked where to place additional charging stations based on their personal needs. For each station, they could indicate the power level (3.7 kW, 22 kW, 50 kW), the projected frequency of use, and the activity while charging at that location (such as work, stop-to-charge, or shopping). Overall, users placed charging stations within cities, preferred 22 kW charging, and wanted activities close to their charging stations (with only 29% of the stations indicating stop-to-charge). Additionally, the activities selected varied considerably between the different power levels, highlighting different usage.

Across the node-based viewpoint, we note the lack of RP data, relying exclusively on choice experiments or survey results. Additionally, while the distance or accessibility of a station is crucial, there is support for the idea that users prefer activities near their public charging stations (an idea which is implicit in the activity-based optimisation). As such, this suggests that the inclusion of such attributes in node-based and activity-based optimisation would be beneficial.

Rather than focusing on the charging stations in isolation, other works consider the station as one part of a user's trip between their origin and destination. In this context, the selection of a charging station can thus be viewed as the deviation of a path for the purposes of charging. As such, this viewpoint is akin to the path-based optimisation models. In all of these works, discrete choice models are used to predict which charging station is selected by the users, however the exact decision being modelled can vary. In both Sun et al. (2016) and Yang et al. (2016), some routes can be completed without charging, so users must decide if they select a route with charging at all and, if applicable, which route with charging. They find that the state of charge and sociodemographic characteristics were significant attributes for selecting a route with charging. In terms of route deviation for charging, Sun et al. (2016) noted that maximum acceptable deviations from the shortest path varied between 500 metres and 1,750 metres depending on vehicle type (private versus commercial) and day (weekday versus weekend). Similarly to Sun et al. (2016),

Yang et al. (2016), in Ashkrof et al. (2020), users must select a route between their origin and destination, with some routes including fast charging stations along the way and some destinations including a slow charger. They find that availability of a slow charging station at the destination decreased the chances of selecting a route with fast charging, while female drivers and younger drivers were more likely to select routes with fast charging. In general, for shorter trips, local streets are preferred while for longer trips freeways and arterial ways are preferred. Rather than selecting a route, in Ge and MacKenzie (2022), users are presented with a route and vehicle characteristics. The process then simulates a real trip, where users arrive at a charging station with given vehicle and trip characteristics (e.g. remaining state of charge and distance to next charging station), and then must decide whether to charge at this charging station or to continue on the route. They find that the remaining state of charge, charging cost, access time, and having access to full amenities (restroom, Wifi, and a restaurant) were significant attributes for users deciding to charge. In terms of data for discrete choice model estimation, we note that only Sun et al. (2016) uses revealed-preference data, while all others use survey data.

Overall, these path-based viewpoints consider analogous attributes to those of node-based, such as the distance to the charging station being replaced by path deviation. However, a major difference is in the data assumption about users, where the researcher is assumed to be aware of the path (or at least the origin and destination) of the user in the path-based viewpoint.

5.2.3 Relation to Our Work

As with many of the prior articles, our work uses discrete choice models to predict the choice of charging station by users, more specifically following the node-based viewpoint for intracity charging. However, our work expands upon the existing literature by estimating with RP data, previously only used in the intercity model of Sun et al. (2016). Additionally, by combining this RP data with GIS information from OpenStreetMaps, we can include amenity information, previously only considered in discrete choice estimation with SP data such as in Sheldon et al. (2019), Visaria et al. (2022). By comparing the available amenities

near a charging station with the usage of the stations, we can then empirically verify the value of the location types proposed in Philipsen et al. (2015, 2016), Anderson et al. (2018).

5.3 Data

In our work, we use a dataset of charging sessions from the charging network operator *Circuit Électrique*. We begin, in Section 5.3.1, with a brief discussion about the charging network and the charging process in Quebec. Additionally, though this dataset has been used in Lamontagne et al. (2023), Elhattab et al. (2023), Parent et al. (2023), descriptive statistics were not provided for charging behaviour. These are provided along with a comparison with other reports on charging behaviour (mentioned previously in the literature review). As we are interested in intracity charging, in Section 5.3.2, we isolate the data for the city of Montreal, Quebec. Finally, in Section 5.3.3, we describe the procedure for obtaining attribute values which are not found in the charging session data.

5.3.1 Data Description

A key component to our charging session data, and a notable difference with other charging networks is the membership card. Indeed, in addition to managing operations of the charging stations, *Circuit Électrique* also has a membership program to which users can register (Circuit Électrique 2023a). Registered users can receive by mail one or more cards with Radio Frequency Identification (RFID) capabilities, and which are connected to their account information; All sessions initiated by a membership card (including at some charging stations not operated by *Circuit Électrique*) are then linked and charged to the associated account. However, a membership card is not required at all charging outlets operated by *Circuit Électrique*, as sessions may be initiated by guest accounts and charged to a credit or debit card. As such, recorded sessions contained within the dataset include those completed by registered and guest members at *Circuit Électrique* charging, as well as some sessions completed by registered members at third-party charging stations.

Since we cannot accurately identify the preferences and habits of guest accounts (which represent roughly 47% of users and 11% of sessions), they are excluded from the analysis and estimation processes. Even for non-guest members, reliable vehicle information is not available for member accounts and, in addition, multiple vehicles may be associated with the same account. As such, it is not directly known if the account corresponds to a private user, or a fleet of commercial vehicles. Since our aim is to evaluate public charging stations from the perspective of private vehicle owners, we must identify and isolate the corresponding member accounts. To do this, we have combined the expertise of our industrial partners, as well as the descriptions of typical charging behaviour from the literature, to create a series of filters for categorisation. For the purposes of these filters, we do not take into account charging behaviour or sessions which occurred between February 1st 2020 and June 30th 2021, as the COVID-19 pandemic had noticeable effects on charging habits which could interfere with the filters.

Unplugged Member accounts which have no charging sessions associated with them. These members may correspond to users who only use home charging (which correspond to 53% of respondents in Lee et al. 2020), or PHEV owners who never charge their vehicles (Chakraborty et al. 2020). Our industrial partners have also suggested that these could correspond to duplicate accounts, where users have forgotten account sign-in information, and have simply created a new account. Since the classification of users excludes the period of February 1st 2020 to June 30th 2021, users are classified as unplugged if their only charging sessions are during this time.

Shared Member accounts presumed to correspond to fleets or commercial vehicles. Several filters identify this case:

- Member accounts which are associated with multiple sessions occurring at the same time.
- Member accounts which have been charged four or more times in a single day. This threshold value is much higher than the average charging rates of 18 to 20 sessions per year in van den Hoed et al. (2013), average 1.47 sessions per day in Axsen et al. (2015d) (median of 1), average 1.17 sessions per day in Tal et al. (2018), median 0.71 sessions per day in

Visaria et al. (2022) (mean of 0.75, maximum of 4.29), and average 1.1 sessions per day in Tal et al. (2020) (highest rate among all vehicle types). Additionally, while less commonly found in the literature, in Tal et al. (2020) the average number of charging sessions on days in which charging occurred was reported to be below 1.66 sessions per day for all vehicle types.

— Member accounts which have an average recharge rate over 500 kWh per month, or 6,000 kWh per year. This threshold is similar to the highest annual energy requirements reported in Tal et al. (2020) (6,565 kWh, followed by 5,043 kWh). While the energy efficiency varies by vehicle and climate, 6,000 kWh per year corresponds to over 30,000 kilometres of travel (van den Hoed et al. 2013, Hardman et al. 2018). By comparison, the average annual driving distances for EVs was 20,150 kilometres in Axsen et al. (2015d), 15,563 kilometres for non-Tesla EVs in Figenbaum and Kolbenstvedt (2016), and 23,367 kilometres for Tesla EVs in Figenbaum and Kolbenstvedt (2016).

Rental Member accounts which have less than 14 days between the creation of the account and the last charging session, and have at least three charging sessions during that time. While this corresponds to a reasonable charging rate, the short duration of the account suggests that this may be a temporary vehicle. As such, the charging behaviour may not correspond to general vehicle ownership, particularly if the rental vehicle is used for long-distance trips to cottages or other vacation destinations (Figenbaum and Kolbenstvedt 2016, Figenbaum and Nordbakke 2019).

Private All remaining accounts.

We note that a different classification of users was proposed in Helmus et al. (2020), partly based on the types of charging sessions initiated by that user. However, this relies on (unavailable to us) vehicle information, and the resulting classifications do not isolate car sharing and taxis from private vehicles. As such, they are not of practical interest for our study. The total number of members in each month and of each type is given in Figure 5.1.

In total, there are 2,873,345 valid recorded sessions by 120,952 non-guest mem-

ber accounts at 81,239 outlets and 43,056 stations, which take place between January 2018 to August 2022. For each charging session (of level 2 or level 3), the unique identifiers for the charging outlet and the member account are recorded, along with the time that the charging connection started, the time the connection ended, and the amount of energy charged. Additionally, for some level 3 charging outlets, the starting and ending state of charge are also recorded. However, we note that the price of charging is not available, nor is waiting time before charging. The number of sessions in each month and by each type of member is given in Figure 5.2.

We present summary statistics of charging session characteristics in Figures 5.3-5.5. These statistics are separated, as applicable, by level of the charging outlet. However, these statistics are similar among different account types, and thus account types are aggregated. These values are compared with reports of level 2 charging sessions on public charging infrastructure in van den Hoed et al. (2013), Morrissey et al. (2016), Helmus et al. (2020) and level 3 sessions on public charging in Morrissey et al. (2016). While charging sessions information is presented in Tal et al. (2020), home charging is not separated from public charging, rendering the comparability questionable. However, as level 3 charging is not available at home, the relevant charging session information in Tal et al. (2020) can be used.

— In Figure 5.3, we report the distribution of the duration of charging sessions. In this graph, the horizontal lines indicate the 25th, 50th, and 75th percentile, while the width of the shaded background illustrates the distribution of each duration (with larger width corresponding to more sessions). As vehicles may be connected to chargers much longer than their charging time (e.g. Morrissey et al. 2016, Helmus et al. 2020), we cap the duration at 720 minutes, which applies for around 2.2% of level 2 sessions and only two level 3 sessions. The median of 116 minutes for level 2 and 23 minutes for level 3 is comparable to the corresponding values of 128.78 minutes and 26.62 minutes for level 2 and level 3 presented in Morrissey et al. (2016), and within the distribution of around 17 minutes to 37 minutes (depending on vehicle type and day) reported in Tal et al. (2020). However, this does differ significantly from the average level 2 connection time of 435 minutes presented in van den Hoed et al. (2013) and median of 537 minutes in Helmus et al. (2020). In

Helmus et al. (2020), they note that over 75% of EV users are dependent on public charging facilities. As such, a higher ratio of overnight charging may contribute to this increased duration.

— In Figure 5.4, we report the distribution of energy (in kWh) charged during the session. The median energy per level 2 session is 6.9 kWh while the median for level 3 session is 13.4 kWh. The value for level 2 charging matches with those in the literature, with 6.8 kWh per session in Morrissey et al. (2016) and Helmus et al. (2020), and 8.31 kWh in van den Hoed et al. (2013). The value for level 3 charging is higher than the 8.32 kWh reported in Morrissey et al. (2016), and within the distribution of 7.9 kWh to 26.3 kWh (depending on vehicle type) reported in Tal et al. (2020).

— In Figure 5.5, we report the distribution for the starting and ending state of charge for level 3 charging sessions, with median values of 30% and 73%, respectively. We recall that state of charge information is not available for level 2 sessions. These values are slightly below the distribution of 30.3 to 48.4% for starting and 74.7 to 92.5% for ending state of charge (depending on vehicle type) presented in Tal et al. (2020). State of charge information is not reported in Morrissey et al. (2016).

Rather than reporting on charging sessions, in Figures 5.6-5.9, we present summary statistics for private vehicle accounts. Summary statistics for shared accounts are presented and discussed in A.3.1, while they are not presented for rental vehicle or unplugged accounts. For rental vehicle accounts this is due to the small sample size, while there is no charging activity to report for unplugged accounts.

— By construction, the average number of sessions and total energy charged are lower for private vehicles (Figures 5.6 and 5.7) than for shared accounts. Median values for the number of charging sessions and total energy per month for private vehicles are, respectively, 0.57 sessions and 5.89 kWh, while the median values for shared accounts are 2.75 sessions and 34.7 kWh. Comparable values in the literature were discussed at the beginning of this section as part of our user classification process.

— In Figures 5.8, we present the distribution for the average amount of time spent charging every month, with the duration of each charging session

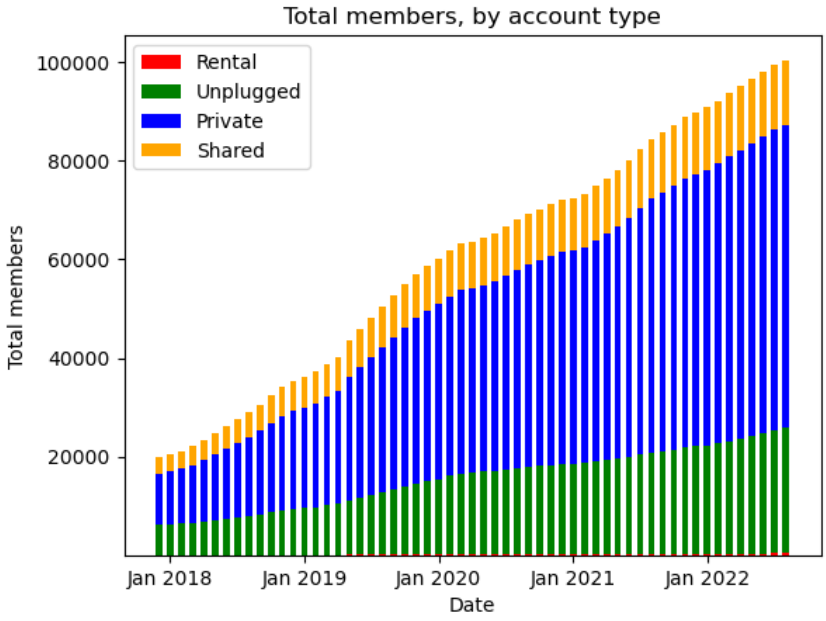

Figure 5.1 – Number of total members, by date and account type.

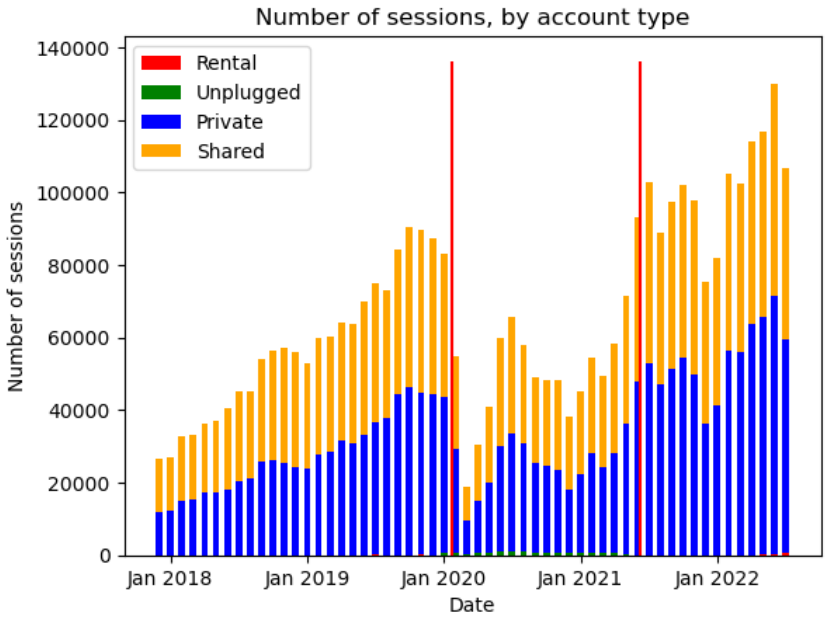

Figure 5.2 – Number of sessions, by date and account type. The narrow red lines indicate the excluded period for the COVID 19 pandemic.

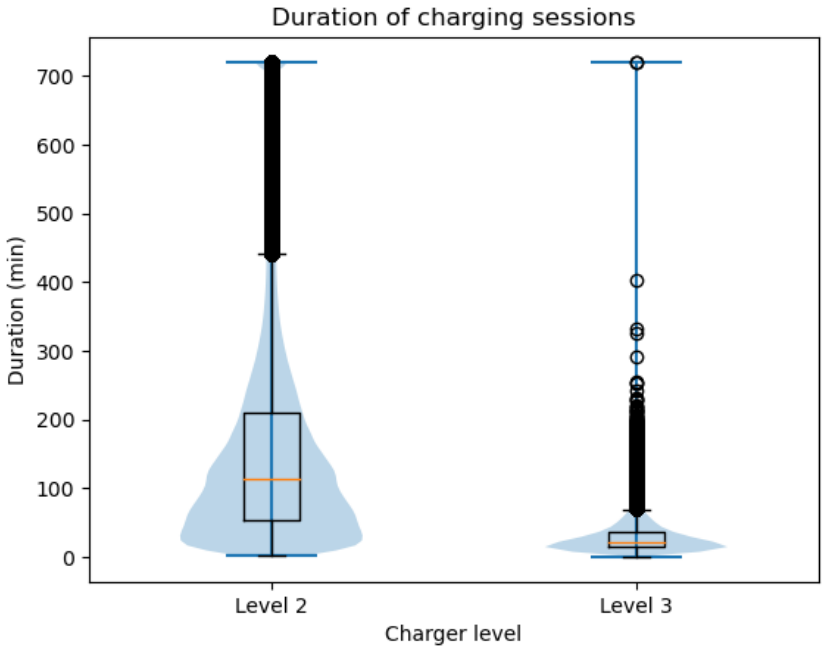

Figure 5.3 – Distribution of duration of charging, by level of charging outlet.

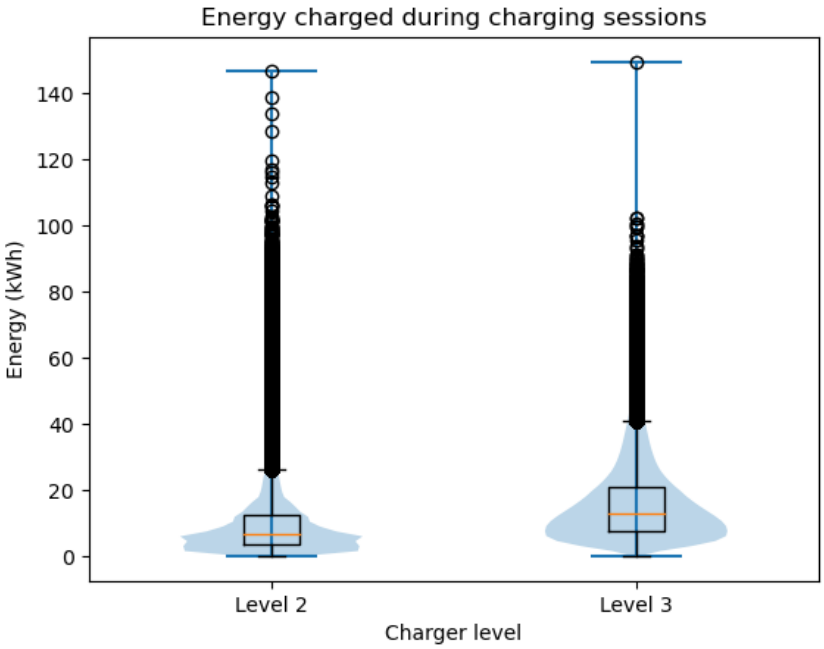

Figure 5.4 – Distribution of energy from charging, by level of charger.

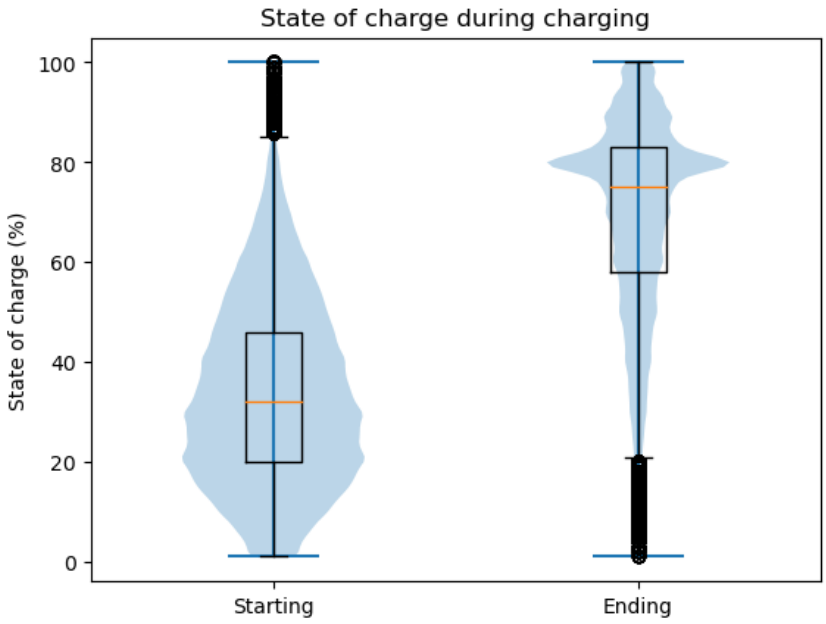

Figure 5.5 – Distribution of starting and ending state of charge at level 3 chargers.

capped at 720 minutes as before. The median value is 47.7 minutes for private vehicles. In terms of comparable values, Tal et al. (2020) reports an average *daily* duration of between 97.33 and 266.96 minutes (depending on vehicle type). However, we note that this charging duration includes home charging and, as such, may not be an accurate proxy for public charging, even for those that lack access to home chargers. For public charging specifically, by combining the average number of 18 to 20 charging sessions per year and 7.25 hour session duration in van den Hoed et al. (2013), we obtain a monthly average of between 652.5 and 720 minutes. As with the duration of individual sessions, this higher value for members may be attributed to a higher rate of overnight charging.

— In Figure 5.9, we present the distribution for the average number of different stations visited each month. The median value is 0.45 stations for private vehicles. Only van den Hoed et al. (2013) reported the number of stations visited, with an average of 4 and 77 different locations visited per year for private vehicles and car sharing vehicles, respectively. Accordingly, the value for private vehicles is quite comparable to that of van den Hoed et al. (2013).

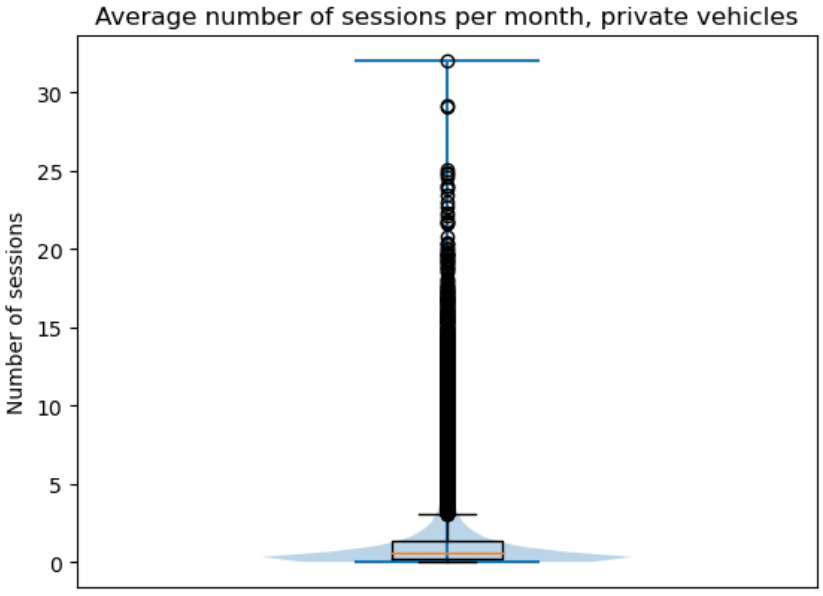

Figure 5.6 – Distribution of average number of sessions per month, private vehicles.

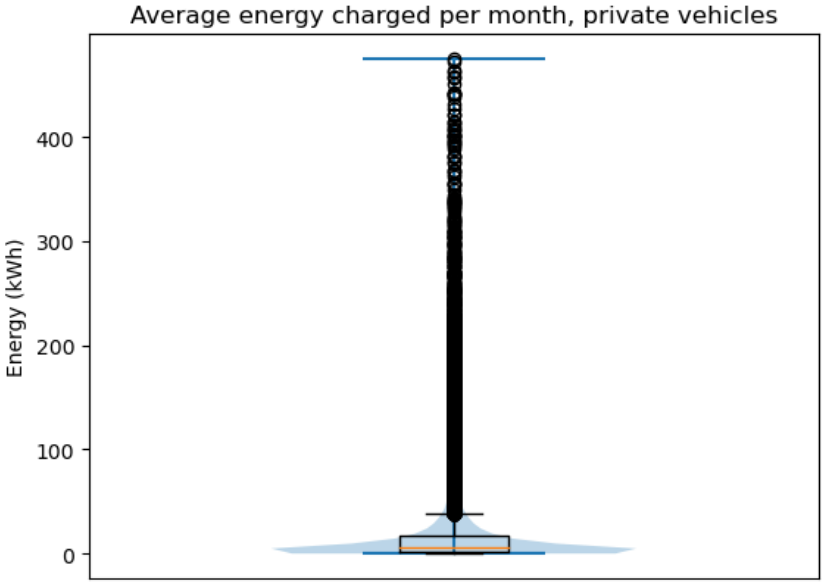

Figure 5.7 – Distribution of average energy charged per month, private vehicles.

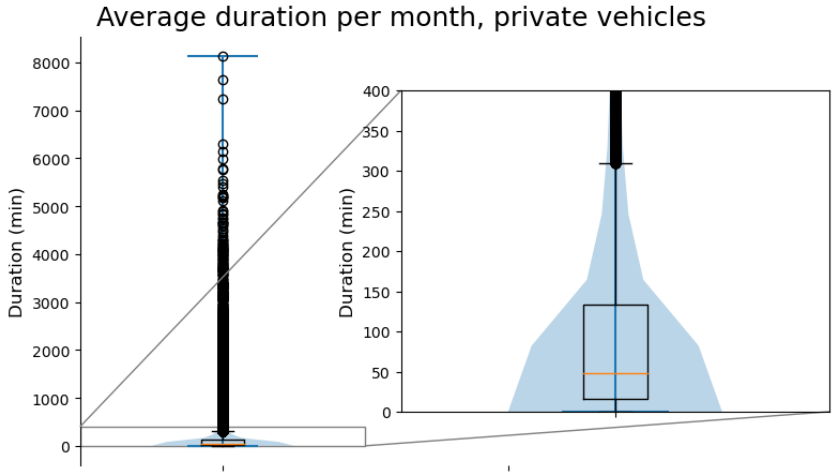

Figure 5.8 – Distribution of average monthly time spent charging, private vehicles.

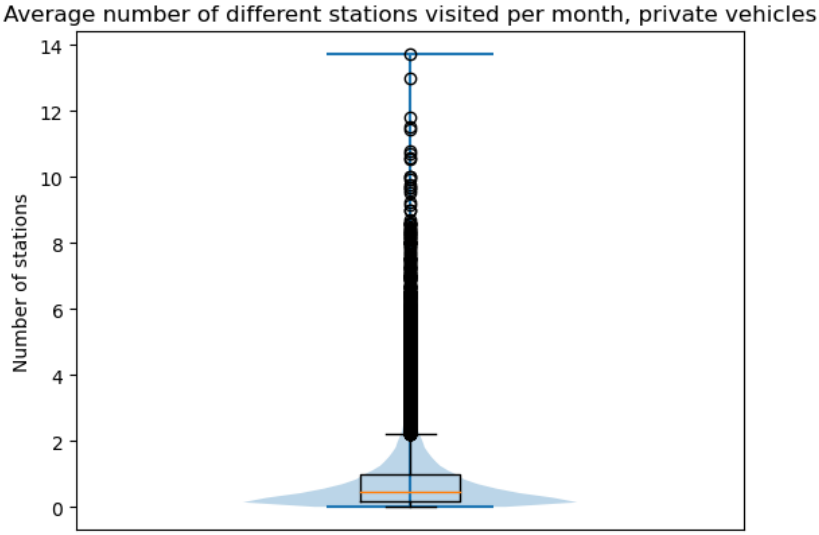

Figure 5.9 – Distribution of average number of different stations per month, private vehicles.

5.3.2 Data Processing

For the estimation process, we use the public charging network on the island of Montreal. As we consider intracity charging by private vehicle owners in this work, we only select members who have provided a postal code, and whose postal code lies within the island. Furthermore, since our industrial partners have advised us that there are many taxi accounts in Montreal, we exclude users from our estimation process if they have ever charged three or more times within the island in a day. These two conditions –postal code within Montreal, and maximum of two or fewer daily charging sessions on the island– are applied in addition to the filters for private vehicle owners in Section 5.3.1.

As for the charging stations, they are excluded if they are private or semi-private stations (similar to Sun et al. 2016) , or if they were permanently closed before January 1st 2018. Additionally, while members can use their *Circuit Électrique* membership cards at charging stations operated by *ChargePoint*, this incurs an additional fee (Circuit Électrique 2023c). These stations have few recorded sessions, likely due to users using a *ChargePoint* rather than a *Circuit Électrique* membership card to avoid the additional fee. As such, to avoid incorrectly biasing the results, we exclude the charging stations operated by *ChargePoint*. After filtering, there are 736 charging stations of level 2 charging stations, and 19 charging stations of level 3. The stations are displayed in Figure 5.10.

5.3.3 Attribute Encoding

In order to estimate parameter values, we must first determine the appropriate value of each attribute. As the session data spans from January 2018 to August 2022, it is important to get historical data. For charging station attributes, we use the data directly from *Circuit Électrique* as well as publicly available charging station information (Circuit Électrique 2023c). For network information and available amenities, we use OpenStreetMaps (OpenStreetMap contributors 2017) data, queried at the start of every month. We use attributes which have been examined, or for which similar attributes have been examined, previously in the literature. These attributes are:

Distance: The distance between the user and the charging station (or the devi-

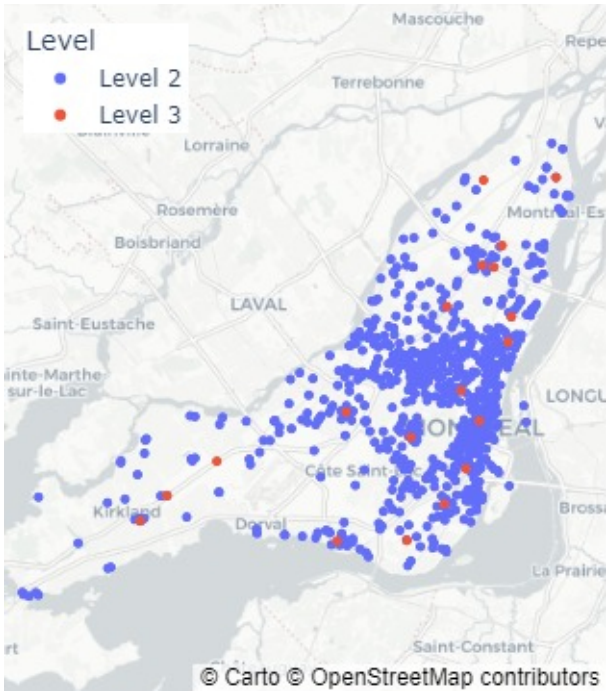

Figure 5.10 – Public charging stations within the Island of Montreal.

ation from their path between home and destination) is the most common attribute in charging station choice modelling, and has consistently been found to be a significant attribute for the user's choices (e.g. Yang et al. 2016, Lamontagne et al. 2023, Ma et al. 2022, Visaria et al. 2022). A shorter distance between the user's home and the charging station improves the *accessibility* of the station as described in Philipsen et al. (2015, 2016). We use two measures for these distances; First, we use OpenStreetMaps to calculate the road network distance between the user's home and the charging station. Second, we include a binary flag indicating whether the Euclidean (i.e. walking) distance between the charging station and the user's home is less than 400 metres, which indicates that the charging station may be convenient for charging near home (Lee et al. 2020). Though Lee et al. (2020) proposes a distance of 300 metres, we adjust this threshold slightly to account for the distance errors due to having postal codes rather than precise addresses.

Number of outlets: Included in Lamontagne et al. (2023), Visaria et al. (2022), this attribute indicates the total number of outlets at each charging station.

A higher number of outlets at the station increases the likelihood that one is available when needed, thus improving the *reliability* of the station as described in Philipsen et al. (2015, 2016). The number of outlets in each station is calculated from the *Circuit Électrique* data based on the installation and closure dates of each outlet.

Is at a gas station: Somewhat surprisingly, the charging station being installed at a gas station has been found to be beneficial for users (Philipsen et al. 2015, Sun et al. 2016, Philipsen et al. 2016). This is attributed in Philipsen et al. (2015) to habit, where the gas stations are those previously used by the users for their ICEVs. In our case, we use a binary variable to indicate whether or not the charging station is located at a gas station, and is determined by the presence of a gas station within 50 metres of the charging station in OpenStreetMaps.

Proximity to amenities: In Anderson et al. (2018), Figenbaum and Nordbakke (2019), it was reported that users prefer to do activities while their vehicle is charging, with activities differing between users and charging level. Various location types and activities have been proposed across the literature, which we discuss in detail below. For each amenity type, we calculate density measures by taking the logarithm of the number of amenities of that type in OpenStreetMaps within various threshold distances around the charging station.

Restaurants, Fast food: The presence of restaurants was included as an attribute in the demand models of Luo et al. (2015), Cui et al. (2019), though the value was not estimated. The highest tier of amenities in Ge and MacKenzie (2022), Visaria et al. (2022), Anderson et al. (2023) included access to the combination of washrooms, a restaurant, and free Wifi. As such it is unclear if the presence of a restaurant alone is sufficient. Restaurants are included as part of an "Other" category in Anderson et al. (2018, 2023), while the location is not included in Philipsen et al. (2016). Additionally, while less than 1% of respondents in Burroughs et al. (2021) indicated that they currently used charging stations near restaurants, cafés, or bars, 76% of respondents indicated

that they prefer to eat and drink while charging. In summary, while restaurants have been included in many surveys and reports, there are conflicting assessments as to the value of such amenities. For our estimation, we separate fast food restaurants from other types; Due to the difference in preparation time, fast food restaurants may be more beneficial for level 3 charging sessions.

Shopping, Supermarkets, Shopping malls: At an aggregate level, the presence of general shopping facilities was found to increase charging station usage for some users in Anderson et al. (2023), while the demand models in Luo et al. (2015), Cui et al. (2019), Sheldon et al. (2019) includes separate attributes for supermarkets and shopping malls. Notably, in Sheldon et al. (2019), both supermarkets and shopping malls were found to increase the likelihood that users select a station in comparison to locations near entertainment venues, with supermarkets having a larger impact than malls. The overall benefit of shopping is consistent with the findings in Anderson et al. (2018), where 18.4% of the placed charging outlets were designated for shopping purposes, and in Philipsen et al. (2016), where shopping was rated as important for users. In practice, Anderson et al. (2023) report that around 20-32% of respondents charged at least once a month near shopping locations. In Axsen et al. (2015d), shopping malls were reported as the most frequent location type for public charging (though they note that public charging was overall infrequently used), while Figenbaum and Kolbenstvedt (2016) report that around 7% of BEVs recharge at least weekly at shopping centres and similar commercial locations. In Burroughs et al. (2021), only 3% and 2% of respondents indicated that they recharged near supermarkets and shopping malls (respectively), while 55% of respondents said they liked to go shopping while recharging their vehicle. In summary, the presence of shopping facilities (and, where applicable, supermarkets and shopping centres) are generally seen as important by users, though they may be used in practice less often than anticipated. For our estimation, we consider supermarkets and shopping malls separately from other types of shopping. For supermarkets, this is due to the habitual

and more frequent usage (as discussed in Philipsen et al. 2015). On the contrary, for shopping malls (a category which also includes the public marketplaces in Montreal), this is due to the presence of multiple types of different shopping in one location, often not individually identified in OpenStreetMaps. As such, using a separate attribute for shopping malls can better capture the more diverse shopping opportunities available.

Leisure, Sports: Combined into one category, sport locations (such as tracks or arenas) and leisure locations (such as cinemas or dog parks) were considered in Anderson et al. (2023) and found to be important for some users. In Sheldon et al. (2019), entertainment venues were used as the baseline location type for other types, and found that gyms and sports facilities were dispreferred compared with this baseline, with high variability among users. In Anderson et al. (2018), around 18.3% of the placed charging outlets were designated for leisure purposes, almost identical to those for shopping purposes. By contrast, in Philipsen et al. (2016), leisure locations were deemed less important than shopping. Likewise, in Anderson et al. (2023) report that only around 4% of respondents charged at least once a month near leisure locations. This is consistent with the findings in Burroughs et al. (2021), who report that 1% of respondents charged in the "Other" category (which includes entertainment venues and sports facilities), while 13% of respondents indicated that they would like to use such facilities while charging. In summary, the use of charging stations near entertainment venues or sports facilities is typically lower than other amenities, though is important for some users. As with fast food restaurants, we separate sports and leisure locations due to potential variations in the duration of these activities.

The maximum value for each of the attributes for each charging level are presented in Table 5.1. Additionally, we present the associated notation x_k for each attribute k in the model.

We note that some common attributes from the literature have not been included, either because they are not appropriate for our case study or because accurate values can not be determined:

Charging power and duration: The power supplied by the charging station or, similarly, the duration of charging has been shown to have an impact on the selection of charging stations, with higher power or lower duration being preferred (e.g. Yang et al. 2016, Ge and MacKenzie 2022, Visaria et al. 2022). However, in Quebec, the charging power can be set independently for each charging outlet, and as such may not be consistent within each charging station. Additionally, while over 95% of the level 2 outlets have a charging power of 7.2 kW (Circuit Électrique 2023c), the charging power for level 3 outlets varies between 24-100 kW with different power levels deliberately placed at the same stations (Circuit Électrique 2023b).

Charging price: As expected, users have been found to avoid charging stations which have higher costs compared to others (Ge and MacKenzie 2022, Visaria et al. 2022, Wang et al. 2021). However, while the cost of charging in Quebec can vary slightly by location and provider, it is subject to governmental regulation, and is determined based on the charging power of the outlet, the charging power drawn by the vehicle, and state of charge of the vehicle (Circuit Électrique 2023b). As a consequence, the charging price can vary not only within a charging station but based on the charging profile of each individual vehicle. In Montreal, over 95% of the level 2 charging stations have a cost of 1$ per hour which, given the median duration of a level 2 session, results in a per-session cost of around 1.93$ (Circuit Électrique 2023c). By contrast, the cost for level 3 charging varies between 6.39-15.73$ per hour, with the majority having a cost of 12.77$ per hour (resulting in a per-session median cost of around 4.90$).

Charging stations are considered to be available for users if at least one charging outlet is installed at the time of the charging, and if a path is found between the users' home and the charging station.

Attribute name	Notation	Level 2	Level 3
Network distance to station (km)	x_{dist}	98.658	49.668
Is the station within a short walk	$x_{\text{isWalkHome}}$	1	1
Number of outlets	x_{outlets}	13	5
Is at a gas station	x_{isGas}	1	1
Restaurant density	x_{rest}	4.635	3.638
Fast food density	x_{ff}	4.060	2.079
Shopping facility density	x_{shop}	5.257	4.007
Supermarket density	x_{sm}	2.303	0.693
Shopping mall density	x_{mall}	1.099	0.693
Leisure density	x_{leis}	3.526	3.091
Sports facility density	x_{sport}	2.833	2.565

Table 5.1 – Maximum value of attributes for level 2 and level 3 charging sessions.

5.4 Methods

Similar to many of the works described in Section 5.2, we use Random Utility Maximisation (RUM) discrete choice models for predicting the selection of charging station by users. As mentioned previously, the reasons why we use these models are twofold: *(i)* the comprehensive nature of our data, which offers an exceptional setup for their estimation, and *(ii)* the existing literature permitting their direct integration into optimisation models.

In Section 5.4.1, we provide the specifications of the model as to the interactions of the attributes and attribute levels. While in Section 5.4.2, we describe the validation process used to compare the various models.

5.4.1 Model Specification

For the sake of simplicity, in this section, we only detail aspects of our models which are relevant for the discussion of results. For the model properties and derivations, we refer to McFadden (1974), Revelt and Train (1998), McFadden and Train (2000), Train (2002). We provide the specifications for both MNL and MXL

models, with the latter considering panel effects. As noted in, e.g., Philipsen et al. (2016), Sheldon et al. (2019), Burroughs et al. (2021), the evaluation of location types and amenities vary significantly among individuals, making the MXL well-suited for this application. The high number of alternatives (i.e. charging stations), the total number of users, and the small number of observations for many users (in many cases just a single observation) make it computationally infeasible to compute alternative-specific or user-specific constants. Additionally, while such constants are useful in predicting individual behaviour, they are not practical for large-scale network operation. As such, we adopt a random parameters specification for our MXL model. Rather than identifying parameter values for specific individuals, this specification aims to estimate the distribution of parameter values across the population. This makes it well-suited for predicting aggregate-level demand, as it can be applied to users who have not been observed.

In our application, each user i must select a charging station alternative j based on the attributes $k = 1, \ldots, K$ given in Section 5.3.3. Each alternative is assumed to have a *utility function* $u_{ij} = V_{ij} + \varepsilon_{ij}$, a prediction of the value of alternative j for user i, which combines *observable* attributes V_{ij} known by the modeller and *unobservable* attributes ε which are known only to the user. In both the MNL and MXL models, we assume that our observable utility takes the standard form which is linear in parameters

$$V_{ij} = \sum_{k=1}^{K} \beta_k x_{ijk}.$$

We recall that x_{ijk} denotes the value of attribute k for user i and charging station j. We note that the parameters β_k are independent of the user i in this formulation, and the dependence of the observable utility on the user appears only via the attributes x_{ijk}. In the case of our MXL model, the mean β_k^{μ} and standard deviation β_k^{σ} are estimated for each attribute k, while only the mean value is estimated for MNL.

We assume that users are either charging near their home or charging while performing daily activities (Hardman et al. 2018), with different attributes considered for each case. We note that Hardman et al. (2018) also list workplace charging and charging during long-distance travel, which do not apply in our situation. Since the charging session dataset does not include the paths travelled by the user (cf.

Sun et al. 2016), it is not possible to determine whether the user is charging near their home or while performing daily activities (most notably, their activity may be near their home). As such, we use a cutoff threshold based on the distance from home, with charging sessions within 1.5 km (network distance) being considered as charging near home and charging sessions outside of 1.5 km being considered as charging near an activity. This threshold distance was selected based on the attributes for walking proximity to home, and is also similar to the maximum path deviation distance of 1.75 km for charging by private vehicle users in Sun et al. (2016).

More specifically, the observable utility within 1.5 km is given by

$$V = \beta_{\text{distNear}} x_{\text{dist}} + \beta_{\text{outletsNear}} x_{\text{outlets}} + \beta_{\text{isWalkHome}} x_{\text{isWalkHome}},$$

where the indices for user i and station j have been omitted from the attribute levels x for ease of reading. The parameters β_{distNear}, $\beta_{\text{outletsNear}}$, and $\beta_{\text{isWalkHome}}$ are respectively those for the distance to home, the number of outlets, and the station being a short walk from home.

When outside of 1.5 km, the observable utility is given by

$$\begin{aligned} V = \beta_{\text{distFar}} x_{\text{dist}} + \beta_{\text{outletsFar}} x_{\text{outlets}} + \beta_{\text{isGas}} x_{\text{isGas}} + \beta_{\text{leis}} x_{\text{leis}} + \beta_{\text{sport}} x_{\text{sport}} \\ + \beta_{\text{sm}} x_{\text{sm}} + \beta_{\text{shop}} x_{\text{ishop}} + \beta_{\text{mall}} x_{\text{mall}} + \beta_{\text{rest}} x_{\text{rest}} + \beta_{\text{ff}} x_{\text{f}}, \end{aligned}$$

where the indices i and j have been omitted as before. The parameters β_{distFar} and $\beta_{\text{outletsFar}}$, as well as the attribute levels x_{dist} and x_{outlets} are equivalent to the prior case. The parameter and attribute level β_{isGas} and x_{isGas} are those for whether station j is located at a gas station. The parameters $\beta_{\text{leis}}, \beta_{\text{sport}}, \beta_{\text{sm}}, \beta_{\text{shop}}, \beta_{\text{mall}}, \beta_{\text{rest}}$, and β_{ff} are those for the proximity to amenities, respectively for leisure facilities, sports facilities, supermarkets, shopping facilities, shopping malls, restaurants, and fast food locations.

5.4.2 Estimation and Validation

To estimate, validate, and compare the MNL and MXL models, we employ internal five-fold cross-validation (Parady et al. 2021). More specifically, due to

the presence of panel data, we use a grouped sampling approach based on the users to prevent *data leakage* (Hillel 2020, Hillel et al. 2021). In this approach, users are randomly divided into five groups, while keeping a similar number of observations in each group. The observations from some groups are used for estimation, while the others are kept for validation (the specifics of which observations are different for level 2 and level 3 charging, and are given below). For validation, only the last observation (i.e. the latest observation in time) is used.

For level 3 charging, each group contains 214 users and approximately 853 observations. For each fold, the estimation set is composed of four out of the five groups, with the last observation of the users in the remaining group reserved for validation. This results in a roughly 94-6 split of observations between estimation and validation. For level 2 charging, each group contains approximately 1,180 users and 11,682 observations. However, the high number of observations and alternatives make it intractable to solve even one group. As such, for each fold, the estimation set samples 5,000 observations from one group, with the last observation of the users in the remaining groups reserved for validation. This results in a roughly 51-49 split of observations between estimation and validation.

In addition to parameter values, we report a series of standard performance indicators about the results in both the estimation and validation sets, such as the log-likelihood (of both the final parameter values and with all parameter values set to 0), ρ, $\bar{\rho}^2$, Akaike Information Criterion, and Bayesian Information Criterion (Parady et al. 2021, Bierlaire 2023). In addition, for the validation set, we present some statistics relating to the distribution of the probability of the chosen alternatives for the estimated model, denoted "DPSA, final" in the tables below. The mean of this distribution – given by $\frac{1}{|N|}\sum_{i\in N}\sum_{j\in M} y_{ij}P(\beta^*, x_{ij})$ with β^* the final parameter values – corresponds to the *fitting factor* described in Parady et al. (2021). Since the number of available alternatives is not constant throughout the observations, we also present the distribution of the choice probabilities corresponding to the uniform distribution, denoted "DPSA, null" in the tables below. Higher values are preferred for the log-likelihoods, ρ, $\bar{\rho}^2$, and DPSA, while lower values are desirable for the Akaike Information Criterion and the Bayesian Information Criterion.

5.5 Results

In this section, we present the results of the estimation and validation processes, obtaining the parameter values using Biogeme version 3.2.12 (Bierlaire 2023). A total of 1,000 draws are used for the simulations, where required. The results for level 2 and level 3 charging are presented, respectively, in Sections 5.5.1 and 5.5.2, while a discussion of these results is reserved for Section 5.6.

Further computational results are presented in A.3.3.

5.5.1 Level 2

Parameter ratio values for both MNL and MXL models in each fold are presented in Table 5.2, while the averages of these ratios across folds are presented in Table 5.3. We note that the parameter values for all but one fold (Fold 2) in the MXL model are preliminary, as the convergence criteria has not been achieved. In particular, the simulated log-likelihood and its derivatives are highly time consuming to obtain, given the number of observations. Statistical significance is not yet available for the folds which have not converged.

Performance indicators for MNL and MXL models in the estimation sets are, respectively, presented in Tables 5.4 and 5.5. In addition to the standard performance indicators, we include the gradient norm in each fold for the MXL model. We recall that the estimation results are not comparable between the MNL and MXL models, due to the panel effect in the MXL model. In Table 5.6 we present the performance indicators of both models in the validation sets, which can be compared.

5.5.2 Level 3

Parameter values for both MNL and MXL models are presented in Table 5.7, while the average of the parameter ratios are presented in Table 5.11. Performance indicators for MNL and MXL models in the estimation sets are, respectively, presented in Tables 5.8 and 5.9. As with level 2 charging, the estimation results are not comparable between the MNL and MXL models. In Table 5.10, we present the performance indicators of both models in the validation sets, which can be

Table 5.2 – Parameter ratio values across models and folds for level 2 charging. *** indicates significance at 1% level, ** significance at 5% level, and * significance at 10% level. Statistical significance is not available for entries in **bold**.

Fold	0		1		2		3		4	
Model	MNL	MXL	MNL	MXL	MNL	MXL	MNL	MXL	MNL	MXL
$\beta^{\mu}_{distNear}$	0.2062***	**−0.3309**	0.3309***	**−0.249**	0.2246***	-0.4948***	0.2079***	**−0.2749**	0.2693***	**−0.2251**
$\beta^{\sigma}_{distNear}$	-	**0.8242**	-	**0.8297**	-	0.9905***	-	**0.7534**	-	**0.7715**
$\beta^{\mu}_{distFar}$	-0.0526***	**−0.159**	-0.0462***	**−0.0769**	-0.0371***	-0.0982***	-0.0496***	**−0.1052**	-0.049***	**−0.0816**
$\beta^{\sigma}_{distFar}$	-	**0.1192**	-	**0.0755**	-	0.0834***	-	**0.0923**	-	**0.0704**
β^{μ}_{ff}	-0.031***	**−0.1302**	-0.0369***	**−0.1271**	-0.0314***	-0.1352***	-0.0396***	**−0.1146**	-0.03***	**−0.0985**
β^{σ}_{ff}	-	**0.2849**	-	**0.2128**	-	0.3942***	-	**0.1604**	-	**0.1532**
β^{μ}_{leis}	-0.0513***	**−0.0598**	-0.037***	**−0.0241**	-0.0746***	-0.1005***	-0.0528***	**−0.0298**	-0.0583***	**−0.0434**
β^{σ}_{leis}	-	**0.4915**	-	**0.2666**	-	0.363***	-	**0.3001**	-	**0.2855**
β^{μ}_{mall}	0.0875***	**−0.1184**	0.0945***	**−0.0676**	0.0564***	-0.0865	0.2021***	**0.0808**	0.1511***	**0.0318**
β^{σ}_{mall}	-	**0.8005**	-	**0.5455**	-	0.6543***	-	**0.5454**	-	**0.621**
$\beta^{\mu}_{outletsNear}$	0.1049***	**0.0688**	0.0851***	**−0.0999**	0.0687***	0.0579*	0.0738***	**0.0226**	0.0565***	**0.0209**
$\beta^{\sigma}_{outletsNear}$	-	**0.3485**	-	**0.5712**	-	0.4055***	-	**0.2377**	-	**0.3823**
$\beta^{\mu}_{outletsFar}$	0.0367***	**0.0182**	0.0339***	**0.023**	0.0274***	0.0262***	0.0279***	**0.0321**	0.022***	**0.024**
$\beta^{\sigma}_{outletsFar}$	-	**0.1281**	-	**0.0701**	-	0.091***	-	**0.0586**	-	**0.0518**
β^{μ}_{rest}	0.1147***	**0.3019**	0.1242***	**0.2111**	0.1076***	0.2587***	0.1142***	**0.1759**	0.1204***	**0.1962**
β^{σ}_{rest}	-	**0.3913**	-	**0.2158**	-	0.3426***	-	**0.2177**	-	**0.2549**
β^{μ}_{shop}	-0.0316***	**−0.1163**	-0.0312***	**−0.0549**	-0.0142**	-0.0651**	-0.0341***	**−0.0581**	-0.0455***	**−0.0624**
β^{σ}_{shop}	-	**0.1808**	-	**0.1413**	-	0.22***	-	**0.1094**	-	**0.1453**
β^{μ}_{sport}	0.0258***	**−0.0406**	0.022***	**0.0076**	0.0219***	0.0562**	0.0353***	**0.0222**	0.0126	**−0.0069**
β^{σ}_{sport}	-	**0.3975**	-	**0.3012**	-	0.4046***	-	**0.2573**	-	**0.2614**
β^{μ}_{sm}	0.0325***	**0.002**	0.0358***	**−0.0202**	0.0125	0.0253	0.0514***	**0.0368**	0.0783***	**0.0431**
β^{σ}_{sm}	-	**0.4785**	-	**0.4456**	-	0.4074***	-	**0.3554**	-	**0.3719**
β^{μ}_{isGas}	-0.0779**	**−0.3685**	-0.1074***	**−0.4726**	0.0352	-0.8033***	-0.1437***	**−0.2005**	-0.1265***	**−0.3104**
β^{σ}_{isGas}	-	**0.4689**	-	**0.4605**	-	0.9415***	-	**0.2131**	-	**0.43**
$\beta^{\mu}_{isWalkHome}$	1.0***	**1.0**	1.0***	**1.0**	1.0***	1.0***	1.0***	**1.0**	1.0***	**1.0**
$\beta^{\sigma}_{isWalkHome}$	-	**1.5797**	-	**1.0219**	-	1.5057***	-	**1.2341**	-	**0.9119**

	MNL	MXL
$\beta^{\mu}_{distNear}$	0.2478	-0.4948
$\beta^{\sigma}_{distNear}$	-	0.9905
$\beta^{\mu}_{distFar}$	-0.0469	-0.0982
$\beta^{\sigma}_{distFar}$	-	0.0834
β^{μ}_{ff}	-0.0338	-0.1352
β^{σ}_{ff}	-	0.3942
β^{μ}_{leis}	-0.0548	-0.1005
β^{σ}_{leis}	-	0.3630
β^{μ}_{mall}	0.1183	-0.0865
β^{σ}_{mall}	-	0.6543
$\beta^{\mu}_{outletsNear}$	0.0778	0.0579
$\beta^{\sigma}_{outletsNear}$	-	0.4055
$\beta^{\mu}_{outletsFar}$	0.0296	0.0262
$\beta^{\sigma}_{outletsFar}$	-	0.0910
β^{μ}_{rest}	0.1162	0.2587
β^{σ}_{rest}	-	0.3426
β^{μ}_{shop}	-0.0313	-0.0651
β^{σ}_{shop}	-	0.2200
β^{μ}_{sport}	0.0235	0.0562
β^{σ}_{sport}	-	0.4046
β^{μ}_{sm}	0.0421	0.0253
β^{σ}_{sm}	-	0.4074
β^{μ}_{isGas}	-0.0841	-0.8033
β^{σ}_{isGas}	-	0.9415
$\beta^{\mu}_{isWalkHome}$	1.000	1.000
$\beta^{\sigma}_{isWalkHome}$	-	1.5057

Table 5.3 – Parameter ratios for MNL and MXL models for level 2 charging, average across folds. Only Fold 2 is included for the MXL model, as the other folds have not converged.

	0	1	2	3	4
Null log-likelihood	-30989.9555	-30883.5489	-30834.3888	-30905.2845	-30896.4595
Final log-likelihood	-26169.0401	-26370.6137	-25960.7399	-25492.0146	-25590.8942
ρ	0.1556	0.1461	0.1581	0.1752	0.1717
$\bar{\rho}^2$	0.1551	0.1457	0.1576	0.1747	0.1713
Akaike Information Criterion	52364.0801	52767.2274	51947.4798	51010.0292	51207.7885
Bayesian Information Criterion	52448.8036	52851.9509	52032.2033	51094.7527	51292.5120

Table 5.4 – Performance indicators for level 2 charging and the MNL model, estimation sets.

	0	1	2	3	4
Null log-likelihood	-30989.9555	-30883.5489	-30834.3888	-30905.2845	-30896.4595
Final log-likelihood	-22556.2595	-23046.4296	-23108.1584	-22717.0839	-22595.5230
ρ	0.2721	0.2538	0.2506	0.2649	0.2687
$\bar{\rho}^2$	0.2713	0.2529	0.2497	0.2641	0.2678
Akaike Information Criterion	45164.5190	46144.8592	46268.3168	45486.1679	45243.0460
Bayesian Information Criterion	45333.9660	46314.3062	46437.7638	45655.6149	45412.4930
Gradient norm	3e+01	1e+00	3.37e-02	1e+02	5e+01

Table 5.5 – Performance indicators for level 2 charging and the MXL model, estimation sets.

Fold	0		1		2		3		4	
Model	MNL	MXL	MNL	MXL	MNL	MXL	MNL	MXL	MNL	MXL
Null log-likelihood	-30187.7778	-30187.7778	-30193.6513	-30193.6513	-30195.0828	-30195.0828	-30212.3235	-30212.3235	-30206.8255	-30206.8255
Final log-likelihood	-26625.7833	-26974.2261	-26393.6309	-26630.9121	-26527.7925	-26761.5221	-26584.7775	-26709.8950	-26511.3104	-26593.9676
ρ	0.1180	0.1065	0.1259	0.1180	0.1215	0.1137	0.1201	0.1159	0.1223	0.1196
$\bar{\rho}^2$	0.1176	0.1056	0.1254	0.1171	0.1210	0.1129	0.1196	0.1151	0.1219	0.1187
Akaike Information Criterion	53277.5665	54000.4522	52813.2617	53313.8242	53081.5850	53575.0442	53195.5549	53471.7901	53048.6209	53239.9353
Bayesian Information Criterion	53361.5464	54168.4119	52897.2416	53481.7838	53165.5649	53743.0039	53279.5375	53639.7553	53132.6035	53407.9005
DPSA null, min	0.0014	0.0014	0.0014	0.0014	0.0014	0.0014	0.0014	0.0014	0.0014	0.0014
DPSA null, mean	0.0017	0.0017	0.0017	0.0017	0.0017	0.0017	0.0017	0.0017	0.0017	0.0017
DPSA null, max	0.0037	0.0037	0.0038	0.0038	0.0038	0.0038	0.0038	0.0038	0.0038	0.0038
DPSA final, min	0.0000	0.0001	0.0000	0.0001	0.0000	0.0001	0.0000	0.0001	0.0000	0.0001
DPSA final, mean	0.0210	0.0220	0.0197	0.0191	0.0224	0.0186	0.0212	0.0235	0.0223	0.0218
DPSA final, max	0.5830	0.4413	0.5820	0.2998	0.5699	0.3494	0.6041	0.4587	0.6341	0.4190

Table 5.6 – Performance indicators for level 2 charging, validation sets.

Fold	0		1		2		3		4	
Model	MNL	MXL	MNL	MXL	MNL	MXL	MNL	MXL	MNL	MXL
$\beta^{\mu}_{distNear}$	0.6148***	0.2005*	0.8744***	0.1413	0.6265***	0.1687	0.8691***	0.2696	0.8801***	0.3891*
$\beta^{\sigma}_{distNear}$	-	0.1192***	-	1.0022***	-	0.2401***	-	0.7604**	-	0.3439**
$\beta^{\mu}_{distFar}$	-0.0885***	-0.0752***	-0.1029***	-0.1428***	-0.1003***	-0.055***	-0.1305***	-0.1937***	-0.0924***	-0.1358***
$\beta^{\sigma}_{distFar}$	-	0.0577***	-	0.1078***	-	0.0429***	-	0.1548***	-	0.1004***
β^{μ}_{ff}	-0.2159***	-0.2602***	-0.322***	-0.4012***	-0.2377***	-0.1274***	-0.1939***	-0.5005***	-0.1899***	-0.2837***
β^{σ}_{ff}	-	0.2689***	-	0.363***	-	0.1339***	-	0.4024***	-	0.3189***
β^{μ}_{leis}	0.079***	0.0347	0.1419***	0.169***	0.0463*	0.0595***	0.1723***	0.1447***	0.0934***	0.1081***
β^{σ}_{leis}	-	0.263***	-	0.5392***	-	0.2202***	-	0.619***	-	0.3361***
β^{μ}_{mall}	0.1057***	-0.0343	0.0783*	-0.2957***	0.2267***	0.0078	0.287***	-0.021	0.1566***	-0.071
β^{σ}_{mall}	-	0.4823***	-	0.9875***	-	0.2797***	-	0.9135***	-	0.8865***
$\beta^{\mu}_{outletsNear}$	0.0064	0.0603	-0.0464	0.2259	0.0979**	0.0744	0.1238*	0.2778*	-0.1152***	-0.0411
$\beta^{\sigma}_{outletsNear}$	-	0.4151***	-	0.4682***	-	0.3678***	-	0.6916***	-	0.3747***
$\beta^{\mu}_{outletsFar}$	0.148***	0.0705***	0.1714***	0.0769***	0.1819***	0.0365***	0.2136***	0.1537***	0.178***	0.1119***
$\beta^{\sigma}_{outletsFar}$	-	0.101***	-	0.2959***	-	0.0691***	-	0.2806***	-	0.2313***
β^{μ}_{rest}	-0.1446***	-0.064	-0.1612***	-0.1294***	-0.1733***	-0.0406***	-0.2922***	-0.1984***	-0.2136***	-0.1714***
β^{σ}_{rest}	-	0.1593***	-	0.4012***	-	0.1401***	-	0.5425***	-	0.2956***
β^{μ}_{shop}	0.0614***	0.0372	0.0657***	-0.0166	0.1015***	-0.0003	0.0726**	0.0306	0.0754***	-0.0005
β^{σ}_{shop}	-	0.1069**	-	0.1347**	-	0.0682***	-	0.3185***	-	0.1981***
β^{μ}_{sport}	-0.1595***	-0.188***	-0.2952***	-0.4407***	-0.1611***	-0.0924***	-0.2435***	-0.3894***	-0.1968***	-0.2663***
β^{σ}_{sport}	-	0.2872***	-	0.6739***	-	0.1487***	-	0.771***	-	0.3883***
β^{μ}_{sm}	0.0067	-0.1492**	0.0236	-0.0852	-0.0088	-0.0696**	0.013	-0.1616	-0.0266	-0.2381***
β^{σ}_{sm}	-	0.4688***	-	0.8234***	-	0.2523***	-	1.0051***	-	0.8895***
β^{μ}_{isGas}	-0.0929***	-0.1387***	-0.116***	-0.2974***	-0.2335***	-0.093***	-0.1718***	-0.5714**	-0.1261***	-0.178***
β^{σ}_{isGas}	-	0.3896***	-	0.6172***	-	0.188***	-	0.9149***	-	0.3139***
$\beta^{\mu}_{isWalkHome}$	1.0***	1.0***	1.0***	1.0***	1.0***	1.0***	1.0***	1.0***	1.0***	1.0***
$\beta^{\sigma}_{isWalkHome}$	-	0.3111***	-	0.3686	-	0.1263	-	0.785***	-	0.6906***

Table 5.7 – Parameter ratio values across models and folds for level 3 charging. *** indicates significance at 1% level, ** significance at 5% level, and * significance at 10% level

compared.

5.6 Discussion

We begin by discussing aspects which apply to both the level 2 and level 3 models. Firstly, we note that both the MNL and MXL models have a DPSA (notably, a fitting factor) that is better than the null model (which reflects random assignment). Combined with the ρ and $\bar{\rho}^2$, this indicates an increased predictive power in comparison with random assignment. Secondly, consistent with the literature, we observe a high level of heterogeneity among the population. Notably, the standard deviation terms in the MXL models are nearly always highly statistically significant, and larger than their mean counterpart. In addition, we note that there

Fold	0	1	2	3	4
Null log-likelihood	-8419.7258	-8385.2235	-8356.5570	-8627.8104	-8605.7668
Final log-likelihood	-5345.6229	-5280.0078	-5208.7181	-5335.3427	-5281.3956
ρ	0.3651	0.3703	0.3767	0.3816	0.3863
$\bar{\rho}^2$	0.3636	0.3688	0.3751	0.3801	0.3848
Akaike Information Criterion	10717.2458	10586.0156	10443.4361	10696.6854	10588.7913
Bayesian Information Criterion	10796.8367	10665.6603	10523.1001	10776.6114	10668.7399

Table 5.8 – Performance indicators for level 3 charging and the MNL model, estimation sets.

Fold	0	1	2	3	4
Null log-likelihood	-8419.7258	-8385.2235	-8356.5570	-8627.8104	-8605.7668
Final log-likelihood	-3766.3995	-3623.5473	-3562.6887	-3637.0272	-3744.4518
ρ	0.5527	0.5679	0.5737	0.5785	0.5649
$\bar{\rho}^2$	0.5496	0.5648	0.5706	0.5754	0.5619
Akaike Information Criterion	7584.7989	7299.0947	7177.3773	7326.0543	7540.9036
Bayesian Information Criterion	7743.9806	7458.3842	7336.7052	7485.9064	7700.8007

Table 5.9 – Performance indicators for level 3 charging and the MXL model, estimation sets.

Fold	0		1		2		3		4	
Model	MNL	MXL	MNL	MXL	MNL	MXL	MNL	MXL	MNL	MXL
Null log-likelihood	-550.7606	-550.7606	-552.2736	-552.2736	-545.7064	-545.7064	-549.6208	-549.6208	-545.3061	-545.3061
Final log-likelihood	-357.6648	-349.7332	-404.1204	-399.0165	-387.7339	-373.2738	-426.1003	-413.0833	-389.8922	-375.0958
ρ	0.3506	0.3650	0.2683	0.2775	0.2895	0.3160	0.2247	0.2484	0.2850	0.3121
$\bar{\rho}^2$	0.3270	0.3178	0.2447	0.2304	0.2657	0.2683	0.2011	0.2011	0.2612	0.2645
Akaike Information Criterion	741.3296	751.4663	834.2408	850.0330	801.4677	798.5476	878.2005	878.1667	805.7844	802.1917
Bayesian Information Criterion	785.0873	838.9817	877.9985	937.5483	845.2254	886.0630	921.8973	965.5603	849.4812	889.5853
DPSA null, min	0.0556	0.0556	0.0556	0.0556	0.0556	0.0556	0.0556	0.0556	0.0556	0.0556
DPSA null, mean	0.0825	0.0825	0.0824	0.0824	0.0858	0.0858	0.0805	0.0805	0.0843	0.0843
DPSA null, max	0.2500	0.2500	0.2500	0.2500	0.2500	0.2500	0.2500	0.2500	0.2500	0.2500
DPSA final, min	0.0027	0.0066	0.0014	0.0037	0.0008	0.0046	0.0006	0.0042	0.0025	0.0027
DPSA final, mean	0.3106	0.3136	0.2959	0.2844	0.3210	0.3125	0.2654	0.2591	0.2944	0.2985
DPSA final, max	0.9364	0.9275	0.9419	0.8582	0.9515	0.9139	0.9544	0.7882	0.9462	0.8183

Table 5.10 – Performance indicators for level 3 charging, validation sets.

	MNL	MXL
$\beta^{\mu}_{distNear}$	0.7730	0.2338
$\beta^{\sigma}_{distNear}$	-	0.4455
$\beta^{\mu}_{distFar}$	-0.1029	-0.1205
$\beta^{\sigma}_{distFar}$	-	0.0093
β^{μ}_{ff}	-0.2319	-0.3146
β^{σ}_{ff}	-	0.2974
β^{μ}_{leis}	0.1066	0.1032
β^{σ}_{leis}	-	0.3955
β^{μ}_{mall}	0.1709	-0.0828
β^{σ}_{mall}	-	0.7099
$\beta^{\mu}_{outletsNear}$	0.0133	0.1195
$\beta^{\sigma}_{outletsNear}$	-	0.4635
$\beta^{\mu}_{outletsFar}$	0.1786	0.0899
$\beta^{\sigma}_{outletsFar}$	-	0.1956
β^{μ}_{rest}	-0.1970	-0.1207
β^{σ}_{rest}	-	0.3077
β^{μ}_{shop}	0.0753	0.0101
β^{σ}_{shop}	-	0.0861
β^{μ}_{sport}	-0.2112	-0.2754
β^{σ}_{sport}	-	0.4538
β^{μ}_{sm}	0.0016	-0.1408
β^{σ}_{sm}	-	0.6878
β^{μ}_{isGas}	-0.1481	-0.2557
β^{σ}_{isGas}	-	0.4847
$\beta^{\mu}_{isWalkHome}$	1.0000	1.0000
$\beta^{\sigma}_{isWalkHome}$	-	0.7922

Table 5.11 – Parameter ratios for MNL and MXL models for level 3 charging, average across folds.

are some differences in sign or significance between the two models, such as the network distance when near home, the density of shopping malls, and the density of shopping facilities. For the average parameter ratios for level 2 in Table 5.3, we also note that the parameter value for the network distance in the MXL model is more than double that of the MNL model. These factors suggests that the MXL model should be privileged for optimisation models, despite the similar performances of the MNL and MXL models in the validation sets. We note that the MXL model performed worse than the MNL model in the validation set for Fold 2, the only fold for which the MXL model converged. This warrants further investigation, once final results are available for all folds. Given the differences between the models, we concentrate on the MXL model in the discussion below, only considering the fold that successfully converged in the level 2 case. Thirdly, when considering charging close to home, the effects of the network distance and the charging station being a short walk from home are comparable (since, by assumption, the distance is bound by 1.5 km in this case), while the number of outlets has a lesser (though still positive and statistically significant) effect. However, when considering charging far from home, the most important attribute is certainly the distance. More specifically, there is a higher bound on the attribute values for the distance compared with the other parameters, with a maximum of around 50 km for level 3 and 100 km for level 2. By contrast, the density measures for the amenities have a maximum of around 5, while the number of outlets has a maximum of 5 outlets for level 3 and 13 outlets for level 2. Fourthly, we observe different preferences between level 2 and level 3 charging stations, particularly as it pertains to the amenities. This highlights the different use cases for the types of charging, consistent with Anderson et al. (2018).

As it pertains to the impact of amenities for level 2 charging in Table 5.3, the only overall positive and statistically significant effects were for the density of restaurants and sports facilities. In addition to this, the effects of the density of shopping malls and supermarkets were overall neutral, with a standard deviation term at least an order of magnitude higher than the mean terms. Despite the positive impact of restaurants, the density of fast food locations had a negative and statistically significant effect, suggesting a preference for longer duration or possible other confounding factors. Likewise, the charging station being located at a gas station likewise had a negative and statistically significant effect, as did

the densities of leisure locations and shopping facilities. As the main value of gas stations was associated with habit in Philipsen et al. (2015, 2016), this suggests that the long-term habits of EV users have adapted around the new refueling requirements. Given their respective bounds, the effects of the amenities near the charging station can have a larger impact than the number of outlets.

For level 3 charging, we first note that the average parameter ratios in Table 5.11 indicates a positive effect for the network distance when charging close to home. As discussed previously, a possible explanation for the positive effect of the distance is that users with access to home charging may prefer to use that rather than a public charger when near home. However, in over 75% of the observations, there are no charging stations are within 1.5 km of the user (for more details, see Table A.10 in A.3.2). As such, unexpected phenomena may be due to a lack of observations. For the amenities, the density of leisure locations has a positive and statistically significant effect, while fast food locations, restaurants, sports facilities, supermarkets, and gas stations had negative and statistically significant average effects. The aversion to restaurants, sports facilities, and supermarkets for level 3 charging may be attributable to longer duration of these activities in comparison with the charging time. The impacts of shopping malls and shopping facilities were overall neutral, but with a standard deviation terms nearly an order of magnitude higher than the mean terms.

5.7 Conclusion

In this work, we estimated multinomial logit and mixed logit models for analysing and predicting electric vehicle charging station usage, for both level 2 and level 3 locations. Our models rely on characteristics of charging stations that are readily available for charging network operators, and thus make them well-suited for optimisation purposes. Internal 5-fold cross validation was performed to evaluate the accuracy and predictive power of our models, demonstrating improved performance over random selection.

By design, these estimation results can be integrated into electric vehicle charging stations network design models such as Luo et al. (2015), Cui et al. (2019),

Lamontagne et al. (2023). In addition, our findings indicate that the demand models integrated into these optimisation programs should factor panel effects. Notably, users who recharge frequently on the public network significantly influence the average preferences of the MNL model, while the MXL model can identify the outlying behaviour. As a consequence, optimisation models which do not include panel effects may integrate unrealistic user behaviour, thus incorrectly evaluating the potential benefits of stations.

Overall, users prefer level 2 charging stations closer to their home (especially within walking distance), while preferences for level 3 charging stations were more variable. Far from home, the most significant attribute was the distance between the home area of the users and the charging locations, with the number of outlets having a positive (if more muted) impact. High heterogeneity was observed for nearly all attributes, suggesting the existence of users with higher preference for all attributes (even those for which a general aversion is observed).

For the amenities, we observe that the network distance between charging stations at gas stations or near fast food locations are avoided, regardless of charging level. For level 2 charging stations, locations near restaurants were preferred while locations near shopping facilities, shopping malls, leisure activities, and restaurants had a neutral effect, with high variability among users. For level 3 charging stations, locations near leisure locations were favored while longer duration activities (including restaurants, sports facilities, supermarkets, and shopping malls) were avoided. As the locations of amenities are primarily identified via the definitions from OpenStreetMaps (OpenStreetMap contributors 2017), it is possible that further refinement may be able to better distinguish the impacts of these attributes. For example, the 'leisure' category includes locations such as public parks and cinemas, which have notably different durations. However, further study would be necessary as to partitioning types of locations.

Our work focuses on the intracity case, where both the charging stations and the users are located within the same city. However, future work could extend this approach to the intercity case, where the charging stations are being used during the course of long-distance trips. Additionally, while not relevant in this market, future work could also incorporate charging price to the selection process.

Acknowledgements

The authors gratefully acknowledge the assistance of Jean-Luc Dupre from *Direction Mobilité* of *Hydro-Québec* for sharing his expertise on EV charging stations and the network. We also gratefully acknowledge Miguel F. Anjos, Ismail Sevim, and Nagisa Sugishita for their insights into the project.

This research was supported by Hydro-Québec, NSERC Collaborative Research and Development Grant CRDPJ 536757 - 19, and the FRQ-IVADO Research Chair in Data Science for Combinatorial Game Theory.

6 Conclusion

While the advances are presented in the context of promoting EV adoption, the articles contained within this work also provide contributions in more general contexts. For the first article (Chapter 3), the efficient reformulation into a MCLP can be used alongside the simulation-based approach of Pacheco Paneque et al. (2021) whenever it is not necessary to know the exact alternative selected by users. For the second article (Chapter 4), both the accelerated Benders decomposition and the local branching method can be applied to dynamic MCLP applications with only covering constraints on the users. Notably, our results indicate that the accelerated Benders decomposition method we propose constitutes the fastest exact method for such cases. For the third article (Chapter 5), our parameter estimations are specifically designed for integration into more general EV charging network optimisation, such as the ones in Luo et al. (2015) and Cui et al. (2019), rather than simply for EV adoption. Additionally, as these discrete choice models are for predicting charging station selection without user-specific characteristics, they are well suited for tasks such as demand forecasting for strategic planning.

In conclusion, this thesis has provided important stepping stones for more accurate EV charging network design models and their solving methodologies. Building upon our findings, future research should expand the limitations of our assumptions. This is discussed in the next sections.

Joint Optimisation of Intracity and Intercity Network The EV adoption model of Anjos et al. (2020) is designed to optimise both intracity and intercity placement of EV charging stations simultaneously. Using the notation from the first article (Chapter 3), the availability sets C_i^{1t} in the single-level model and the coverage parameters a_{jik}^{rt} in the maximum covering model can handle multiple disjoint cities. One must simply not include charging stations in different cities from the users in their availability sets, or set the associated coverage parameter

to 0. This would result in a multi-period MCLP with disjoint covering constraints for each city, with the budget constraints being the only ones linking the problem among different cities.

However, this neglects intercity traveling, and thus, the best way to handle the intercity network design remains an open question. This is particularly important for the province of Quebec given its vast territory. Ideally, one could include the intercity charging network as a component to the utility functions (i.e. a better intercity network increases the utility for all charging alternatives). Unfortunately, this approach breaks the separability of the utility functions by alternative, a crucial component for the maximum covering reformulation. Additionally, it is not clear if data sources exist to accurately estimate the effect of the intercity network on EV adoption. For instance, it would likely be necessary to have disaggregate origin-destination or paths for individual users within each city.

Alternatively, a simple way to take into account the intercity charging network without modifying the utility functions would be as a bound constraint:

$$\sum_{j \in \text{IC}} \sum_{k=1}^{m_j} k \left(x_{jk}^t - x_{jk-1}^t \right) \geq \alpha \sum_{i \in N} \sum_{r=1}^{R_i} \frac{N_i^{t-1}}{R_i} w_i^{rt-1}, 1 \leq t \leq T,$$

where IC is a particular section of the intercity network and $\alpha \geq 0$. Effectively, this constraint ensures that there are at least $\frac{1}{\alpha}$ outlets on the intercity network per user. With this approach, the formulation remains an MCLP model. Moreover, for the accelerated Benders decomposition in the second article (Chapter 4), the term on the right-hand side is given by the auxiliary variables θ^{t-1}. As a consequence, this constraint does not affect the Benders subproblem structure, and the accelerated Benders decomposition and local branching methods are still valid.

Capacity Constraints on Alternatives In our first article (Chapter 3), we assume that there is no capacity limit for each alternative, which differs from the capacity constraint for each charging station imposed in Anjos et al. (2020). While our assumption is not a strict requirement of the single-level model (notably, capacity constraints are used in the original formulation of Pacheco Paneque et al. 2021), this does interfere with the maximum covering reformulation. In particular, the covering variables w_i^{rt} and associated covering constraints $w_i^{rt} \leq \sum_{j \in M} \sum_{k=1}^{m_j} a_{jik}^{rt} x_{jk}^t$ are

built around the assumption that we do not need to track the alternative selected by the users.

A partial workaround that allows for capacity constraints can be obtained by using different partial coverage variables w_{ji}^{rt} and covering constraints $w_{ji}^{rt} \leq \sum_{k=1}^{m_j} a_{jik}^{rt} x_{jk}^{t}$. Capacity constraints can then be imposed on these partial coverage variables:

$$\sum_{(t,i,r)\in P} \frac{N_i^{t-1}}{R_i} w_{ji}^{rt} \leq \text{Cap}(k),$$

where $\text{Cap}(k)$ is a predefined capacity function which depends on the number of outlets. We then define a new coverage variable $\bar{w}_i^{rt}$ with constraints $\bar{w}_i^{rt} \leq w_{ji}^{rt}, j \in M$, which replaces our original covering variables w_i^{rt} in the objective function.

Using this preserves the maximum covering reformulation. A feasible solution to this new model ensures that there is at least one valid assignment of users to alternatives which satisfies our capacity constraints and the preferences of the users. However, this method may result in some econometric issues. For example, consider a situation with two users (i_1 and i_2), along with two charging stations (j_1 and j_2) each with a capacity of 1. The charging station j_1 covers users i_1 and i_2, while the charging station j_2 only covers the user i_1. Naturally, the optimal solution will assign user i_1 to station j_2 and user i_2 to station j_1. But it is possible that the utility of user i_1 for station j_1 is higher than the utility for station j_2. In other words, in this situation, the selection of user i_1 does not follow the utility maximisation principle.

Considering the second article (Chapter 4) instead, we note that these modifications do change the structure of the Benders subproblem. Notably, the capacity constraints (which must be added to the Benders subproblem) have several detrimental effects:

— As the capacity depends on the assignment of all of the users, this breaks the separability of the subproblem by user. As a consequence, the efficiency of the subproblem solution is likely to be impacted.

— Currently, the Benders subproblem (and its dual) has an analytical solution. It is not clear that this would hold in the capacitated case, further impacting the efficiency of the subproblem solution.

— For standard Benders decomposition to apply, we rely on the relaxation of

the integrality constraints on the variables z_j^t in the Benders subproblem. However, integrality is highly unlikely to hold when considering the capacity. As such, a generalised Benders approach would be necessary (see, e.g. Rahmaniani et al. 2017).

These effects pose serious concerns as to the applicability and viability of the proposed Benders approach in the capacitated case. As such, adaptations may be necessary for an efficient implementation.

In summary, a simple adaptation of the model can allow for capacity considerations. While this does pose some econometric concerns, it does preserve the maximum covering formulation. However, serious modifications would be necessary for the accelerated Benders decomposition, and it may not be applicable at all.

Alternative-dependent Objective Function An additional assumption in the first article (Chapter 3) is that alternatives can broadly be categorised as either "good" or "bad" in the objective function. In our case, this means that the opt-out alternative has a value of 0 in the objective, while the home charging and public charging alternatives all correspond to a value of $\frac{N_i^t}{R_i}$. However, there are cases, such as in pricing problems (e.g. Bortolomiol et al. 2021a,b, Pinzon et al. 2023), where each alternative may correspond to a different profit in the objective function.

The same workaround can be applied as for the capacitated case, with partial coverage variables w_{ji}^{rt} and covering constraints $w_{ji}^{rt} \leq \sum_{k=1}^{m_j} a_{jik}^{rt} x_{jk}^t$. The objective function can then be modified as

$$\sum_{(t,i,r)\in P} \sum_{j\in M} p_j w_{ji}^{rt},$$

where p_j is the profit associated with the alternative j. In this way, the maximum covering reformulation can still be applied. The coverage variables w_i^{rt} or $\bar{w}_i^{rt}$ are not necessary in this case, though the constraints $\sum_{j\in M} w_{ji}^{rt} \leq 1$ would be necessary to ensure users are only assigned to one alternative.

However, this poses even more serious econometric concerns than the capacitated case. Notably, the solver will assign each user i to the alternative j which corresponds to the maximum profit, subject to the coverage. That is, for each user

i, the optimal solutions $w_{ji}^{rt}, j \in M$ solve the following problem

$$\begin{aligned}
\text{Maximise } & \sum_{j \in M} p_j w_{ji}^{rt}, \\
\text{subject to } & \sum_{j \in M} w_{ji}^{rt} \leq 1, \\
& w_{ji}^{rt} \leq \sum_{k=1}^{m_j} a_{jik}^{rt} x_{jk}^{t}, \quad j \in M, \\
& w_{ji}^{rt} \leq 1, \qquad\qquad j \in M, \\
& w_{ji}^{rt} \geq 0, \qquad\qquad j \in M.
\end{aligned} \tag{6.1}$$

This problem can be solved by inspection, and has an analytical solution given by $w_{ji}^{rt} = 1$ if $j \in \text{argmax}_{j' \in M} \left\{ p_{j'} : \sum_{k=1}^{m_{j'}} a_{j'ik}^{rt} x_{j'k}^{t} \geq 1 \right\}$, and $w_{ji}^{rt} = 0$ otherwise. If multiple alternatives have the same profit, then the assignment among the associated alternatives is arbitrary. However, as with the capacitated case, there is the concern that selection of users does not follow the utility maximisation principle. But, contrary to the capacitated case, the interests of the users and the decision maker are diametrically opposed: Users want the cheapest option, while the decision maker wants users to select the most profitable (and usually expensive) alternative. As such, the maximum covering formulation may greatly over evaluate the profit compared to the simulation-based approach (bilevel model), as the former pushes users to select more expensive alternatives than the latter.

While the econometric concerns are more severe than the capacitated case, the application of the accelerated Benders decomposition from the second article (Chapter 4) is simpler. Notably, the Benders subproblem would be separable for each (t, i, r), as given in Equation (6.1). As we noted, it has an analytical solution which clearly preserves the integrality property. As a consequence, while the modifications would change the exact form of the Benders optimality cuts, it is likely that the methodology would still be applicable, as would the acceleration techniques.

To summarise, a similar modification to the capacitated case could also allow for an alternative-dependent objective function. While the maximum covering reformulation is likely amenable for the accelerated Benders decomposition, there

are serious econometric concerns as to the validity of this transformation.

Connecting Charging Preferences and EV Adoption In the third article (Chapter 5), we estimated a discrete choice model for predicting EV charging station selection, under the assumption that better charging stations would correlate with higher EV adoption. It remains to determine how this correlation works, particularly in regards to the parameters β^t_{jik} and κ^t_{ji} from the first article (Chapter 3).

Similar to the maximum likelihood estimation process used to obtain the parameter values $\beta_k, 1 \leq k \leq K$ in the third article (Chapter 5), we can use maximum likelihood again to estimate the contributions for EV adoption. To improve the readability, we denote by $\bar{\beta}^t_{jik}$ and $\bar{\kappa}^t_{ji}$ the parameters in the first article (i.e. relating to EV adoption), while we denote by β^μ_{k} the parameters values in the third article (i.e. relating to charging station selection). As per the third article, the parameter values β^μ_{k} are known, while $\bar{\beta}^t_{jik}$ and $\bar{\kappa}^t_{ji}$ are not. For simplicity, while we present the process using only the mean values, one could use a simulation approach to consider the standard deviation terms as well. For a given user i and charging station j, if the network distance between i and j is less than 1.5 km, then we set

$$\begin{aligned}
\bar{\beta}^t_{jik} &= \beta^\mu_{\mathrm{outletsNear}}, \\
\bar{\kappa}^t_{ji} &= \beta^\mu_{\mathrm{distNear}} x_{\mathrm{dist}} + \beta^\mu_{\mathrm{isWalkHome}} x_{\mathrm{isWalkHome}},
\end{aligned}$$

where the parameters β^μ and attribute values x are defined as in the third article (Chapter 5). We note that the values of β^μ depend on the level of the charging station, and so should be chosen appropriately for station j. Analogously, if the network distance between user i and station j is greater than 1.5 km, then we set

$$\begin{aligned}
\bar{\beta}^t_{jik} =& \beta^\mu_{\mathrm{outletsFar}}, \\
\bar{\kappa}^t_{ji} =& \beta^\mu_{\mathrm{distFar}} x_{\mathrm{dist}} + \beta^\mu_{\mathrm{isGas}} x_{\mathrm{isGas}} + \beta^\mu_{\mathrm{leis}} x_{\mathrm{leis}} + \beta^\mu_{\mathrm{sport}} x_{\mathrm{sport}} \\
&+ \beta^\mu_{\mathrm{sm}} x_{\mathrm{sm}} + \beta^\mu_{\mathrm{shop}} x_{\mathrm{ishop}} + \beta^\mu_{\mathrm{mall}} x_{\mathrm{mall}} + \beta^\mu_{\mathrm{rest}} x_{\mathrm{rest}} + \beta^\mu_{\mathrm{ff}} x_{\mathrm{f}},
\end{aligned}$$

where, as before, β^μ and x are defined as in the third article and set appropriate for the charging level.

With the values $\bar{\beta}^t_{jik}$ and $\bar{\kappa}^t_{ji}$ set for all charging stations, it remains to deter-

mine an appropriate value for the opt-out alternative $\bar{\kappa}_{0i}^t$ (and all other exogenous alternatives, which can use a similar process). There is also an additional hurdle in this case compared to the charging preferences: While disaggregate charging preferences are available (i.e. the charging stations selected by each individual user), it is possible that only aggregate EV adoption is known (i.e. the total number of EVs in each region). As such, rather than the index i representing a single user, in the EV adoption context it may represent a class of users sharing similar sociodemographic and geographic characteristics. We then estimate the value of $\bar{\kappa}_{0i}^t$ in the resulting discrete choice model for EV adoption

$$\begin{aligned}
\bar{u}_{0i}^t &= \bar{\kappa}_{0i}^t + \bar{\varepsilon}_{0i}^t, \\
\bar{u}_{ji}^{rt} &= \sum_{k=1}^{m_j} \bar{\beta}_{jik}^t x_{jk}^t + \bar{\kappa}_{ji}^t + \bar{\varepsilon}_{ji}^{rt}, \quad j \in C_i^{1t},
\end{aligned}$$

for which $\bar{\beta}_{jik}^t$ and $\bar{\kappa}_{ji}^t$ are kept fixed. More specifically, this estimates the value of $\bar{\kappa}_{0i}^t$ which maximises the likelihood of achieving the distribution of EV adoption for each user class i. As such, this requires data on the EV adoption rate of each user class i and time period t.

An extension of this method can be found in Sifringer et al. (2020), where they combine machine learning and discrete choice models. Machine learning is used on a portion of the terms in the utility functions, which allows for better predictive power compared to typical utility functions. However, they maintain interpretability of the resulting hybrid approach by forcing the machine learning component of utility to have an elasticity of zero. Alternatively, another method to determine appropriate values to use for $\bar{\kappa}_{0i}^t$ can be found in Berry et al. (1995). There, they provide a methodology specifically designed for aggregate measures, such as the EV adoption in each region. This method determines the values as to replicate the *moments* of the distribution for the aggregate measure.

Bibliography

Aboolian, R., Berman, O., Krass, D., 2007. Competitive facility location model with concave demand. European Journal of Operational Research 181, 598–619.

Achtnicht, M., Bühler, G., Hermeling, C., 2012. The impact of fuel availability on demand for alternative-fuel vehicles. Transportation Research Part D: Transport and Environment 17, 262–269.

Adenso-Díaz, B., Rodríguez, F., 1997. A simple search heuristic for the MCLP: Application to the location of ambulance bases in a rural region. Omega 25, 181–187.

Albareda-Sambola, M., Fernández, E., Hinojosa, Y., Puerto, J., 2009. The multi-period incremental service facility location problem. Computers & Operations Research 36, 1356–1375.

Alizadeh, R., Nishi, T., Bagherinejad, J., Bashiri, M., 2021. Multi-period maximal covering location problem with capacitated facilities and modules for natural disaster relief services. Applied Sciences 11.

Anderson, J.E., Bergfeld, M., Nguyen, D.M., Steck, F., 2023. Real-world charging behavior and preferences of electric vehicles users in Germany. International Journal of Sustainable Transportation 17, 1032–1046.

Anderson, J.E., Lehne, M., Hardinghaus, M., 2018. What electric vehicle users want: Real-world preferences for public charging infrastructure. International Journal of Sustainable Transportation 12, 341–352.

Anjos, M., Gendron, B., Joyce-Moniz, M., 2020. Increasing electric vehicle adoption through the optimal deployment of fast-charging stations for local and long-distance travel. European Journal of Operational Research 285, 263–278.

Arakaki, R.G.I., Lorena, L.A.N., 2001. A constructive genetic algorithm for the maximal covering location problem, in: Proceedings of metaheuristics international conference, pp. 13–17.

Arulselvan, A., Bley, A., Ljubić, I., 2019. The incremental connected facility location problem. Computers & Operations Research 112, 104763.

Asamer, J., Reinthaler, M., Ruthmair, M., Straub, M., Puchinger, J., 2016. Optimizing charging station locations for urban taxi providers. Transportation Research Part A: Policy and Practice 85, 233–246.

Ashkrof, P., Homem de Almeida Correia, G., van Arem, B., 2020. Analysis of the effect of charging needs on battery electric vehicle drivers' route choice behaviour: A case study in the netherlands. Transportation Research Part D: Transport and Environment 78, 102206.

de Assis Corrêa, F., Lorena, L.A.N., Ribeiro, G.M., 2009. A decomposition approach for the probabilistic maximal covering location-allocation problem. Computers & Operations Research 36, 2729–2739.

Association des Véhicules Électrique du Québec, 2021. Statistiques SAAQ-AVÉQ sur l'électromobilité au Québec en date du 30 juin 2021.

Association des véhicules électriques du Québec, 2023. Réseaux de bornes. https://www.aveq.ca/reacuteseaux-de-bornes.html [Last accessed: December 4th 2023].

Association des véhicules électriques du Québec, 2024. L'installation d'une borne à votre domicile. https://www.aveq.ca/domicile.html [Last accessed: January 16th 2024].

Atkinson, D.S., Vaidya, P.M., 1995. A cutting plane algorithm for convex programming that uses analytic centers. Mathematical Programming , 1–43.

Axsen, J., Bailey, J., Castro, M.A., 2015a. Preference and lifestyle heterogeneity among potential plug-in electric vehicle buyers. Energy Economics 50, 190–201.

Axsen, J., Goldberg, S., Bailey, J., Kamiya, G., Langman, B., Cairns, J., Wolinetz, M., Miele, A., 2015b. Electrifying Vehicles: Insights from the Canadian Plug-in Electric Vehicle Study. Technical Report. Simon Fraser University.

Axsen, J., Goldberg, S., Bailey, J., Kamiya, G., Langman, B., Cairns, J., Wolinetz, M., Miele, A., 2015c. Electrifying Vehicles: Insights from the Canadian Plug-in Electric Vehicle Study. Technical Report. Simon Fraser University.

Axsen, J., Goldberg, S., Bailey, J., Kamiya, G., Langman, B., Cairns, J., Wolinetz, M., Miele, A., 2015d. Electrifying Vehicles: Insights from the Canadian Plug-in Electric Vehicle Study. Technical Report. Simon Fraser University.

Badri-Koohi, B., Tavakkadi-Moghaddam, R., Asghari, M., 2019. Optimizing number and locations of alternative fuel stations using a multi-criteria approach. Engineering, Technology & Applied Science Research 9, 3715–3720.

Bagherinejad, J., Shoeib, M., 2018. Dynamic capacitated maximal covering location problem by considering dynamic capacity. International Journal of Industrial Engineering Computations 9, 249–264.

Bailey, J., Miele, A., Axsen, J., 2015. Is awareness of public charging associated with consumer interest in plug-in electric vehicles? Transportation Research Part D: Transport and Environment 36, 1–9.

Ben-Ameur, W., Neto, J., 2007. Acceleration of cutting-plane and column generation algorithms: Applications to network design. Networks 49, 3–17.

Benati, S., 1999. The maximum capture problem with heterogeneous customers. Computers & Operations Research 26, 1351–1367.

Benati, S., Hansen, P., 2002. The maximum capture problem with random utilities: Problem formulation and algorithms. European Journal of Operational Research 143, 518–530.

Benders, J.F., 1962. Partitioning procedures for solving mixed-variables programming problems. Numerische mathematik 4, 238–252.

Bengio, Y., Lodi, A., Prouvost, A., 2021. Machine learning for combinatorial optimization: A methodological tour d'horizon. European Journal of Operational Research 290, 405–421.

Berman, O., Drezner, T., Drezner, Z., Krass, D., 2014. Modeling competitive facility location problems: New approaches and results. INFORMS TutORials in Operations Research 14, 156–181.

Berman, O., Drezner, Z., Krass, D., 2010. Generalized coverage: New developments in covering location models. Computers & Operations Research 37, 1675–1687.

Berman, O., Hajizadeh, I., Krass, D., 2013. The maximum covering problem with travel time uncertainty. IIE Transactions 45, 81–96.

Berry, S., Levinsohn, J., Pakes, A., 1995. Automobile prices in market equilibrium. Econometrica 63, 841–890.

Bienstock, D., Zuckerberg, M., 2010. Solving LP relaxations of large-scale precedence constrained problems, in: Eisenbrand, F., Shepherd, F.B. (Eds.), Integer Programming and Combinatorial Optimization, Springer Berlin Heidelberg, Berlin, Heidelberg. pp. 1–14.

Bierlaire, M., 2020. A short introduction to Biogeme. Technical Report. Technical report TRANSP-OR 230620. Transport and Mobility Laboratory, ENAC, EPFL.

Bierlaire, M., 2023. A short introduction to Biogeme. Technical Report. Technical report TRANSP-OR 230620. Transport and Mobility Laboratory, ENAC, EPFL.

Birge, J.R., Louveaux, F.V., 1988. A multicut algorithm for two-stage stochastic linear programs. European Journal of Operational Research 34, 384–392.

Bodur, M., Luedtke, J.R., 2017. Mixed-integer rounding enhanced Benders decomposition for multiclass service-system staffing and scheduling with arrival rate uncertainty. Management Science 63, 2073–2091.

Bonami, P., Salvagnin, D., Tramontani, A., 2020. Implementing automatic Benders decomposition in a modern MIP solver, in: Bienstock, D., Zambelli, G. (Eds.), Integer Programming and Combinatorial Optimization, Springer International Publishing. pp. 78–90.

Bortolomiol, S., Lurkin, V., Bierlaire, M., 2021a. Price-based regulation of oligopolistic markets under discrete choice models of demand. Transportation 49, 1441–1463.

Bortolomiol, S., Lurkin, V., Bierlaire, M., 2021b. A simulation-based heuristic to find approximate equilibria with disaggregate demand models. Transportation Science 55, 1025–1045.

Burroughs, N., Kolich, K., Byers, T., Nordstrom, V., 2021. Electric Vehicle Charging Survey – Insights into EV owners' charging habits, and use of public EV charging. Technical Report. Energy Efficiency and Conservation Authority.

Calderín, J.F., Masegosa, A.D., Pelta, D.A., 2017. An algorithm portfolio for the dynamic maximal covering location problem. Memetic Computing 9, 141–151.

Capar, I., Kuby, M., Leon, V.J., Tsai, Y.J., 2013. An arc cover–path-cover formulation and strategic analysis of alternative-fuel station locations. European Journal of Operational Research 227, 142–151.

Chakraborty, D., Bunch, D.S., Lee, J.H., Tal, G., 2019. Demand drivers for charging infrastructure-charging behavior of plug-in electric vehicle commuters. Transportation Research Part D: Transport and Environment 76, 255–272.

Chakraborty, D., Hardman, S., Tal, G., 2020. Why do some consumers not charge their plug-in hybrid vehicles? evidence from californian plug-in hybrid owners. Environmental Research Letters 15, 084031.

Chen, L., Chen, S.J., Chen, W.K., Dai, Y.H., Quan, T., Chen, J., 2023. Efficient presolving methods for solving maximal covering and partial set covering location problems. European Journal of Operational Research 311, 73–87.

Church, R., ReVelle, C., 1974. The maximal covering location problem, in: Papers of the regional science association, Springer-Verlag Berlin/Heidelberg. pp. 101–118.

Church, R.L., Stoms, D.M., Davis, F.W., 1996. Reserve selection as a maximal covering location problem. Biological Conservation 76, 105–112.

Circuit Électrique, 2023a. Become a member. https://lecircuitelectrique.com/en/become-a-member/ [Last accessed: November 17th 2023].

Circuit Électrique, 2023b. Cost of charging. https://lecircuitelectrique.com/en/cost/ [Last accessed: October 11th 2023].

Circuit Électrique, 2023c. Find a station. https://lecircuitelectrique.com/en/find-a-station/ [Last accessed: October 11th 2023].

Circuit Électrique, 2024. Charging. https://lecircuitelectrique.com/en/stations/level-2-station/ [Last accessed: January 16th 2024].

Codato, G., Fischetti, M., 2006. Combinatorial Benders' cuts for mixed-integer linear programming. Operations Research 54, 756–766.

Coffman, M., Bernstein, P., Wee, S., 2017. Electric vehicles revisited: a review of factors that affect adoption. Transport Reviews 37, 79–93. doi:10.1080/01441647.2016.1217282, arXiv:https://doi.org/10.1080/01441647.2016.1217282.

Colombo, F., Cordone, R., Lulli, G., 2016. The multimode covering location problem. Computers & Operations Research 67, 25–33.

Coniglio, S., Furini, F., Ljubić, I., 2022. Submodular maximization of concave utility functions composed with a set-union operator with applications to maximal covering location problems. Mathematical Programming 196, 9–56.

Contreras, I., Cordeau, J.F., Laporte, G., 2011. Benders decomposition for large-scale uncapacitated hub location. Operations Research 59, 1477–1490.

Cordeau, J., Furini, F., Ljubić, I., 2019. Benders decomposition for very large scale partial set covering and maximal covering location problems. European Journal of Operational Research 275, 882–896.

Costa, A.M., Cordeau, J.F., Gendron, B., Laporte, G., 2012. Accelerating Benders decomposition with heuristic master problem solutions. Pesquisa Operacional 32, 3–19.

Crainic, T.G., Hewitt, M., Maggioni, F., Rei, W., 2021. Partial Benders decomposition: General methodology and application to stochastic network design. Transportation Science 55, 414–435.

Crainic, T.G., Hewitt, M., Rei, W., 2014. Scenario grouping in a progressive hedging-based meta-heuristic for stochastic network design. Computers & Operations Research 43, 90–99.

Cui, Q., Weng, Y., Tan, C., 2019. Electric vehicle charging station placement method for urban areas. IEEE Transactions on Smart Grid 10, 6552–6565.

Dam, T., Ta, T., Mai, T., 2021. Submodularity and local search approaches for maximum capture problems under generalized extreme value models. European Journal of Operational Research .

Daskin, M.S., 1983. A maximum expected covering location model: Formulation, properties and heuristic solution. Transportation Science 17, 48–70.

Deb, S., 2021. Machine learning for solving charging infrastructure planning problems: A comprehensive review. Energies 14.

Degel, D., Wiesche, L., Rachuba, S., Werners, B., 2015. Time-dependent ambulance allocation considering data-driven empirically required coverage. Health Care Management Science 18, 444–458.

Dell'Olmo, P., Ricciardi, N., Sgalambro, A., 2014. A multiperiod maximal covering location model for the optimal location of intersection safety cameras on an urban traffic network. Procedia - Social and Behavioral Sciences 108, 106–117.

Downs, B.T., Camm, J.D., 1996. An exact algorithm for the maximal covering problem. Naval Research Logistics (NRL) 43, 435–461.

Dupačová, J., Gröwe-Kuska, N., Römisch, W., 2003. Scenario reduction in stochastic programming. Mathematical Programming 95, 493–511.

Eiselt, H.A., Marianov, V., Drezner, T., 2019. Competitive location models, in: Laporte, G., Nickel, S., Saldanha da Gama, F. (Eds.), Location Science. Springer. chapter 14, pp. 391–429.

Elhattab, M., Khabbaz, M., Al-Dahabreh, N., Atallah, R., Assi, C., 2023. Leveraging real-world data sets for qoe enhancement in public electric vehicles charging networks. IEEE Transactions on Network and Service Management , 1–1.

Environment and Climate Change Canada, 2021. Greenhouse gas sources and sinks: executive summary 2021.

Environment and Climate Change Canada, 2023. Greenhouse gas sources and sinks: executive summary 2023.

Figenbaum, E., Kolbenstvedt, M., 2016. Learning from Norwegian Battery Electric and

Plug-in Hybrid Vehicle users – Results from a survey of vehicle owners. Technical Report. Institute of Transport Economics. Norwegian Centre for Transport Research.

Figenbaum, E., Nordbakke, S., 2019. Battery electric vehicle user experiences in norway's maturing market. Technical Report. Institute of Transport Economics. Norwegian Centre for Transport Research.

Fischetti, M., Lodi, A., 2003. Local branching. Mathematical Programming 98, 23–47.

Frade, I., et al., 2011. Optimal location of charging stations for electric vehicles in a neighborhood in Lisbon, Portugal. Transportation Research Record Journal of the Transportation Research Board 2252, 91–98.

Franke, T., Krems, J.F., 2013. Understanding charging behaviour of electric vehicle users. Transportation Research Part F: Traffic Psychology and Behaviour 21, 75–89.

Freire, A., Moreno, E., Yushimitoa, W., 2016. A branch-and-bound algorithm for the maximum capture problem with random utilities. European Journal of Operational Research 252, 204–212.

Galvão, R.D., Espejo, L., Boffey, B., 2000. A comparison of Lagrangean and surrogate relaxations for the maximal covering location problem. European Journal of Operational Research 124, 377–389.

Galvão, R.D., ReVelle, C., 1996. A Lagrangean heuristic for the maximal covering location problem. European Journal of Operational Research 88, 114–123.

Gavranović, H., Barut, A., Ertek, G., Yüzbaşıoğlu, O., Pekpostalcı, O., Önder Tombuş, 2014. Optimizing the electric charge station network of EŞARJ, in: Procedia Computer Science. 2nd International Conference on Information Technology and Quantitative Management, ITQM 2014.

Ge, Y., MacKenzie, D., 2022. Charging behavior modeling of battery electric vehicle drivers on long-distance trips. Transportation Research Part D: Transport and Environment 113, 103490.

Gendreau, M., Laporte, G., Semet, F., 1997. Solving an ambulance location model by tabu search. Location Science 5, 75–88.

Gendreau, M., Laporte, G., Semet, F., 2001. A dynamic model and parallel tabu search heuristic for real-time ambulance relocation. Parallel Computing 27, 1641–1653.

González, S., Feijooa, F., Bassoa, F., Subramanianb, V., Sankaranarayananc, S., Dasd, T., 2022. Routing and charging facility location for EVs under nodal pricing of

electricity: A bilevel model solved using special ordered set. IEEE Transactions on Smart Grid 13, 3059–3068.

Guennebaud, G., Jacob, B., et al., 2010. Eigen v3. http://eigen.tuxfamily.org.

Gunawardane, G., 1982. Dynamic versions of set covering type public facility location problems. European Journal of Operational Research 10, 190–195.

Güney, E., Leitner, M., Ruthmair, M., Sinnl, M., 2021. Large-scale influence maximization via maximal covering location. European Journal of Operational Research 289, 144–164.

Haase, K., 2009. Discrete Location Planning. Technical Report. Institute for Transport and Logistics Studies, University of Sydney.

Haase, K., Müller, S., 2014. A comparison of linear reformulations for multinomial logit choice probabilities in facility location models. European Journal of Operational Research 232, 689–691.

Hackbarth, A., Madlener, R., 2013. Consumer preferences for alternative fuel vehicles: A discrete choice analysis. Transportation Research Part D: Transport and Environment 25, 5–17.

Haghani, M., Bliemer, M., Rose, J., Oppewal, H., Lancsar, E., 2021a. Hypothetical bias in stated choice experiments: Part I. macro-scale analysis of literature and integrative synthesis of empirical evidence from applied economics, experimental psychology and neuroimaging. Journal of Choice Modelling 41, 100309.

Haghani, M., Bliemer, M., Rose, J., Oppewal, H., Lancsar, E., 2021b. Hypothetical bias in stated choice experiments: Part II. conceptualisation of external validity, sources and explanations of bias and effectiveness of mitigation methods. Journal of Choice Modelling 41, 100322.

Han, Z., Li, S., Cui, C., Song, H., Kong, Y., Qin, F., 2019. Camera planning for area surveillance: A new method for coverage inference and optimization using location-based service data. Computers, Environment and Urban Systems 78, 101396.

Hardman, S., Jenn, A., Tal, G., Axsen, J., Beard, G., Daina, N., Figenbaum, E., Jakobsson, N., Jochem, P., Kinnear, N., Plötz, P., Pontes, J., Refa, N., Sprei, F., Turrentine, T., Witkamp, B., 2018. A review of consumer preferences of and interactions with electric vehicle charging infrastructure. Transportation Research Part D: Transport and Environment 62, 508–523.

Helmus, J.R., Lees, M.H., van den Hoed, R., 2020. A data driven typology of electric

vehicle user types and charging sessions. Transportation Research Part C: Emerging Technologies 115, 102637.

Hidrue, M.K., et al., 2011. Willingness to pay for electric vehicles and their attributes. Resource and Energy Economics doi:10.1016/j.reseneeco.2011.02.002.

Hillel, T., 2020. New perspectives on the performance of machine learning classifiers for mode choice prediction. Technical Report. Ecole Polytechnique Fédérale de Lausanne Lausanne, Switzerland.

Hillel, T., Bierlaire, M., Elshafie, M., Jin, Y., 2021. A systematic review of machine learning classification methodologies for modelling passenger mode choice. Journal of Choice Modelling 38, 100221.

Hodgson, M.J., 1990. A flow-capturing location-allocation model. Geographical analysis 22, 270–279.

van den Hoed, R., Helmus, J.R., de Vries, R., Bardok, D., 2013. Data analysis on the public charge infrastructure in the city of Amsterdam, in: 2013 World Electric Vehicle Symposium and Exhibition (EVS27), pp. 1–10.

IBM, 2022. CPLEX C++ reference manual. URL: https://www.ibm.com/docs/en/icos/22.1.1?topic=optimizers-cplex-c-reference-manual. last accessed: May 19th 2023.

Iloglu, S., Albert, L.A., 2020. A maximal multiple coverage and network restoration problem for disaster recovery. Operations Research Perspectives 7, 100132.

International Energy Agency, 2021. Greenhouse gas emissions from energy: Overview.

International Energy Agency, 2023. Greenhouse gas emissions from energy: Overview.

Javid, R.J., Nejat, A., 2017. A comprehensive model of regional electric vehicle adoption and penetration. Transport Policy 54, 30–42.

Jung, J., Chow, J.Y., Jayakrishnan, R., Park, J.Y., 2014. Stochastic dynamic itinerary interception refueling location problem with queue delay for electric taxi charging stations. Transportation Research Part C: Emerging Technologies 40, 123–142.

Kadri, A.A., Perrouault, R., Boujelben, M.K., Gicquel, C., 2020. A multi-stage stochastic integer programming approach for locating electric vehicle charging stations. Computers & Operations Research 117, 104888.

Karasakal, O., Karasakal, E.K., 2004. A maximal covering location model in the presence of partial coverage. Computers & Operations Research 31, 1515–1526.

Kchaou-Boujelben, M., 2021. Charging station location problem: A comprehensive re-

view on models and solution approaches. Transportation Research Part C: Emerging Technologies 132, 103376.

Khuller, S., Moss, A., Naor, J.S., 1999. The budgeted maximum coverage problem. Information Processing Letters 70, 39–45.

Kleinert, T., Labbé, M., Plein, F., Schmidt, M., 2020. Technical note—there's no free lunch: On the hardness of choosing a correct big-m in bilevel optimization. Operations Research 68, 1716–1721.

Kuby, M., Lim, S., 2005. The flow-refueling location problem for alternative-fuel vehicles. Socio-Economic Planning Sciences 39, 125–145.

Lamontagne, S., Carvalho, M., Frejinger, E., Gendron, B., Anjos, M.F., Atallah, R., 2023. Optimising electric vehicle charging station placement using advanced discrete choice models. INFORMS Journal on Computing 35, 1195–1213.

Lee, J.H., Chakraborty, D., Hardman, S.J., Tal, G., 2020. Exploring electric vehicle charging patterns: Mixed usage of charging infrastructure. Transportation Research Part D: Transport and Environment 79, 102249.

Legault, R., Frejinger, E., 2023. A model-free approach for solving choice-based competitive facility location problems using simulation and submodularity. URL: https://arxiv.org/abs/2203.11329.

Li, L., Wei, Z., Hao, J.K., He, K., 2021. Probability learning based tabu search for the budgeted maximum coverage problem. Expert Systems with Applications 183, 115310.

Lim, S., Kuby, M., 2010. Heuristic algorithms for siting alternative-fuel stations using the Flow-Refueling Location Model. European Journal of Operational Research 204, 51–61.

Ljubić, I., Moreno, E., 2018. Outer approximation and submodular cuts for maximum capture facility location problems with random utilities. European Journal of Operational Research 266, 46–56.

Luo, C., Huang, Y.F., Gupta, V., 2015. Placement of EV charging stations–balancing benefits among multiple entities. IEEE Transactions on Smart Grid 10, 1–10.

Ma, S.C., Yi, B.W., Fan, Y., 2022. Research on the valley-filling pricing for EV charging considering renewable power generation. Energy Economics 106, 105781.

Magnanti, T.L., Wong, R.T., 1981. Accelerating Benders decomposition: Algorithmic enhancement and model selection criteria. Operations research 29, 464–484.

Mai, T., Lodi, A., 2020. A multicut outer-approximation approach for competitive facility location under random utilities. European Journal of Operational Research 284, 874–881.

Martín-Forés, I., Guerin, G.R., Munroe, S.E.M., Sparrow, B., 2021. Applying conservation reserve design strategies to define ecosystem monitoring priorities. Ecology and Evolution 11, 17060–17070.

Marín, A., Martínez-Merino, L.I., Rodríguez-Chía, A.M., Saldanha-da-Gama, F., 2018. Multi-period stochastic covering location problems: Modeling framework and solution approach. European Journal of Operational Research 268, 432–449.

McFadden, D., 1974. Conditional logit analysis of qualitative choice behavior, in: Zarembka, P. (Ed.), Frontiers in Econometrics. Academic Press, New York, pp. 105–142.

McFadden, D., Train, K., 2000. Mixed mnl models for discrete response. Journal of Applied Econometrics 15, 447–470.

Metais, M., Jouini, O., Perez, Y., Berrada, J., Suomalainen, E., 2022. Too much or not enough? planning electric vehicle charging infrastructure: A review of modeling options. Renewable and Sustainable Energy Reviews 153, 111719.

Moon, H., Park, S.Y., Jeong, C., Lee, J., 2018. Forecasting electricity demand of electric vehicles by analyzing consumers' charging patterns. Transportation Research Part D: Transport and Environment 62, 64–79.

Morrissey, P., Weldon, P., O'Mahony, M., 2016. Future standard and fast charging infrastructure planning: An analysis of electric vehicle charging behaviour. Energy Policy 89, 257–270.

Muñoz, G., Espinoza, D., Goycoolea, M., Moreno, E., Queyranne, M., Letelier, O., 2018. A study of the Bienstock–Zuckerberg algorithm: applications in mining and resource constrained project scheduling. Computational Optimization and Applications 69, 501–534.

Muren, Li, H., Mukhopadhyay, S.K., Wu, J., Zhou, L., Du, Z., 2020. Balanced maximal covering location problem and its application in bike-sharing. International Journal of Production Economics 223, 107513.

Murray, A.T., 2016. Maximal coverage location problem: Impacts, significance, and evolution. International Regional Science Review 39, 5–27.

Murray, A.T., Church, R.L., 1996. Applying simulated annealing to location-planning models. Journal of Heuristics 2, 31–53.

Máximo, V.R., Nascimento, M.C., Carvalho, A.C., 2017. Intelligent-guided adaptive search for the maximum covering location problem. Computers & Operations Research 78, 129–137.

Nelas, J., Dias, J., 2020. Optimal emergency vehicles location: An approach considering the hierarchy and substitutability of resources. European Journal of Operational Research 287, 583–599.

Nemhauser, G.L., Wolsey, L.A., Fisher, M.L., 1978. An analysis of approximations for maximizing submodular set functions—i. Mathematical programming 14, 265–294.

Nicholas, M., Hall, D., Lutsey, N., 2019. Quantifying the Electric Vehicle Charging Infrastructure Gap Across U.S. Markets. Technical Report. International Council on Clean Transportation.

Nicholas, M.A., Tal, G., Turrentine, T.S., 2017. Advanced Plug-in Electric Vehicle Travel and Charging Behavior Interim Report. Technical Report. UC Davis. Institute of Transportation Studies.

OpenStreetMap contributors, 2017. Planet dump retrieved from https://planet.osm.org . https://www.openstreetmap.org.

Pacheco Paneque, M., et al., 2021. Integrating advanced discrete choice models in mixed integer linear optimization. Transportation Research Part B: Methodological 146, 26–49.

Papadakos, N., 2008. Practical enhancements to the Magnanti–Wong method. Operations Research Letters 36, 444–449.

Parady, G., Ory, D., Walker, J., 2021. The overreliance on statistical goodness-of-fit and under-reliance on model validation in discrete choice models: A review of validation practices in the transportation academic literature. Journal of Choice Modelling 38, 100257.

Parent, P.L., Carvalho, M., Anjos, M.F., Atallah, R., 2023. Maximum flow-based formulation for the optimal location of electric vehicle charging stations.

Pereira, M.A., Lorena, L.A.N., Senne, E.L.F., 2007. A column generation approach for the maximal covering location problem. International Transactions in Operational Research 14, 349–364.

Pevec, D., Babic, J., Kayser, M.A., Carvalho, A., Ghiassi-Farrokhfal, Y., Podobnik, V., 2018. A data-driven statistical approach for extending electric vehicle charging infrastructure. International Journal of Energy Research 42, 3102–3120.

Philipsen, R., Schmidt, T., van Heek, J., Ziefle, M., 2016. Fast-charging station here, please! user criteria for electric vehicle fast-charging locations. Transportation Research Part F: Traffic Psychology and Behaviour 40, 119–129.

Philipsen, R., Schmidt, T., Ziefle, M., 2015. A charging place to be - users' evaluation criteria for the positioning of fast-charging infrastructure for electro mobility. Procedia Manufacturing 3, 2792–2799. 6th International Conference on Applied Human Factors and Ergonomics (AHFE 2015) and the Affiliated Conferences, AHFE 2015.

Pineda, S., Morales, J.M., 2019. Solving linear bilevel problems using big-ms: Not all that glitters is gold. IEEE Transactions on Power Systems 34, 2469–2471.

Pinzon, D., Frejinger, E., Gendron, B., 2023. A logistics provider's profit maximization facility location problem with random utility maximizing followers. URL: https://arxiv.org/abs/2303.06749.

Porras, C., Calderín, J.F., Rosete, A., 2019. Multi-coverage dynamic maximal covering location problem. Investigación Operacional 40, 140–149.

Potoglou, D., Song, R., Santos, G., 2023. Public charging choices of electric vehicle users: A review and conceptual framework. Transportation Research Part D: Transport and Environment 121, 103824.

Rahmaniani, R., Ahmed, S., Crainic, T.G., Gendreau, M., Rei, W., 2020. The Benders dual decomposition method. Operations Research 68, 878–895.

Rahmaniani, R., Crainic, T.G., Gendreau, M., Rei, W., 2017. The Benders decomposition algorithm: A literature review. European Journal of Operational Research 259, 801–817.

Ramírez-Pico, C., Ljubić, I., Moreno, E., 2023. Benders adaptive-cuts method for two-stage stochastic programs. Transportation Science 57, 1252–1275.

Rei, W., Cordeau, J.F., Gendreau, M., Soriano, P., 2009. Accelerating Benders decomposition by local branching. INFORMS Journal on Computing 21, 333–345.

Resende, M., 1998. Computing approximate solutions of the maximum covering problem with GRASP. Journal of Heuristics 4, 161–177.

Resende, M., Ribeiro, C., 2018. Optimisation By GRASP: Greedy Randomized Adaptive Search Procedures. SPRINGER.

ReVelle, C., Scholssberg, M., Williams, J., 2008. Solving the maximal covering location problem with heuristic concentration. Computers & Operations Research 35, 427–435.

Revelt, D., Train, K., 1998. Mixed logit with repeated choices: Households' choices of appliance efficiency level. The Review of Economics and Statistics 80, 647–657.

Rezvani, Z., Jansson, J., Bodin, J., 2015. Advances in consumer electric vehicle adoption research: A review and research agenda. Transportation Research Part D: Transport and Environment 34, 122–136.

Rodriguez, F.J., Blum, C., Lozano, M., García-Martínez, C., 2012. Iterated greedy algorithms for the maximal covering location problem, in: Hao, J.K., Middendorf, M. (Eds.), Evolutionary Computation in Combinatorial Optimization, Springer Berlin Heidelberg, Berlin, Heidelberg. pp. 172–181.

Roulons Électrique, 2023. Choose a plug-in vehicle that meets your nees. https://www.roulonselectrique.ca/documents/77/Brochure-Electro-EN-2023_web.pdf [Last accessed: January 16th 2024].

Santoso, T., Ahmed, S., Goetschalckx, M., Shapiro, A., 2005. A stochastic programming approach for supply chain network design under uncertainty. European Journal of Operational Research 167, 96–115.

Schilling, D.A., 1980. Dynamic location modeling for public-sector facilities: A multicriteria approach. Decision Sciences 11, 714–724.

Senne, E.L., Lorena, L.A., 2002. Stabilizing column generation using Lagrangean/surrogate relaxation: an application to p-median location problems. European Journal of Operational Research .

Sheldon, T.L., DeShazo, J.R., Carson, R.T., 2019. Demand for green refueling infrastructure. Environmental and Resource Economics 74, 1231–157.

Shukla, A., Pekny, J., Venkatasubramanian, V., 2011. An optimization framework for cost effective design of refueling station infrastructure for alternative fuel vehicles. Computers & Chemical Engineering 35, 1431–1438.

Sifringer, B., Lurkin, V., Alahi, A., 2020. Enhancing discrete choice models with representation learning. Transportation Research Part B: Methodological 140, 236–261.

Sinha, A., Malo, P., Deb, K., 2017. A review on bilevel optimization: From classical to evolutionary approaches and applications. IEEE Transactions on Evolutionary Computation 22, 276–295.

Statistics Canada, 2017. 2016 census, catalogue no. 98-401-x2016044.

Straka, M., De Falco, P., Ferruzzi, G., Proto, D., Van Der Poel, G., Khormali, S., Buzna, L., 2020. Predicting popularity of electric vehicle charging infrastructure in urban context. IEEE Access 8, 11315–11327.

Sun, X.H., Yamamoto, T., Morikawa, T., 2016. Fast-charging station choice behavior among battery electric vehicle users. Transportation Research Part D: Transport and Environment 46, 26–39.

Sun, Z., Gao, W., Li, B., Wang, L., 2020. Locating charging stations for electric vehicles. Transport Policy 98, 48–54.

Tal, G., Lee, J., Nicholas, M., 2018. Observed Charging Rates in California. Technical Report. UC Davis: Plug-In Hybrid & Electric Vehicle Research Center.

Tal, G., et al., 2020. Advanced Plug-in Electric Vehicle Travel and Charging Behavior Final Report. Technical Report. UC Davis. Institute of Transportation Studies, prepared for California Environmental Protection Agency.

Train, K., 2002. Discrete Choice Methods with Simulation. Cambridge University Press, Berkeley.

Vatsa, A.K., Jayaswal, S., 2016. A new formulation and Benders decomposition for the multi-period maximal covering facility location problem with server uncertainty. European Journal of Operational Research 251, 404–418.

Vermeulen, I., Helmus, J.R., Lees, M., van den Hoed, R., 2019. Simulation of future electric vehicle charging behavior–effects of transition from PHEV to FEV. World Electric Vehicle Journal 10.

Visaria, A.A., Jensen, A.F., Thorhauge, M., Mabit, S.E., 2022. User preferences for EV charging, pricing schemes, and charging infrastructure. Transportation Research Part A: Policy and Practice 165, 120–143.

Walker, J., Ben-Akiva, M., Bolduc, D., 2004. Identification of the logit kernel (or mixed logit) model, in: 10th International Conference on Travel Behavior Research.

Wang, Y., Yao, E., Pan, L., 2021. Electric vehicle drivers' charging behavior analysis considering heterogeneity and satisfaction. Journal of Cleaner Production 286, 124982.

Wang, Y.W., Lin, C.C., 2009. Locating road-vehicle refueling stations. Transportation Research Part E: Logistics and Transportation Review 45, 821–829.

Wei, Z., Hao, J.K., 2023. Iterated hyperplane search for the budgeted maximum coverage problem. Expert Systems with Applications 214, 119078.

Wolbertus, R., van den Hoed, R., Kroesen, M., Chorus, C., 2021. Charging infrastructure roll-out strategies for large scale introduction of electric vehicles in urban areas: An agent-based simulation study. Transportation Research Part A: Policy and Practice 148, 262–285.

Woo, J., Choi, H., Ahn, J., 2017. Well-to-wheel analysis of greenhouse gas emissions for electric vehicles based on electricity generation mix: A global perspective. Transportation Research Part D: Transport and Environment 51, 340–350.

Xia, L., Xie, M., Xu, W., Shao, J., Yin, W., Dong, J., 2009. An empirical comparison of five efficient heuristics for maximal covering location problems, in: 2009 IEEE/INFORMS International Conference on Service Operations, Logistics and Informatics, pp. 747–753.

Yang, J., Wu, F., Yan, J., Lin, Y., Zhan, X., Chen, L., Liao, S., Xu, J., Sun, Y., 2020. Charging demand analysis framework for electric vehicles considering the bounded rationality behavior of users. International Journal of Electrical Power & Energy Systems 119, 105952.

Yang, Y., Yao, E., Yang, Z., Zhang, R., 2016. Modeling the charging and route choice behavior of bev drivers. Transportation Research Part C: Emerging Technologies 65, 190–204.

Zarandi, M.H.F., Davari, S., Sisakht, S.A.H., 2013. The large-scale dynamic maximal covering location problem. Mathematical and Computer Modelling 57, 710–719.

Zhang, A., Kang, J.E., Kwon, C., 2017a. Incorporating demand dynamics in multi-period capacitated fast-charging location planning for electric vehicles. Transportation Research Part B: Methodological 103, 5–29.

Zhang, B., Peng, J., Li, S., 2017b. Covering location problem of emergency service facilities in an uncertain environment. Applied Mathematical Modelling 51, 429–447.

Ziegler, A., 2012. Individual characteristics and stated preferences for alternative energy sources and propulsion technologies in vehicles: A discrete choice analysis for Germany. Transportation Research Part A: Policy and Practice 46, 1372–1385.

A Appendix

In this chapter, we present supplemental information for each of the articles. These are presented sequentially for each article in Sections A.1 to A.3.

A.1 First Article

A.1.1 Bilevel Optimisation Model

The natural hierarchical structure of our problem suggests a bilevel formulation. Bilevel optimisation models sequential decision making, where first, the leader takes a decision (*upper level*) and then, the followers react by solving an optimisation problem (*lower level*). The optimal solution of a bilevel model are the decision values for the leader that optimise its objective function, based on the optimal reaction of the lower-level users to the values of those variables. In our case, the decision maker is in the upper-level while the users are in the lower-level.

The choice in the lower-level to purchase an EV is modelled via a discrete choice model, where the users (followers) maximise their *utility*. More specifically, the users must choose an alternative from a finite set of available alternatives (here, open stations, home charging, and opt-out). The value of each alternative is predicted through the use of a *utility function*, which associates the value of a given alternative for users based on observable and unobservable factors. Under the RUM assumption, users then, as rational beings, select the alternative which presents the maximum benefit to them, as represented by the alternative with the highest utility. For each period $1 \leq t \leq T$, user class $i \in N$, and alternative $j \in \mathcal{C}_i^t(\mathbf{x})$, the utility is denoted u_{ji}^t.

The analyst has imperfect knowledge of the utility of the users, so we model it as a random variable. Hence, instead of a deterministic model identifying the

alternative chosen by the users, we obtain a probability distribution over the set of available alternatives. Consequently, the leader maximises the expected number of users purchasing an EV or, equivalently, minimises the expected number of users that *do not* purchase an EV. This is given by

$$\min_{x \in X} \sum_{t=1}^{T} \sum_{i \in N} N_i^t \mathbb{P}_\varepsilon \left[u_{0i}^t(x, \varepsilon) \geq u_{ji}^t(x, \varepsilon), \forall j \in \mathcal{C}_i^t(x) \right], \tag{A.1}$$

where X denotes the upper-level constraints, and ε denotes the random error term. These constraints are discussed in more detail in Appendix A.1.1. We recall that index $j = 0$ indicates the opt-out alternative, thus u_{0i}^t is the opt-out utility for user class i in year t.

If the error terms are independent, and identically extreme-value type I distributed, the choice probabilities have an analytic formula (the well-known MNL model). In our application, this assumption may not hold. For example, if stations are near each other, they will also have similar amenities near them (e.g. restaurants, shopping centres, etc.). If a user places high value in those amenities (and they are not explicitly included in the observable factors), the error terms for those stations may be highly correlated. To allow for general discrete choice models which relax this restriction and support flexible substitution patterns, we use the simulation-based approach of Pacheco Paneque et al. (2021).

Recall that R_i is the number of *scenarios* for user class i, P is the set of triplets (t, i, r) for user class i, alternative j, scenario r, and period t, and ε_{ji}^{rt} is the realisation of the random variable ε in triplet (t, i, r) . Then, $\forall j \in C_i^t(x)$, we denote

$$w_{ji}^{rt} = \begin{cases} 1, \text{ if } j \in \operatorname{argmax}_{j' \in C_i^t(x)} \left\{ u_{j'i}^t(x, \varepsilon_{j'i}^{rt}) \right\}, \\ 0, \text{ otherwise.} \end{cases} \tag{A.2}$$

The details of the lower-level problem are discussed in Appendix A.1.1. For the sake of simplicity, in a flagrant abuse of notation, we denote the vector $\mathbf{w} = \left\{ w_{ji}^{rt} \right\}$ with w_{ji}^{rt} given by (A.2) for each $(t, i, r), j \in C_i^t(x)$ as $\mathbf{w} \in \operatorname{argmax}_{j \in C(x)} \{u(x, \varepsilon)\}$.

Then, we can write a sample average approximation of (A.1) as

$$\min_{x \in X} \sum_{(t,i,r) \in P} \frac{N_i^t}{R_i} w_{0i}^{rt},$$
$$\text{s.t. } \mathbf{w} = \text{argmax}_{j \in C(x)} \left\{ u(x, \varepsilon) \right\}.$$

Lower-Level Problem

The lower-level problem is assumed to be separable for each user class, each period, and each scenario, meaning that there is no interaction among them. Therefore, in what follows, we concentrate on detailing a given triplet (t, i, r). For each alternative $j \in \mathcal{C}_i^t(x)$, let $u_{ji}^{rt} = u_{ji}^t(x, \varepsilon_{ji}^{rt})$ be the *simulated utility*.

We previously remarked that the choice set $\mathcal{C}_i^t(\mathbf{x})$ depends on which stations are open and we defined the choice sets C_i^{0t} and C_i^{1t} as the sets related to alternatives exogenous and endogenous to the optimisation model, respectively. To ensure that the alternative associated with a closed station $j \in C_i^{1t}$ cannot be chosen, we set the simulated utility u_{ji}^{rt} to a lower bound if $x_{j1}^t = 0$. This concept is referred to as the "discounted utility" in Pacheco Paneque et al. (2021). Let $\underline{a}_i^t = \min\left(\left\{\kappa_{ji}^t + \varepsilon_{ji}^{rt}, j \in C_i^{1t}, 1 \leq r \leq R_i\right\}\right)$ and $b_{ji}^{rt} = \sum_{k=1}^{m_j} \beta_{jik}^t + \kappa_{ji}^t + \varepsilon_{ji}^{rt}$ be respectively lower and upper bounds on the simulated utility u_{ji}^{rt}, and let $\nu_{ji}^t = b_{ji}^{rt} - \underline{a}_i^t$. For each $i \in N$, we assume that R_i is sufficiently large such that for each $1 \leq t \leq T, 1 \leq r \leq R_i$ we have $\underline{a}_i^t < u_{0i}^{rt}$. We note that the lower bound $\underline{a}_i^t$ could be strengthened by adding the utility of one outlet, (e.g. $\min\left\{\beta_{j1}^{rt} + \kappa_{ji}^t + \varepsilon_{ji}^{rt}\right\}$). However, in our testing, this did not have a significant impact. We also note that, since the error terms ε_{ji}^{rt} can come from unbounded distributions, it is not generally possible to use a fixed lower bound for u_{0i}^{rt}, e.g. $\underline{a}_i^t = 0$.

The linear formulation for the simulated utility u_{ji}^{rt} is given by

$$u_{ji}^{rt} \geq \underline{a}_i^t, \qquad j \in C_i^{1t}, (t,i,r) \in P, \tag{A.3}$$

$$u_{ji}^{rt} \leq \underline{a}_i^t + \nu_{ji}^{rt} x_{j1}^t, \qquad j \in C_i^{1t}, (t,i,r) \in P, \tag{A.4}$$

$$u_{ji}^{rt} \geq \sum_{k=1}^{m_j} \beta_{jik}^t x_{jk}^t + \kappa_{ji}^t + \varepsilon_{ji}^{rt} - \nu_{ji}^{rt} \left(1 - x_{j1}^t\right), \qquad j \in C_i^{1t}, (t,i,r) \in P, \tag{A.5}$$

$$u_{ji}^{rt} \leq \sum_{k=1}^{m_j} \beta_{jik}^t x_{jk}^t + \kappa_{ji}^t + \varepsilon_{ji}^{rt}, \qquad j \in C_i^{1t}, (t,i,r) \in P. \tag{A.6}$$

For each $(t,i,r) \in P$, the value of w_{ji}^{rt} for $j \in C_i^{0t} \cup C_i^{1t}$ is then given by the solution of the following optimisation problem, which acts as the lower-level problem in our bilevel optimisation model:

$$\text{Maximise} \sum_{j \in C_i^{0t}} w_{ji}^{rt} u_{ji}^{rt} + \sum_{j \in C_i^{1t}} w_{ji}^{rt} u_{ji}^{rt}, \tag{A.7a}$$

$$\text{subject to} \sum_{j \in C_i^{0t}} w_{ji}^{rt} + \sum_{j \in C_i^{1t}} w_{ji}^{rt} = 1, \tag{A.7b}$$

$$w_{ji}^{rt} \in \{0,1\}, \quad j \in C_i^{0t} \cup C_i^{1t}. \tag{A.7c}$$

It is easy to see that the binary requirements can be relaxed.

Upper-Level Problem

The placement of charging outlets and stations in the upper-level is restricted by the following set of constraints

$$\sum_{j \in M} \sum_{k=1}^{m_j} c_{jk}^t \left(x_{jk}^t - x_{jk}^{t-1}\right) \leq B^t, \qquad 1 \leq t \leq T. \tag{A.8}$$

$$x_{jk}^t \leq x_{jk-1}^t, \qquad 1 \leq t \leq T, j \in M, \tag{A.9}$$

$$x_{jk}^t \geq x_{jk}^{t-1}, \qquad 1 \leq t \leq T, j \in M, 1 \leq k \leq m_j. \tag{A.10}$$

These correspond to Constraints (3.2b)-(3.2d) presented in Section 3.3.4. Note that it would also be possible to supplement the per-period budget with an overall budget, as was done in Anjos et al. (2020).

Constraints (A.9) enforces that if we have at least k outlets, we must also have at least $k-1$ outlets.

Constraints (A.10) forbid the model from removing charging outlets. These constraints assume that it would be suboptimal to remove a station.

Bilevel Model

We now introduce the full, bilevel model

$$\text{Minimise} \sum_{(t,i,r)\in P} \frac{N_i^t}{R_i} w_{0i}^{rt}, \tag{A.11}$$

$$\begin{aligned}
\text{subject to } & (3.1), (A.3)-(A.6), (A.8)-(A.10) \\
& w_{ji}^{rt} \in \operatorname{argmax}\left\{ \sum_{j\in C_i^{0t}} w_{ji}^{rt} u_{ji}^{rt} + \sum_{j\in C_i^{1t}} w_{ji}^{rt} u_{ji}^{rt} : (A.7b)-(A.7c) \right\} \\
& u_{ji}^{rt} \in \mathbb{R}, \\
& x_{jk}^{t} \in \{0,1\}.
\end{aligned}$$

We consider the *optimistic* version of the bilevel problem which means that the users do not select the opt-out alternative if a different alternative has equal utility. While this in theory has a zero probability (given that the error terms are drawn from continuous distributions), this can occur in practice due to numerical precision.

In order to solve the model, we reformulate it as a single-level optimisation problem by transforming the lower-level model (A.7) into a series of constraints for the upper-level model. To this end, we apply the Karush-Kuhn-Tucker conditions which are necessary and sufficient for the optimality of the (linear) lower-level problem (Sinha et al. 2017), and we linearize the terms $w_{ji}^{rt} \cdot u_{ji}^{rt}$ through Big-M constraints. In this way, for each $(t,i,r) \in P$, the lower-level problem (A.7) is

replaced by the following constraints:

$$u_{ji}^{rt} - \alpha_i^{rt} + \left(1 - w_{ji}^{rt}\right) \mu_{ji}^{rt} \geq 0,\ j \in C_i^{0t} \cup C_i^{1t}, \tag{A.12}$$

$$\sum_{j \in C_i^{0t}} w_{ji}^{rt} + \sum_{j \in C_i^{1t}} w_{ji}^{rt} = 1, \tag{A.13}$$

$$\alpha_i^{rt} \geq u_{ji}^{rt},\ j \in C_i^{0t} \cup C_i^{1t}, \tag{A.14}$$

$$w_{ji}^{rt} \in \{0,1\}, j \in C_i^{0t} \cup C_i^{1t}, \tag{A.15}$$

$$\alpha_i^{rt} \in \mathbb{R}, \tag{A.16}$$

where the Big-M constants, μ_{ji}^{rt}, are given by

$$\mu_{ji}^{rt} = \begin{cases} \max\left(\left\{b_{ji}^{rt}, j \in C_i^{1t}\right\} \cup \left\{\kappa_{ji}^{rt} + \varepsilon_{ji}^{rt}, j \in C_i^{0t}\right\}\right) - \kappa_{ji}^{rt} - \varepsilon_{ji}^{rt}, & j \in C_i^{0t}, \\ \max\left(\left\{b_{ji}^{rt}, j \in C_i^{1t}\right\} \cup \left\{\kappa_{ji}^{rt} + \varepsilon_{ji}^{rt}, j \in C_i^{0t}\right\}\right) - \underline{a}_i^t, & j \in C_i^{1t}. \end{cases}$$

A.1.2 Parameter Values

In this section, we describe the parameter values for each dataset, as well as the mechanism for drawing error terms for each of the instances. We start by describing the general framework used for the error terms, as that is common to all of the datasets. Table A.1 provides a list of parameter values, with more detailed explanations in the following subsections for parameter values which differ. Unless otherwise specified, parameter values are set arbitrarily. We note that, in all datasets, the number of scenarios is set to $15 \times |C_0^{it} \cup C_1^{it}|$. In the case of the Simple, Distance, and HomeCharging datasets, the size of C_1^{it} varies by user class, due to the maximum distance of 10km for considering a charging station. As a consequence, the number of scenarios varies from 15 (only the opt-out is considered) to 105 (opt-out plus six charging stations). On the contrary, in the Price and LongSpan datasets, there is no maximum distance for consideration, and thus every station is included in the set C_1^{it}. As a consequence, $|C_0^{it} \cup C_1^{it}| = 31$, and the number of scenarios is always 465.

In all of our datasets:

— Each user class $i \in N$ includes the home location (as a node in the network). This allows us to estimate population based on the census data (Statistics

Canada 2017), with the number of user classes per node and the partitioning method depending on the dataset.

— Each dataset includes 20 instances, where each instance generates different sets of error terms $\varepsilon_{ji}^{rt}, j \in C_{0i}^{rt} \cup C_{1i}^{rt}$.

— For each $i \in N, 1 \leq t \leq T$, the alternative-specific constant for the opt-out option κ_{0i}^{t} is set to 4.5.

In order to simulate the error terms for the demand model, we employ the error components formulation of the mixed logit model to approximate a nested logit model, as described in Train (2002) and Walker et al. (2004). The notation in what follows matches the latter work, and we refer to the aforementioned work for detailed explanations of the process.

For each $i \in N, 1 \leq t \leq T, 1 \leq r \leq R_i$, the vector of error terms $\varepsilon_i^{rt} = (\varepsilon_i^{rt})_{j \in C_i^{0t} \cup C_i^{1t}}$ is given by

$$\varepsilon_i^{rt} = FT\xi^r + \zeta^r, \tag{A.17}$$

with

— F a *factor loading* matrix.

— T a diagonal matrix with the standard deviation of each factor.

— ξ^r a vector of IID random terms from a normal distribution.

— ζ^r a vector of IID random terms from a Gumbel distribution.

The form of the matrices F and T vary in each dataset. However, in all datasets, ξ^r has a location of zero and a scale of one, and ζ^r has location of zero and a scale of three.

Simple Dataset

The set of user classes N includes one user class for every node in the network. The population of user class i, N_i^t, is given by the population of the node in the 2016 census multiplied by a factor of 0.1. In other words, 10% of the population in each node are deciding to purchase a vehicle each year.

For each $i \in N, 1 \leq t \leq T$, the choice set C_i^{1t} includes all stations which are within ten kilometres of the location of the user class. The utility for $j \in C_i^{1t}$ is

Parameter	Simple	Distance	HomeCharging	LongSpan	Price
T	4	4	4	10	4
$\|M\|$	10	10	10	30	30
$\|N\|$	317	317	634	317	1397
$\|C_0^{it}\|$	1	2	1	1	1
$\|C_1^{it}\|$	Varies	Varies	Varies	30	30
x_{jk}^0 (all stations and outlets)	0	0	0	0	0
R_i	$15-105$	$15-105$	$15-105$	465	465
B^t (per year)	400	400	400	400	400
m_j (all stations)	2	6	6	6	6
c_{j1}^t (all stations and years)	150	150	150	150	150
c_{jk}^t (all other outlets)	50	50	50	50	50

Table A.1 – Parameter values for the generated instances

linear in terms of the number of charging outlets, with

$$\beta_{jik}^t = 0.281k, \forall j \in C_i^{1t}. \tag{A.18}$$

Additionally, the alternative-specific constant for each station $j \in C_i^{1t}$ is calculated as

$$\kappa_{ji}^t = 1.464\delta_1 - 0.063\delta_2 + 0.174\delta_3, \tag{A.19}$$

with

— δ_1: binary coefficient indicating if the station is level 3 (i.e. fast charging). We note that in our tests all stations were considered level 3.

— δ_2: the distance (in kilometres, shortest path in the network) between the user's home and the charging station,

— δ_3: binary coefficient indicating if the station is in the city center (defined as a subset of the nodes in the network).

The coefficients for these parameters were estimated using real-world data. A discrete choice model was created which examined which charging station was selected by EV owners when recharging their vehicle. A MNL model was estimated with the maximum likelihood approach with the BIOGEME package in Python (Bierlaire 2020), using real charging data for EV owners in the province of Québec.

For the error terms for each $i \in N, 1 \leq t \leq T$, the options $j \in C_i^{0t} \cup C_i^{1t}$ are divided into two nests: one for the opt-out option and one for all charging stations. The $|C_i^{0t} \cup C_i^{1t}| \times 2$ factor loading matrix F and 2×2 diagonal matrix T are given

by

$$F = \begin{bmatrix} 1 & 0 \\ 0 & 1 \\ \vdots & \vdots \\ 0 & 1 \end{bmatrix}, \quad T = \begin{bmatrix} 1 & 0 \\ 0 & 1 \end{bmatrix}. \tag{A.20}$$

Distance Dataset

The user classes, choice sets, and error terms are all identical to the Simple dataset.

The coefficient for distance in the alternative-specific constant has been increased by a factor of ten. More specifically, for each $i \in N, 1 \leq t \leq T$, the alternative-specific constant for each station $j \in C_i^{1t}$ is calculated as

$$\kappa_{ji}^t = 1.464\delta_1 - 0.63\delta_2 + 0.174\delta_3, \tag{A.21}$$

with $\delta_1, \delta_2, \delta_3$ defined as in the Simple dataset.

Home Charging Dataset

The set of user classes N includes two user classes for every node in the network: one which has access to home charging, and one which does not. We estimate the access to home charging via the housing information in the 2016 census (Statistics Canada 2017). Based on recommendations from our industrial partners, we assume that 90% of users in single homes have access to home charging, while 75% of those in attached homes, and 40% of those in apartments also have access. The population of each of the two user classes are given by the respective estimates multiplied by a factor of 0.1.

For user classes i which have access to home charging and for each $1 \leq t \leq T$, the utility for $j \in C_i^{1t}$ is linear in terms of the number of charging outlets, with

$$\beta_{jik}^t = 0.211k, \forall j \in C_i^{1t}. \tag{A.22}$$

For user classes i which do not have access to home charging and for each $1 \leq t \leq T$,

the utility for $j \in C_i^{1t}$ is linear in terms of the number of charging outlets, with

$$\beta_{jik}^t = 0.351k, \forall j \in C_i^{1t}. \tag{A.23}$$

In both cases, the choice set C_i^{1t} includes all stations which are within ten kilometres of the location of the user class and the alternative-specific constants are identical to the Simple dataset.

For user classes i which do not have access to home charging, the error terms are identical to the Simple dataset. For user classes i which have access to home charging and for each $1 \leq t \leq T$, the options $j \in C_i^{0t} \cup C_i^{1t}$ are divided into three nests: one for the opt-out option, one for home charging, and one for all charging stations. The $|C_i^{0t} \cup C_i^{1t}| \times 3$ factor loading matrix F and 3×3 diagonal matrix T are given by

$$F = \begin{bmatrix} 1 & 0 & 0 \\ 0 & 1 & 0 \\ 0 & 0 & 1 \\ \vdots & \vdots & \vdots \\ 0 & 0 & 1 \end{bmatrix}, \quad T = \begin{bmatrix} 1 & 0 & 0 \\ 0 & 1 & 0 \\ 0 & 0 & 1 \end{bmatrix}. \tag{A.24}$$

LongSpan Dataset

The mechanisms for the user classes, alternative-specific constants, and error terms are all identical to the Simple dataset. However, the choice sets for each user class now include all stations, not only those within ten kilometres. This, combined with the increased number of stations and the longer time span, results in a significantly more difficult problem to solve.

Price Dataset

The alternative-specific constants, error terms, and choice sets are identical to the LongSpan dataset.

In this dataset, we simulate a price decrease year-by-year, which affects different user classes differently based on their income. The set of user classes N includes five user classes for every node in the network, based on the partitioning in Javid

and Nejat (2017) for income. In the aforementioned work, a logit model for EV acquisition was estimated, with one of the considered factors being the annual household income. The income level was classified as a categorical variable, with the categories defined via income

— Less than 25 000$,

— 25 000$ - 49 999$,

— 50 000$ - 74 999$,

— 75 000 - 99 999$,

— Greater or equal to 100 000$.

In the final estimation of the logit model, the income variable was found to be significantly significant. The utility coefficient for the categorical variable was estimated as 0.443.

In our work, we estimate the population in each node that falls within each of the five income brackets using the household income field in the 2016 Statistics Canada census (Statistics Canada 2017), and assigned each to a user class. [1] The population of each of the five user classes are given by the respective estimates multiplied by a factor of 0.1, and any user class which would have a population < 1 are removed.

An additional term is added to the alternative specific constants for all charging stations based on the income bracket, in increments of 0.443. We then modify the value of the penalisation term each year to account for a decrease in price affecting each user class differently (with the modification affecting the lower income brackets more). More specifically, for each $i \in N, 1 \leq t \leq T$, the alternative-specific constant for each station $j \in C_i^{1t}$ is calculated as

$$\kappa_{ji}^t = 1.464\delta_1 - 0.063\delta_2 + 0.174\delta_3 + 0.443\delta_{4i} + 0.443\,(t-1)\left(\frac{2-\delta_{4i}}{4}\right), \quad \text{(A.25)}$$

with $\delta_1, \delta_2, \delta_3$ defined as in the Simple dataset and δ_{4i} given in Table A.2.

1. The census provides data in brackets of 10 000$, and so the population in certain fields was divided evenly into two user classes (e.g. half of the population of the "20 000$ to 29 999$" field in the census was assigned to the "Less than 25 000$" user class whereas the other half was added to the "25 000$ - 49 999$" user class.)

Income level of user class i	δ_{4i}
Less than 25 000$	-2
25 000$ - 49 999$	-1
50 000$ - 74 999$	0
75 000 - 99 999$	1
Greater or equal to 100 000$	2

Table A.2 – Values of parameter δ_{4i}

A.1.3 Growth Function model

Intracity model

For comparing the GF model of Anjos et al. (2020) to the MC model (3.3), it must be reduced to an intracity form. More precise definitions and development of each of these variables and equations, we refer to the previous work. Note that some variable names have been changed from the original work to avoid confusion with notation in MC model (3.3) and the SL model (3.2). We assume that the city occupies a single urban centre u. We also eliminate the path-based constraints from the optimisation model, as these represent users travelling between urban centres. Given these simplifications, we use the following notation:

— T: Set of investment periods.

— N: Set of population centers.

— M: Set of candidate locations.

— $N_j, j \in M$: Set of locations which are willing to charge at location j.

— $e_j, j \in M$: Maximum number of charging outlets at location j.

— r: Population of the city.

— r_i: Population in location i.

— $l_j, j \in M$: Number of charging outlets already installed at location j.

— c^U: Cost for installing a charging outlet at any location.

— $c_j^F, j \in M$: One-time cost for opening location j.

— $B^t, t \in T$: Budget for year t.

— α: Fraction of EV users that choose to charge at home.

— $a^t, t \in T$: Capacity increase for each charging outlet in year t.

— S: Set of segments in the (piecewise linear) GF.

— $q^{s-1}, q^s, s \in S$: Breakpoints of segment s in the growth function.

— $m^s, s \in S$: Slope of segment s in the growth function.

— $o^s, s \in S$: Intercept of segment s in the growth function.

— $x_j^t, j \in M, t \in T$: Number of charging outlets at station i in year t.

— $y_j^t, j \in M, t \in T$: 1 if station is open in year t, 0 otherwise.

— $w^{st}, s \in S, t \in T$: 1 if the city is at penetration level s at the beginning of year t, 0 otherwise.

— $h_{ij}^t, i \in N, j \in M, t \in T$: Number of EVs based in location i choosing to charge in location j in year t.

— $z^{st}, s \in S, t \in T$: Number of EVs in the city which is at penetration level s at the beginning of year t.

The list of parameter values can be found in Table A.3.

The model used for the comparisons is the following:

$$\text{Maximise} \sum_{j \in M} \sum_{i \in N_j} h_{ij}^{t-1}, \tag{A.26}$$

$$\text{subject to} \sum_{j \in M} c_U \left(x_j^t - x_j^{t-1} \right) + \sum_{j \in M} c_j^F \left(y_j^t - y_j^{t-1} \right) \leq B^t, \quad t \in T, \tag{A.27}$$

$$x_j^t \leq e_j y_j^t, \quad j \in M, 1 \leq t \leq T, \tag{A.28}$$

$$x_j^t \geq x_j^{t-1}, \quad j \in M, 1 \leq t \leq T, \tag{A.29}$$

$$y_j^t \geq y_j^{t-1}, \, j \in M, 1 \leq t \leq T, \tag{A.30}$$

$$\sum_{s \in S} z^{st} = \sum_{j \in M} \sum_{i \in N_j} h_{ij}^{t-1}, t \in T, \tag{A.31}$$

$$q^{s-1} w^{st} \leq z^{st} \leq q^s w^{st}, s \in S, t \in T, \tag{A.32}$$

$$\sum_{s \in S} w^{st} \leq 1, t \in T, \tag{A.33}$$

$$\sum_{i \in N_j} h_{ij}^t \leq \sum_{i \in N_j} h_{ij}^{t-1} + \frac{r_i}{r} \sum_{s \in S} \left(o^s w^{st} + (m^s - 1) \, z^{st} \right), j \in M, t \in T, \tag{A.34}$$

$$\sum_{i \in N_j} h_{ij}^{t-1} \leq \sum_{i \in N_j} h_{ij}^t, j \in M, t \in T, \tag{A.35}$$

$$\alpha \sum_{i \in N_j} h_{ij}^t \leq a^t \left(x_j^0 + \sum_{t' \leq t} x_j^{t'} \right) j \in N, t \in T. \tag{A.36}$$

The objective function (A.26) aims to maximise the total number of EV users in the final year. Constraints (A.27) are budget constraints, ensuring that the cost of opening charging stations and installing charging outlets does not exceed the budget for that year. Constraints (A.28) both enforce a maximum number of charging outlets at each station and also ensures that the one-time cost to open charging stations is paid. Constraints (A.29) prevent removing charging outlets and constraints (A.30) prevent closing charging stations from one year to the next. Constraints (A.31) set the number of EVs at the start of one year as the number at the end of the previous year. Constraints (A.32) find the segment of the growth function that the current EV population is in. Constraints (A.33) ensure that only one segment of the growth function is selected. Constraints (A.34) cap the the number of EVs by the end of the year by following the growth function.

Parameter	Value
T	4
$\|N\|$	317
$\|M\|$	10
$\|N_j\|$	Varies
e_j (all stations)	6
r	181624
l_j (all stations)	0
c^U (all stations)	50
c_j^F (all stations)	100
B^t (per year)	400
α	0.566
a^t (all years)	$+\infty$
$\|S\|$	5
q^{s-1}, q^s	Varies
m^s	Varies
o^s	Varies

Table A.3 – Growth Function parameter values

Constraints (A.35) ensure that the total number of EVs does not decrease from year to year. Constraints (A.36) are capacity constraints, ensuring that potential new EV users will only decide to purchase an EV if there exists sufficient charging infrastructure.

Generating the Growth Function

The growth function in the GF model gives the number of EVs in the current year as a function of the number of EVs in the previous year. In the absence of the capacity contraints (A.36), the growth function would directly dictate the number of EVs each year via Constraints (A.31). We can ensure that the EV growth remains comparable between the MC and GF models by using the output from the MC model to create the growth function.

More specifically, we assume there are no EV owners at the start of the optimi-

sation period. While this is not a realistic assumption, it ensures feasibility in the GF model. Given a candidate solution $(\mathbf{x}, \mathbf{y})$, we solve the MC model (3.3) with the desired user classes and parameters over the 20 instances in the dataset. In each instance and for $1 \leq t \leq T$ we calculate the number of users who are covered by $\mathbf{x}$ (given by $\sum_{i \in N} \sum_{r=1}^{R_i} \frac{N_i^t}{R_i} w_i^{rt}$). To calculate the total number of EVs, we add the new EVs in each year to the EVs from the previous year (or the starting EVs in the case of the first year). We take the average result over all instances for each year as our desired growth function, which mimics perfectly the EV growth from the MC model (3.3).

After normalising for the population–which gives the percentage of the population with EVs in the following year given the percentage of the population with EVs in the current year–, we extend the growth function to cover the entire $[0, 1]$ domain. Both of these steps allow the growth function to be used regardless of population. An example of the normalised, extended growth function is given in Figure A.1.

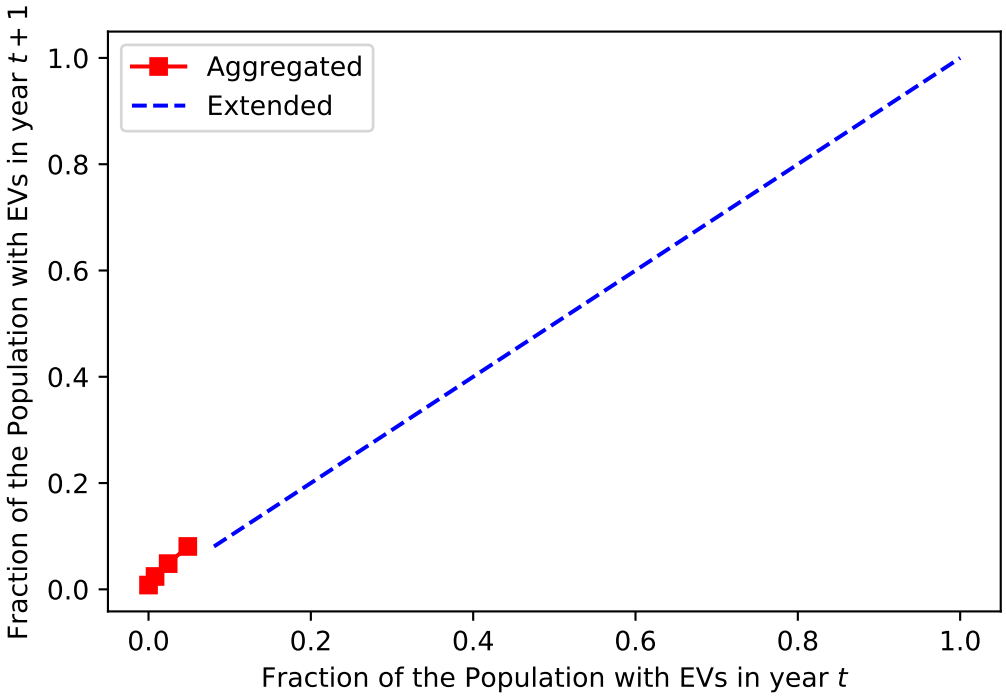

Figure A.1 – Growth Function Example

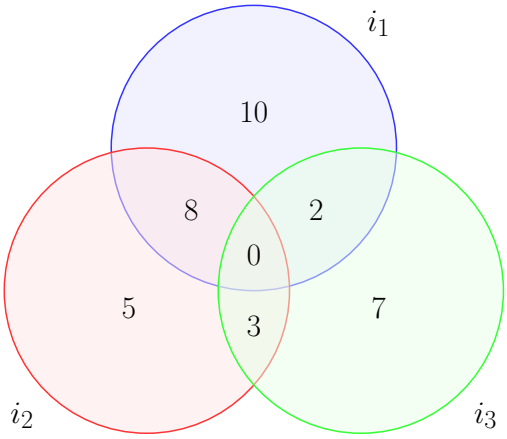

Figure A.2 – A simple example, with $T = 1$, three facilities $\{i_1, i_2, i_3\}$ and user coverage given by the numbers within the regions. Numbers within the intersection of facilities indicate overlapping coverage.

A.2 Second Article

A.2.1 Example of Benders Cuts

We present a simple example of this in Figure A.2. We drop the superscript t as there is only one time period. In this case, the domain Ω is given simply by $\Omega = \{(x_{i_1}, x_{i_2}, x_{i_3}) : x_i \in [0, 1], i = i_1, i_2, i_3\}$. If we generate the optimality cuts for the candidate solution $\tilde{x} = (1, 0, 0)$, i.e. facility i_1 is opened whereas facilities i_2 and i_3 are closed, we have the following optimality cuts

$$\begin{aligned}
&\text{(B0):}\quad 0x_{i_1} + 8x_{i_2} + 10x_{i_3} + 20 \geq \theta,\\
&\text{(B1):}\quad 10x_{i_1} + 8x_{i_2} + 10x_{i_3} + 10 \geq \theta,\\
&\text{(B2):}\quad 20x_{i_1} + 16x_{i_2} + 12x_{i_3} + 0 \geq \theta.
\end{aligned}$$

All three types of cuts correctly identify the objective value of solution $\tilde{x}$ as 20, matching the value in Equation (4.2). However, if we then use these optimality cuts to calculate the objective value of the solution $\bar{x} = (0, 0.75, 0.75)$, we obtain the values 33.5, 23.5, and 21 (for B0, B1, and B2 cuts respectively), while Equation (4.2) gives 19.5.

A.2.2 Links to Submodular Optimisation

The dynamic MCLP (4.1) can be viewed as a particular case of the general submodular problem in Coniglio et al. (2022), with the additional embedded structure of the time periods. For $1 \leq t \leq T$, let $S^t \subset I$ represent the subset of open facilities. Then, we define the real-valued set function $f^t(S^t) = \sum_{j \in J} \min\left\{1, \sum_{i \in S^t} a_{ij}^t\right\} d_j^t$, and the *marginal gains* function $\phi^t(i, S^t) = f^t(S^t \cup \{i\}) - f^t(S^t)$. It can then easily be verified that the function f^t is submodular, for example via the marginal gains property (iii) of Proposition 2.1 in Nemhauser et al. (1978).

We note that submodularity holds not only within each time period, but when considering the time period-facility pairs (t, i) more generally. That is, as the sum of submodular functions, the function $f\left(\cup_{t=1}^T S^t\right) = \sum_{t=1}^T f^t(S^t)$ is also submodular. Accordingly, single-cut equivalents to the multi-cuts described in A.2.2 can be used. However, for the sake of simplicity, we limit our discussion to the multi-cut versions.

Submodular Cuts and Benders Cuts

As mentioned previously, there are submodular cuts analogous to the Benders cuts presented in this work, and which can be used in a branch-and-cut framework. However, these submodular cuts are only defined for integer solutions, contrary to the Benders cuts. For $1 \leq t \leq T$, let x_i^t be an integer feasible solution to the main problem (4.7), and let $S^t(x) = \{i \in I : x_i^t = 1\}$. When there is no risk of confusion, we use $\tilde{S}^t = S^t(\tilde{x}_i^t)$, for $\tilde{x}_i^t$ the integer feasible candidate solution at the current iteration.

As before, let $J_s = \left\{j \in J : \sum_{t=1}^T \sum_{i \in I} a_{ij}^t = 1\right\}$ and $\tilde{I}_j^t = I_j^t(\tilde{x}) = \sum_{i \in I} a_{ij}^t \tilde{x}_i^t$. Then, in Coniglio et al. (2022), the authors propose the following submodular cuts:

$$\theta^t \leq f^t(\tilde{S}^t) + \sum_{i \in I \setminus \tilde{S}^t} \phi^t\left(i, \tilde{S}^t\right) x_i^t - \sum_{i \in \tilde{S}^t} \phi^t\left(i, I \setminus \{i\}\right)(1 - x_i^t), \tag{SC1}$$

$$\theta^t \leq f^t(\tilde{S}^t) + \sum_{i \in I \setminus \tilde{S}^t} \phi^t\left(i, \emptyset\right) x_i^t - \sum_{i \in \tilde{S}^t} \phi^t\left(i, \tilde{S}^t \setminus \{i\}\right)(1 - x_i^t), \tag{SC2}$$

$$\theta^t \leq f^t(\tilde{S}^t) + \sum_{i \in I \setminus \tilde{S}^t} \phi^t\left(i, \tilde{S}^t\right) x_i^t. \tag{SC3}$$

As demonstrated in Coniglio et al. (2022), the submodular cuts (SC1) are equivalent

to the Benders cuts (B1), the cuts(SC3) are equivalent to the cuts (B0), and the cuts (SC2) are weaker than the cuts (B2). This can be easily verified in the example of A.2.1, as well as by rewriting the set functions with respect to $\tilde{I}_j^t$, which yields the following equivalent cuts:

$$\theta^t \leq \sum_{j\in J:\tilde{I}_j^t\geq 1} d_j^t + \sum_{i\in I:\tilde{x}_i^t=0}\left(\sum_{j\in J:\tilde{I}_j^t=0} a_{ij}^t d_j^t\right) x_i^t - \sum_{i\in I:\tilde{x}_i^t=1}\left(\sum_{j\in J_s:\tilde{I}_j^t=1} a_{ij}^t d_j^t\right)(1-x_i^t), \tag{SC1'}$$

$$\theta^t \leq \sum_{j\in J:\tilde{I}_j^t\geq 1} d_j^t + \sum_{i\in I:\tilde{x}_i^t=0}\left(\sum_{j\in J} a_{ij}^t d_j^t\right) x_i^t - \sum_{i\in I:\tilde{x}_i^t=1}\left(\sum_{j\in J:\tilde{I}_j^t=1} a_{ij}^t d_j^t\right)(1-x_i^t), \tag{SC2'}$$

$$\theta^t \leq \sum_{j\in J:\tilde{I}_j^t\geq 1} d_j^t + \sum_{i\in I:\tilde{x}_i^t=0}\left(\sum_{j\in J:\tilde{I}_j^t=0} a_{ij}^t d_j^t\right) x_i^t. \tag{SC3'}$$

Submodular Interpretation of the Local Branching Subproblem

As in A.2.2, for $1 \leq t \leq T$, let $\tilde{x}_i^t$ be an integer feasible solution to the main problem (4.7), $\tilde{S}^t = \{i \in I : \tilde{x}_i^t = 1\}$, and $\tilde{I}_j^t = I_j^t(\tilde{x}) = \sum_{i\in I} a_{ij}^t \tilde{x}_i^t$. The equivalent versions of Propositions 4.5.1 and 4.5.2 using the submodular cuts are, respectively, given in Propositions A.2.1 and A.2.2.

Proposition A.2.1. *Let x be an (integer) feasible solution to the maximum covering model (4.1), and let t be any time period, $1 \leq t \leq T$. Let $\hat{i} \in I$ be such that $x_{\hat{i}}^t = 0$. Then the modified solution $\hat{x}$ with $\hat{x}_{\hat{i}}^t = 1$ and $\hat{x}_i^t = x_i^t, i \neq \hat{i}$ satisfies*

$$f^t\left(S^t(x)\cup\left\{\hat{i}\right\}\right) = f^t(\tilde{S}^t) + \sum_{i\in I\setminus\tilde{S}^t}\phi^t\left(i,\tilde{S}^t\right)x_i^t, \tag{A.37}$$

$$f^t\left(S^t(x)\cup\left\{\hat{i}\right\}\right) = f^t(\tilde{S}^t) + \sum_{i\in I\setminus\tilde{S}^t}\phi^t\left(i,\tilde{S}^t\right)x_i^t - \sum_{i\in\tilde{S}^t}\phi^t\left(i,I\setminus\{i\}\right)(1-x_i^t). \tag{A.38}$$

(A.39)

Proof. As $\hat{x}_i^t = x_i^t$ for $i \in I \setminus \left\{\hat{i}\right\}$, in both cases the summation on the right-hand side reduces to

$$f^t\left(S^t(x)\right) + \phi^t\left(\hat{i}, S^t(x)\right) x_{\hat{i}}^t. \tag{A.40}$$

The result then follows by definition of the marginal gains function ϕ^t. □

Proposition A.2.2. *Let $\hat{x}_j^t$ denote the optimal values for the variables x_j^t in the restricted subproblem* (4.20) *around an integer candidate solution $\tilde{x}$ at distance $\tilde{\kappa} = 2$. Then $\hat{x}_j^t$ are also the optimal values for the variables x_j^t in the following problem:*

$$\text{Maximise } \sum_{t=1}^{T} \theta^t, \tag{A.41a}$$

subject to (4.1b), (4.1d), (4.3b), (4.3c), (4.19c),

$$\sum_{i \in I : \tilde{x}_i^t = 1} \left(1 - x_i^t\right) + \sum_{i \in I : \tilde{x}_i^t = 0} x_i^t \leq 2, \qquad 1 \leq t \leq T, \tag{A.41b}$$

$$f^t(\tilde{S}^t) + \sum_{i \in I \setminus \tilde{S}^t} \phi^t\left(i, \tilde{S}^t\right) x_i^t - \sum_{i \in \tilde{S}^t} \phi^t\left(i, I \setminus \{i\}\right)\left(1 - x_i^t\right) \geq \theta^t,$$

$$1 \leq t \leq T, \tag{A.41c}$$

$$f^t(\tilde{S}^t \cup \left\{\hat{i}\right\}) + \sum_{i \in I \setminus \tilde{S}^t} \phi^t\left(i, \tilde{S}^t \cup \left\{\hat{i}\right\}\right) x_i^t \geq \theta^t, 1 \leq t \leq T, \hat{i} : \tilde{x}_{\hat{i}}^t = 0,$$

(A.41d)

$$f^t(\tilde{S}^t \setminus \left\{\hat{i}\right\}) + \sum_{i \in I \setminus \tilde{S}^t} \phi^t\left(i, \tilde{S}^t \setminus \left\{\hat{i}\right\}\right) x_i^t \geq \theta^t, \ 1 \leq t \leq T, \hat{i} : \tilde{x}_{\hat{i}}^t = 1.$$

(A.41e)

Proof. The proof is identical to that of Proposition 4.5.2. □

As mentioned in Appendix A.2.2, the submodular cuts (SC1) and (SC3) are, respectively, equivalent to the Benders cuts (B1) and (B0). Additionally, since the candidate solutions must be integer valued for the local branching framework, both the submodular and Benders cuts methodologies are entirely equivalent.

Table A.4 – Average performance details without greedy warmstart. Starred entries only include instances for which non-zero incumbent solutions were found. Entries in **bold** indicate the best performance across the exact methods in that dataset and metric.

		Simple	Distance	HomeCharging	LongSpan	Price
Solve time (sec)	Greedy	<0.01	<0.01	<0.01	0.05	0.10
	B&C	0.20	0.70	6.56	7186.12	7194.97
	U-B&BC	0.15	1.57	68.24	7184.25	7184.76
	A-B&BC	**0.11**	**0.51**	**1.37**	7184.35	7184.57
	A-B&BC+LB-SubD-SepD	4.65	4.74	12.70	7313.04	7344.53
Objective value	Greedy	31814.20	16591.75	18016.47	133724.37	33641.74
	B&C	**31820.15**	**16627.14**	**18030.50**	0.00	0.00
	U-B&BC	**31820.15**	**16627.14**	**18030.50**	122803.68*	32563.31
	A-B&BC	**31820.15**	**16627.14**	**18030.50**	133613.34*	33623.02
	A-B&BC+LB-SubD-SepD	**31820.15**	**16627.14**	**18030.50**	**133772.68**	**33655.97**
Optimality gap (%)	B&C	< **0.01**	< **0.01**	< **0.01**	-	-
	U-B&BC	< **0.01**	< **0.01**	< **0.01**	15.79*	15.00
	A-B&BC	< **0.01**	< **0.01**	< **0.01**	**6.20***	**11.49**
	A-B&BC+LB-SubD-SepD	< **0.01**	< **0.01**	< **0.01**	12.04	18.91
Number of nodes	B&C	59.25	43.35	**131.95**	0.00	0.00
	U-B&BC	**52.40**	**27.85**	228.50	0.00	0.00
	A-B&BC	152.10	84.50	1012.55	455.30	0.00
	A-B&BC+LB-SubD-SepD	65.05	187.30	795.25	**6435.35**	**1099.60**
Average lazy cut time (sec)	U-B&BC	< **0.01**	< **0.01**	< **0.01**	**0.04**	**0.08**
	A-B&BC	< **0.01**	< **0.01**	< **0.01**	0.05	0.11
	A-B&BC+LB-SubD-SepD	0.20	0.30	0.51	125.37	72.75
Average user cut time (sec)	U-B&BC	< **0.01**	< **0.01**	< **0.01**	**0.05**	**0.11**
	A-B&BC	< **0.01**	< **0.01**	< **0.01**	0.06	0.12
	A-B&BC+LB-SubD-SepD	0.02	< **0.01**	0.01	0.07	0.75
Number of restricted subproblems	A-B&BC+LB-SubD-SepD	127.90	143.85	185.70	1045.00	1169.95
Number of diversified subproblems	A-B&BC+LB-SubD-SepD	27.10	16.20	25.35	58.60	102.15
Solve time, LP (sec)	A-B&BC	0.01	0.02	0.02	0.82	1.31

A.2.3 Additional Computational Results

Comparison of Methodologies

In Tables A.4 and A.5, we report additional performance details for each of the solution methods compared in Section 4.6.2. The entries with the solve time, objective value, optimality gap, and the number of nodes have been duplicated in this table for ease of comparison. In addition, we present the number and average time for both lazy cuts (for integer candidate solutions) and user cuts (for fractional candidate solutions). Finally, since the local branching method solves the LP relaxation of the model with the multi-cut method independently, we include the LP solve time here.

In Figures A.3-A.5, we see the number of instances solved by each method as a function of time (in seconds).

Table A.5 – Average performance details with greedy warmstart. Entries in **bold** indicate the best performance across the exact methods in that dataset and metric.

		Simple	Distance	HomeCharging	LongSpan	Price
Solve time, (sec)	Greedy	<0.01	<0.01	<0.01	0.05	0.10
	B&C	0.23	0.70	6.46	7187.77	7196.19
	U-B&BC	0.14	1.13	58.23	7184.00	7185.39
	A-B&BC	**0.09**	**0.52**	**1.34**	7184.54	7185.04
	A-B&BC+LB-SubD-SepD	4.67	4.81	13.00	7291.34	7305.71
Objective value	Greedy	31814.20	16591.75	18016.47	133724.37	33641.74
	B&C	**31820.15**	**16627.14**	**18030.51**	133724.36	33641.73
	U-B&BC	**31820.15**	**16627.14**	**18030.51**	133724.36	33641.74
	A-B&BC	**31820.15**	**16627.14**	**18030.51**	133728.65	33642.19
	A-B&BC+LB-SubD-SepD	**31820.15**	**16627.14**	**18030.51**	**133781.88**	**33650.81**
Optimality gap (%)	B&C	< **0.01**	< **0.01**	< **0.01**	25.07	52.84
	U-B&BC	< **0.01**	< **0.01**	< **0.01**	6.25	11.34
	A-B&BC	< **0.01**	< **0.01**	< **0.01**	**6.12**	**11.32**
	A-B&BC+LB-SubD-SepD	< **0.01**	< **0.01**	< **0.01**	11.86	18.66
Number of nodes	B&C	47.40	35.00	**109.30**	0.00	0.00
	U-B&BC	**41.90**	**17.65**	200.75	0.00	0.00
	A-B&BC	65.35	75.05	860.45	0.00	**1499.60**
	A-B&BC+LB-SubD-SepD	65.05	205.60	797.35	**7282.65**	1202.50
Average lazy cut time (sec)	U-B&BC	< **0.01**	< **0.01**	< **0.01**	**0.04**	**0.08**
	A-B&BC	< **0.01**	< **0.01**	< **0.01**	0.06	0.12
	A-B&BC+LB-SubD-SepD	0.20	0.31	0.51	124.45	71.14
Average user cut time (sec)	U-B&BC	< **0.01**	< **0.01**	< **0.01**	**0.05**	**0.11**
	A-B&BC	< **0.01**	< **0.01**	< **0.01**	0.06	0.12
	A-B&BC+LB-SubD-SepD	0.02	< **0.01**	0.01	0.07	1.09
Number of diversified subproblems	A-B&BC+LB-SubD-SepD	27.10	16.10	25.50	59.55	103.10
Solve time, LP (sec)	A-B&BC	0.01	0.01	0.01	0.08	0.11

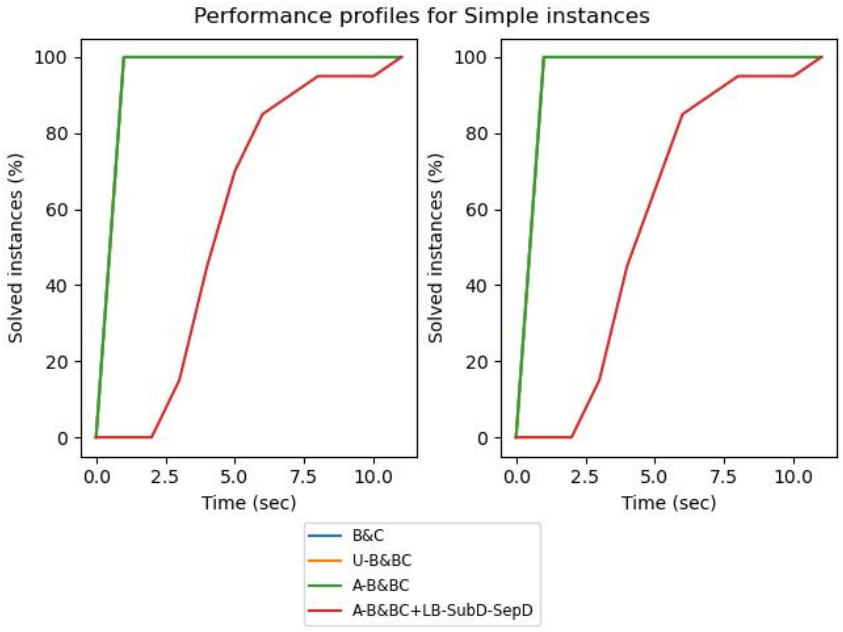

Figure A.3 – Performance profiles showing the number of Simple instances solved by each method as a function of time, both without a warmstart (left) and with a warmstart (right).

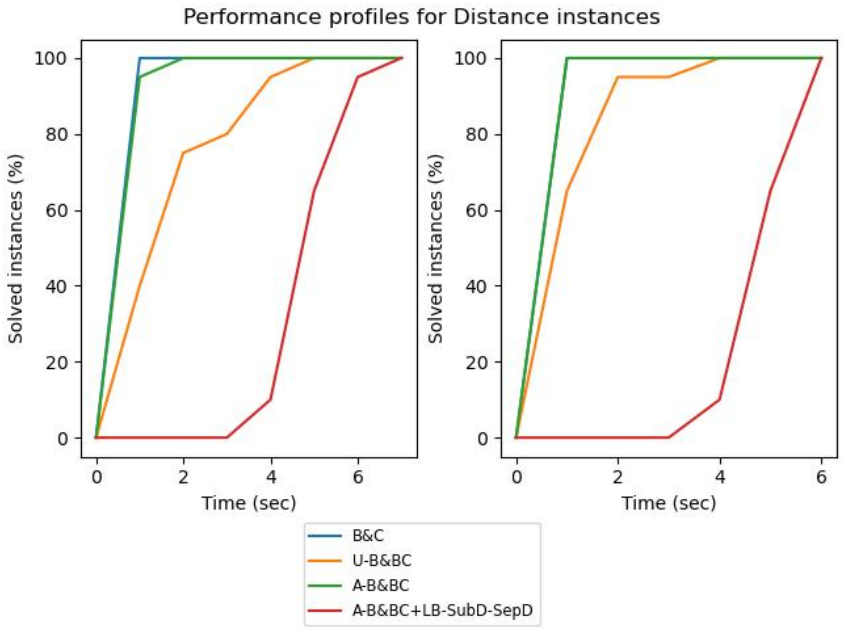

Figure A.4 – Performance profiles showing the number of Distance instances solved by each method as a function of time, both without a warmstart (left) and with a warmstart (right).

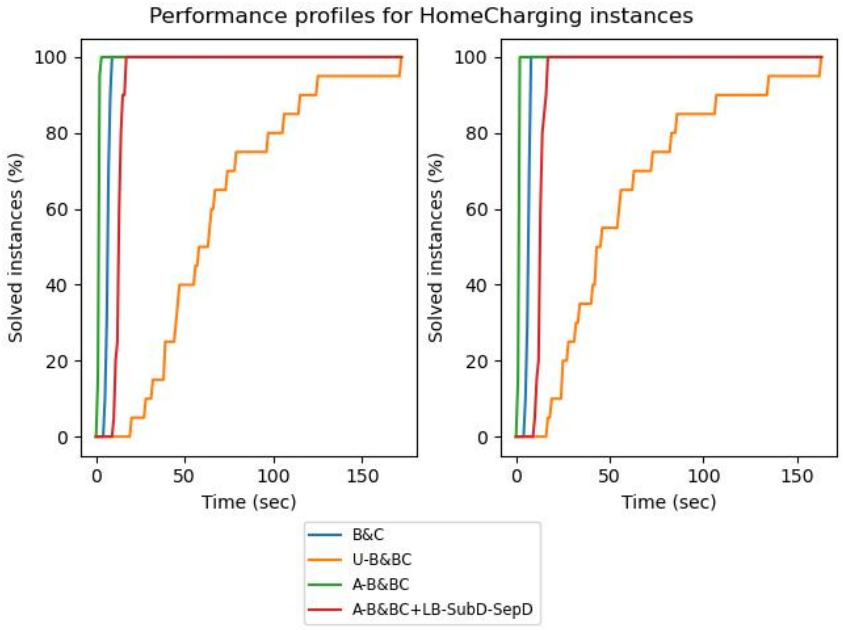

Figure A.5 – Performance profiles showing the number of HomeCharging instances solved by each method as a function of time, both without a warmstart (left) and with a warmstart (right).

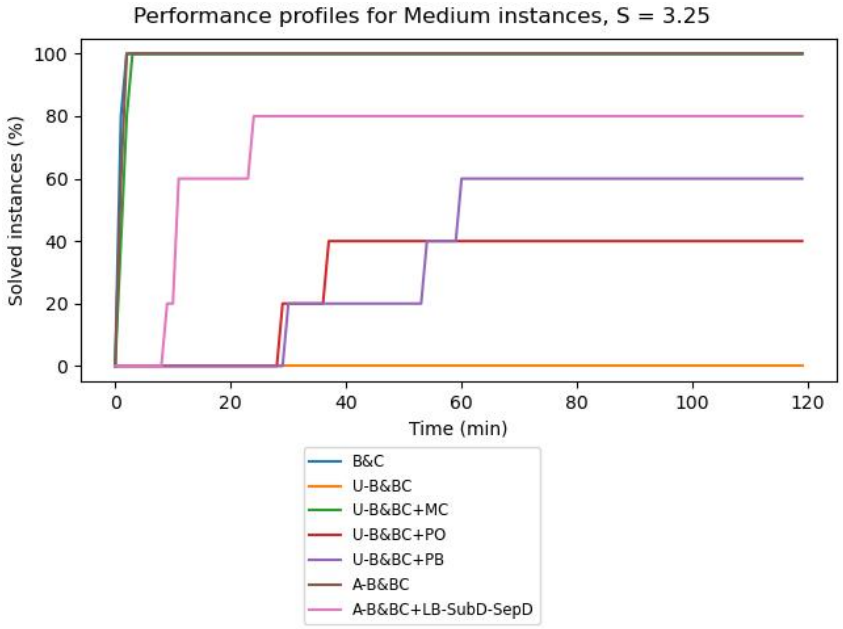

Figure A.6 – Performance profiles showing the number of Medium instances with $S = 3.25$ solved by each method as a function of time.

Comparison of Acceleration Techniques

In Table A.6, we report additional performance details for each of the solution methods compared in Section 4.6.3. The entries with the solve time, objective value, optimality gap, and the number of nodes have been duplicated in this table for ease of comparison. In addition, we present the number and average time for both lazy cuts (for integer candidate solutions) and user cuts (for fractional candidate solutions). Finally, since the local branching method solves the LP relaxation of the model with the multi-cut method independently, we include the LP solve time here.

In Figures A.6-A.8, we present the performance profiles for each method for each value of S. As in Section 4.6.3, these indicate the number of solved instances as a function of time for each method.

Further Results: Local Branching Restricted Subproblem Solution Method

In Figure A.9, we report the average solve time as a function of the number of separated solutions in each of the datasets. We recall that there are 20 instances in

Table A.6 – Average performance details in Medium instances. Entries in **bold** indicate the best performance across the exact methods in that dataset and metric.

		S=3.25	S=3.75	S=4.25
Solve time, MIP (sec)	B&C	**23.40**	187.48	73.31
	U-B&BC	7110.49	6515.51	5001.91
	U-B&BC+MC	79.44	86.67	40.71
	U-B&BC+PO	5009.42	4928.70	4711.18
	U-B&BC+PB	4516.99	4300.18	3403.50
	A-B&BC	56.11	**51.88**	**36.80**
	A-B&BC+LB-SubD-SepD	2077.59	2943.88	3725.03
Objective value	B&C	**1877854.46**	**2398990.73**	**2970338.08**
	U-B&BC	1877081.97	2398147.48	2968357.31
	U-B&BC+MC	**1877854.46**	**2398990.73**	**2970338.08**
	U-B&BC+PO	1877040.15	2396647.52	2967975.96
	U-B&BC+PB	1877179.18	2397067.08	2969571.91
	A-B&BC	**1877854.46**	**2398990.73**	**2970338.08**
	A-B&BC+LB-SubD-SepD	**1877854.46**	**2398990.73**	**2970338.08**
Gap to best known solution (%)	B&C	**0.00**	**0.00**	**0.00**
	U-B&BC	0.04	0.04	0.07
	U-B&BC+MC	**0.00**	**0.00**	**0.00**
	U-B&BC+PO	0.04	0.10	0.08
	U-B&BC+PB	0.04	0.08	0.03
	A-B&BC	**0.00**	**0.00**	**0.00**
	A-B&BC+LB-SubD-SepD	**0.00**	**0.00**	**0.00**
Optimality gap (%)	B&C	$<$ **0.01**	$<$ **0.01**	$<$ **0.01**
	U-B&BC	2.60	1.77	3.00
	U-B&BC+MC	$<$ **0.01**	$<$ **0.01**	$<$ **0.01**
	U-B&BC+PO	1.98	1.89	2.96
	U-B&BC+PB	0.85	1.47	0.93
	A-B&BC	$<$ **0.01**	$<$ **0.01**	$<$ **0.01**
	A-B&BC+LB-SubD-SepD	0.07	0.19	1.13
Number of nodes	B&C	8351.60	62989.40	24196.40
	U-B&BC	22776.80	24473.60	9865.80
	U-B&BC+MC	103045.80	86509.80	52664.80
	U-B&BC+PO	30834.00	25441.00	10147.80
	U-B&BC+PB	19181.20	13130.00	8498.00
	A-B&BC	68917.80	58596.60	49838.20
	A-B&BC+LB-SubD-SepD	**2631.60**	**8132.00**	**4233.40**
Number of solved instances	B&C	**5**	**5**	**5**
	U-B&BC	0	1	2
	U-B&BC+MC	**5**	**5**	**5**
	U-B&BC+PO	2	2	2
	U-B&BC+PB	3	3	3
	A-B&BC	**5**	**5**	**5**
	A-B&BC+LB-SubD-SepD	4	4	4

Table A.7 – Average performance details in Medium instances (continued). Entries in **bold** indicate the best performance across the exact methods in that dataset and metric.

		S=3.25	S=3.75	S=4.25
Average lazy cut time (sec)	U-B&BC	**< 0.01**	**< 0.01**	**< 0.01**
	U-B&BC+MC	**< 0.01**	**< 0.01**	**< 0.01**
	U-B&BC+PO	**< 0.01**	**< 0.01**	**< 0.01**
	U-B&BC+PB	**< 0.01**	**< 0.01**	**< 0.01**
	A-B&BC	**< 0.01**	**< 0.01**	**< 0.01**
	A-B&BC+LB-SubD-SepD	2.75	3.17	2.46
Average user cut time (sec)	U-B&BC	**< 0.01**	**< 0.01**	**< 0.01**
	U-B&BC+MC	**< 0.01**	**< 0.01**	**< 0.01**
	U-B&BC+PO	**< 0.01**	**< 0.01**	**< 0.01**
	U-B&BC+PB	**< 0.01**	**< 0.01**	**< 0.01**
	A-B&BC	**< 0.01**	**< 0.01**	**< 0.01**
	A-B&BC+LB-SubD-SepD	0.29	0.09	0.15
Number of restricted subproblems	A-B&BC+LB-SubD-SepD	2420.40	3363.40	4686.60
Number of diversified subproblems	A-B&BC+LB-SubD-SepD	551.80	817.60	1063.60
Solve time, LP (sec)	A-B&BC	0.18	0.19	0.19

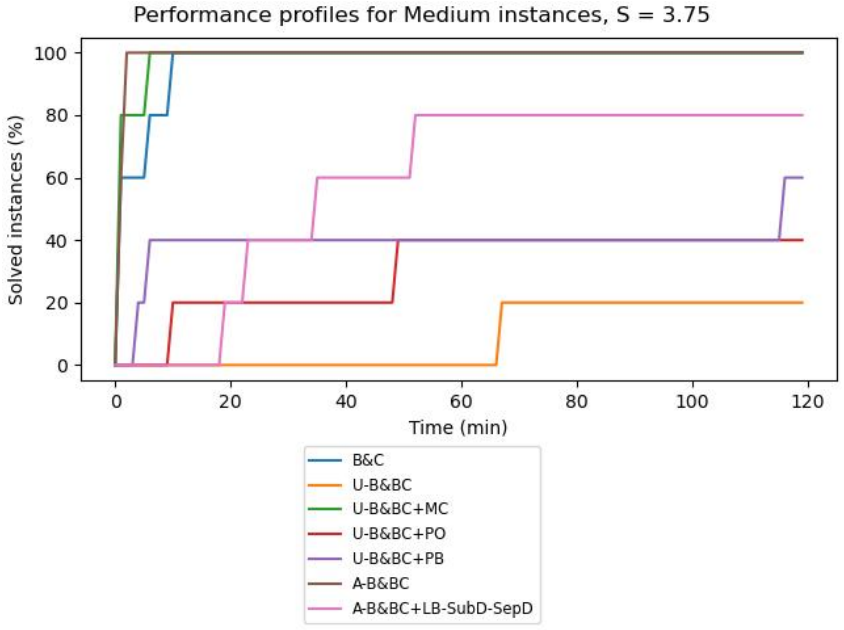

Figure A.7 – Performance profiles showing the number of Medium instances with $S = 3.75$ solved by each method as a function of time.

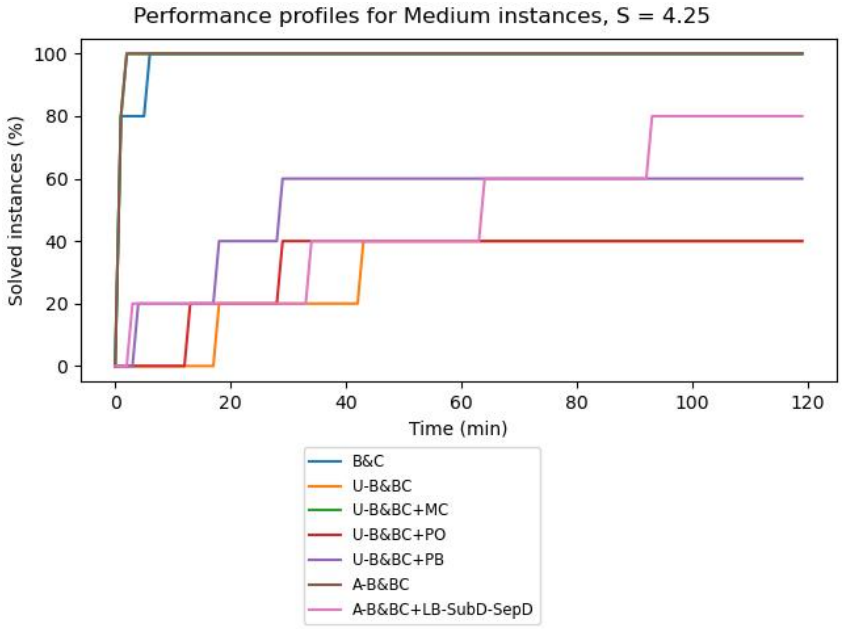

Figure A.8 – Performance profiles showing the number of Medium instances with $S = 4.25$ solved by each method as a function of time.

the dataset, and in each instance we randomly generated a series of 255 candidate solutions. The restricted subproblem (4.20) around each candidate solution was then solved using either the method SubD, which directly solves the reformulation (4.25) with a generic solver, or the method SubB, which solves the restricted subproblem (4.20) via the A-B&BCmethod. By taking the average solve time of the subproblems across all instances for a fixed number of solved subproblems, we can then examine the impact of the increasing number of cuts to both of the methods.

Looking at Figure A.9, we observe, for both methods, that the time to solve the restricted subproblem tends to increases along with the number of separated solutions. This is unsurprising, due to the addition of the Big-M Constraints (4.27a). More interestingly, we remark a much higher variability in the solving times for the SubBmethod, with the solve times shifting rapidly by 50% or more. The only dataset for which we see a higher variability in the SubDmethod is in the LongSpan dataset, where nearly all subproblems terminate at the time limit for the SubBmethod.

In Figures A.10 and A.11, we see the percentage of restricted subproblems

Table A.8 – Average performance details for different feasible space reduction methods. Entries in **bold** indicate the best performance across the exact methods in that dataset and metric. Metrics or datasets with no clear "best" value do not have any entries in bold.

		Simple	Distance	HomeCharging	LongSpan	Price
Solve time (sec)	SepB, all solutions	46.52	2.32	1460.34	7176.68	9045.39
	SepB, improving solutions	**0.72**	**1.17**	8.95	7192.53	7269.47
	SepD	1.12	1.68	**4.99**	7175.38	7292.31
Objective value	SepB, all solutions	**13718.14**	**6635.17**	**8151.72**	18473.34	13439.35
	SepB, improving solutions	**13718.14**	**6635.17**	**8151.72**	**18882.63**	**13601.62**
	SepD	**13718.14**	**6635.17**	**8151.72**	18851.94	13552.85
Optimality gap (%)	SepB, all solutions	< **0.01**	< **0.01**	0.21	21.92	22.41
	SepB, improving solutions	< **0.01**	< **0.01**	< **0.01**	13.38	18.05
	SepD	< **0.01**	< **0.01**	< **0.01**	**12.47**	**17.47**
Number of nodes	SepB, all solutions	509.10	100.60	3061.90	1003.45	589.73
	SepB, improving solutions	12.75	73.95	216.35	2654.30	1117.95
	SepD	**10.00**	**64.10**	**170.80**	**4273.90**	**1592.75**
Average lazy cut time (sec)	SepB, all solutions	**0.05**	**0.09**	0.16	**8.93**	33.00
	SepB, improving solutions	**0.05**	**0.09**	**0.13**	9.13	**31.90**
	SepD	0.06	0.10	0.17	9.05	33.47
Number of lazy cuts	SepB, all solutions	9.50	**3.25**	11.65	23.85	23.15
	SepB, improving solutions	**7.90**	3.35	**11.00**	68.90	47.50
	SepD	11.45	10.05	9.40	42.10	41.35
Average user cut time (sec)	SepB, all solutions	0.03	0.01	0.08	3.76	12.16
	SepB, improving solutions	**0.01**	0.01	0.02	1.01	3.01
	SepD	**0.01**	< **0.01**	**0.01**	**0.33**	**0.95**
Number of user cuts	SepB, all solutions	652.95	23.45	2880.55	736.65	255.12
	SepB, improving solutions	**5.70**	9.70	50.80	820.25	228.80
	SepD	6.55	**5.80**	**21.15**	834.70	227.55
Number of diversified subproblems	SepB, all solutions	662.45	26.70	2892.20	760.50	278.27
	SepB, improving solutions	13.60	13.05	61.80	889.15	276.30
	SepD	18.00	15.85	30.55	876.80	268.90
Number of restricted subproblems	SepB, all solutions	1424.90	98.25	13127.65	4838.15	1708.62
	SepB, improving solutions	31.25	41.60	195.60	4783.15	1338.45
	SepD	87.75	101.95	170.40	6773.35	1973.20
Solve time, LP (sec)	SepB, all solutions	< **0.01**	0.01	0.01	**0.05**	**0.24**
	SepB, improving solutions	< **0.01**	< **0.01**	< **0.01**	0.05	0.27
	SepD	< **0.01**	0.01	0.01	0.14	0.62
Number of user-created branches	SepB, all solutions	654.70	27.00	2887.90	741.20	260.38
	SepB, improving solutions	2.20	4.70	6.70	12.40	9.30

solved by each subproblem solution method as a function of time (for the Price and LongSpan datasets, respectively). As the subproblem solution time in the easy instances is nearly always less than one second regardless of the method, the corresponding figures have not been included.

Further Results: Local Branching Subdomain Separation Scheme

In Table A.8, we report additional performance details for the subproblem solution methods, where values in the table are defined equivalently as A.2.3.

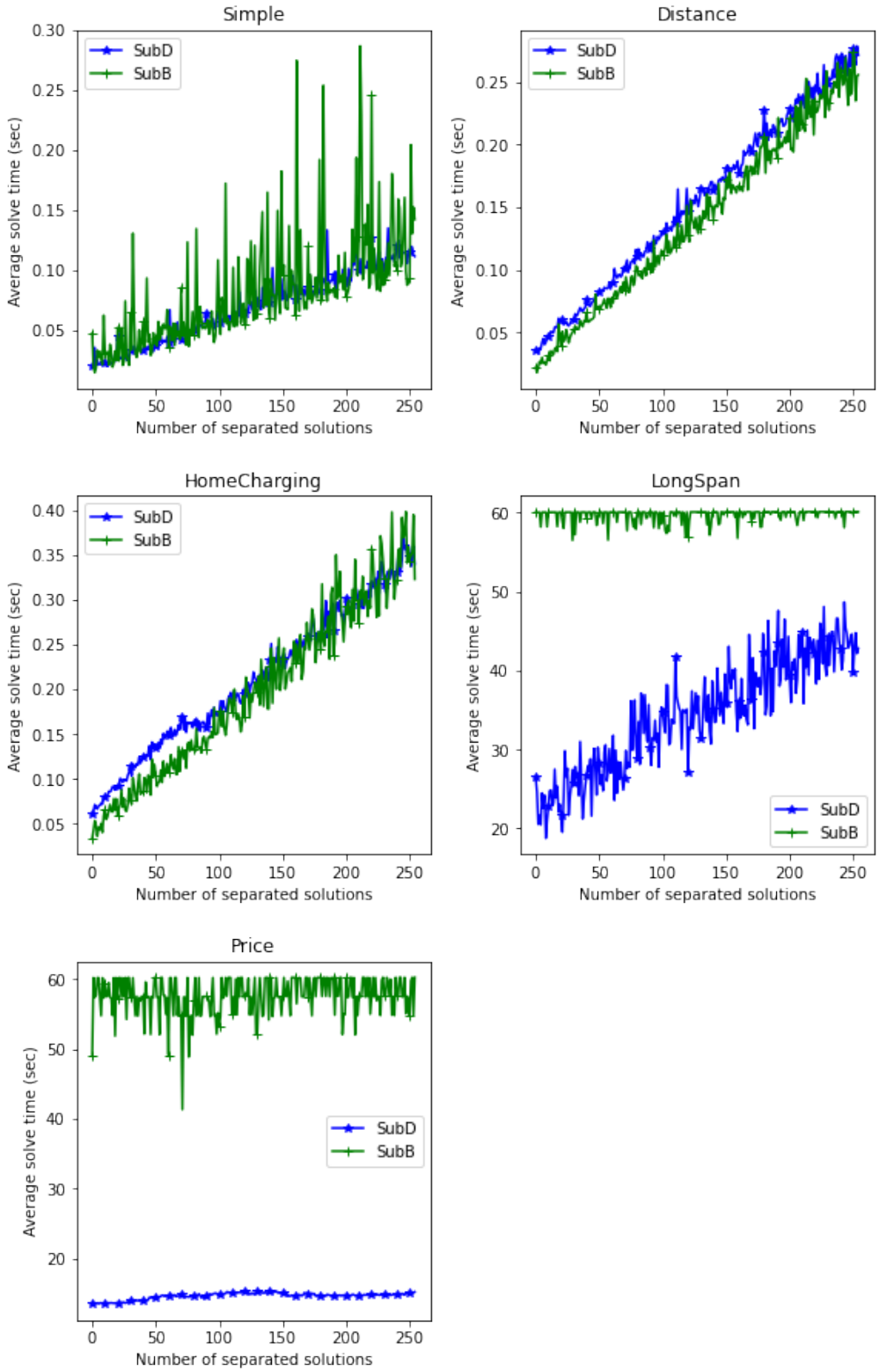

Figure A.9 – Evolution of subproblem solution time as a factor of the number of subproblem separations completed.

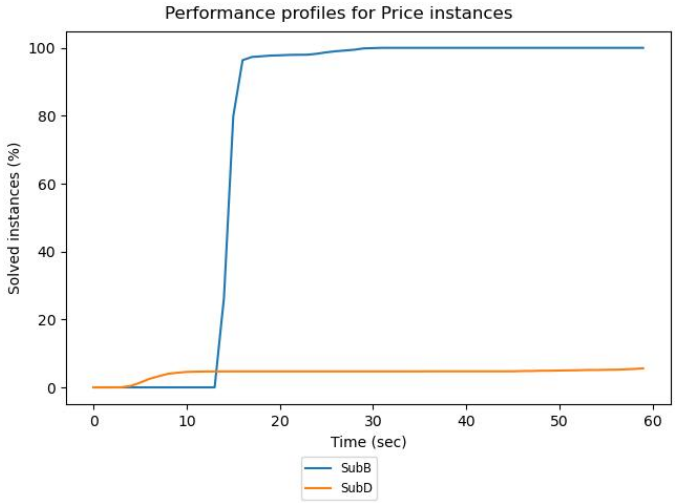

Figure A.10 – Percentage of restricted subproblems solved in the Price dataset by each method as a function of time.

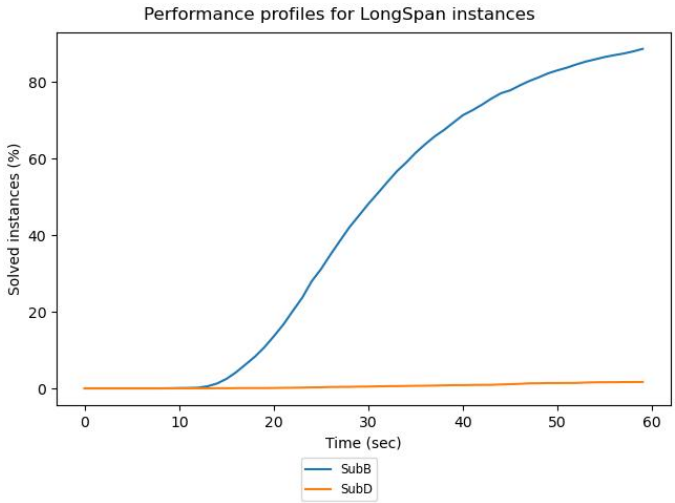

Figure A.11 – Percentage of restricted subproblems solved in the LongSpan dataset by each method as a function of time.

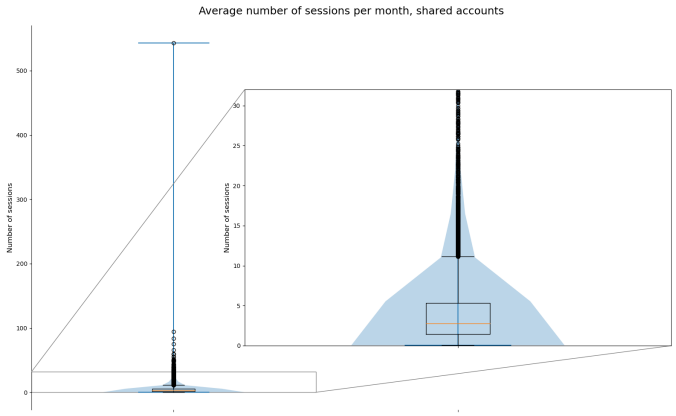

Figure A.12 – Distribution of average number of sessions per month, shared vehicles.

A.3 Third Article

A.3.1 Data Description, Shared Members

In general, shared members have a much higher usage of public charging infrastructure across all metrics. This can be seen by comparing the figures in Section 5.3.1 for private vehicles with their counterpart in Figures A.12-A.15. For ease of reading, the median values for private vehicles are repeated in this section.

— By construction, the average number of sessions and total energy charged are presented in Figures A.12 and A.13. Median values for the number of charging sessions and total energy per month for private vehicles are, respectively, 0.57 sessions and 5.89 kWh, while the median values for shared accounts are 2.75 sessions and 34.7 kWh.

— In Figure A.14, we present the distribution for the average amount of time spent charging every month, with the duration of each charging session capped at 720 minutes as before. The median values are 47.7 minutes for private vehicles and 162.7 minutes for shared accounts.

— In Figure A.15, we present the distribution for the average number of different stations visited each month. The median values are 0.45 and 1.85 stations, respectively, for private vehicles and shared accounts.

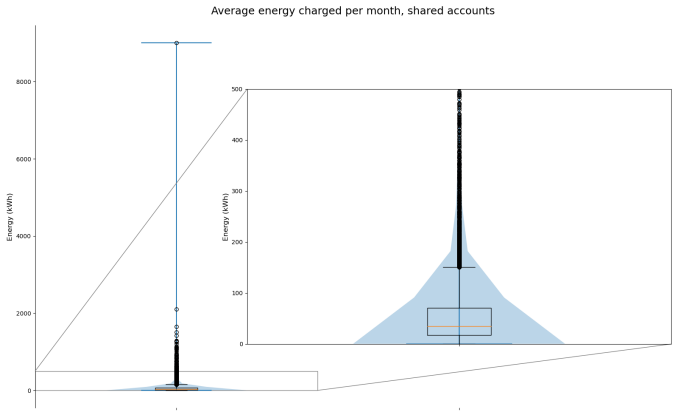

Figure A.13 – Distribution of average energy charged per month, shared vehicles.

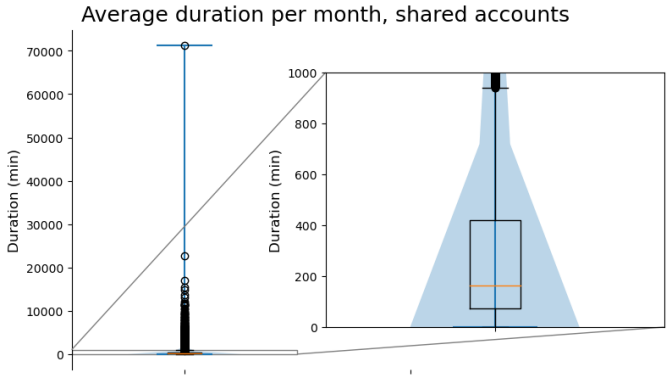

Figure A.14 – Distribution of average monthly time spent charging, shared vehicles.

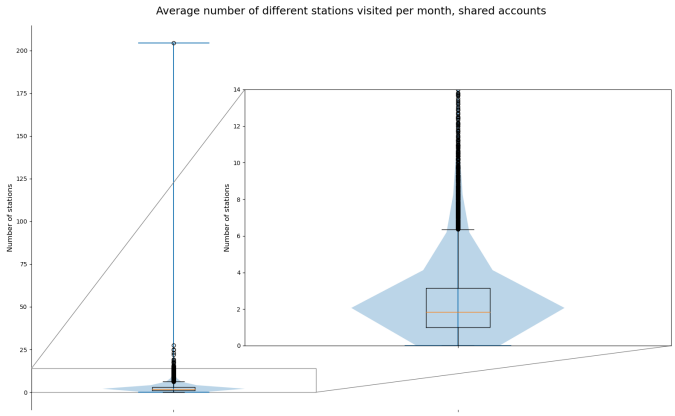

Figure A.15 – Distribution of average number of different stations per month, shared vehicles.

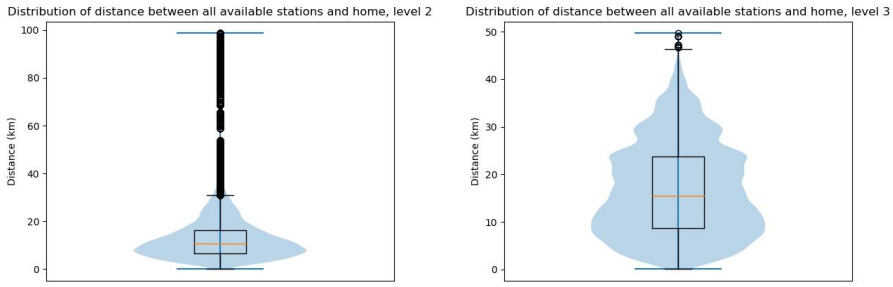

Figure A.16 – Distance from the user's home to the all available charging stations.

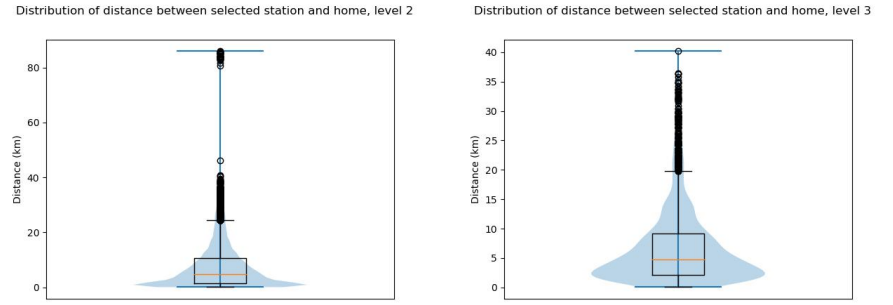

Figure A.17 – Distance from the user's home to the selected charging station.

A.3.2 Distribution of Attributes

	500m	750m	1000m	1250m	1500m
mean	0.8127	2.0735	3.9996	6.5259	9.5881
std	1.1767	2.4713	4.5060	6.9330	9.7409
min	0	0	0	0	0
25%	0	0	1	1	2
50%	0	1	3	5	7
75%	1	3	6	10	15
max	15	23	42	55	70

Table A.9 – Distribution of the number of charging stations with the utility function thresholds for level 2 charging.

	500m	750m	1000m	1250m	1500m
mean	0.0152	0.0658	0.1080	0.1609	0.2223
std	0.1225	0.2480	0.3156	0.3843	0.4442
min	0	0	0	0	0
25%	0	0	0	0	0
50%	0	0	0	0	0
75%	0	0	0	0	0
max	1	1	2	2	2

Table A.10 – Distribution of the number of charging stations with the utility function thresholds for level 3 charging.

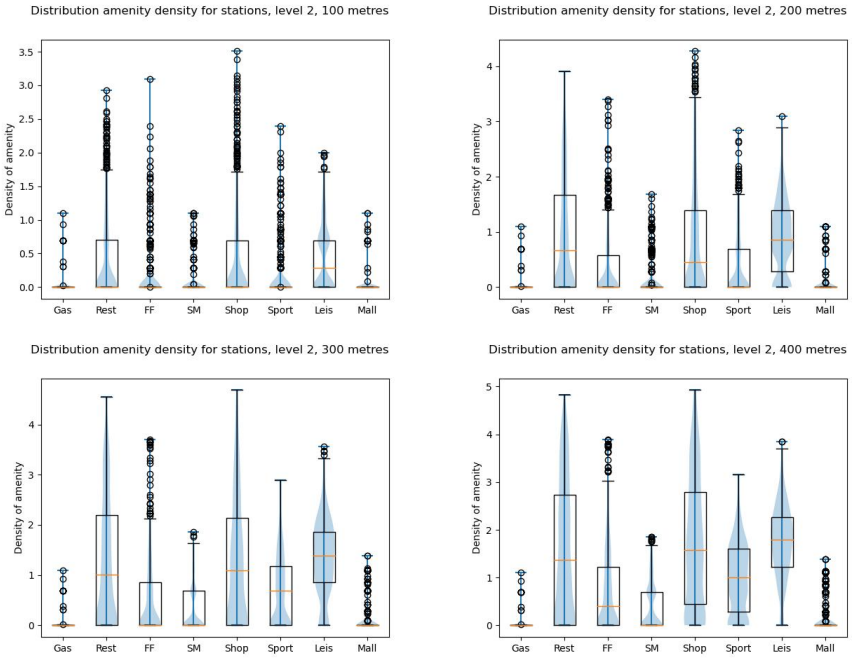

Figure A.18 – Density of amenities at different distance thresholds, level 2.

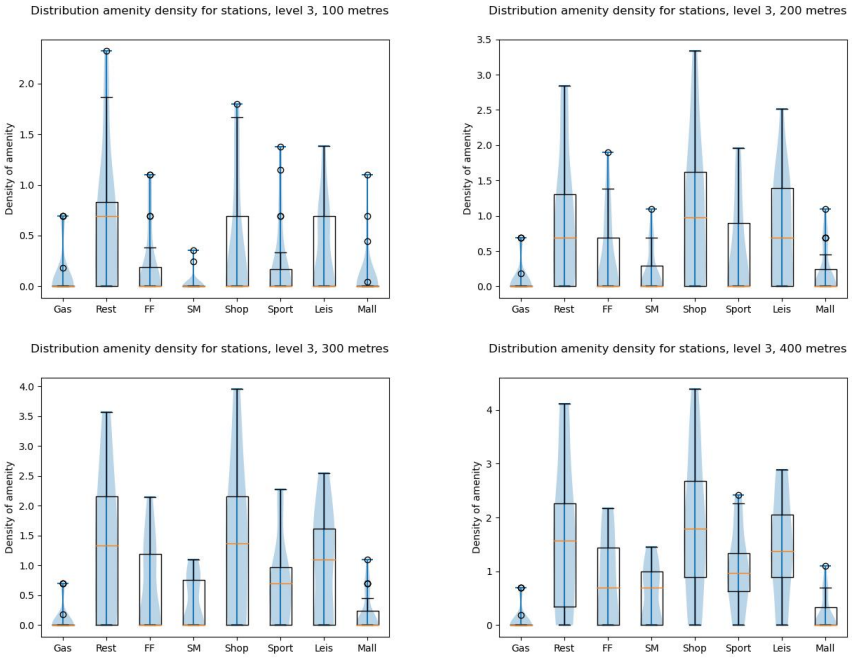

Figure A.19 – Density of amenities at different distance thresholds, level 3.

A.3.3 Additional Estimation Results

Parameter	Distance	0	1	2	3	4
$\beta^{\mu}_{distFar}$	100	-0.1591***	-0.1422***	-0.1283***	-0.1619***	-0.1582***
	200	-0.1616***	-0.145***	-0.1293***	-0.1608***	-0.1608***
	300	-0.163***	-0.1454***	-0.1296***	-0.164***	-0.1608***
	400	-0.1623***	-0.1443***	-0.129***	-0.1628***	-0.1596***
$\beta^{\mu}_{distNear}$	100	0.5991***	1.0374***	0.7813***	0.723***	0.8911***
	200	0.6434***	1.0774***	0.8139***	0.9184***	0.9184***
	300	0.6391***	1.0422***	0.7845***	0.6879***	0.8845***
	400	0.5709***	0.9572***	0.6848***	0.6034***	0.811***
β^{μ}_{ff}	100	0.0005	0.0791**	0.0129	-0.0465	-0.0472
	200	-0.1015***	-0.1728***	-0.2049***	-0.1663***	-0.1663***
	300	-0.0961***	-0.1161***	-0.1098***	-0.1311***	-0.0985***
	400	-0.1042***	-0.0907***	-0.1004***	-0.1099***	-0.0513**
β^{μ}_{isGas}	100	-0.324***	-0.415***	-0.003	-0.4791***	-0.4317***
	200	-0.2123**	-0.3062***	0.1074	-0.3652***	-0.3652***
	300	-0.2414**	-0.3383***	0.1231	-0.4756***	-0.4155***
	400	-0.2582***	-0.3583***	0.08	-0.483***	-0.4052***
$\beta^{\mu}_{isWalkHome}$	100	3.0644***	3.1369***	3.4862***	3.3313***	3.2841***
	200	3.1021***	3.1773***	3.5186***	3.3121***	3.3121***
	300	3.0992***	3.1498***	3.4934***	3.3087***	3.2845***
	400	3.0426***	3.0794***	3.407***	3.2376***	3.2243***
β^{μ}_{leis}	100	-0.1515***	0.0269	-0.2136***	0.2344***	-0.0001
	200	-0.0884***	-0.0846***	-0.1754***	-0.1332***	-0.1332***
	300	-0.159***	-0.1166***	-0.2607***	-0.1748***	-0.1916***
	400	-0.2475***	-0.1591***	-0.3302***	-0.2523***	-0.2983***
β^{μ}_{mall}	100	0.6322***	0.6795***	0.5981***	1.1677***	0.7985***
	200	0.3663***	0.3058***	0.2705***	0.4025***	0.4025***
	300	0.2711***	0.2975***	0.197***	0.6687***	0.4962***
	400	0.1605***	0.2353***	0.2327***	0.5829***	0.3509***
$\beta^{\mu}_{outletsFar}$	100	0.1374***	0.1284***	0.1163***	0.1102***	0.0954***
	200	0.1221***	0.1146***	0.1058***	0.0839***	0.0839***
	300	0.1136***	0.1067***	0.0958***	0.0923***	0.0724***
	400	0.1169***	0.1068***	0.0927***	0.078***	0.0718***
$\beta^{\mu}_{outletsNear}$	100	0.3219***	0.2669***	0.2393***	0.2475***	0.1863***
	200	0.3258***	0.2711***	0.2422***	0.19***	0.19***
	300	0.3251***	0.2681***	0.2399***	0.2442***	0.1857***
	400	0.3181***	0.2602***	0.2314***	0.2347***	0.1766***

Table A.11 – Parameter values for level 2 charging with the MNL model, and various amenity thresholds. The utility function threshold is set at 1.5km and the sample size is 5,000. *** indicates significance at 1% level, ** significance at 5% level, and * significance at 10% level

Parameter	Distance	0	1	2	3	4
β^{μ}_{rest}	100	0.2273***	0.3801***	0.377***	0.2648***	0.3425***
	200	0.3181***	0.4165***	0.3732***	0.3822***	0.3822***
	300	0.3556***	0.3912***	0.376***	0.3777***	0.3956***
	400	0.3469***	0.3746***	0.3966***	0.3989***	0.3719***
β^{μ}_{shop}	100	-0.0223	-0.0575**	-0.0291	0.0453*	-0.0146
	200	-0.0941***	-0.0504***	-0.0095	-0.0692***	-0.0692***
	300	-0.098***	-0.0981***	-0.0496**	-0.1129***	-0.1494***
	400	-0.0785***	-0.1419***	-0.0949***	-0.1603***	-0.1428***
β^{μ}_{sm}	100	0.1547***	0.0994	-0.1608***	0.0734	0.0238
	200	0.1724***	0.1505***	0.0684	0.3255***	0.3255***
	300	0.1006***	0.1129***	0.0437	0.1702***	0.2572***
	400	0.0646*	0.1595***	0.049	0.1336***	0.2197***
β^{μ}_{sport}	100	0.1797***	0.0869**	-0.0112	-0.0255	-0.1036**
	200	0.0814***	0.1227***	-0.0167	0.0039	0.0039
	300	0.0798***	0.0694***	0.0765***	0.1168***	0.0413
	400	0.0895***	0.0161	0.0566**	0.1298***	0.0859***

Table A.12 – Parameter values for level 2 charging with the MNL model, and various amenity thresholds (continued). The utility function threshold is set at 1.5km and the sample size is 5,000. *** indicates significance at 1% level, ** significance at 5% level, and * significance at 10% level

	Distance	100		200		300		400	
		Mean	Std	Mean	Std	Mean	Std	Mean	Std
Test set	Score								
Estimation	Akaike Information Criterion	52019.7700	652.8600	51937.1900	604.2400	51859.3200	668.2300	51865.2400	664.9100
	Bayesian Information Criterion	52104.4900	652.8600	52021.9100	604.2400	51944.0400	668.2300	51949.9600	664.9100
	Final log-likelihood	-25996.8853	326.4277	-25955.5947	302.1192	-25916.6605	334.1137	-25919.6182	332.4531
	Null log-likelihood	-30901.9274	50.3773	-30900.1624	50.3833	-30901.9274	50.3773	-30901.9274	50.3773
	ρ	0.1587	0.0104	0.1600	0.0095	0.1613	0.0107	0.1612	0.0106
	$\bar{\rho}^2$	0.1583	0.0104	0.1596	0.0095	0.1609	0.0107	0.1608	0.0106
Validation	Akaike Information Criterion	53369.9400	193.0700	53115.9900	164.1200	53083.3200	157.7800	53144.9600	162.9300
	Bayesian Information Criterion	53453.9200	193.0700	53199.9700	164.1200	53167.3000	157.7800	53228.9400	162.9300
	DPSA final, max	0.5792	0.0222	0.6033	0.0277	0.5946	0.0226	0.5816	0.0290
	DPSA final, mean	0.0212	0.0009	0.0213	0.0010	0.0213	0.0010	0.0214	0.0010
	DPSA final, min	0.0000	0.0000	0.0000	0.0000	0.0000	0.0000	0.0000	0.0000
	DPSA null, max	0.0038	0.0000	0.0038	0.0000	0.0038	0.0000	0.0038	0.0000
	DPSA null, mean	0.0017	0.0000	0.0017	0.0000	0.0017	0.0000	0.0017	0.0000
	DPSA null, min	0.0014	0.0000	0.0014	0.0000	0.0014	0.0000	0.0014	0.0000
	Final log-likelihood	-26671.9687	96.5372	-26544.9946	82.0617	-26528.6589	78.8882	-26559.4805	81.4667
	Null log-likelihood	-30199.1322	9.0394	-30198.0326	7.5853	-30199.1322	9.0394	-30199.1322	9.0394
	ρ	0.1168	0.0032	0.1210	0.0028	0.1215	0.0026	0.1205	0.0027
	$\bar{\rho}^2$	0.1164	0.0032	0.1205	0.0028	0.1211	0.0026	0.1201	0.0027

Table A.13 – Performance indicators for level 2 charging with the MNL model, and various amenity thresholds. The utility function threshold is set at 1.5km and the sample size is 5,000.

Parameter	Distance	0	1	2	3	4
$\beta^{\mu}_{distFar}$	0.5	-0.1952***	-0.1781***	-0.1632***	-0.1967***	-0.2023***
	0.75	-0.1783***	-0.168***	-0.1517***	-0.1869***	-0.187***
	1.0	-0.17***	-0.1627***	-0.1391***	-0.1801***	-0.1757***
	1.25	-0.1658***	-0.1556***	-0.1331***	-0.1692***	-0.169***
	1.5	-0.163***	-0.1454***	-0.1296***	-0.164***	-0.1608***
$\beta^{\mu}_{distNear}$	0.5	-3.8529***	-2.3207***	-2.7967***	-2.9456***	-3.8382***
	0.75	0.8015***	-0.1358	-0.1549	-0.1444	-0.0426
	1.0	1.2063***	0.5303***	1.4025***	0.4651***	1.1343***
	1.25	0.8708***	0.8543***	1.0689***	0.7694***	0.8666***
	1.5	0.6391***	1.0422***	0.7845***	0.6879***	0.8845***
β^{μ}_{ff}	0.5	-0.1442***	-0.1496***	-0.1927***	-0.1917***	-0.1749***
	0.75	-0.1201***	-0.149***	-0.1523***	-0.1603***	-0.1421***
	1.0	-0.1119***	-0.1504***	-0.1281***	-0.1446***	-0.1093***
	1.25	-0.0973***	-0.1314***	-0.12***	-0.1404***	-0.0938***
	1.5	-0.0961***	-0.1161***	-0.1098***	-0.1311***	-0.0985***
β^{μ}_{isGas}	0.5	-0.2311**	-0.319***	0.1141	-0.3755***	-0.3989***
	0.75	-0.2443***	-0.3863***	0.1015	-0.5085***	-0.4941***
	1.0	-0.2303**	-0.3795***	0.1146	-0.5092***	-0.493***
	1.25	-0.2598***	-0.3775***	0.1121	-0.4966***	-0.4525***
	1.5	-0.2414**	-0.3383***	0.1231	-0.4756***	-0.4155***
$\beta^{\mu}_{isWalkHome}$	0.5	5.6532***	5.3508***	5.5593***	5.5003***	5.691***
	0.75	2.8536***	3.6115***	3.7672***	3.9158***	4.005***
	1.0	2.7698***	3.1226***	3.1435***	3.2018***	3.192***
	1.25	2.9403***	3.1045***	3.2977***	3.2061***	3.2324***
	1.5	3.0992***	3.1498***	3.4934***	3.3087***	3.2845***
β^{μ}_{leis}	0.5	-0.0241	0.0216	-0.1333***	-0.0832***	-0.0384
	0.75	-0.0933***	-0.0416*	-0.1881***	-0.1181***	-0.1134***
	1.0	-0.126***	-0.0662***	-0.2648***	-0.1577***	-0.1477***
	1.25	-0.146***	-0.0819***	-0.2593***	-0.1631***	-0.1747***
	1.5	-0.159***	-0.1166***	-0.2607***	-0.1748***	-0.1916***
β^{μ}_{mall}	0.5	0.1741***	0.2047***	0.0848	0.5263***	0.385***
	0.75	0.216***	0.2582***	0.1505***	0.5834***	0.4625***
	1.0	0.2603***	0.2759***	0.1905***	0.6065***	0.4995***
	1.25	0.28***	0.2754***	0.2038***	0.6376***	0.5029***
	1.5	0.2711***	0.2975***	0.197***	0.6687***	0.4962***
$\beta^{\mu}_{outletsFar}$	0.5	0.1472***	0.1365***	0.1259***	0.1233***	0.1012***
	0.75	0.1249***	0.119***	0.1099***	0.1131***	0.0902***
	1.0	0.1203***	0.1108***	0.0998***	0.0968***	0.0808***
	1.25	0.1153***	0.1102***	0.0969***	0.0971***	0.0744***
	1.5	0.1136***	0.1067***	0.0958***	0.0923***	0.0724***
$\beta^{\mu}_{outletsNear}$	0.5	0.0077	-0.0314	-0.0417	-0.0493	-0.155***
	0.75	0.4203***	0.3154***	0.286***	0.167***	0.0547*
	1.0	0.3627***	0.3354***	0.2588***	0.2853***	0.1637***
	1.25	0.3354***	0.2818***	0.2608***	0.2475***	0.1815***
	1.5	0.3251***	0.2681***	0.2399***	0.2442***	0.1857***

Table A.14 – Parameter values for level 2 charging with the MNL model, and various utility function thresholds. The amenity threshold is set at 300m and the sample size is 5,000. *** indicates significance at 1% level, ** significance at 5% level, and * significance at 10% level

Parameter	Distance	0	1	2	3	4
β^{μ}_{rest}	0.5	0.3192***	0.3079***	0.3368***	0.3564***	0.3023***
	0.75	0.3274***	0.337***	0.3333***	0.3715***	0.3531***
	1.0	0.3458***	0.3468***	0.3735***	0.3875***	0.359***
	1.25	0.3512***	0.3554***	0.3821***	0.3663***	0.3635***
	1.5	0.3556***	0.3912***	0.376***	0.3777***	0.3956***
β^{μ}_{shop}	0.5	-0.0557***	-0.0587***	0.0307	-0.0657***	-0.0481**
	0.75	-0.0798***	-0.0722***	0.0027	-0.0991***	-0.108***
	1.0	-0.0904***	-0.072***	-0.0312	-0.1289***	-0.1207***
	1.25	-0.1044***	-0.0846***	-0.051**	-0.1015***	-0.1376***
	1.5	-0.098***	-0.0981***	-0.0496**	-0.1129***	-0.1494***
β^{μ}_{sm}	0.5	0.1579***	0.1612***	0.0859***	0.3017***	0.3057***
	0.75	0.1599***	0.1292***	0.0871***	0.2691***	0.296***
	1.0	0.1221***	0.121***	0.076**	0.2711***	0.2793***
	1.25	0.1173***	0.1018***	0.056	0.1942***	0.2834***
	1.5	0.1006***	0.1129***	0.0437	0.1702***	0.2572***
β^{μ}_{sport}	0.5	0.1544***	0.111***	0.1451***	0.0881***	0.0904***
	0.75	0.0848***	0.1064***	0.1171***	0.0895***	0.051**
	1.0	0.0801***	0.0838***	0.1129***	0.0802***	0.044*
	1.25	0.0749***	0.0566***	0.0953***	0.0964***	0.0425*
	1.5	0.0798***	0.0694***	0.0765***	0.1168***	0.0413

Table A.15 – Parameter values for level 2 charging with the MNL model, and various utility function thresholds (continued). The amenity threshold is set at 300m and the sample size is 5,000. *** indicates significance at 1% level, ** significance at 5% level, and * significance at 10% level

	Distance	0.5		0.75		1.0		1.25		1.5	
		Mean	Std	Mean	Std	Mean	Std	Mean	Std	Mean	Std
Test set	Score										
Estimation	Akaike Information Criterion	53092.5700	616.9900	52498.7400	653.5600	52118.0600	698.4400	51993.8400	728.4000	51859.3200	668.2300
	Bayesian Information Criterion	53188.3300	617.0400	52594.5000	653.6100	52213.8100	698.5100	52089.5900	728.4600	51944.0400	668.2300
	Final log-likelihood	-26533.2857	308.4955	-26236.3715	326.7782	-26046.0282	349.2219	-25983.9190	364.1997	-25916.6605	334.1137
	Null log-likelihood	-30901.9274	50.3773	-30901.9274	50.3773	-30901.9274	50.3773	-30901.9274	50.3773	-30901.9274	50.3773
	ρ	0.1414	0.0102	0.1510	0.0108	0.1571	0.0113	0.1591	0.0117	0.1613	0.0107
	$\bar{\rho}^2$	0.1409	0.0102	0.1506	0.0108	0.1567	0.0113	0.1587	0.0117	0.1609	0.0107
Validation	Akaike Information Criterion	54012.0549	126.7889	53563.5112	135.7686	53267.2156	135.0333	53126.8781	145.8170	53083.3178	157.7764
	Bayesian Information Criterion	54096.0359	126.7895	53647.4921	135.7692	53351.1965	135.0335	53210.8591	145.8173	53167.2988	157.7766
	DPSA final, max	0.7335	0.0557	0.6304	0.0568	0.6179	0.0535	0.5945	0.0372	0.5946	0.0226
	DPSA final, mean	0.0208	0.0006	0.0211	0.0009	0.0214	0.0010	0.0213	0.0009	0.0213	0.0010
	DPSA final, min	0.0000	0.0000	0.0000	0.0000	0.0000	0.0000	0.0000	0.0000	0.0000	0.0000
	DPSA null, max	0.0000	0.0000	0.0000	0.0000	0.0000	0.0000	0.0000	0.0000	0.0000	0.0000
	DPSA null, mean	0.0000	0.0000	0.0000	0.0000	0.0000	0.0000	0.0000	0.0000	0.0000	0.0000
	DPSA null, min	0.0000	0.0000	0.0000	0.0000	0.0000	0.0000	0.0000	0.0000	0.0000	0.0000
	Final log-likelihood	-26993.0275	63.3945	-26768.7556	67.8843	-26620.6078	67.5166	-26550.4391	72.9085	-26528.6589	78.8882
	Null log-likelihood	-30199.1322	9.0394	-30199.1322	9.0394	-30199.1322	9.0394	-30199.1322	9.0394	-30199.1322	9.0394
	ρ	0.1062	0.0021	0.1136	0.0022	0.1185	0.0022	0.1208	0.0024	0.1215	0.0026
	$\bar{\rho}^2$	0.1057	0.0021	0.1132	0.0022	0.1181	0.0022	0.1204	0.0024	0.1211	0.0026

Table A.16 – Performance indicators for level 2 charging with the MNL model, and various utility function thresholds. The amenity threshold is set at 300m and the sample size is 5,000.

Parameter	Sample size	0	1	2	3	4
$\beta^{\mu}_{distFar}$	1000	-0.1449***	-0.1306***	-0.1213***	-0.1775***	-0.1624***
	3000	-0.1615***	-0.1437***	-0.1263***	-0.1686***	-0.1649***
	5000	-0.163***	-0.1454***	-0.1296***	-0.164***	-0.1608***
	7000	-0.1592***	-0.1478***	-0.1299***	-0.157***	-0.1625***
$\beta^{\mu}_{distNear}$	1000	0.6025***	0.9028***	0.9079***	0.7305***	0.8192***
	3000	0.6146***	1.0851***	0.7936***	0.7123***	0.8924***
	5000	0.6391***	1.0422***	0.7845***	0.6879***	0.8845***
	7000	0.6525***	1.0282***	0.806***	0.6908***	0.8752***
β^{μ}_{ff}	1000	-0.0392	-0.1667***	-0.0084	-0.2112***	-0.0269
	3000	-0.1034***	-0.1426***	-0.1069***	-0.1481***	-0.134***
	5000	-0.0961***	-0.1161***	-0.1098***	-0.1311***	-0.0985***
	7000	-0.1018***	-0.1403***	-0.1041***	-0.1368***	-0.1104***
β^{μ}_{isGas}	1000	-0.3528	-0.3691	0.0597	-0.8249***	-0.6176*
	3000	-0.3125**	-0.2669*	0.0686	-0.5475***	-0.4784***
	5000	-0.2414**	-0.3383***	0.1231	-0.4756***	-0.4155***
	7000	-0.3174***	-0.3788***	0.098	-0.4722***	-0.4213***
$\beta^{\mu}_{isWalkHome}$	1000	3.002***	3.2534***	3.6752***	3.1939***	3.3787***
	3000	3.011***	3.1172***	3.4777***	3.2558***	3.2743***
	5000	3.0992***	3.1498***	3.4934***	3.3087***	3.2845***
	7000	3.1229***	3.1425***	3.561***	3.3311***	3.2716***
β^{μ}_{leis}	1000	-0.1944***	-0.0048	-0.3333***	-0.1536***	-0.1785***
	3000	-0.1494***	-0.1163***	-0.2759***	-0.1645***	-0.185***
	5000	-0.159***	-0.1166***	-0.2607***	-0.1748***	-0.1916***
	7000	-0.153***	-0.1279***	-0.2453***	-0.1823***	-0.1839***
β^{μ}_{mall}	1000	0.3014***	0.1744	0.1894	0.7692***	0.4778***
	3000	0.2275***	0.3175***	0.1614**	0.6539***	0.5013***
	5000	0.2711***	0.2975***	0.197***	0.6687***	0.4962***
	7000	0.2756***	0.2978***	0.1829***	0.6668***	0.4985***
$\beta^{\mu}_{outletsFar}$	1000	0.0991***	0.0999***	0.0861***	0.0845***	0.0768***
	3000	0.1023***	0.1147***	0.0965***	0.087***	0.078***
	5000	0.1136***	0.1067***	0.0958***	0.0923***	0.0724***
	7000	0.1091***	0.1027***	0.1076***	0.0925***	0.0764***
$\beta^{\mu}_{outletsNear}$	1000	0.3372***	0.3***	0.1892***	0.2854***	0.1459***
	3000	0.3411***	0.2747***	0.2403***	0.2348***	0.1898***
	5000	0.3251***	0.2681***	0.2399***	0.2442***	0.1857***
	7000	0.3274***	0.2725***	0.2459***	0.2362***	0.1894***

Table A.17 – Parameter values for level 2 charging with the MNL model, and various sample sizes. The amenity threshold is set at 300m and the utility function threshold is 1,5km. *** indicates significance at 1% level, ** significance at 5% level, and * significance at 10% level

Parameter	Sample size	0	1	2	3	4
β^{μ}_{rest}	1000	0.3016***	0.361***	0.4669***	0.3992***	0.3349***
	3000	0.3439***	0.4012***	0.3932***	0.3741***	0.4106***
	5000	0.3556***	0.3912***	0.376***	0.3777***	0.3956***
	7000	0.362***	0.3917***	0.3821***	0.3659***	0.3892***
β^{μ}_{shop}	1000	-0.1368***	-0.0886*	-0.0983*	-0.1189**	-0.1306***
	3000	-0.0952***	-0.1053***	-0.0405	-0.0872***	-0.138***
	5000	-0.098***	-0.0981***	-0.0496**	-0.1129***	-0.1494***
	7000	-0.0988***	-0.096***	-0.0509***	-0.1044***	-0.1507***
β^{μ}_{sm}	1000	0.2847***	0.2098***	-0.0212	0.2968***	0.3009***
	3000	0.1377***	0.1048**	0.056	0.1673***	0.2358***
	5000	0.1006***	0.1129***	0.0437	0.1702***	0.2572***
	7000	0.0922***	0.1252***	0.026	0.1392***	0.2698***
β^{μ}_{sport}	1000	0.0518	0.0961*	0.1639***	0.1914***	0.0185
	3000	0.0706**	0.0936***	0.0882***	0.0938***	0.071**
	5000	0.0798***	0.0694***	0.0765***	0.1168***	0.0413
	7000	0.0589***	0.0807***	0.0931***	0.1125***	0.027

Table A.18 – Parameter values for level 2 charging with the MNL model, and various sample sizes. The amenity threshold is set at 300m and the utility function threshold is 1,5km (continued). *** indicates significance at 1% level, ** significance at 5% level, and * significance at 10% level

	Sample size	1000		3000		5000		7000	
		Mean	Std	Mean	Std	Mean	Std	Mean	Std
Test set	Score								
Estimation	Akaike Information Criterion	10480.7700	240.7100	31224.4800	442.5100	51859.3200	668.2300	72541.2300	820.6900
	Bayesian Information Criterion	10544.5700	240.7100	31302.5700	442.5100	51944.0400	668.2300	72630.3200	820.6900
	Final log-likelihood	-5227.3846	120.3561	-15599.2423	221.2528	-25916.6605	334.1137	-36257.6129	410.3451
	Null log-likelihood	-6185.5388	15.4519	-18539.4485	35.4542	-30901.9274	50.3773	-43262.0048	79.5915
	ρ	0.1549	0.0191	0.1586	0.0122	0.1613	0.0107	0.1619	0.0091
	$\bar{\rho}^2$	0.1528	0.0191	0.1579	0.0122	0.1609	0.0107	0.1616	0.0091
Validation	Akaike Information Criterion	53148.7700	179.0100	53081.9700	161.1900	53083.3200	157.7800	53084.3000	137.1300
	Bayesian Information Criterion	53232.7500	179.0100	53165.9500	161.1900	53167.3000	157.7800	53168.2800	137.1300
	DPSA final, max	0.5802	0.0412	0.5903	0.0300	0.5946	0.0226	0.5969	0.0204
	DPSA final, mean	0.0207	0.0014	0.0208	0.0009	0.0213	0.0010	0.0215	0.0009
	DPSA final, min	0.0000	0.0000	0.0000	0.0000	0.0000	0.0000	0.0000	0.0000
	DPSA null, max	0.0038	0.0000	0.0038	0.0000	0.0038	0.0000	0.0038	0.0000
	DPSA null, mean	0.0017	0.0000	0.0017	0.0000	0.0017	0.0000	0.0017	0.0000
	DPSA null, min	0.0014	0.0000	0.0014	0.0000	0.0014	0.0000	0.0014	0.0000
	Final log-likelihood	-26561.3830	89.5047	-26527.9849	80.5963	-26528.6589	78.8882	-26529.1505	68.5667
	Null log-likelihood	-30199.1322	9.0394	-30199.1322	9.0394	-30199.1322	9.0394	-30199.1322	9.0394
	ρ	0.1205	0.0029	0.1216	0.0027	0.1215	0.0026	0.1215	0.0023
	$\bar{\rho}^2$	0.1200	0.0029	0.1211	0.0027	0.1211	0.0026	0.1211	0.0023

Table A.19 – Performance indicators for level 2 charging with the MNL model, and various sample sizes. The amenity threshold is set at 300m and the utility function threshold is 1,5km. *** indicates significance at 1% level, ** significance at 5% level, and * significance at 10% level

Parameter	Distance	0	1	2	3	4
$\beta^{\mu}_{distFar}$	100	-0.176***	-0.1741***	-0.1832***	-0.1832***	-0.1837***
	200	-0.1737***	-0.1715***	-0.1798***	-0.1791***	-0.1806***
	300	-0.1739***	-0.1738***	-0.1807***	-0.1819***	-0.1823***
	400	-0.1742***	-0.1733***	-0.1817***	-0.1797***	-0.1831***
$\beta^{\mu}_{distNear}$	100	1.411***	1.743***	1.322***	1.3636***	1.9477***
	200	1.2063***	1.4573***	1.1227***	1.1926***	1.7204***
	300	1.1971***	1.4446***	1.0276***	1.0765***	1.6485***
	400	1.2011***	1.508***	1.0773***	1.1526***	1.6488***
β^{μ}_{ff}	100	-0.3821***	-0.6857***	-0.4282***	-0.3854***	-0.5555***
	200	-0.4237***	-0.5366***	-0.4259***	-0.266***	-0.3712***
	300	-0.0479	-0.1621***	0.1073	0.0505	0.0409
	400	0.2099***	0.0838	0.329***	0.3817***	0.2778***
β^{μ}_{isGas}	100	0.1049	0.0454	-0.1722**	0.0253	0.0037
	200	-0.1824***	-0.1933***	-0.4185***	-0.2357***	-0.2465***
	300	-0.3423***	-0.3846***	-0.5826***	-0.4111***	-0.4357***
	400	-0.1634***	-0.1328**	-0.4461***	-0.2873***	-0.2091***
$\beta^{\mu}_{isWalkHome}$	100	2.0464***	1.7839***	1.8796***	1.4404***	2.0454***
	200	1.9622***	1.6666***	1.7922***	1.3722***	1.9548***
	300	1.9035***	1.5773***	1.6888***	1.2823***	1.8437***
	400	1.9187***	1.6313***	1.7537***	1.3088***	1.8588***
β^{μ}_{leis}	100	0.2584***	0.3385***	0.1879**	0.3869***	0.2217***
	200	0.1551***	0.2365***	0.083*	0.2364***	0.1826***
	300	0.3323***	0.4502***	0.2744***	0.3302***	0.3286***
	400	0.0084	0.1055***	-0.0594	-0.0429	0.0155
β^{μ}_{mall}	100	0.3925***	0.4002***	0.51***	0.4583***	0.4416***
	200	0.2075***	0.1304*	0.4064***	0.3938***	0.3062***
	300	0.6607***	0.6946***	0.8865***	0.7802***	0.7251***
	400	0.8997***	0.9646***	1.0536***	0.9838***	0.9663***
$\beta^{\mu}_{outletsFar}$	100	0.3965***	0.4726***	0.4457***	0.4166***	0.494***
	200	0.2905***	0.2857***	0.326***	0.2931***	0.3479***
	300	0.2022***	0.1823***	0.1993***	0.1692***	0.2174***
	400	0.3001***	0.3195***	0.3038***	0.297***	0.3428***
$\beta^{\mu}_{outletsNear}$	100	0.0506	-0.0115	0.2013***	0.2003**	-0.1789**
	200	0.0126	-0.0773	0.1754**	0.1698*	-0.2252***
	300	-0.0107	-0.1007	0.1431*	0.1367	-0.2777***
	400	0.0371	-0.0357	0.1799**	0.1862**	-0.2063***

Table A.20 – Parameter values for level 3 charging with the MNL model, and various amenity thresholds. The utility function threshold is set to 1,5km. *** indicates significance at 1% level, ** significance at 5% level, and * significance at 10% level

Parameter	Distance	0	1	2	3	4
β^{μ}_{rest}	100	-0.1871***	-0.1848***	-0.2134***	-0.2781***	-0.2602***
	200	-0.2837***	-0.2687***	-0.3107***	-0.401***	-0.4175***
	300	-0.1182***	-0.0878*	-0.1855***	-0.204***	-0.2553***
	400	-0.1324**	-0.0559	-0.1809***	-0.2868***	-0.2071***
β^{μ}_{shop}	100	-0.3348***	-0.3325***	-0.3579***	-0.4193***	-0.3614***
	200	0.1204***	0.1095***	0.1818***	0.0996**	0.1475***
	300	-0.2306***	-0.3053***	-0.2609***	-0.2551***	-0.2172***
	400	-0.4168***	-0.4875***	-0.4565***	-0.3506***	-0.4777***
β^{μ}_{sm}	100	0.5238	1.0688***	1.2679***	0.9772***	0.7517**
	200	0.0131	0.0393	-0.0158	0.0178	-0.0521
	300	0.2098***	0.4397***	0.333***	0.43***	0.306***
	400	0.8362***	0.9826***	0.9871***	0.9231***	1.0172***
β^{μ}_{sport}	100	-0.4973***	-0.7591***	-0.5213***	-0.6338***	-0.6354***
	200	-0.3129***	-0.4919***	-0.2887***	-0.3342***	-0.3847***
	300	-0.2794***	-0.4374***	-0.3163***	-0.2945***	-0.337***
	400	-0.1467***	-0.3012***	-0.0911**	-0.146***	-0.2263***

Table A.21 – Parameter values for level 3 charging with the MNL model, and various amenity thresholds. The utility function threshold is set to 1,5km (continued). *** indicates significance at 1% level, ** significance at 5% level, and * significance at 10% level

	Distance	100		200		300		400	
		Mean	Std	Mean	Std	Mean	Std	Mean	Std
Test set	Score								
Estimation	Akaike Information Criterion	10693.9800	88.9800	10606.4300	97.6900	10735.1200	105.4700	10655.0700	113.7000
	Bayesian Information Criterion	10773.7300	88.9800	10686.1900	97.7200	10814.8700	105.5200	10734.8200	113.7200
	Final log-likelihood	-5333.9900	44.4899	-5290.2174	48.8472	-5354.5580	52.7369	-5314.5332	56.8513
	Null log-likelihood	-8479.0167	114.4676	-8479.0167	114.4676	-8479.0167	114.4676	-8479.0167	114.4676
	ρ	0.3708	0.0083	0.3760	0.0076	0.3684	0.0069	0.3731	0.0081
	$\bar{\rho}^2$	0.3693	0.0083	0.3745	0.0076	0.3669	0.0069	0.3716	0.0081
Validation	Akaike Information Criterion	825.2300	44.2000	812.2000	44.7700	823.3700	45.3500	816.9000	48.3000
	Bayesian Information Criterion	868.9600	44.1800	855.9400	44.7500	867.1100	45.3400	860.6400	48.2800
	DPSA final, max	0.9549	0.0053	0.9461	0.0065	0.9462	0.0117	0.9497	0.0117
	DPSA final, mean	0.2884	0.0190	0.2974	0.0188	0.2910	0.0179	0.2938	0.0210
	DPSA final, min	0.0011	0.0006	0.0016	0.0009	0.0015	0.0008	0.0016	0.0009
	DPSA null, max	0.2500	0.0000	0.2500	0.0000	0.2500	0.0000	0.2500	0.0000
	DPSA null, mean	0.0831	0.0018	0.0831	0.0018	0.0831	0.0018	0.0831	0.0018
	DPSA null, min	0.0556	0.0000	0.0556	0.0000	0.0556	0.0000	0.0556	0.0000
	Final log-likelihood	-399.6134	22.0993	-393.1023	22.3839	-398.6860	22.6755	-395.4509	24.1482
	Null log-likelihood	-548.7335	2.7691	-548.7335	2.7691	-548.7335	2.7691	-548.7335	2.7691
	ρ	0.2717	0.0402	0.2836	0.0406	0.2735	0.0409	0.2793	0.0438
	$\bar{\rho}^2$	0.2481	0.0402	0.2599	0.0406	0.2498	0.0409	0.2556	0.0438

Table A.22 – Performance indicators for level 3 charging with the MNL model, and various amenity thresholds. The utility function threshold is set to 1,5km. *** indicates significance at 1% level, ** significance at 5% level, and * significance at 10% level

Parameter	Distance	0	1	2	3	4
$\beta^{\mu}_{distFar}$	0.5	-0.1935***	-0.1915***	-0.198***	-0.2002***	-0.2004***
	0.75	-0.1858***	-0.184***	-0.1941***	-0.1934***	-0.1928***
	1.0	-0.182***	-0.1821***	-0.1897***	-0.1897***	-0.1891***
	1.25	-0.1812***	-0.1787***	-0.1856***	-0.1837***	-0.1866***
	1.5	-0.1737***	-0.1715***	-0.1798***	-0.1791***	-0.1806***
$\beta^{\mu}_{distNear}$	0.5	-6.9284	0.2229	-1.5196	-0.0655	0.927
	0.75	1.0473	1.606***	3.2752***	1.035	0.7309
	1.0	2.4474***	1.9191***	2.1093***	1.7397***	2.4352***
	1.25	0.676**	1.3522***	1.1083***	1.9382***	1.5369***
	1.5	1.2063***	1.4573***	1.1227***	1.1926***	1.7204***
β^{μ}_{ff}	0.5	-0.3137***	-0.3711***	-0.3261***	-0.0649	-0.2145***
	0.75	-0.409***	-0.4809***	-0.3713***	-0.145*	-0.3271***
	1.0	-0.4871***	-0.5187***	-0.4233***	-0.234***	-0.4081***
	1.25	-0.4619***	-0.5708***	-0.448***	-0.2716***	-0.4395***
	1.5	-0.4237***	-0.5366***	-0.4259***	-0.266***	-0.3712***
β^{μ}_{isGas}	0.5	-0.1969***	-0.1714***	-0.412***	-0.215***	-0.2436***
	0.75	-0.1866***	-0.1533***	-0.4001***	-0.2062***	-0.2324***
	1.0	-0.1954***	-0.1842***	-0.4277***	-0.24***	-0.2675***
	1.25	-0.1831***	-0.191***	-0.4147***	-0.2197***	-0.2533***
	1.5	-0.1824***	-0.1933***	-0.4185***	-0.2357***	-0.2465***
$\beta^{\mu}_{isWalkHome}$	0.5	5.0925***	1.5596	1.3657	2.2746	1.9765
	0.75	2.0835***	2.2644***	2.4458***	2.1489***	2.7706***
	1.0	2.1762***	1.6867***	1.7287***	1.6861***	1.8825***
	1.25	2.0271***	1.7278***	1.8199***	1.4059***	1.9651***
	1.5	1.9622***	1.6666***	1.7922***	1.3722***	1.9548***
β^{μ}_{leis}	0.5	0.2254***	0.3259***	0.0838*	0.3032***	0.2357***
	0.75	0.1603***	0.2512***	0.0655	0.2482***	0.1637***
	1.0	0.1541***	0.2312***	0.0688	0.2346***	0.1586***
	1.25	0.164***	0.2443***	0.0873*	0.2495***	0.1824***
	1.5	0.1551***	0.2365***	0.083*	0.2364***	0.1826***
β^{μ}_{mall}	0.5	0.1487*	0.1024	0.398***	0.378***	0.2917***
	0.75	0.1426*	0.0967	0.3991***	0.3692***	0.2826***
	1.0	0.1358*	0.0847	0.3637***	0.3512***	0.2548***
	1.25	0.1729**	0.0943	0.3861***	0.3862***	0.2687***
	1.5	0.2075***	0.1304*	0.4064***	0.3938***	0.3062***
$\beta^{\mu}_{outletsFar}$	0.5	0.2343***	0.2247***	0.2872***	0.2343***	0.2886***
	0.75	0.2517***	0.2514***	0.2987***	0.2485***	0.3119***
	1.0	0.2695***	0.2576***	0.2994***	0.26***	0.3255***
	1.25	0.2702***	0.2648***	0.3075***	0.2797***	0.3354***
	1.5	0.2905***	0.2857***	0.326***	0.2931***	0.3479***
$\beta^{\mu}_{outletsNear}$	0.5	0.1295	0.3088	1.5361	0.2389	0.2481
	0.75	0.0711	-0.2416	-0.3532	-0.0263	-0.162
	1.0	-0.3237**	-0.2531*	0.0082	-0.1406	-0.3656***
	1.25	0.0723	-0.1202	0.1297	-0.0614	-0.2175**
	1.5	0.0126	-0.0773	0.1754**	0.1698*	-0.2252***

Table A.23 – Parameter values for level 3 charging with the MNL model, and various utility function thresholds. The amenity threshold is set to 200m. *** indicates significance at 1% level, ** significance at 5% level, and * significance at 10% level

Parameter	Distance	0	1	2	3	4
β^{μ}_{rest}	0.5	-0.3397***	-0.3278***	-0.3376***	-0.4622***	-0.4658***
	0.75	-0.3234***	-0.2961***	-0.3353***	-0.4532***	-0.4447***
	1.0	-0.2814***	-0.2873***	-0.3237***	-0.4247***	-0.4209***
	1.25	-0.2738***	-0.2495***	-0.2926***	-0.3968***	-0.3898***
	1.5	-0.2837***	-0.2687***	-0.3107***	-0.401***	-0.4175***
β^{μ}_{shop}	0.5	0.1114***	0.0837**	0.2038***	0.0527	0.1318***
	0.75	0.1562***	0.1185***	0.211***	0.0999**	0.1733***
	1.0	0.1593***	0.1298***	0.2143***	0.1215***	0.1841***
	1.25	0.1278***	0.1146***	0.1824***	0.1038***	0.1556***
	1.5	0.1204***	0.1095***	0.1818***	0.0996**	0.1475***
β^{μ}_{sm}	0.5	0.0736	0.1047	0.0131	0.1807*	-0.0009
	0.75	0.0795	0.1253	0.0237	0.1745*	-0.0027
	1.0	0.0137	0.0752	0.0063	0.0998	-0.0743
	1.25	0.0097	0.0386	-0.0262	0.0294	-0.0782
	1.5	0.0131	0.0393	-0.0158	0.0178	-0.0521
β^{μ}_{sport}	0.5	-0.1829***	-0.3273***	-0.1623***	-0.1981***	-0.2401***
	0.75	-0.225***	-0.3769***	-0.1746***	-0.2331***	-0.282***
	1.0	-0.2736***	-0.3935***	-0.2045***	-0.276***	-0.3285***
	1.25	-0.3075***	-0.4727***	-0.2753***	-0.3279***	-0.3778***
	1.5	-0.3129***	-0.4919***	-0.2887***	-0.3342***	-0.3847***

Table A.24 – Parameter values for level 3 charging with the MNL model, and various utility function thresholds (continued). The amenity threshold is set to 200m. *** indicates significance at 1% level, ** significance at 5% level, and * significance at 10% level

	Distance	0.5		0.75		1.0		1.25		1.5	
		Mean	Std	Mean	Std	Mean	Std	Mean	Std	Mean	Std
Test set	Score										
Estimation	Akaike Information Criterion	10909.0800	90.5500	10791.4700	81.5900	10758.3700	96.0200	10704.4000	94.7800	10606.4300	97.6900
	Bayesian Information Criterion	10988.8300	90.6100	10871.2300	81.6500	10838.1200	96.0600	10784.1600	94.7800	10686.1900	97.7200
	Final log-likelihood	-5441.5394	45.2774	-5382.7351	40.7970	-5366.1834	48.0075	-5339.2006	47.3914	-5290.2174	48.8472
	Null log-likelihood	-8479.0167	114.4676	-8479.0167	114.4676	-8479.0167	114.4676	-8479.0167	114.4676	-8479.0167	114.4676
	ρ	0.3582	0.0067	0.3651	0.0065	0.3671	0.0070	0.3702	0.0085	0.3760	0.0076
	$\bar{\rho}^2$	0.3566	0.0068	0.3636	0.0065	0.3655	0.0070	0.3687	0.0085	0.3745	0.0076
Validation	Akaike Information Criterion	832.1997	38.0500	826.7232	35.6112	820.5784	37.9845	820.2844	42.8279	812.2046	44.7679
	Bayesian Information Criterion	875.9330	38.0377	870.4565	35.5982	864.3118	37.9693	864.0177	42.8114	855.9379	44.7517
	DPSA final, max	0.9563	0.0241	0.9555	0.0137	0.9551	0.0130	0.9441	0.0092	0.9461	0.0065
	DPSA final, mean	0.2820	0.0177	0.2842	0.0150	0.2885	0.0173	0.2889	0.0173	0.2974	0.0188
	DPSA final, min	0.0009	0.0004	0.0012	0.0005	0.0013	0.0007	0.0014	0.0007	0.0016	0.0009
	DPSA null, max	0.2500	0.0000	0.2500	0.0000	0.2500	0.0000	0.2500	0.0000	0.2500	0.0000
	DPSA null, mean	0.0800	0.0000	0.0800	0.0000	0.0800	0.0000	0.0800	0.0000	0.0800	0.0000
	DPSA null, min	0.0600	0.0000	0.0600	0.0000	0.0600	0.0000	0.0600	0.0000	0.0600	0.0000
	Final log-likelihood	-403.0998	19.0250	-400.3616	17.8056	-397.2892	18.9923	-397.1422	21.4140	-393.1023	22.3839
	Null log-likelihood	-548.7335	2.7691	-548.7335	2.7691	-548.7335	2.7691	-548.7335	2.7691	-548.7335	2.7691
	ρ	0.2654	0.0339	0.2704	0.0320	0.2760	0.0343	0.2763	0.0389	0.2836	0.0406
	$\bar{\rho}^2$	0.2417	0.0339	0.2467	0.0319	0.2523	0.0343	0.2526	0.0389	0.2599	0.0406

Table A.25 – Performance indicators for level 3 charging with the MNL model, and various utility function thresholds. The amenity threshold is set to 200m. *** indicates significance at 1% level, ** significance at 5% level, and * significance at 10% level